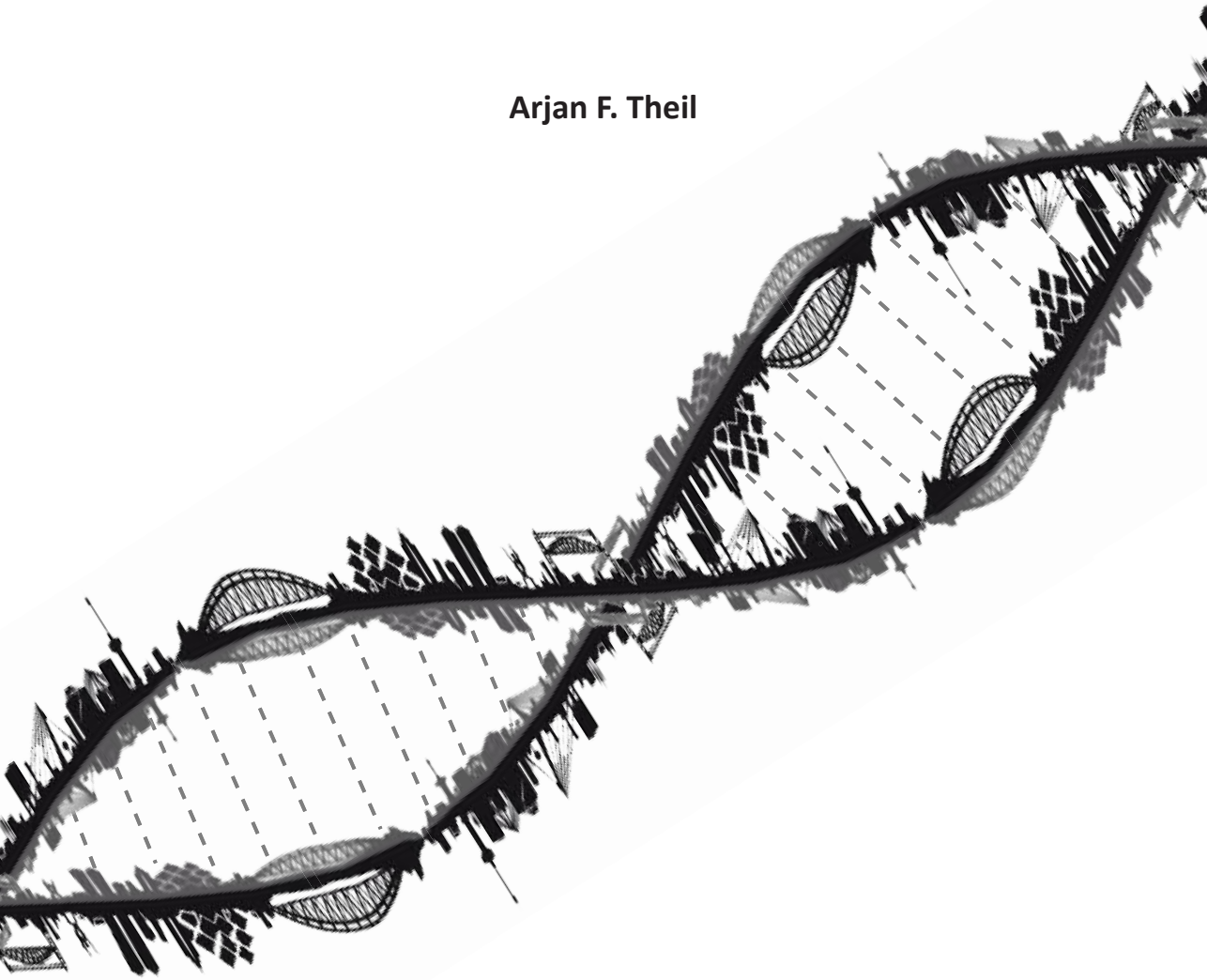


Functional Analysis of TTDA: From Human to Mouse

- Big impact of a small protein -

Arjan F. Theil



Colofon

ISBN: 978-90-8891-880-3

Cover illustration: DNA helix made from Skyline of Rotterdam
Cover design: Arjan F. Theil
Lay-out: Arjan F. Theil
Printed by: Proefschriftmaken.nl || Uitgeverij BOXPress
Published by: Uitgeverij BOXPress, 's-Hertogenbosch

The studies presented in this thesis were mainly performed at the department of Genetics of the Erasmus University Medical Center, Rotterdam, The Netherlands

Copyright © Arjan F. Theil 2014, Rotterdam, The Netherlands

All rights reserved. No part of this thesis may be reproduced, stored in a retrieval system, or transmitted in any form or by any means, without prior written permission of the author.

**Functional Analysis of TTDA: From Human to Mouse
- Big impact of a small protein -**

Functionele analyse van TTDA: van mens tot muis
- Grote impact van een klein eiwit -

Proefschrift

ter verkrijging van de graad van doctor aan de
Erasmus Universiteit Rotterdam
op gezag van de
rector magnificus

Prof.dr. H.A.P. Pols

en volgens besluit van het College voor Promoties.

De openbare verdediging zal plaatsvinden op
woensdag 04 juni 2014 om 13.30 uur
door

Arjan Friso Theil
geboren te 's-Gravenhage



Promotiecommissie

Promotor: Prof.dr. J.H.J. Hoeijmakers

Overige leden: Dr. J. Essers
Prof.dr. L.H.F. Mullenders
Prof.dr. J. Gribnau

Copromotor: Dr. W. Vermeulen

Contents

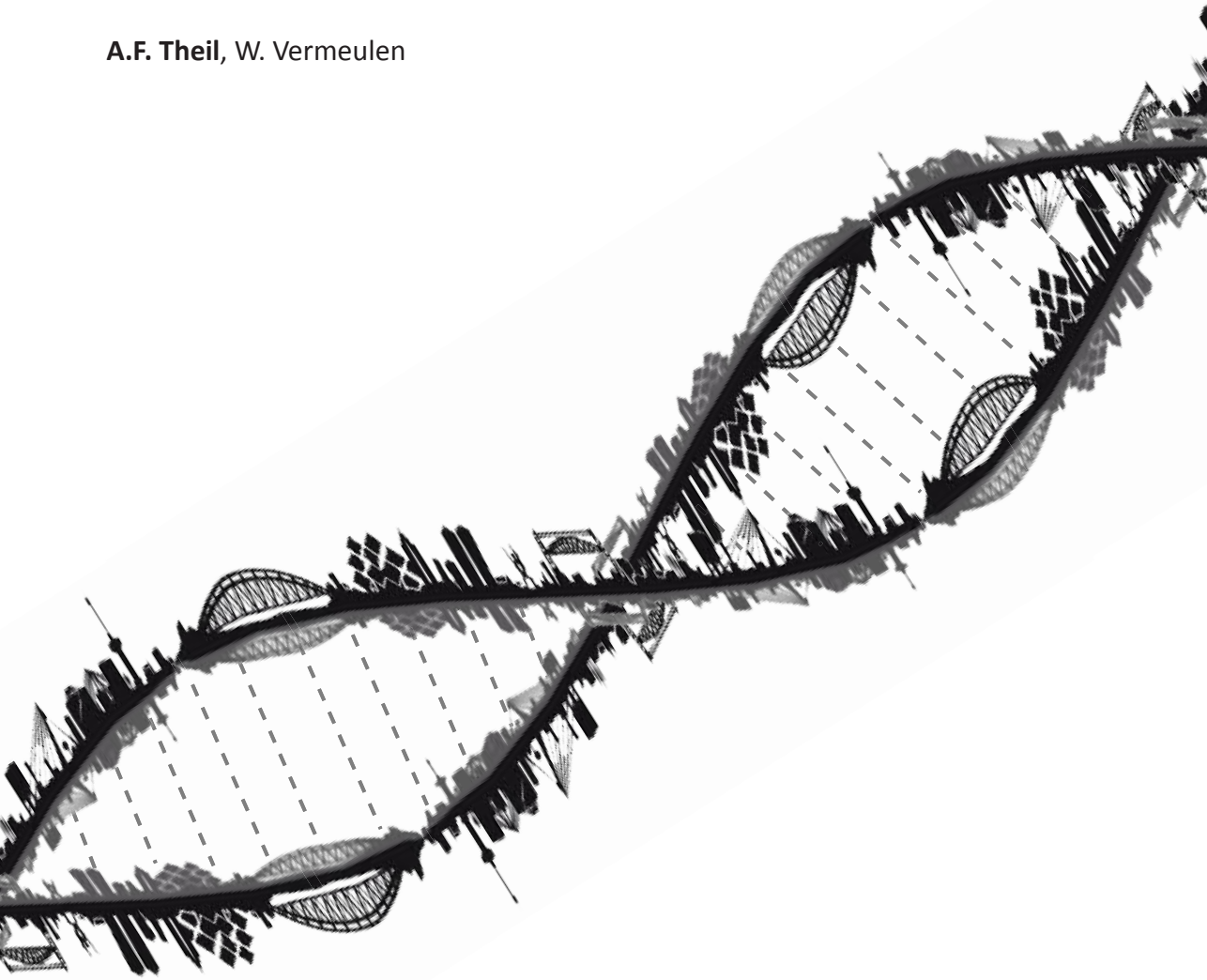
Chapter		Page
Chapter 1	Scope of the Thesis	10
	Introduction	12
Chapter 2	Slowly progressing Nucleotide Excision Repair in Trichthiodystrophy Group A Patient Fibroblasts	32
Chapter 3	Dynamic Interaction of TTDA with TFIIH is Stabilized by Nucleotide Excision Repair in Living Cells	50
Chapter 4	Differentiation Driven Changes in the Dynamic Organization of Basal Transcription Initiation	74
Chapter 5	Disruption of TTDA Results in Complete Nucleotide Excision Repair Deficiency and Embryonic Lethality	100
Chapter 6	Discussion	126
Chapter 7	Summary	136
	Nederlandse samenvatting	140
	List of Abbreviations	144
	Curriculum Vitae	146
	List of Publications	147
	PhD Portfolio	149
	Acknowledgements	152



CHAPTER 1

Scope of the Thesis
Introduction

A.F. Theil, W. Vermeulen



Scope of the Thesis

1

The integrity of genomic DNA is continuously exposed to intracellularly produced genotoxins, and environmental chemicals and radiation that lead to a wide variety of DNA lesions. To counteract the deleterious effects of DNA damage, all living organisms have developed multiple DNA repair mechanisms, each with their own lesion specificity and characteristics. Nucleotide excision repair (NER) is responsible for recognition and repair of numerous structurally unrelated helix-distorting lesions, including UV-induced 6-4-photoproducts (6-4PPs) and cyclobutane pyrimidine dimers (CPDs). TFIIH is an important multi-subunit protein complex crucial not only for NER, but also essential for RNA polymerase II (RNAP2) driven transcription. In both processes, TFIIH unwinds the DNA to allow either initiation of transcription or strand excision in NER. Mutations in the TFIIH subunits XPB, XPD and TTDA are associated with a large variety of clinical features associated with inherited NER-disorders: cancer-prone Xeroderma Pigmentosum (XP), severe neuro-developmental and premature ageing syndromes Trichothiodystrophy (TTD) and Cockayne Syndrome (CS) or XP combined with CS (XP/CS) or TTD (XP/TTD).

The work presented in this thesis is aimed to better understand the molecular mechanism underlying the clinical features presented in TTD patients, with a focus on the analysis of cellular features associated with inherited mutations in the *TTDA* gene. Patients carrying mutations in the *TTDA* gene belong to the rare neurodevelopment repair syndrome trichothiodystrophy group A (TTD-A). The small 8 kDa protein encoded by this gene is part of TFIIH and important for maintaining its stability and its role in NER. Fibroblasts derived from TTD-A patients present a low DNA repair synthesis capacity after UV irradiation (measured by Unscheduled DNA Synthesis). Despite this low repair capacity (UDS level of approximately 20%), a surprising moderate UV-hypersensitivity was found (overall 2-3 fold UV sensitivity). To investigate this apparent inconsistency, we have performed a detailed analysis on the repair kinetics and NER complex assembly within TTD-A cells (**Chapter 1**). We showed that the repair activity in TTD-A cells is not completely abolished, but occurs at a slower rate. The data presented in this chapter suggest that TTDA is not an essential NER factor, however, its presence clearly stimulates the efficiency of the repair reaction.

To understand how TTDA participates in DNA repair, we measured the kinetic engagement of TTDA during repair in living cells. A fluorescently tagged and biologically active version of TTDA (TTDA-GFP) was expressed in TTD-A mutant cells and analyzed using confocal microscopy (**Chapter 2**). Experiments performed in this chapter showed that TTDA is not tightly associated with TFIIH, but dynamically switches between a TFIIH-bound and a TFIIH-free form of TTDA. However, when cells are exposed to DNA damage, the equilibrium is quickly shifted towards a TFIIH-bound TTDA that is actively engaged in NER. Our data further suggest that TTDA is implicated in licensing the NER reaction by its role in the damage-verification function of TFIIH.

Analysis of TTD-A patient cells in **Chapter 1 and 2** have provided valuable information on the function of TTDA in NER. However, the majority of the disease-specific symptoms of TTD-A patients are expressed in the neuronal and epithelial tissue (ichthyosis, brittle hair) and not in the fibroblasts lineage. In order to provide important clues on the molecular basis of TFIIH-related diseases, two mouse models have been generated: an *XpbYFP* knock-in and a *Ttda*^{-/-} knock-out mouse model. *XpbYFP* mice expresses in all cells a fluorescently tagged XPB (subunit of TFIIH) from its endogenous gene locus, which allowed us to study the role of TFIIH in both transcription and NER in different cells in living tissues (**Chapter 3**). This mouse model provided valuable information on how transcription is

organized in highly differentiated post-mitotic cells. We have shown that in post-mitotic cells (e.g.: neurons, myocytes, and hepatocytes), TFIIH is bound to promoters with a much longer residence time than in proliferative cells (e.g.: keratinocytes and fibroblasts). This observation might help to better understand the cell-specific expression of TTD features, which are known to be also derived from transcriptional defects. In addition, the fluorescent TFIIH was also used to study the fate of TFIIH in the absence of TTDA in *Ttda* knock-out mice. The *Ttda*^{-/-} mouse model was generated to investigate the molecular mechanism leading to a TTD-specific phenotype (**Chapter 4**). Unexpectedly, and in striking contrast to TTD-A patients, *Ttda*^{-/-} embryos die in utero between 10.5 days of gestation and birth. Moreover, cells isolated from these mice present a complete inactivation of NER, also contrasting to the only mild NER defect in TTD-A patient cells. We found that this rather mild TTD-phenotype observed in TTD-A patients is due to the presence of partly functional mutant proteins. Another surprising observation was that *Ttda*-deficient cells were also hyper-sensitive to oxidative DNA damage. These observations suggest that TTDA, and most likely the entire TFIIH, has additional functions in DNA repair extending beyond NER, possibly causing synergistic effects when inactivated. Oxidative DNA damage is the most abundant lesion produced by endogenous cellular processes. We propose a model that the lethal phenotype of *Ttda*^{-/-} or severely disturbed embryonic development is most likely caused by a combination of affected embryonic transcriptional program and a defect in repairing endogenously produced oxidative DNA lesions.

Introduction

1 Maintenance of genetic information is important for proper cell function and ensures faithful transmission of an intact genome to the next generation. Every cell in all organisms is constantly attacked by endogenous and environmental stresses that can damage genetic information. DNA lesions generated by endogenous sources are a result of spontaneous hydrolysis, oxidation or methylation. For example, reactive oxygen species (ROS) are generated by the cell's own respiration, which produces several types of oxidative DNA lesions [1]. The number of DNA lesions produced by normal cellular metabolism is estimated to be approximately 10,000-50,000 lesions per cell per day in humans [2,3]. DNA lesions generated by environmental stresses can arise from solar UV irradiation, ionizing radiation (IR) or various chemicals. For instance, ultraviolet radiation produces helical-distorting lesions cyclobutane pyrimidine dimers (CPDs) and pyrimidine-(6-4)-pyrimidone products (6-4PPs) [4,5]. On the other hand, IR can cause formation of single strand breaks (SSBs) and double strand breaks (DSBs) [6].

DNA lesions can directly interfere with both transcription elongation and DNA replication. Unrepaired lesions in actively transcribing genes interfere with the elongation of both RNA polymerase I (RNAP1) and RNA polymerase II (RNAP2). This physical block in transcription may inactivate gene expression and could eventually result in permanent cell cycle arrest (senescence) or cell death (apoptosis) [7]. If these cells are not replaced in the tissues or organs, it can result in progeria [8]. Unrepaired lesions can also interfere with DNA replication, affecting the progression and fidelity of the DNA replication machinery. Replication errors may result in mutations, genome instability and can lead to carcinogenesis [8]. As a consequence, unrepaired lesions may lead to long-term consequences that are implicated in human pathologies, such as cancer and premature ageing [9].

To ensure preservation of genetic information, and to allow on-going DNA-transacting processes, the cell harbours multiple DNA repair systems and associated DNA-damage signalling pathways—collectively called the DNA-damage response (DDR). The three kinases that play a crucial role in the DDR are ataxia telangiectasia-mutated (ATM), ataxia telangiectasia and Rad3-related kinase (ATR) and DNA-dependent protein kinase catalytic subunit (DNA-PKcs) [10,11]. These kinases respond to various forms of genotoxic stress and as a consequence initiate a phosphorylation cascade that affect key regulatory proteins [12,13], like p53 and the effector kinases Chk1 and Chk2. ATM is the main kinase required for early responses to DSBs, whereas ATR is mainly required in response to UV light-induced DNA damage and stalled replication forks. Research over the last decade has provided clear evidence that short-term consequences of the DDR are to either arrest the cell cycle (via cell cycle checkpoints) or, when necessary, trigger apoptosis (programmed cell death). In response to UV-light for instance, the checkpoint protein p53 becomes activated in a cell cycle independent manner, triggering either cell cycle arrest or apoptosis [14-16]. The DNA-damage signalling pathway is not solely mediated via ATM/ATR, it also involves other regulatory factors and post-translational modifications. For instance, the c-Jun NH₂-terminal kinases (JNK)—a known sub-group of mitogen-activated protein kinases (MAPK)—play also an important regulatory role in the response to environmental stress [17].

DNA Repair Pathways

Multiple DNA repair mechanisms are constantly monitoring the DNA structure in order

to counteract the continuous attacks, and collectively restrict the impact of these DNA lesions. There are at least six major multi-step DNA repair pathways, each with their own lesion specificity and characteristics. Which repair pathway is finally used depends on the type of lesion, its genomic localization and the phase of the cell cycle [18]. The major DNA repair pathways in mammals include: nucleotide excision repair (NER) that removes helical-distorting lesions [19]; base excision repair (BER) that removes non-bulky lesions and single strand breaks [20]; mismatch repair (MMR) [21,22] that removes single-nucleotide mismatches, insertions or deletions; interstrand crosslink (ICL) repair [23,24] that repairs covalently attached duplex DNA strands; homologous recombination (HR) [25] that repairs double strand breaks (DSB); and non-homologous end-joining (NHEJ) [26-28] that also repairs DSBs, but in a less error-free manner (Figure 1). When damage is not recognized or repaired before it is encountered by the replicating machinery, it may result in replication stalling. A class of alternative DNA polymerases is required to catalyse DNA synthesis over many of these replication-blocking lesions, devoted specifically to overcome replication stress. Lesion bypass by these translesion synthesis (TLS) polymerases occurs in a relatively error-prone manner and thus facilitates mutations, due to less selective nucleotide selection in the active site. Although TLS polymerases do not remove lesions, they are important in protecting the genome by preventing replication fork collapse [29-31].

In mammalian cells, various DNA repair mechanisms partly overlap in their lesion specificity and characteristics. DNA lesions involving one damaged strand are predominantly repaired by excision repair (both the BER and NER pathway). Helix-distorting lesions are a result of both endogenous and exogenous sources. These lesions block transcription and replication and are recognized by NER. Lesions that are substrate for BER are mainly a result from endogenous sources, which are less helix-distorting and do not block transcription and replication. Most of the experimental work described in this thesis are on the further analysis of molecular details of the NER reaction. In addition,

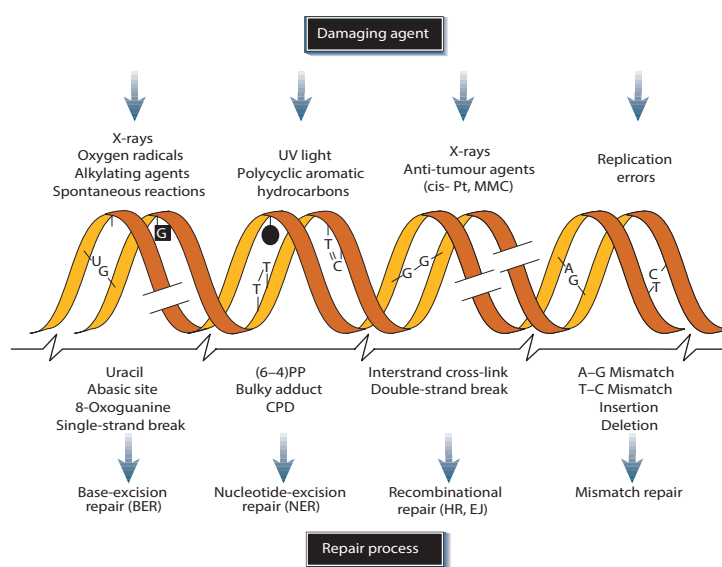


Figure 1. DNA damage, repair mechanisms and consequences.

Common DNA damaging agents (top); examples of DNA lesions induced by these agents (middle); and most relevant DNA repair mechanism responsible for the removal of the lesions (bottom). Abbreviations: cis-Pt and MMC, cisplatin and mitomycin C, respectively (both DNA-crosslinking agents); (6-4)PP and CPD, 6-4 photoproduct and cyclobutane pyrimidine dimer, respectively (both induced by UV light); BER and NER, base and nucleotide-excision repair, respectively; HR, homologous recombination; EJ, end joining. Figure obtained from J.H.J. Hoeijmakers, Nature 2001.

experiments described in this thesis disclose a novel interaction between NER and BER.

Base excision repair

The BER pathway is responsible for the repair of damaged DNA bases, sites of base loss and single strand breaks, induced by either endogenous or exogenous mutagens [32,33]. Oxidative DNA damage is considered to be the most abundant class of insults that are repaired by BER. Repair of base lesions is essential for maintaining genome integrity and survival, since knockout mice lacking one of the core BER proteins (such as *Apex1* and *Polβ*) are embryonic lethal [34-36]. BER can be roughly divided in five distinctive steps: (1) damage recognition and removal; (2) strand cleavage; (3) end cleaning; (4) gap filling; and (5) nick sealing, illustrated in Figure 2.

Damage recognition and removal (1)

DNA damage recognition by the BER pathway is achieved by a limited set of different so-called glycosylases, of which there are at least 10 known in mammals. The relatively low number of DNA glycosylases described have a broad overlap in their specificity, responsible for the recognition of a rather large number of different damaged bases identified in the genome. Because of this redundancy, a mouse model lacking one DNA glycosylase hardly shows any phenotype [37-40]. There are two types of DNA glycosylases: the mono-functional DNA glycosylases and the bi-functional DNA glycosylases. Mono-functional DNA glycosylases recognize mainly alkylated bases [20] and only exhibit glycosylase activity. Mono-functional glycosylases cleave the N-glycosidic bond between the damaged base and the phosphor-sugar backbone, creating a mutagenic repair intermediate: an abasic (AP)-site. In general, bi-functional DNA glycosylases specifically recognize oxidized bases and exhibit both a glycosylase and an additional AP endonuclease activity. This AP-site is created by hydrolysing the phosphodiester backbone, producing a single-strand nick [41].

Strand cleavage (2)

The second step in the BER pathway is the strand cleavage, formation of a single-strand break. As mentioned in the previous paragraph, bi-functional DNA glycosylases have an additional lyase activity. These bi-functional DNA glycosylases are therefore able to perform the strand cleavage themselves, able to generate a single nucleotide gap with different modified DNA ends. For instance, some bi-functional DNA glycosylases generate an α,β -unsaturated aldehyde dehydration product of deoxyribose phosphate at the 3'-site and a phosphate residue at the 5'-site (OGG1), while others will generate a phosphate residue at both sites (NEIL1-3). After base lesion recognition by a mono-functional DNA glycosylase (such as uracil DNA glycosylase [42]), the produced AP-site is cleaved by another protein called AP-endonuclease 1 (APE1), creating a single nucleotide gap harbouring DNA ends with a 5'-deoxyribose phosphate (5'-dRP) and a 3'-hydroxyl group (3'-OH).

End cleaning (3)

The third step in the BER pathway involves cleaning the DNA ends of the single-strand break, to produce a substrate that allows gap-filling nucleotide incorporation and subsequent ligation. Polymerase beta (*Polβ*), harbouring an intrinsic dRP lyase activity, will specifically remove dRP residues at the 5'-site of the single nucleotide gap, generated by mono-functional DNA glycosylases and APE1 endonuclease. Residues at the DNA ends of a single nucleotide gap which are generated by bi-functional DNA glycosylases [43], are cleaned by proteins APE1 or polynucleotide kinase (PNK) [44]. After end cleaning, the final

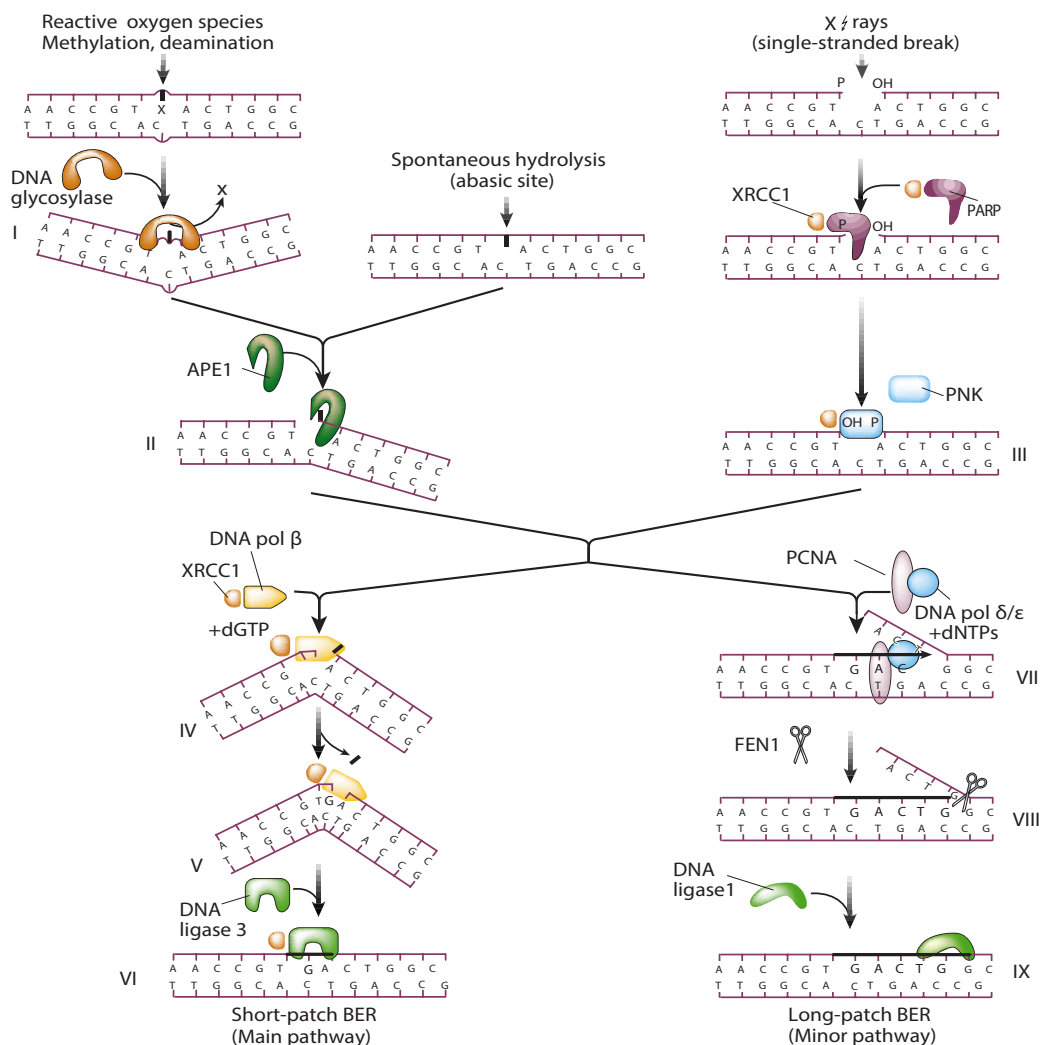


Figure 2. Mechanism for base-excision repair. A battery of glycosylases, each dealing with a relatively narrow, partially overlapping spectrum of lesions, feeds into a core reaction. Glycosylases flip the suspected base out of the helix by DNA backbone compression to accommodate it in an internal cavity of the protein. Inside the protein, the damaged base is cleaved from the sugar-phosphate backbone (stage I in the figure). The resulting abasic site can also occur spontaneously by hydrolysis. The core BER reaction is initiated by strand incision at the abasic site by the APE1 endonuclease (II). Poly(ADP-ribose) polymerase (PARP), which binds to and is activated by DNA strand breaks, and the recently identified polynucleotide kinase (PNK)59 may be important when BER is initiated from a SSB to protect and trim the ends for repair synthesis (III). In mammals, the so-called short-patch repair is the dominant mode for the remainder of the reaction. DNA pol β performs a one-nucleotide gap-filling reaction (IV) and removes the 5'-terminal baseless sugar residue via its lyase activity (V); this is then followed by sealing of the remaining nick by the XRCC1–ligase3 complex (VI). The XRCC1 scaffold protein interacts with most of the above BER core components and may therefore be instrumental in protein exchange. The long-patch repair mode involves DNA pol δ/ϵ and proliferating cell nuclear antigen (PCNA) for repair synthesis (2–10 bases) as well as the FEN1 endonuclease to remove the displaced DNA flap and DNA ligase 1 for sealing (VII–IX). The above BER reaction operates across the genome. However, some BER lesions block transcription, and in this case the problem is dealt with by the TCR pathway described above, including TFIIF, XPG (which also stimulates some of the glycosylases) and probably the remainder of the core NER apparatus. Figure obtained from J.H.J. Hoeijmakers, *Nature* 2001.

product of end cleaning will be a 5'-phosphate residue (5'-P) and a 3'-hydroxyl group (3'-OH), which can be further processed by gap filling proteins.

Gap filling (4)

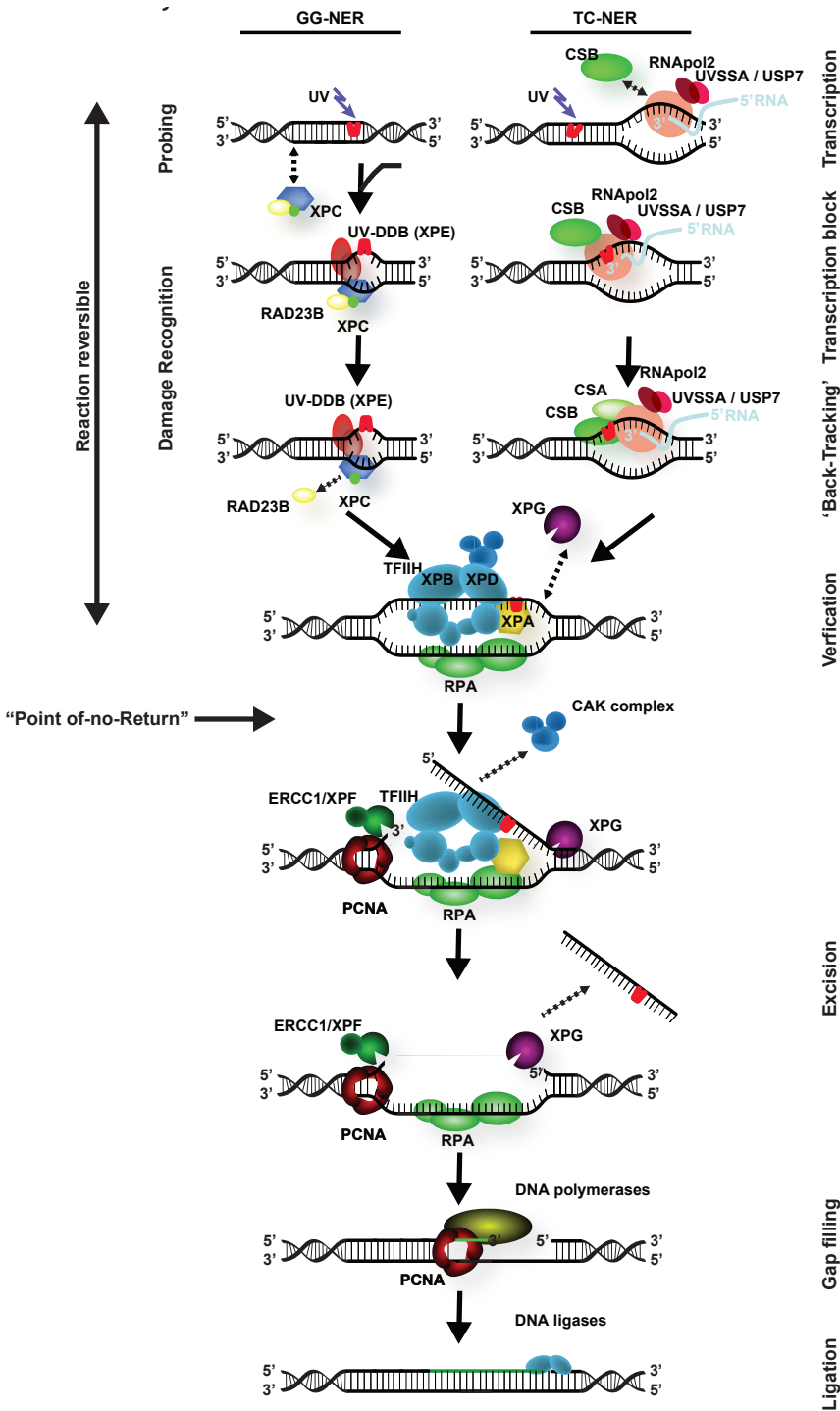
Two sub-pathways in BER have been characterized—namely short-patch BER (SP-BER) and long-patch BER (LP-BER) [45]—and differ in the length of the repair patch produced in the reaction. In both these repair sub-pathways, activated poly (ADP-ribose) polymerase 1 (PARP1) is recruited very early to sites of SSBs and is thought to help loading downstream repair proteins involved in BER. In SP-BER, Pol β is the DNA polymerase that performs the single nucleotide incorporation. However, DNA-ends containing a 5'-dRP residue are potentially vulnerable to oxidation. In that case, Pol β is not able to efficiently remove these oxidized 5-dRP residues generated by APE1, despite its intrinsic dRP lyase activity. Such modified residues will block downstream steps in SP-BER [46,47] and can only be repaired by LP-BER in which DNA polymerases displace the damaged 5'-nucleotide. This sub-pathway is initiated by the loading of proliferating cell nuclear antigen (PCNA) at the 3'-OH of the duplex DNA by replication factor C (RFC). Since Pol β is unable to effectively catalyse strand-displacement DNA synthesis in LP-BER and has no intrinsic 3' to 5' exonuclease activity [48], other DNA polymerases, e.g. δ/ϵ are needed. By the action of these DNA replication factors, the strand-displacement DNA synthesis step will create an oxidized 5'-dRP-containing segment, displaced as a flap of approximately 2-8 nucleotides. Subsequently, 5'-flap endonuclease 1 (FEN1) is needed to remove the oxidized 5'-dRP containing fragment [49]. Although the precise mechanism is still under debate, it has been shown that APE1, FEN1 and PARP1 (and subsequent poly(ADP-ribosylation)) are important to regulate the activity of Pol β [50,51].

Nick sealing (5)

The final step in BER is the sealing of the nick in the DNA backbone, which involves two DNA ligases: DNA ligase III α (LigIII α) or Ligase I (LigI). In SP-BER, sealing of the remaining nick is facilitated by X-ray cross complementing protein-1 (XRCC1), which plays also a role as scaffold protein earlier in BER, and DNA ligase III α [52,53], which seals approximately 80% of the lesions. In LP-BER, the remaining nick is sealed by LigI, independently of XRCC1 [54,55]. It has been proposed that LP-BER is the mode of repair, not only when 5'-dRP residues are oxidized, but also when nicks are persistent due to chromatin context or when induced during replication [56].

Nucleotide Excision Repair

NER is a highly coordinated multistep pathway that removes a wide range of DNA lesions that disturb Watson and Crick base pairing [57], including the UV-light induced photoproducts CPDs and 6-4PPs, and various bulky chemical adducts. NER can be divided into two sub-pathways that differ in the recognition step. Global genome NER (GG-NER) removes lesions that are located anywhere in the genome [58]. Transcription-coupled NER (TC-NER) recognizes lesions located in the transcribed strand of active genes that physically block RNA polymerase II (RNAP2) elongation [59]. More than 30 proteins are involved in the multistep pathways of NER and can be roughly divided in five distinctive steps: (1) damage recognition (1a: TC-NER, 1b: GG-NER); (2) DNA unwinding; (3) complex stabilization and lesion verification; (4) excision of damaged DNA; and (5) DNA synthesis and ligation, as indicated in Figure 3.



presence of a lesion. XPA is capable of detecting a lesion in a single-strand DNA conformation and together with RPA and XPG properly orients the pre-incision complex on the DNA damage. Next is the recruitment and subsequent 5' incision by the endonuclease complex ERCC1-XPF which enables gap-filling DNA synthesis by DNA polymerases Pol δ , Pol ϵ or Pol η . The endonuclease XPG cuts at the 3' site of the lesion resulting in the excision of the 22-30 oligonucleotide containing the injury. The NER reaction is completed by sealing of the final nick by DNA ligase I or III. Figure obtained from J.A. Marteijn et al., Nature Reviews MCB 2014.

Figure 3. Global Genome and Transcription-coupled Nucleotide Excision Repair. NER is subdivided by two damage recognition modes; GG-NER (left) and TC-NER (right). In GG-NER, the damage sensor XPC, in complex with RAD23B and centrin2 is constantly probing the DNA for NER substrates. Helix-distorting lesions are recognized by the joint action of the UV-DDB complex and XPC. Upon binding of XPC to the damage, RAD23B dissociates. In TC-NER damage is indirectly recognized by the stalling of elongating RNAPol2 on a lesion. During normal transcription elongation UVSSA, USP7 and CSB transiently interact with the RNAPol2. Upon stalling of RNAPol2 on the lesion the affinity of CSB for RNAPol2 is increased. The buildup of the CSA-CSB complex most likely results in the back-tracking or reverse translocating of RNAPol2, rendering the DNA lesion accessible for the downstream NER reaction, which is similar for both GG-NER and TC-NER. TFIIH is recruited to the recognized damage, resulting in the release of its CAK subcomplex, further opening of the DNA and verification of the DNA and verification of the DNA and verification of the DNA

Damage recognition in TC-NER (1a)

The DNA damage recognition step that initiates TC-NER is facilitated by the stalling of elongating RNAP2 upon a DNA lesion. The stalling of RNAP2 will trigger binding of TC-NER specific proteins. The first proteins to play a role after damage recognition by RNAP2 are Cockayne syndrome group B (CSB), Cockayne syndrome group A (CSA), ubiquitin-specific protease 7 (USP7) and UV-stimulated scaffold protein A (UVSSA). The last two were only very recently identified [60-62]. CSB monitors progression of transcription by elongating RNAP2 and becomes more tightly associated upon stalling at lesions [63], fulfilling a key role as a coupling factor to attract downstream TC-NER proteins [64]. CSA is part of an E3-ubiquitin ligase complex which is most likely responsible for the poly-ubiquitination of CSB, triggering an UV-dependent proteasomal degradation [65]. Besides poly-ubiquitination of CSB, CSA also facilitates binding of additional factors: High mobility group nucleosome-binding protein 1 (HMGN1) and p300 (chromatin remodelers), XPA-binding protein 2 (XAB2; splicing factor) and transcription factor II S (TFIIS; backtracking of RNAP2) [64]. UVSSA interacts with (stalled) RNAP2 (at UV-induced lesions) and is implicated in stabilizing CSB by delivering the de-ubiquitinating enzyme USP7 to TC-NER complexes [61]. This de-ubiquitination by USP7 counteracts the UV-induced poly-ubiquitination of CSB—thereby protecting against proteasomal degradation. This creates an extended time-window of bound CSB to ensure proper loading of the downstream NER factors.

Damage recognition in GG-NER (1b)

In GG-NER, recognition of the damaged DNA is initiated by the DNA binding protein Xeroderma pigmentosum group C (XPC), which forms a stable complex with either RAD23A or RAD23B and Centrin-2. The XPC complex does not directly bind to the lesion, instead it binds to short ssDNA opposite the helix-distorting lesion [66,67]. It is because of this indirect binding to the damage that the XPC complex is able to recognize a wide range of DNA base lesions. However, for some lesions it has been shown that the generated helix-distortion is not enough to initiate XPC binding. For instance, CPDs—the most abundant UV-induced DNA lesion—are known to only slightly disturb the DNA double-helix [68-70]. For these specific type of lesions the UV-damaged DNA-binding (UV-DDB) protein (a hetero-dimeric protein complex consisting of the DDB1 and DDB2 subunits) initiates the damage recognition step [71,72]. Binding of DDB2 to lesions stimulates the recruitment of XPC by direct protein interaction. Binding of DDB2 also enhances the DNA helix-distortion, exposing a ssDNA substrate for XPC [71]. Subsequent binding of UV-DDB and XPC associated factors (such as CUL4A [73], CBP/p300 [74,75], PARP1 [76] and RNF111 [77]) will further coordinate multiple UV-induced post-translational modifications (PTM) of UV-DDB, XPC, histones and/or other proteins, preparing the local chromatin environment for efficient repair reactions.

DNA unwinding (2)

After initial damage recognition, both GG-NER and TC-NER funnel into a common process that involves the opening of the DNA helix by the helicase function of the basal transcription factor II H (TFIIH) [78,79]. TFIIH is a multifunctional complex performing several important functions in the cell nucleus, including DNA helix opening for both NER [78] and transcription [80,81]. TFIIH contains two subunits that are ATP-dependent helicases: the 3'-5'-directed Xeroderma pigmentosum group B (XPB) [82] and the 5'-3'-directed Xeroderma pigmentosum group D (XPD) [83]. It has been shown that after damage recognition, the XPD helicase activity of TFIIH is mainly responsible for the damage search, which has a 5'-to-3' directionality [78]. The XPB helicase activity is not needed for

NER [84,85], however, the ATPase activity of both XPD and XPB are needed to open the DNA helix around the lesion.

complex stabilization and lesion verification (3)

After DNA unwinding, Xeroderma Pigmentosum group A (XPA) together with Replication protein A (RPA) bind to the opened DNA structure, facilitated by TFIIH. XPA was long thought to be the damage recognition factor in NER, however, it has been shown that XPA prefers to bind close to 5'-side of a bubble structure, by monitoring the electrostatic potential of distorted DNA repair sites rather than binding directly to the lesion [86-88]. Because XPA interacts with TFIIH, RPA, XPC-HR23B, DDB2, ERCC1 and PCNA, it is considered to be a central player of the NER complex, positioning all NER factors in the right place for the incision to occur [19]. Especially its interaction with RPA is believed to be important for stabilization and also in positioning the NER incision [89,90]. The hetero-trimeric RPA—consisting of the three subunits: RPA14, RPA32 and RPA70—is a single-stranded binding protein complex and is known to be involved in replication and several repair pathways, of which NER is one. RPA is not only important to protect ssDNA [91], but also to properly direct or orient the two structure-specific endonucleases Xeroderma pigmentosum group G (XPG) [92,93] and heterodimer excision repair cross-complementing protein 1-Xeroderma pigmentosum group F (ERCC1-XPF) complex [94], to the damaged strand [95].

Excision of damaged DNA (4)

Once the two endonucleases ERCC1-XPF and XPG are in place, dual incision of the lesion-containing oligonucleotide can be initiated [96-98]. ERCC1-XPF performs the incision 5' to the damage side [94], whereas incision by XPG is oriented 3' to the damaged side [92]. The order of incision is tightly regulated and is initiated by ERCC1-XPF, since it requires the presence, but not catalytic activity of XPG. Indeed, it has been shown that the repair synthesis step of NER can be initiated in the absence of XPG incision [99]. After the excision step, lesion-containing oligonucleotides are released from duplex DNA in complex with TFIIH [100], strengthening the model that XPD is indeed the damage verifying protein.

DNA synthesis and ligation (5)

The last step in NER is DNA synthesis to fill the single-stranded gap by DNA polymerases (δ , ϵ and κ) [101,102]. Replication factor C, PCNA and RPA are also needed for loading of the polymerases and regulating the repair synthesis step of NER [103]. The intact strand is used here as a template to incorporate the correct nucleotides. Ligation of the nick in the DNA backbone is catalysed by either LigI or LigIII, depending on the proliferation status of the cell [104].

Cross talk between the BER and NER pathway

Endogenously generated and environmental ROS can generate oxidative DNA lesions, likely contributing to a large number of human cancers [105] and also play a role in the pathogenesis of aging and many degenerative diseases [106,107]. Several types of oxidative DNA lesions are being formed, primarily small, helix non-distorting base lesions and abasic sites [108]. In non-challenged cells and induced by normal cellular metabolism, the most frequently produced oxidation product is 7,8-dihydro-8-oxoguanine (8-oxoG), estimated to vary between 0.1 and 1 lesion per million bases [109]. Endogenously produced DNA lesions are typically repaired by BER, however, there might exist some overlap with other DNA repair pathways, including NER. It has been shown, at least for some rare bulky oxidative lesions (such as 8,5'-cyclopurine-2'-deoxynucleosides, malondialdehyde and

4-hydroxynonenal) that they are substrate for the NER pathway. Direct involvement of NER or an interplay between NER and BER to repair “non-bulky” oxidative DNA lesions is under debate and currently widely studied [110].

It has been suggested that XPC/HR23B may either directly bind to some DNA glycosylases or indirectly stimulate the binding of some DNA glycosylases to damaged DNA [111]. For example, it has been shown that XPC/HR23B directly interacts with 3-methyladenine DNA glycosylase [112] and thymine DNA glycosylase (TDG) [113]. It can also stimulate the activity of OGG1, possibly by promoting the release of OGG1 from the created AP site [113].

The involvement of CSB in the repair of oxidative DNA lesions is supported by an even larger number of publications. Several studies have shown that cells deficient for CSB are besides UV-hypersensitive, also hypersensitive to oxidative DNA damaging agents [114-117]. However, the issue whether the CS proteins participate in TC-R of oxidative DNA damage is subject to long lasting debate. TC-R was originally documented for DNA damage only induced by UV-light and believed to operate through the NER pathway. Later reports suggested that oxidative damage is also preferentially repaired in a transcription-dependent manner [118-120]. It has been suggested that RNA polymerases also arrest at oxidative lesions, to initiate TC-R. However, 8-oxoG only slightly inhibited RNAPII during transcription elongation [121] which argues against the involvement of TC-R in repairing oxidative DNA lesions. Contrary, a novel laser-assisted procedure to locally inflict oxidative DNA lesions shows strong binding of TC-NER factor CSB, to these damaged areas. This binding does not trigger the canonical NER reaction and was linked with transcription elongation [122,123]. Using a newly developed procedure to monitor strand specific repair, it was recently shown that 8-oxoG is preferentially repaired in the transcribed strand and that this process requires OGG1, XPA, CSB, UVSSA and actively elongating RNAPII [120].

It has been speculated that particularly a transcription-coupled defect in repairing oxidative lesions might contribute to the severe human pathologies associated with inborn TC-NER deficiencies [124]. In contrast, genetic disorders based on BER-deficiency are not described. However, great redundancy is observed in mice lacking one of the DNA glycosylases. Mice lacking essential core-BER proteins are embryonic lethal, and most likely also in humans. The human syndromes discussed in the next paragraph are therefore primarily focussing on those caused by a NER defect.

Clinical consequences of NER defects

The importance of DNA repair mechanisms and other vital genome maintenance pathways is clearly shown by the severe clinical consequences associated with inherited defects in these systems. The UV-hypersensitive human NER syndromes Xeroderma Pigmentosum (XP), Cockayne syndrome (CS), combined XP and CS (XP/CS), Trichothiodystrophy (TTD) or combined XP and TTD (XP/TTD) [125-127] are associated with either a strongly enhanced cancer-risk or accelerated ageing.

Xeroderma pigmentosum

Xeroderma Pigmentosum (XP) is an autosomal recessive inherited disorder and is the first identified human DNA repair disease [128]. XP can be caused by mutations in any of the *XPA* through *XPG* genes and these patients suffer from extreme UV-hypersensitivity, abnormal skin pigmentation, increased risk of skin cancer (>2000 fold), and a slight elevated risk of developing internal tumours [129]. It is suggested that XP features result from defects in GG-NER that leads to accumulation of lesions throughout the genome. These lesions can

give rise to elevated mutation rates in proliferative tissue leading to the strong cancer risk, especially in UV-exposed areas of the skin. Moreover, many mutations in XP genes do not cause a complete inactivation of proteins, providing the cell with residual repair activity. This will probably cause milder forms of XP [129]. A minority of XP patients suffer from accelerated neurodegeneration [130-133]. The additional neurodegeneration features are thought to be derived from combined defects in GG-NER and TC-NER. Neurological symptoms only occur in XP patients that have mutations in *XPA*, *XPB*, *XPD*, *XPF* or *XPG* genes, resulting in a severely/completely defective NER [134].

Cockayne syndrome

The Cockayne syndrome is a rare genetic disorder caused by a specific defect in TC-NER and has an occurrence frequency of approximately 2.7 per million in western Europe [135,136]. On average, individuals with CS have a lifespan of only 12-13 years, although some reports describe individuals that lived longer [137]. CS syndrome results from mutations in the *CSA* or *CSB* genes and is characterized by sun hypersensitivity and neurodevelopmental abnormalities, however, they lack the increased cancer risk typically observed in XP patients. In contrast to XP patients, CS patients exhibit other very severe phenotypes, including pigmentary retinopathy and cataracts, sensorineural hearing loss, ataxia, dental caries, premature aging and cachectic dwarfism [138], most likely caused by an increased apoptosis rate that removes affected cells from tissues. Many of the phenotypes mentioned above are also observed in normally ageing individuals, which has led to the classification of CS as being a segmental accelerated aging syndrome.

Usually, XP and CS are clinically and genetically distinct. However, in rare cases, patients have been shown to have combined pathology XP/CS [139]. These patients harbour mutations in *XPB*, *XPD* and *XPG* genes. In contrast to the classical CS features, these patients are cancer prone.

Trichothiodystrophy

Trichothiodystrophy (TTD) is a genetic disorder with symptoms that affect several tissues and organs. Four genes have been identified as being responsible for the TTD phenotype: *XPB*, *XPD*, *TTDA* and *TTDN1* [127]. TTD patients show a broad spectrum of phenotypes that is usually characterized by a combination of photosensitivity, ichthyosis, brittle hair and nails, intellectual impairment, decreased fertility and short stature (the acronyms, PIBIDS, IBIDS and BIDS represent the initials of these characterizations [140]). TTD patients can be divided in two groups: Photosensitive TTD and non-photosensitive TTD, depending on the affected gene. The photosensitive form of TTD is caused by mutations in the TFIIH subunits *XPB*, *XPD* and *TTDA*. Although photosensitive TTD patients have a defect in the same gene as some XP patients characterized by photo-induced skin cancers, the TTD patients do not have an increased incidence of skin cancers [141]. On the other hand, non-photosensitive TTD patients display a normal NER activity [142] and this form of TTD is caused by mutations in the *TTDN1* gene. Severity of the clinical features of patients with a mutation in *TTDN1* do not correlate with the mutation map, suggesting that non-photosensitive TTD patients might be a multi-factorial disorder [143].

A complex phenotype of moderate severity with some features of both TTD and XP has been described in several patients. It has been suggested that the observed features may be caused by both a transcriptional and NER impairment [144].

Transcription factor II H

1 The central NER factor TFIIH is a multi-functional complex, which plays a fundamental role in opening the helix of DNA around the lesion and setting the stage for the incision of the damaged strand [78]. Initially, TFIIH was isolated as a general transcription factor (GTF) [82,145], though this multi-subunit complex displays several functions including, transcription of ribosomal genes, activated transcription and cell cycle control [80{Zurita, 2003 #964}. TFIIH is composed of 10 proteins [146]: seven subunits (XPB, XPD, p62, p52, p44, p34 and TTDA) form the core complex and three subunits form the TFIIH-associated cyclin activating kinase-subcomplex (CAK complex: CDK7, MAT1 and CCNH). The CAK complex is linked to the core via interactions with the XPD subunit [147] and plays a role in the phosphorylation of the C-terminal domain (CTD) of RNAP2 [148] and in cell cycle control [149]. The two DNA-dependent helicases; XPB and XPD catalyse DNA unwinding, which is required for both RNAP2 promoter escape and for the DNA repair reaction [96,147,150]. Because of its diverse cellular functions, mutations in TFIIH subunits (XPB, XPD and TTDA) are associated with a surprisingly heterogeneous panel of phenotypes [151] and include: the tumorigenic XP and the non-tumorigenic, neuro-degenerative and premature ageing syndromes CS and TTD and combined forms of these syndromes, XP/CS [130] and XP/TTD [144]. Interestingly, while XP and CS phenotypes can arise from mutations in different NER-related genes, photosensitive TTD is caused by mutations exclusively in TFIIH.

Trichothiodystrophy group A

The photosensitive form of TTD is a very rare disorder that is caused by mutations in three genes: XPB, XPD and TTDA. Thus far, only three different TTDA mutations were identified in three non-related TTD-A patients [146]: 1) Patient TTD99RO; homozygous nonsense mutation at codon 56, converting an Arginine to a stop codon (truncating the protein with 20%); 2) Patient TTD1BR is heterozygous for the TTD99RO allele, the other allele has a mis-sense mutation at codon 21, converting a conserved Leucine into Proline; 3) Siblings TTD13PV and TTD14PV carry a homozygous mutation in the ATG start codon, aborting TTDA protein synthesis.

TTDA is an 8 kDa protein that binds to TFIIH core components XPD and p52 [152-154] and controls the steady state level of cellular TFIIH in human fibroblasts [146,155]. The steady state level of most TFIIH subunits in cultured fibroblasts of TTD-A appeared only about 30% as compared to TTDA proficient cells [155]. Remarkably, TTD-A patient cells present a low repair capacity after UV irradiation. Nevertheless, despite this low repair capacity, cell survival after UV irradiation is higher than expected. TTDA appeared to be the sole TFIIH subunit dispensable for transcription *in vitro*, however its presence stimulates this reaction [156]. TTDA was also found to be associated with the pre-incision complex (PIC) and although it is not essential for transcription, yeast cells deficient for *Ttda* have a slow growth [157]. TTDA exists in two cellular pools; a TFIIH-bound nuclear pool and a free-pool which shuttles passively (due to its small size) from the cytoplasm to the nucleus [158]. During active NER, TTDA binds more tightly to TFIIH and possibly plays a role in stabilizing TFIIH on lesions to allow the transition between NER-intermediates [158]. This NER-dependent TFIIH-stabilization role can also partly restore the DNA repair deficiency in p52 D. melanogaster mutants (*Dmp52*), when enough TTDA molecules are available [156]. Moreover, it was found that TTDA is important for the DNA-damage-dependent ATPase activity of XPB, stimulating the opening of the helix and the translocation of XPA to UV-damaged DNA [152]. Coin and co-workers [152] further suggest that in cells derived from

TTD-A patients, TFIIH loaded on the damaged DNA cannot recruit the subsequent NER factors and that in its absence NER is fully compromised. This model of fully compromised NER does however not match the only relative mild UV-hypersensitivity observed in patients derived cells. Based on these observations, TTDA was suggested to be specifically required for the NER reaction.

The work presented in this thesis is aimed to better understand the molecular mechanism underlying the clinical features presented in TTD patients, with a focus on the analysis of cellular features associated with inherited mutations in the TTDA gene.

References

1. De Bont R, van Larebeke N (2004) Endogenous DNA damage in humans: a review of quantitative data. *Mutagenesis* 19: 169-185.
2. Lindahl T (1993) Instability and decay of the primary structure of DNA. *Nature* 362: 709-715.
3. Friedberg EC (1995) Out of the shadows and into the light: the emergence of DNA repair. *Trends Biochem Sci* 20: 381.
4. Sancar A (1996) DNA excision repair. *Annu Rev Biochem* 65: 43-81.
5. Ravanat JL, Douki T, Cadet J (2001) Direct and indirect effects of UV radiation on DNA and its components. *J Photochem Photobiol B* 63: 88-102.
6. van Gent DC, Hoeijmakers JH, Kanaar R (2001) Chromosomal stability and the DNA double-stranded break connection. *Nat Rev Genet* 2: 196-206.
7. Ljungman M, Zhang F (1996) Blockage of RNA polymerase as a possible trigger for u.v. light-induced apoptosis. *Oncogene* 13: 823-831.
8. Mitchell JR, Hoeijmakers JH, Niedernhofer LJ (2003) Divide and conquer: nucleotide excision repair battles cancer and ageing. *Curr Opin Cell Biol* 15: 232-240.
9. Hoeijmakers JH (2001) Genome maintenance mechanisms for preventing cancer. *Nature* 411: 366-374.
10. Falck J, Coates J, Jackson SP (2005) Conserved modes of recruitment of ATM, ATR and DNA-PKcs to sites of DNA damage. *Nature* 434: 605-611.
11. Jackson SP, Bartek J (2009) The DNA-damage response in human biology and disease. *Nature* 461: 1071-1078.
12. Kim ST, Lim DS, Canman CE, Kastan MB (1999) Substrate specificities and identification of putative substrates of ATM kinase family members. *J Biol Chem* 274: 37538-37543.
13. Abraham RT (2001) Cell cycle checkpoint signaling through the ATM and ATR kinases. *Genes Dev* 15: 2177-2196.
14. Yamaizumi M, Sugano T (1994) U.v.-induced nuclear accumulation of p53 is evoked through DNA damage of actively transcribed genes independent of the cell cycle. *Oncogene* 9: 2775-2784.
15. Ljungman M, Zhang F, Chen F, Rainbow AJ, McKay BC (1999) Inhibition of RNA polymerase II as a trigger for the p53 response. *Oncogene* 18: 583-592.
16. McKay BC, Ljungman M, Rainbow AJ (1998) Persistent DNA damage induced by ultraviolet light inhibits p21waf1 and bax expression: implications for DNA repair, UV sensitivity and the induction of apoptosis. *Oncogene* 17: 545-555.
17. Ip YT, Davis RJ (1998) Signal transduction by the c-Jun N-terminal kinase (JNK)--from inflammation to development. *Curr Opin Cell Biol* 10: 205-219.
18. Saleh-Gohari N, Helleday T (2004) Conservative homologous recombination preferentially repairs DNA double-strand breaks in the S phase of the cell cycle in human cells. *Nucleic Acids Res* 32: 3683-3688.
19. Scharer OD (2013) Nucleotide Excision Repair in Eukaryotes. *Cold Spring Harb Perspect Biol* 5.
20. Hegde ML, Hazra TK, Mitra S (2008) Early steps in the DNA base excision/single-strand interruption repair pathway in mammalian cells. *Cell Res* 18: 27-47.
21. Hsieh P (2001) Molecular mechanisms of DNA mismatch repair. *Mutat Res* 486: 71-87.
22. Jiricny J (2006) The multifaceted mismatch-repair system. *Nat Rev Mol Cell Biol* 7: 335-346.
23. Knipscheer P, Raschle M, Smogorzewska A, Enou M, Ho TV, et al. (2009) The Fanconi anemia pathway promotes

- replication-dependent DNA interstrand cross-link repair. *Science* 326: 1698-1701.
24. Raschle M, Knipscheer P, Enoiu M, Angelov T, Sun J, et al. (2008) Mechanism of replication-coupled DNA interstrand crosslink repair. *Cell* 134: 969-980.
 25. Jackson SP (2002) Sensing and repairing DNA double-strand breaks. *Carcinogenesis* 23: 687-696.
 26. Lieber MR (2010) The mechanism of double-strand DNA break repair by the nonhomologous DNA end-joining pathway. *Annu Rev Biochem* 79: 181-211.
 27. Mao Z, Bozzella M, Seluanov A, Gorbunova V (2008) Comparison of nonhomologous end joining and homologous recombination in human cells. *DNA Repair (Amst)* 7: 1765-1771.
 28. Lundin C, Erixon K, Arnaudeau C, Schultz N, Jenssen D, et al. (2002) Different roles for nonhomologous end joining and homologous recombination following replication arrest in mammalian cells. *Mol Cell Biol* 22: 5869-5878.
 29. Lehmann AR (2005) Replication of damaged DNA by translesion synthesis in human cells. *FEBS Lett* 579: 873-876.
 30. Goodman MF, Tiffin B (2000) The expanding polymerase universe. *Nat Rev Mol Cell Biol* 1: 101-109.
 31. Kunkel TA, Bebenek K (2000) DNA replication fidelity. *Annu Rev Biochem* 69: 497-529.
 32. Lindahl T, Barnes DE (2000) Repair of endogenous DNA damage. *Cold Spring Harb Symp Quant Biol* 65: 127-133.
 33. Mitra S, Boldogh I, Izumi T, Hazra TK (2001) Complexities of the DNA base excision repair pathway for repair of oxidative DNA damage. *Environ Mol Mutagen* 38: 180-190.
 34. Xanthoudakis S, Smeyne RJ, Wallace JD, Curran T (1996) The redox/DNA repair protein, Ref-1, is essential for early embryonic development in mice. *Proc Natl Acad Sci U S A* 93: 8919-8923.
 35. Ludwig DL, MacInnes MA, Takiguchi Y, Purtymun PE, Henrie M, et al. (1998) A murine AP-endonuclease gene-targeted deficiency with post-implantation embryonic progression and ionizing radiation sensitivity. *Mutat Res* 409: 17-29.
 36. Tebbs RS, Flannery ML, Meneses JJ, Hartmann A, Tucker JD, et al. (1999) Requirement for the Xrcc1 DNA base excision repair gene during early mouse development. *Dev Biol* 208: 513-529.
 37. Klungland A, Rosewell I, Hollenbach S, Larsen E, Daly G, et al. (1999) Accumulation of premutagenic DNA lesions in mice defective in removal of oxidative base damage. *Proc Natl Acad Sci U S A* 96: 13300-13305.
 38. Engelward BP, Weeda G, Wyatt MD, Broekhof JL, de Wit J, et al. (1997) Base excision repair deficient mice lacking the Aag alkyladenine DNA glycosylase. *Proc Natl Acad Sci U S A* 94: 13087-13092.
 39. Hang B, Singer B, Margison GP, Elder RH (1997) Targeted deletion of alkylpurine-DNA-N-glycosylase in mice eliminates repair of 1,N⁶-ethenoadenine and hypoxanthine but not of 3,N⁴-ethenocytosine or 8-oxoguanine. *Proc Natl Acad Sci U S A* 94: 12869-12874.
 40. Elder RH, Jansen JG, Weeks RJ, Willington MA, Deans B, et al. (1998) Alkylpurine-DNA-N-glycosylase knockout mice show increased susceptibility to induction of mutations by methyl methanesulfonate. *Mol Cell Biol* 18: 5828-5837.
 41. Fortini P, Parlanti E, Sidorkina OM, Laval J, Dogliotti E (1999) The type of DNA glycosylase determines the base excision repair pathway in mammalian cells. *J Biol Chem* 274: 15230-15236.
 42. Lindahl T (1974) An N-glycosidase from *Escherichia coli* that releases free uracil from DNA containing deaminated cytosine residues. *Proc Natl Acad Sci U S A* 71: 3649-3653.
 43. Wiederhold L, Leppard JB, Kedar P, Karimi-Busheri F, Rasouli-Nia A, et al. (2004) AP endonuclease-independent DNA base excision repair in human cells. *Mol Cell* 15: 209-220.
 44. Jilani A, Ramotar D, Slack C, Ong C, Yang XM, et al. (1999) Molecular cloning of the human gene, PNKP, encoding a polynucleotide kinase 3'-phosphatase and evidence for its role in repair of DNA strand breaks caused by oxidative damage. *J Biol Chem* 274: 24176-24186.
 45. Robertson AB, Klungland A, Rognes T, Leiros I (2009) DNA repair in mammalian cells: Base excision repair: the long and short of it. *Cell Mol Life Sci* 66: 981-993.
 46. Matsumoto Y, Kim K, Bogenhagen DF (1994) Proliferating cell nuclear antigen-dependent abasic site repair in *Xenopus laevis* oocytes: an alternative pathway of base excision DNA repair. *Mol Cell Biol* 14: 6187-6197.
 47. Matsumoto Y, Kim K (1995) Excision of deoxyribose phosphate residues by DNA polymerase beta during DNA repair. *Science* 269: 699-702.

48. Beard WA, Wilson SH (2006) Structure and mechanism of DNA polymerase Beta. *Chem Rev* 106: 361-382.
49. Levin DS, Vijayakumar S, Liu X, Bermudez VP, Hurwitz J, et al. (2004) A conserved interaction between the replicative clamp loader and DNA ligase in eukaryotes: implications for Okazaki fragment joining. *J Biol Chem* 279: 55196-55201.
50. Sukhanova M, Khodyreva S, Lavrik O (2010) Poly(ADP-ribose) polymerase 1 regulates activity of DNA polymerase beta in long patch base excision repair. *Mutat Res* 685: 80-89.
51. Jelezcova E, Trivedi RN, Wang XH, Tang JB, Brown AR, et al. (2010) Parp1 activation in mouse embryonic fibroblasts promotes Pol beta-dependent cellular hypersensitivity to alkylation damage. *Mutat Res* 686: 57-67.
52. Cappelli E, Taylor R, Cevasco M, Abbondandolo A, Caldecott K, et al. (1997) Involvement of XRCC1 and DNA ligase III gene products in DNA base excision repair. *J Biol Chem* 272: 23970-23975.
53. Caldecott KW, McKeown CK, Tucker JD, Ljungquist S, Thompson LH (1994) An interaction between the mammalian DNA repair protein XRCC1 and DNA ligase III. *Mol Cell Biol* 14: 68-76.
54. Podlitsky AJ, Dianova, II, Podust VN, Bohr VA, Dianov GL (2001) Human DNA polymerase beta initiates DNA synthesis during long-patch repair of reduced AP sites in DNA. *EMBO J* 20: 1477-1482.
55. Frosina G, Fortini P, Rossi O, Carrozzino F, Raspaglio G, et al. (1996) Two pathways for base excision repair in mammalian cells. *J Biol Chem* 271: 9573-9578.
56. Fortini P, Pascucci B, Parlanti E, D'Errico M, Simonelli V, et al. (2003) 8-Oxoguanine DNA damage: at the crossroad of alternative repair pathways. *Mutat Res* 531: 127-139.
57. Nospikel T (2009) DNA repair in mammalian cells: So DNA repair really is that important? *Cell Mol Life Sci* 66: 965-967.
58. Sugasawa K, Ng JM, Masutani C, Iwai S, van der Spek PJ, et al. (1998) Xeroderma pigmentosum group C protein complex is the initiator of global genome nucleotide excision repair. *Mol Cell* 2: 223-232.
59. Hanawalt PC (2002) Subpathways of nucleotide excision repair and their regulation. *Oncogene* 21: 8949-8956.
60. Nakazawa Y, Sasaki K, Mitsutake N, Matsuse M, Shimada M, et al. (2012) Mutations in UVSSA cause UV-sensitive syndrome and impair RNA polymerase IIo processing in transcription-coupled nucleotide-excision repair. *Nat Genet* 44: 586-592.
61. Schwertman P, Lagarou A, Dekkers DH, Raams A, van der Hoek AC, et al. (2012) UV-sensitive syndrome protein UVSSA recruits USP7 to regulate transcription-coupled repair. *Nat Genet* 44: 598-602.
62. Zhang X, Horibata K, Saijo M, Ishigami C, Ukai A, et al. (2012) Mutations in UVSSA cause UV-sensitive syndrome and destabilize ERCC6 in transcription-coupled DNA repair. *Nat Genet* 44: 593-597.
63. van den Boom V, Citterio E, Hoogstraten D, Zotter A, Egly JM, et al. (2004) DNA damage stabilizes interaction of CSB with the transcription elongation machinery. *J Cell Biol* 166: 27-36.
64. Fousteri M, Vermeulen W, van Zeeland AA, Mullenders LH (2006) Cockayne syndrome A and B proteins differentially regulate recruitment of chromatin remodeling and repair factors to stalled RNA polymerase II in vivo. *Mol Cell* 23: 471-482.
65. Groisman R, Kuraoka I, Chevallier O, Gaye N, Magnaldo T, et al. (2006) CSA-dependent degradation of CSB by the ubiquitin-proteasome pathway establishes a link between complementation factors of the Cockayne syndrome. *Genes Dev* 20: 1429-1434.
66. Sugasawa K, Shimizu Y, Iwai S, Hanaoka F (2002) A molecular mechanism for DNA damage recognition by the xeroderma pigmentosum group C protein complex. *DNA Repair (Amst)* 1: 95-107.
67. Min JH, Pavletich NP (2007) Recognition of DNA damage by the Rad4 nucleotide excision repair protein. *Nature* 449: 570-575.
68. Sugasawa K, Okamoto T, Shimizu Y, Masutani C, Iwai S, et al. (2001) A multistep damage recognition mechanism for global genomic nucleotide excision repair. *Genes Dev* 15: 507-521.
69. McAteer K, Jing Y, Kao J, Taylor JS, Kennedy MA (1998) Solution-state structure of a DNA dodecamer duplex containing a Cis-syn thymine cyclobutane dimer, the major UV photoproduct of DNA. *J Mol Biol* 282: 1013-1032.
70. Kusumoto R, Masutani C, Sugasawa K, Iwai S, Araki M, et al. (2001) Diversity of the damage recognition step in the global genomic nucleotide excision repair in vitro. *Mutat Res* 485: 219-227.
71. Scrima A, Konickova R, Czyzewski BK, Kawasaki Y, Jeffrey PD, et al. (2008) Structural basis of UV DNA-damage recognition by the DDB1-DDB2 complex. *Cell* 135: 1213-1223.

72. Moser J, Volker M, Kool H, Alekseev S, Vrieling H, et al. (2005) The UV-damaged DNA binding protein mediates efficient targeting of the nucleotide excision repair complex to UV-induced photo lesions. *DNA Repair (Amst)* 4: 571-582.
73. Kapetanaki MG, Guerrero-Santoro J, Bisi DC, Hsieh CL, Rapic-Otrin V, et al. (2006) The DDB1-CUL4A/CUL4B ubiquitin ligase is deficient in xeroderma pigmentosum group E and targets histone H2A at UV-damaged DNA sites. *Proc Natl Acad Sci U S A* 103: 2588-2593.
74. Rapic-Otrin V, McLenigan MP, Bisi DC, Gonzalez M, Levine AS (2002) Sequential binding of UV DNA damage binding factor and degradation of the p48 subunit as early events after UV irradiation. *Nucleic Acids Res* 30: 2588-2598.
75. Datta A, Bagchi S, Nag A, Shiyonov P, Adami GR, et al. (2001) The p48 subunit of the damaged-DNA binding protein DDB associates with the CBP/p300 family of histone acetyltransferase. *Mutat Res* 486: 89-97.
76. Pines A, Vrouwe MG, Marteiijn JA, Typas D, Luijsterburg MS, et al. (2012) PARP1 promotes nucleotide excision repair through DDB2 stabilization and recruitment of ALC1. *J Cell Biol* 199: 235-249.
77. Poulsen SL, Hansen RK, Wagner SA, van Cuijk L, van Belle GJ, et al. (2013) RNF111/Arkadia is a SUMO-targeted ubiquitin ligase that facilitates the DNA damage response. *J Cell Biol* 201: 797-807.
78. Sugawara K, Akagi J, Nishi R, Iwai S, Hanaoka F (2009) Two-step recognition of DNA damage for mammalian nucleotide excision repair: Directional binding of the XPC complex and DNA strand scanning. *Mol Cell* 36: 642-653.
79. Volker M, Mone MJ, Karmakar P, van Hoffen A, Schul W, et al. (2001) Sequential assembly of the nucleotide excision repair factors in vivo. *Mol Cell* 8: 213-224.
80. Egly JM (2001) The 14th Datta Lecture. TFIIH: from transcription to clinic. *FEBS Lett* 498: 124-128.
81. Zurita M, Merino C (2003) The transcriptional complexity of the TFIIH complex. *Trends Genet* 19: 578-584.
82. Schaeffer L, Roy R, Humbert S, Moncollin V, Vermeulen W, et al. (1993) DNA repair helicase: a component of BTF2 (TFIIH) basic transcription factor. *Science* 260: 58-63.
83. Coin F, Marinoni JC, Rodolfo C, Fribourg S, Pedrini AM, et al. (1998) Mutations in the XPD helicase gene result in XP and TTD phenotypes, preventing interaction between XPD and the p44 subunit of TFIIH. *Nat Genet* 20: 184-188.
84. Coin F, Oksenysh V, Egly JM (2007) Distinct roles for the XPB/p52 and XPD/p44 subcomplexes of TFIIH in damaged DNA opening during nucleotide excision repair. *Mol Cell* 26: 245-256.
85. Fan L, Arvai AS, Cooper PK, Iwai S, Hanaoka F, et al. (2006) Conserved XPB core structure and motifs for DNA unwinding: implications for pathway selection of transcription or excision repair. *Mol Cell* 22: 27-37.
86. Missura M, Buterin T, Hindges R, Hubscher U, Kasparkova J, et al. (2001) Double-check probing of DNA bending and unwinding by XPA-RPA: an architectural function in DNA repair. *EMBO J* 20: 3554-3564.
87. Camenisch U, Dip R, Schumacher SB, Schuler B, Naegeli H (2006) Recognition of helical kinks by xeroderma pigmentosum group A protein triggers DNA excision repair. *Nat Struct Mol Biol* 13: 278-284.
88. Camenisch U, Dip R, Vitanescu M, Naegeli H (2007) Xeroderma pigmentosum complementation group A protein is driven to nucleotide excision repair sites by the electrostatic potential of distorted DNA. *DNA Repair (Amst)* 6: 1819-1828.
89. de Laat WL, Appeldoorn E, Jaspers NG, Hoeijmakers JH (1998) DNA structural elements required for ERCC1-XPF endonuclease activity. *J Biol Chem* 273: 7835-7842.
90. Hermanson-Miller IL, Turchi JJ (2002) Strand-specific binding of RPA and XPA to damaged duplex DNA. *Biochemistry* 41: 2402-2408.
91. Rademakers S, Volker M, Hoogstraten D, Nigg AL, Mone MJ, et al. (2003) Xeroderma pigmentosum group A protein loads as a separate factor onto DNA lesions. *Mol Cell Biol* 23: 5755-5767.
92. O'Donovan A, Davies AA, Moggs JG, West SC, Wood RD (1994) XPG endonuclease makes the 3' incision in human DNA nucleotide excision repair. *Nature* 371: 432-435.
93. Zotter A, Luijsterburg MS, Warmerdam DO, Ibrahim S, Nigg A, et al. (2006) Recruitment of the nucleotide excision repair endonuclease XPG to sites of UV-induced dna damage depends on functional TFIIH. *Mol Cell Biol* 26: 8868-8879.
94. Sijbers AM, de Laat WL, Ariza RR, Biggerstaff M, Wei YF, et al. (1996) Xeroderma pigmentosum group F caused by

- a defect in a structure-specific DNA repair endonuclease. *Cell* 86: 811-822.
95. de Laat WL, Appeldoorn E, Sugawara K, Weterings E, Jaspers NG, et al. (1998) DNA-binding polarity of human replication protein A positions nucleases in nucleotide excision repair. *Genes Dev* 12: 2598-2609.
 96. Evans E, Moggs JG, Hwang JR, Egly JM, Wood RD (1997) Mechanism of open complex and dual incision formation by human nucleotide excision repair factors. *EMBO J* 16: 6559-6573.
 97. Mu D, Hsu DS, Sancar A (1996) Reaction mechanism of human DNA repair excision nuclease. *J Biol Chem* 271: 8285-8294.
 98. Mu D, Wakasugi M, Hsu DS, Sancar A (1997) Characterization of reaction intermediates of human excision repair nuclease. *J Biol Chem* 272: 28971-28979.
 99. Staresincic L, Fagbemi AF, Enzlin JH, Gourdin AM, Wijgers N, et al. (2009) Coordination of dual incision and repair synthesis in human nucleotide excision repair. *EMBO J* 28: 1111-1120.
 100. Kemp MG, Reardon JT, Lindsey-Boltz LA, Sancar A (2012) Mechanism of release and fate of excised oligonucleotides during nucleotide excision repair. *J Biol Chem* 287: 22889-22899.
 101. Ogi T, Limsirichaikul S, Overmeer RM, Volker M, Takenaka K, et al. (2010) Three DNA polymerases, recruited by different mechanisms, carry out NER repair synthesis in human cells. *Mol Cell* 37: 714-727.
 102. Overmeer RM, Moser J, Volker M, Kool H, Tomkinson AE, et al. (2011) Replication protein A safeguards genome integrity by controlling NER incision events. *J Cell Biol* 192: 401-415.
 103. Shivji MK, Podust VN, Hubscher U, Wood RD (1995) Nucleotide excision repair DNA synthesis by DNA polymerase epsilon in the presence of PCNA, RFC, and RPA. *Biochemistry* 34: 5011-5017.
 104. Moser J, Kool H, Giakzidis I, Caldecott K, Mullenders LH, et al. (2007) Sealing of chromosomal DNA nicks during nucleotide excision repair requires XRCC1 and DNA ligase III alpha in a cell-cycle-specific manner. *Mol Cell* 27: 311-323.
 105. Doll R, Peto R (1981) The causes of cancer: quantitative estimates of avoidable risks of cancer in the United States today. *J Natl Cancer Inst* 66: 1191-1308.
 106. Hastay P, Campisi J, Hoesjmakers J, van Steeg H, Vijg J (2003) Aging and genome maintenance: lessons from the mouse? *Science* 299: 1355-1359.
 107. Cooke MS, Evans MD, Dizdaroglu M, Lunec J (2003) Oxidative DNA damage: mechanisms, mutation, and disease. *FASEB J* 17: 1195-1214.
 108. Lindahl T, Wood RD (1999) Quality control by DNA repair. *Science* 286: 1897-1905.
 109. Cadet J, Douki T, Ravanat JL (2011) Measurement of oxidatively generated base damage in cellular DNA. *Mutat Res* 711: 3-12.
 110. Brooks PJ (2008) The 8,5'-cyclopurine-2'-deoxynucleosides: candidate neurodegenerative DNA lesions in xeroderma pigmentosum, and unique probes of transcription and nucleotide excision repair. *DNA Repair (Amst)* 7: 1168-1179.
 111. D'Errico M, Parlanti E, Teson M, de Jesus BM, Degan P, et al. (2006) New functions of XPC in the protection of human skin cells from oxidative damage. *EMBO J* 25: 4305-4315.
 112. Miao F, Bouziane M, Dammann R, Masutani C, Hanaoka F, et al. (2000) 3-Methyladenine-DNA glycosylase (MPG protein) interacts with human RAD23 proteins. *J Biol Chem* 275: 28433-28438.
 113. Shimizu Y, Iwai S, Hanaoka F, Sugawara K (2003) Xeroderma pigmentosum group C protein interacts physically and functionally with thymine DNA glycosylase. *EMBO J* 22: 164-173.
 114. Stevnsner T, Muftuoglu M, Aamann MD, Bohr VA (2008) The role of Cockayne Syndrome group B (CSB) protein in base excision repair and aging. *Mech Ageing Dev* 129: 441-448.
 115. Sunesen M, Stevnsner T, Brosh RM, Jr., Dianov GL, Bohr VA (2002) Global genome repair of 8-oxoG in hamster cells requires a functional CSB gene product. *Oncogene* 21: 3571-3578.
 116. Tuo J, Chen C, Zeng X, Christiansen M, Bohr VA (2002) Functional crosstalk between hOgg1 and the helicase domain of Cockayne syndrome group B protein. *DNA Repair (Amst)* 1: 913-927.
 117. de Waard H, de Wit J, Gorgels TG, van den Aardweg G, Andressoo JO, et al. (2003) Cell type-specific hypersensitivity to oxidative damage in CSB and XPA mice. *DNA Repair (Amst)* 2: 13-25.
 118. Banerjee D, Mandal SM, Das A, Hegde ML, Das S, et al. (2011) Preferential repair of oxidized base damage in the transcribed genes of mammalian cells. *J Biol Chem* 286: 6006-6016.

119. Khobta A, Kitsera N, Speckmann B, Epe B (2009) 8-Oxoguanine DNA glycosylase (Ogg1) causes a transcriptional inactivation of damaged DNA in the absence of functional Cockayne syndrome B (Csb) protein. *DNA Repair (Amst)* 8: 309-317.
120. Guo J, Hanawalt PC, Spivak G (2013) Comet-FISH with strand-specific probes reveals transcription-coupled repair of 8-oxoGuanine in human cells. *Nucleic Acids Res.*
121. Tornaletti S, Maeda LS, Kolodner RD, Hanawalt PC (2004) Effect of 8-oxoguanine on transcription elongation by T7 RNA polymerase and mammalian RNA polymerase II. *DNA Repair (Amst)* 3: 483-494.
122. Menoni H, Hoeijmakers JH, Vermeulen W (2012) Nucleotide excision repair-initiating proteins bind to oxidative DNA lesions in vivo. *J Cell Biol* 199: 1037-1046.
123. Thorslund T, von Kobbe C, Harrigan JA, Indig FE, Christiansen M, et al. (2005) Cooperation of the Cockayne syndrome group B protein and poly(ADP-ribose) polymerase 1 in the response to oxidative stress. *Mol Cell Biol* 25: 7625-7636.
124. Sedelnikova OA, Redon CE, Dickey JS, Nakamura AJ, Georgakilas AG, et al. (2010) Role of oxidatively induced DNA lesions in human pathogenesis. *Mutat Res* 704: 152-159.
125. Lehmann AR (2003) DNA repair-deficient diseases, xeroderma pigmentosum, Cockayne syndrome and trichothiodystrophy. *Biochimie* 85: 1101-1111.
126. de Boer J, Hoeijmakers JH (2000) Nucleotide excision repair and human syndromes. *Carcinogenesis* 21: 453-460.
127. Stefanini M, Botta E, Lanzafame M, Orioli D (2010) Trichothiodystrophy: from basic mechanisms to clinical implications. *DNA Repair (Amst)* 9: 2-10.
128. Cleaver JE (1968) Defective repair replication of DNA in xeroderma pigmentosum. *Nature* 218: 652-656.
129. Botta E, Nardo T, Lehmann AR, Egly JM, Pedrini AM, et al. (2002) Reduced level of the repair/transcription factor TFIIH in trichothiodystrophy. *Hum Mol Genet* 11: 2919-2928.
130. Kraemer KH, Lee MM, Andrews AD, Lambert WC (1994) The role of sunlight and DNA repair in melanoma and nonmelanoma skin cancer. The xeroderma pigmentosum paradigm. *Arch Dermatol* 130: 1018-1021.
131. Kraemer KH, Herlyn M, Yuspa SH, Clark WH, Jr., Townsend GK, et al. (1989) Reduced DNA repair in cultured melanocytes and nevus cells from a patient with xeroderma pigmentosum. *Arch Dermatol* 125: 263-268.
132. Bootsma D, Hoeijmakers JH (1991) The genetic basis of xeroderma pigmentosum. *Ann Genet* 34: 143-150.
133. Jeppesen DK, Bohr VA, Stevnsner T (2011) DNA repair deficiency in neurodegeneration. *Prog Neurobiol* 94: 166-200.
134. Brooks PJ (2002) DNA repair in neural cells: basic science and clinical implications. *Mutat Res* 509: 93-108.
135. Kleijer WJ, Laugel V, Berneburg M, Nardo T, Fawcett H, et al. (2008) Incidence of DNA repair deficiency disorders in western Europe: Xeroderma pigmentosum, Cockayne syndrome and trichothiodystrophy. *DNA Repair (Amst)* 7: 744-750.
136. Kleijer WJ, van der Sterre ML, Garritsen VH, Raams A, Jaspers NG (2006) Prenatal diagnosis of the Cockayne syndrome: survey of 15 years experience. *Prenat Diagn* 26: 980-984.
137. Nance MA, Berry SA (1992) Cockayne syndrome: review of 140 cases. *Am J Med Genet* 42: 68-84.
138. Kraemer KH, Patronas NJ, Schiffmann R, Brooks BP, Tamura D, et al. (2007) Xeroderma pigmentosum, trichothiodystrophy and Cockayne syndrome: a complex genotype-phenotype relationship. *Neuroscience* 145: 1388-1396.
139. Lindenbaum Y, Dickson D, Rosenbaum P, Kraemer K, Robbins I, et al. (2001) Xeroderma pigmentosum/cockayne syndrome complex: first neuropathological study and review of eight other cases. *Eur J Paediatr Neurol* 5: 225-242.
140. Faghri S, Tamura D, Kraemer KH, Digiovanna JJ (2008) Trichothiodystrophy: a systematic review of 112 published cases characterises a wide spectrum of clinical manifestations. *J Med Genet* 45: 609-621.
141. Leibel D, Laspe P, Emmert S (2006) Nucleotide excision repair and cancer. *J Mol Histol* 37: 225-238.
142. Stefanini M, Lagomarsini P, Arlett CF, Marinoni S, Borroni C, et al. (1986) Xeroderma pigmentosum (complementation group D) mutation is present in patients affected by trichothiodystrophy with photosensitivity. *Hum Genet* 74: 107-112.
143. Zhang Y, Tian Y, Chen Q, Chen D, Zhai Z, et al. (2007) TTDN1 is a Plk1-interacting protein involved in maintenance of cell cycle integrity. *Cell Mol Life Sci* 64: 632-640.

144. Broughton BC, Berneburg M, Fawcett H, Taylor EM, Arlett CF, et al. (2001) Two individuals with features of both xeroderma pigmentosum and trichothiodystrophy highlight the complexity of the clinical outcomes of mutations in the XPD gene. *Hum Mol Genet* 10: 2539-2547.
145. Conaway RC, Conaway JW (1993) General initiation factors for RNA polymerase II. *Annu Rev Biochem* 62: 161-190.
146. Giglia-Mari G, Coin F, Ranish JA, Hoogstraten D, Theil A, et al. (2004) A new, tenth subunit of TFIIH is responsible for the DNA repair syndrome trichothiodystrophy group A. *Nat Genet* 36: 714-719.
147. Tirode F, Busso D, Coin F, Egly JM (1999) Reconstitution of the transcription factor TFIIH: assignment of functions for the three enzymatic subunits, XPB, XPD, and cdk7. *Mol Cell* 3: 87-95.
148. Kaldis P, Pitluk ZW, Bany IA, Enke DA, Wagner M, et al. (1998) Localization and regulation of the cdk-activating kinase (Cak1p) from budding yeast. *J Cell Sci* 111 (Pt 24): 3585-3596.
149. Fisher RP, Morgan DO (1994) A novel cyclin associates with MO15/CDK7 to form the CDK-activating kinase. *Cell* 78: 713-724.
150. Guzder SN, Sung P, Bailly V, Prakash L, Prakash S (1994) RAD25 is a DNA helicase required for DNA repair and RNA polymerase II transcription. *Nature* 369: 578-581.
151. Vermeulen W, Scott RJ, Rodgers S, Muller HJ, Cole J, et al. (1994) Clinical heterogeneity within xeroderma pigmentosum associated with mutations in the DNA repair and transcription gene ERCC3. *Am J Hum Genet* 54: 191-200.
152. Coin F, Proietti De Santis L, Nardo T, Zlobinskaya O, Stefanini M, et al. (2006) p8/TTD-A as a repair-specific TFIIH subunit. *Mol Cell* 21: 215-226.
153. Zhou Y, Kou H, Wang Z (2007) Tfb5 interacts with Tfb2 and facilitates nucleotide excision repair in yeast. *Nucleic Acids Res* 35: 861-871.
154. Kainov DE, Vitorino M, Cavarelli J, Poterszman A, Egly JM (2008) Structural basis for group A trichothiodystrophy. *Nat Struct Mol Biol* 15: 980-984.
155. Vermeulen W, Bergmann E, Auriol J, Rademakers S, Frit P, et al. (2000) Sublimiting concentration of TFIIH transcription/DNA repair factor causes TTD-A trichothiodystrophy disorder. *Nat Genet* 26: 307-313.
156. Aguilar-Fuentes J, Fregoso M, Herrera M, Reynaud E, Braun C, et al. (2008) p8/TTDA overexpression enhances UV-irradiation resistance and suppresses TFIIH mutations in a *Drosophila* trichothiodystrophy model. *PLoS Genet* 4: e1000253.
157. Ranish JA, Hahn S, Lu Y, Yi EC, Li XJ, et al. (2004) Identification of TFB5, a new component of general transcription and DNA repair factor IIH. *Nat Genet* 36: 707-713.
158. Giglia-Mari G, Miquel C, Theil AF, Mari PO, Hoogstraten D, et al. (2006) Dynamic interaction of TTDA with TFIIH is stabilized by nucleotide excision repair in living cells. *PLoS Biol* 4: e156.



CHAPTER 2

Slowly progressing Nucleotide Excision Repair in Trichothiodystrophy Group A Patient Fibroblasts

A.F. Theil, J. Nonnekens, N. Wijgers, W. Vermeulen, G. Giglia-Mari

MCB, Sept. 2011



Abstract

Trichothiodystrophy (TTD) is a rare autosomal premature-ageing and neuroectodermal disease. The photohypersensitive form of TTD is caused by inherited mutations in three of the 10 subunits of the basal transcription factor TFIIH. TFIIH is an essential transcription initiation factor that is also pivotal for nucleotide excision repair (NER). Photosensitive TTD is explained by deficient NER, dedicated to removing UV-induced DNA lesions. TTD group A (TTD-A) patients carry mutations in the smallest TFIIH subunit, TTDA, which is an 8-kDa protein that dynamically interacts with TFIIH. TTD-A patients display a relatively mild TTD phenotype, and TTD-A primary fibroblasts exhibit moderate UV sensitivity despite a rather low level of UV-induced unscheduled DNA synthesis (UDS). To investigate the rationale of this seeming discrepancy, we studied the repair kinetics and the binding kinetics of TFIIH downstream NER factors to damaged sites in TTD-A cells. Our results show that TTD-A cells do repair UV lesions, although with reduced efficiency, and that the binding of downstream NER factors on damaged DNA is not completely abolished but only retarded. We conclude that in TTD-A cells repair is not fully compromised but only delayed, and we present a model that explains the relatively mild photosensitive phenotype observed in TTD-A patients.

Introduction

DNA lesions that disturb proper Watson-Crick base pairing are targets for the nucleotide excision repair (NER) pathway (32). NER is a versatile DNA repair system able to recognize and remove a large variety of DNA lesions, including the major UV light-induced photoproducts cyclobutane pyrimidine dimers (CPD) and 6-4 pyrimidine-pyrimidone photoproducts (6-4PPs). The biological importance of NER is illustrated by the severe clinical consequences associated with hereditary photohypersensitive NER deficiency disorders: the cancer-prone syndrome xeroderma pigmentosum (XP [MIM 278700-780]) and the neurodevelopmental conditions Cockayne syndrome (CS [MIM 214150]) and trichothiodystrophy (TTD [MIM 601675]) (2, 26).

NER is a highly coordinated multistep process initiated by two lesion recognition pathways: transcription-coupled NER (TC-NER) and global genome NER (GG-NER) (14, 21). TC-NER is initiated by lesions located in the transcribed strand of active genes that stall elongating RNA polymerase II (RNAP2); CSB (Cockayne syndrome B protein) senses stalled RNAP2 and recruits the preincision NER factors (15). Damage recognition of lesions located anywhere in the genome by GG-NER is achieved by the concerted action of the XPC-RAD23B-Cen2 and UV-damaged DNA-binding protein (UV-DDB) complexes (43). After initial damage recognition, these two subpathways funnel into a common process that involves the opening of the DNA helix by the helicase function of the basal transcription factor II H (TFIIH) (44, 57). Subsequently, TFIIH (28), together with XPA (xeroderma pigmentosum group A), verifies the lesion (44) and with RPA (replication protein A) properly orients the two structure-specific endonucleases XPG (xeroderma pigmentosum group G) (33, 61) and ERCC1-XPF complex (for excision repair cross-complementing protein 1 and xeroderma pigmentosum group F protein) (38) (responsible for the 3' and 5' incisions, respectively). The highly coordinated dual incision of XPG and ERCC1-XPF (39) excises a stretch of 27 to 29 nucleotides containing the lesion. The resulting single-strand gap is filled in by DNA replication proteins (34) and sealed by DNA ligases (30).

The central NER factor TFIIH is a multifunctional complex that plays a fundamental role in opening the helix of DNA around the lesion and setting the stage for the incision

of the damaged strand (44). Initially, TFIIH was isolated as a general transcription factor (GTF) (8), though this multisubunit complex displays several functions, including ribosomal transcription, activated transcription, and cell cycle control (9, 62).

TFIIH is composed of 10 proteins (17): seven subunits (XPB, XPD, p62, p52, p44, p34, and TTDA) form the core complex, and three subunits (CDK7, MAT1, and CCNH) form the TFIIH-associated cyclin-activating kinase (CAK) subcomplex. The CAK complex is linked to the core via interactions with the XPD subunit (46) and plays a role in the phosphorylation of the C-terminal domain (CTD) of RNAP2 (23) and in cell cycle control (13). The two DNA-dependent helicases XPB and XPD catalyze DNA unwinding, which is required for both RNAP2 promoter escape and the DNA repair reaction (10, 20, 46). Most likely because of its diverse cellular functions, mutations in TFIIH subunits (XPB, XPD, and TTDA) are associated with a surprisingly heterogeneous panel of phenotypes (55) and include the tumorigenic XP; the nontumorigenic, neurodegenerative, and premature-ageing syndromes CS and TTD; and combined forms of these syndromes, XP-CS (24) and XP-TTD (3). Interestingly, while XP and CS phenotypes can arise from mutations in different NER-related genes, photosensitive TTD is an exclusively TFIIH-related syndrome.

TTD is a premature-ageing syndrome, with the hallmark features of brittle hair and nails, ichthyosis, and progressive mental and physical retardation (12). Within photosensitive TTD, three TFIIH-coding genes have been found to be mutated: XPB (58), XPD (4, 42), and TTDA (17).

TTDA is an 8-kDa protein that binds to the TFIIH core components XPD and p52 (7, 22, 60) and controls the steady-state level of cellular TFIIH in human fibroblasts (17, 51). TTDA appeared to be the sole TFIIH subunit dispensable for transcription *in vitro*; however, its presence stimulates this reaction (1), and the TTDA component is present in the preincision complex (PIC) and is required for transcription *in vivo* in yeast (35). TTDA exists in two cellular pools, a TFIIH-bound nuclear pool and a free pool that shuttles passively (due to its small size) from the cytoplasm to the nucleus (18). During active NER, TTDA binds more tightly to TFIIH and possibly plays a role in stabilizing TFIIH on lesions to allow the transition between NER intermediates (18). This NER-dependent TFIIH stabilization role can also partly restore the DNA repair deficiency in p52 *Drosophila melanogaster* mutants (*Dmp52*) when enough TTDA molecules are available (1). Moreover, it was found that TTDA is important for the DNA damage-dependent ATPase activity of XPB, stimulating the opening of the helix and the translocation of XPA to UV-damaged DNA (7). Coin and coworkers (7) further suggested that without TTDA, TFIIH, although loaded on the damaged DNA, cannot recruit the subsequent NER factors and that in its absence NER is fully compromised. Based on these observations, TTDA was suggested to be specifically required for the NER reaction. Indeed TTD-A primary fibroblasts exhibit a rather low level of UV-induced unscheduled DNA synthesis (UDS), the levels of which range from 10% (TTD13/14PV) to 25% (TTD1BR) of residual UDS activity (17), indicative of a severe NER defect. Surprisingly, however, the UV sensitivity of TTD-A primary fibroblasts is relatively mild compared to other complementation groups (e.g., XP-A, XP-B, and XP-G) with similarly low UDS levels (17). Because of this seeming discrepancy, we further studied the repair kinetics and the binding kinetics of TFIIH downstream NER factors to damaged sites in TTD-A cells. Our results show that TTD-A cells do not repair UV lesions at early time points after UV irradiation, explaining the low UDS levels. However, at later time points post-UV irradiation (6 to 8 h), most of the UV-induced 6-4PPs appeared to be removed. In addition, we found that the binding of downstream NER factors on damaged DNA is not completely abolished but retarded. Our results suggest that in TTD-A cells repair is not fully compromised but only retarded, which explains the relatively mild photosensitive

phenotype observed in patients.

Materials and Methods

Cell culture and specific treatments.

The primary human fibroblast strains used were XP12RO (XP-A), TTD1BR (TTD-A), TTD99RO (TTD-A), TTD14PV (TTD-A), and the NER-proficient C5RO cell line. The cells were cultured in Ham's F10 (Gibco) supplemented with antibiotics and 10% fetal calf serum at 37°C, 3% O₂, and 5% CO₂.

The simian virus 40 (SV40)-immortalized human cell lines used were XP2OS-sv (XP-A), TTD1BR-sv (TTD-A), and TTD1BR-sv (TTD-A), stably expressing TTDA-hemagglutinin (HA) and the NER-proficient MRC5-sv cell line. The cell lines were cultured in a 1:1 mixture of Ham's F10 and Dulbecco's modified Eagle's medium (DMEM) (Gibco) supplemented with antibiotics and 10% fetal calf serum at 37°C, 20% O₂, and 5% CO₂.

Treatment with UV-C (254 nm) was performed using a Philips germicidal lamp. Doses of 5 J/m² for enzyme-linked immunosorbent assay (ELISA) on primary fibroblasts; 25 J/m² for chromatin immunoprecipitation (ChIP); and 1, 2, 4, and 8 J/m² for UV survival were used for total irradiation. For local irradiation through a microporous filter (5 μm), a dose of 60 J/m² was used.

UV cell survival.

Primary fibroblasts were plated on 6-well culture dishes (5 × 10³ per well) in quadruplicate (0 J/m²) or triplicate (others) in 3 ml medium. Two days after seeding, the cells were washed with phosphate-buffered saline (PBS) and UV irradiated at various doses. The cells were pulse-labeled 5 days after irradiation with [methyl-³H]thymidine (40 to 60 Ci/mmol; 5 μCi/ml), chased for 30 min in unlabeled medium, washed with PBS, lysed in 0.25 M NaOH, and harvested. The cell lysates were transferred into scintillation flasks and supplemented with 7.5 ml Hionic Fluor scintillation fluid (Packard). Each sample was counted in the scintillation counter for 10 min, and the results were expressed as the percentage of surviving cells at a given dose over the nonirradiated cells.

UV-induced UDS.

Three days before the UDS assay (52), wild-type (WT) or XP-A primary fibroblasts were labeled with latex beads (0.79 μm) by adding a suspension of beads to normal culture medium (54). After trypsinization, the labeled primary fibroblasts were extensively washed to remove free beads. Cells (0.5 × 10⁶) were mixed in a 1:1 ratio with different TTD-A primary fibroblasts seeded on 24-mm coverslips, and after 2 days, they were irradiated with 16 J/m² UV-C. At various time points after UV irradiation, the cells were incubated for 2 h with culture medium containing 10 μCi [methyl-³H]thymidine (110 Ci/mmol; Amersham Biosciences)/ml, washed with PBS, and fixed. Coverslips with radioactively labeled cells were mounted onto slides and dipped in a photosensitive emulsion (Ilford K2). After exposure (2 to 7 days), the slides were developed and stained. Repair capacity was quantified by counting autoradiographic grains above the nuclei of at least 25 cells. UDS levels are expressed as either an absolute grain count per nucleus (Fig. 1c) or the percentage of UDS in wild-type cells assayed directly after UV irradiation (0 to 2 h), which was set at 100% (Fig. 1b).

Quantification of 6-4PP and CPD UV photoproducts by ELISA.

Seventy to 80% confluent cultures of cells to be analyzed were washed with PBS, UV

irradiated, and incubated for various times. Cells were harvest in PBS, and DNA was isolated using a QIAamp DNA Blood Mini Kit (Qiagen). Concentrations were measured by the optical density at 260 nm. Ninety-six-well polyvinylchloride flat-bottom microtiter plates were precoated with 0.003% protamine sulfate (50 μ l/well; Sigma) and dried in the dark overnight at 37°C. DNA samples were denatured for 10 min at 95°C and immediately cooled on ice for 20 min. Vortexed DNA solution (50 μ l/well) was loaded in the precoated 96-well dish to a final concentration of 6 μ g/ml for the detection of 6-4PP or 0.3 μ g/ml for CPD. The plate was dried overnight at 37°C and washed 5 times with PBS plus 0.05% Tween 20 (150 μ l/well). The wells were preabsorbed with PBS plus 2% fetal calf serum (FCS) for 30 min at 37°C and subsequently washed 5 times with PBS-Tween 20 prior to incubation with 100 μ l/well primary antibody: 6-4PP (1:1,000; Bioconnect/MBL) or CPD (1:1,000; TDM-2; Bioconnect/MBL) diluted in PBS. After 5 washes with PBS-Tween 20, samples were incubated for 30 min at 37°C with a secondary antibody, goat anti-mouse IgG(H+L) conjugated to horseradish peroxidase (HRP) (1:2,000; Southern Biotech). After 5 washes with PBS-Tween 20, samples were treated with 100 μ l/well citrate-phosphate buffer (24 mM $C_6H_8O_7 \cdot H_2O$ and 41 mM $Na_2HPO_4 \cdot 2H_2O$; Sigma). Samples were then incubated with 100 μ l/well of freshly made ODP buffer (0.4% o-phenylene diamine and 0.02% citrate-phosphate buffer; Sigma) at 37°C for 30 min. The reaction was stopped by adding 50 μ l/well of 2 M H_2SO_4 , and absorbance was directly measured at 490 nm.

Immunofluorescence.

Cells were grown on glass coverslips (24 mm) for 3 days prior to the experiments and fixed with 2% paraformaldehyde at 37°C for 15 min. Coverslips were washed with PBS containing 0.1% Triton X-100 three times for 5 min each time. To visualize the DNA photoproducts, nuclear DNA was denatured by incubation with 0.07 N NaOH at room temperature for 5 min, washed with 0.1% Triton X-100 three times for 5 min each time, and subsequently washed with PBS+ (PBS containing 0.15% glycine and 0.5% bovine serum albumin [BSA]). The cells were incubated at room temperature with primary antibodies for 2 h in a moist chamber. Subsequently, the coverslips were washed three times with PBS-Triton X-100 and PBS+, incubated for 1 h with secondary antibodies at room temperature, and again washed three times in PBS-Triton X-100. Samples were embedded in Vectashield mounting medium (Vector Laboratories, Burlingame, CA). Images were obtained by confocal laser scanning microscopy imaging, carried out with an LSM 510 microscope (Zeiss, Oberkochen, Germany).

For this procedure, the primary antibodies used were rabbit anti-XPA (1:2,000; kindly provided by K. Tanaka), rabbit anti-XPB (1:1,000; S-19; Santa Cruz Biotechnology), rabbit anti-XPC (1:1,000) (48), mouse anti-CPD (1:1,000; TDM-2; BioConnect/MBL), and rat anti-HA (1:500; 3F10; Roche). The secondary antibodies used were Cy3-conjugated goat anti-mouse antiserum (1:1,000; Jackson ImmunoResearch Laboratories), Alexa Red-conjugated goat anti-rabbit antiserum (1:1,000; Molecular Probes), Alexa Fluor 350 goat anti-mouse antiserum (1:250; Molecular Probes), and Alexa Green 488 goat anti-rat antiserum (1:1,000; Molecular Probes).

Cross-linking and ChIP.

In vivo cross-linking to identify chromatin-bound NER proteins 1 h after UV irradiation (ChIP on Western) was performed as previously described (15): 20 confluent grown petri dishes (14.5 cm) for each sample were treated with freshly prepared 1% formaldehyde solution containing 50 mM HEPES, pH 8.0, 1 mM EDTA, 0.5 mM EGTA, and 0.1 M NaCl for 16 min at 4°C. Cross-linking was stopped by adding glycine to a final concentration of 0.125

2

M. The cells were washed with cold PBS and isolated after centrifugation (1,300 rpm for 5 min). Cell lysis was achieved by rotation of the cell pellet resuspended in 7 ml of PDB buffer (50 mM HEPES, pH 7.8, 1 mM EDTA, 0.5 mM EGTA, 0.15 M NaCl, 0.5% NP-40, 0.25% Triton X-100, 10% glycerol, 1 mM phenylmethylsulfonyl fluoride [PMSF], and 5 µg/ml proteinase inhibitors) at 4°C for 10 min. The resulting nuclei were collected by centrifugation (1,300 rpm for 5 min) and washed with 7 ml buffer (10 mM Tris-HCl, pH 8.0, 1 mM EDTA, 0.5 mM EGTA, 0.2 M NaCl, 1 mM PMSF, and 5 µg/ml proteinase inhibitors). The crude nuclei were resuspended in 2.5 ml of 1× RIPA buffer (PBS containing 1% NP-40, 0.5% Na deoxycholate, and 0.1% SDS) and sonicated (power setting 5) on ice using repeated 20-s bursts with a Soniprep 150 (Beun De Ronde), followed by 1 min of cooling on ice between sonications to obtain DNA fragments with an average length of 0.3 to 0.7 kb. Samples were centrifuged at 13,000 rpm for 45 min at 4°C, and the supernatants were stored at -80°C. The DNA size was regularly checked between sonication steps by electrophoresis on agarose after proteinase K treatment and phenol chloroform extraction.

Cross-linked cellular extracts were incubated overnight at 4°C in RIPA buffer with rabbit polyclonal anti-XPB (S-19; Santa Cruz Biotechnology) or normal rabbit IgG (Santa Cruz Biotechnology) cross-linked to protein A-Sepharose beads (Amersham Biosciences). Before immunoprecipitation, the cross-linked beads were preabsorbed with 100 µg/ml sonicated (denatured) salmon sperm DNA and 100 µg/ml BSA for 2 h at 4°C. After immunoprecipitation, the beads were washed twice with 1× RIPA buffer, once with RIPA buffer containing 100 µg/ml single-stranded DNA (ssDNA), and twice with 1× RIPA buffer containing 100 µg/ml ssDNA plus 0.5 M NaCl. Finally, the beads were washed with LiCl buffer (20 mM Tris, pH 8.0, 1 mM EDTA, 250 mM LiCl, 1% Na deoxycholate, 1 mM PMSF, and 5 µg/ml proteinase inhibitors). For protein analysis, beads were mixed with an equal volume of 2× SDS-sample buffer and boiled for 30 min to 1 h at 94°C. Proteins were separated on 8% SDS-PAGE and transferred to 0.45-µm nitrocellulose membranes (Millipore). The membranes were hybridized with either rabbit polyclonal ERCC1 (1:1,000) (50), rabbit polyclonal XPF (1:1,000; affinity purified), mouse monoclonal anti-p62 (3C9), or rabbit anti-XPA (1:1,000; kindly provided by K. Tanaka) antibody, followed by a secondary antibody (either donkey anti-rabbit or rabbit anti-mouse) conjugated with horseradish peroxidase (Biosource International) and detected using enhanced chemiluminescence (ECL+ Detection Kit; Amersham Biosciences).

Results

Prolonged residual UDS levels in TTD-A primary fibroblasts.

To gain further insight into the apparent discrepancy between low UDS and relatively mild UV sensitivity of TTD-A cells, we systematically analyzed the NER parameters of the three different TTD-A primary fibroblasts (TTD1BR, TTD99RO, and TTD14PV) in a time-resolved manner. First, we systematically determined the UV hypersensitivities of the different TTD-A primary fibroblasts assayed in parallel in the same experiment. As shown in Fig. 1a, all TTD-A primary fibroblasts exhibit markedly similar and mild UV sensitivities compared to a completely NER-deficient (XP-A) primary fibroblasts. Next, we determined the UDS levels of these three TTD-A patient cells and of NER-proficient wild-type primary fibroblasts (C5RO) at different time points after UV irradiation. To avoid systematic intersample variations of UDS measurements, we performed these measurements in a setup in which, for each of the separate cell strains used and time points measured, the same internal wild-type control was included. To that end, we labeled wild-type primary fibroblasts (C5RO) with latex beads and mixed them with unlabeled TTD-A primary XP-A primary fibroblasts with

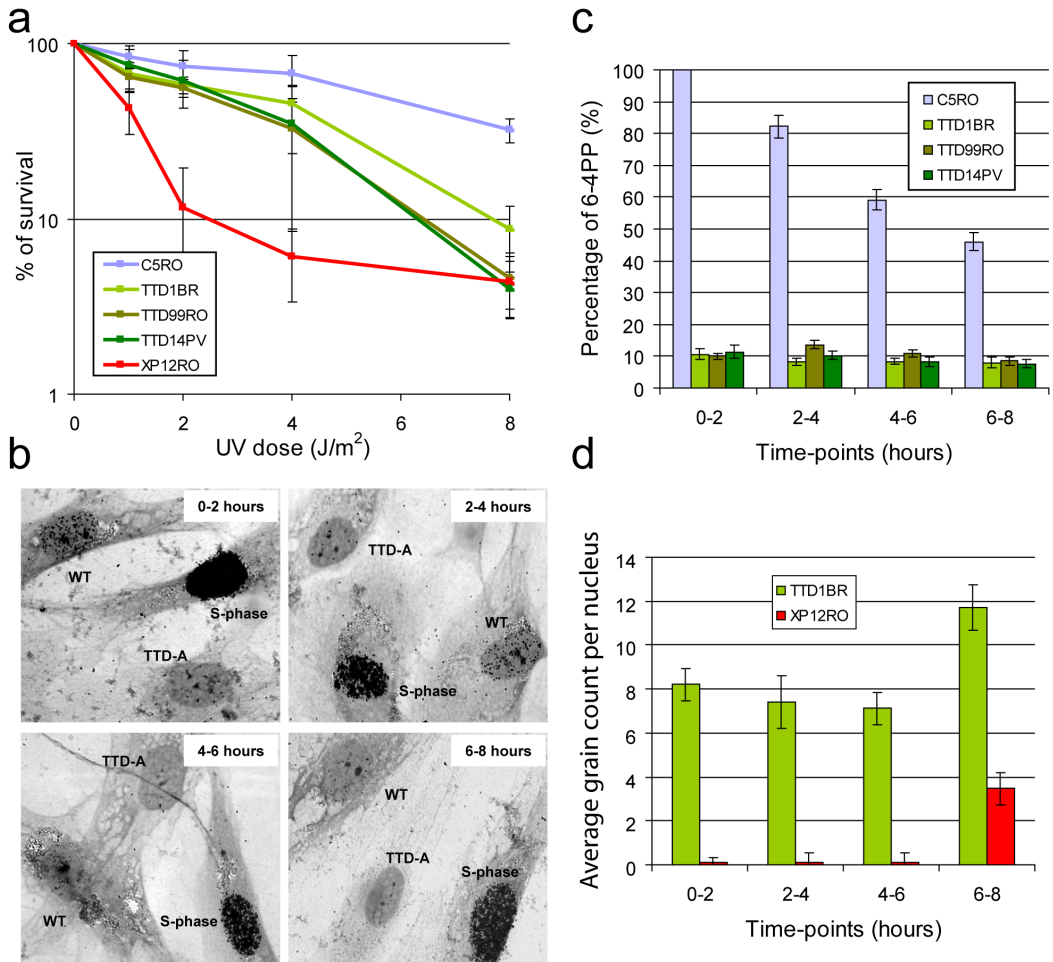


Fig. 1. Time-lapse UDS capacity. (a) Graph showing the surviving fraction of cells after different doses of UV irradiation of wild-type C5RO, TTD-A, and XP-A primary fibroblasts. The percentage of surviving cells was plotted against the applied UV dose, measured by [³H]thymidine incorporation. The error bars indicate the standard errors of the mean (SEM). (b) Representative pictures of UDS experiments of TTD-A (TTD1BR) mixed with WT (C5RO) primary fibroblasts at different time points, as indicated, after UV irradiation. WT cells are recognized by the presence of small beads in the cytoplasm, and the heavily labeled cells are in S phase. (c) Graph showing the relative UDS levels at different time points after UV irradiation obtained after counting the autoradiographic grains above the nuclei expressed as percentages of wild-type UDS measured directly after UV irradiation, which was set at 100%. The UDS levels of the different TTD-A primary fibroblasts are indicated in green. The error bars indicate the SEM of at least 25 nuclei counted. (d) Graph showing the absolute UDS levels at different time points after UV irradiation obtained after counting the autoradiographic grains above the nuclei of TTD-A (TTD1BR) and XP-A (XP12RO) primary fibroblasts. The error bars indicate the SEM of at least 50 nuclei counted.

latex beads, mixed them with unlabeled TTD-A primary fibroblasts, and measured UDS levels at the various time points (Fig. 1d). The absolute grain count measured in TTD-A cells was significantly higher than in XP-A primary fibroblasts (indistinguishable from non-UV-induced UDS), showing that this persistent low level of UDS is not background staining. Our results suggest that the incorporation of nucleotides during NER-induced DNA synthesis at the site of damage (i.e., the penultimate gap-filling step of the NER process) is not completely abolished but slowly progresses in TTD-A primary fibroblasts.

2

Retarded 6-4PP removal in TTD-A cells.

The low but persistent UDS can be explained by slow but continuous UV-induced lesion removal in TTD-A cells. UDS in the first hours after UV irradiation in NER-proficient cells is mainly derived from 6-4PP repair (29, 37), and the majority of these lesions are removed within 4 to 6 h after UV irradiation (49). To verify whether the observed low, continuous UDS is in part derived from partial and slow repair of 6-4PP, we determined 6-4PP elimination kinetics in primary fibroblasts by using ELISA (31) (Fig. 2a). At different time points after UV irradiation (5 J/m^2), DNA was isolated, and the number of UV-induced lesions was determined in wild-type (blue), TTD-A (green hues), and XP-A (red) (the last are fully NER deficient) primary fibroblasts. As previously determined (11, 49), we also found that in wild-type cells the vast majority of 6-4PP lesions were removed within only 2 h after UV irradiation (Fig. 2a). In accordance with the low but persistent UDS, TTD-A primary fibroblasts do exhibit 6-4PP lesion removal (Fig. 2a). This removal, however, is severely delayed compared to wild-type cells, with approximately 5 to 20% removal of 6-4PPs in 2 h and 50 to 75% repair after 8 h. In contrast, NER-deficient primary fibroblasts from an XP-A patient (XP12RO) were fully deficient in repairing 6-4PP even after 8 h. Under the same experimental conditions, the CPD removal was also measured in these primary fibroblasts (Fig. 2b). Due to their structural properties, CPD lesions are poor substrates for NER, and its removal is less efficient. As expected, NER-deficient primary fibroblasts were unable to repair CPD lesions even after 24 h. NER-proficient primary fibroblasts completely remove CPD lesions within 16 h after UV irradiation. Surprisingly, CPD removal as measured in two independent TTD-A primary fibroblasts (TTD1BR and TTD99RO) showed virtually the same CPD repair kinetics as measured in a NER-proficient cell line. These experiments clearly show that the slow repair kinetics measured in TTD-A primary fibroblasts is solely dependent on inefficient 6-4PP removal.

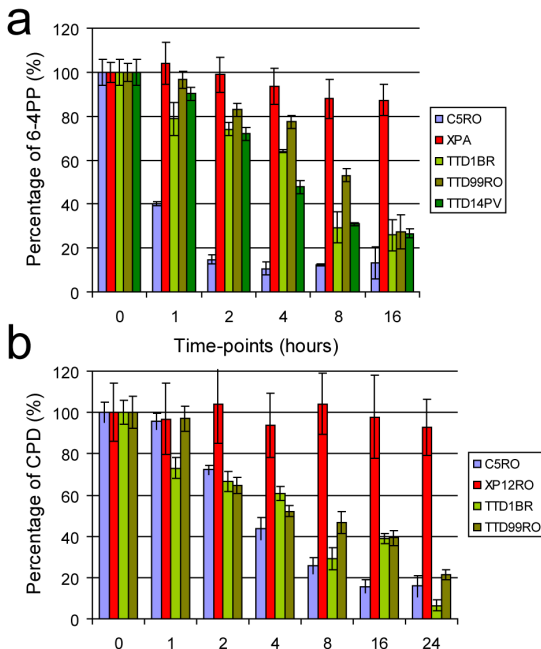


Fig. 2. UV photolesion repair. Wild-type (C5RO), TTD-A (TTD1BR, TTD99RO, and TTD14PV), and XPA (XP12RO) primary fibroblasts were grown in a 14.5-cm dish. The cells were washed with PBS and UV irradiated at 5 J/m^2 . DNA was isolated at different time points (0, 1, 2, 4, 8, 16, and 24 h) after UV irradiation. (a) Amount of 6-4PP measured by ELISA, using a 6-4PP-specific antibody. The amount of 6-4PP measured directly after UV irradiation was set at 100%. (b) Amount of CPD measured by ELISA, using a CPD-specific antibody. The amount of CPD measured directly after UV was set at 100%.

Delayed NER complex assembly in TTD-A cells.

Previously, the TTD-A NER defect was explained by the observed absence of NER complex assembly in experiments using local UV damage induction (7). In these experiments, however, assembly of NER factors was determined at only a single time point (i.e., 30 min) after UV irradiation. As we found retarded damage removal in TTD-A cells here, slower NER factor assembly at damaged DNA can also be envisaged. To determine whether the delayed repair observed in TTD-A cells is derived from inefficient NER complex assembly, we investigated the accumulation of several NER proteins at local UV-damaged (LUD) sites over time, using comparative immunofluorescence (51). A mixed cell population containing both TTD-A and TTD-A corrected cells that stably express TTDA-HA (18) (here, wild-type cells) was subjected to local-damage irradiation. LUD was visualized using a CPD antibody, and to distinguish TTDA-HA corrected cells from TTD-A cells, an HA antibody was used. Initially, we tested XPC binding (Fig. 3a and Table 1) on LUDs, as XPC is one of the first

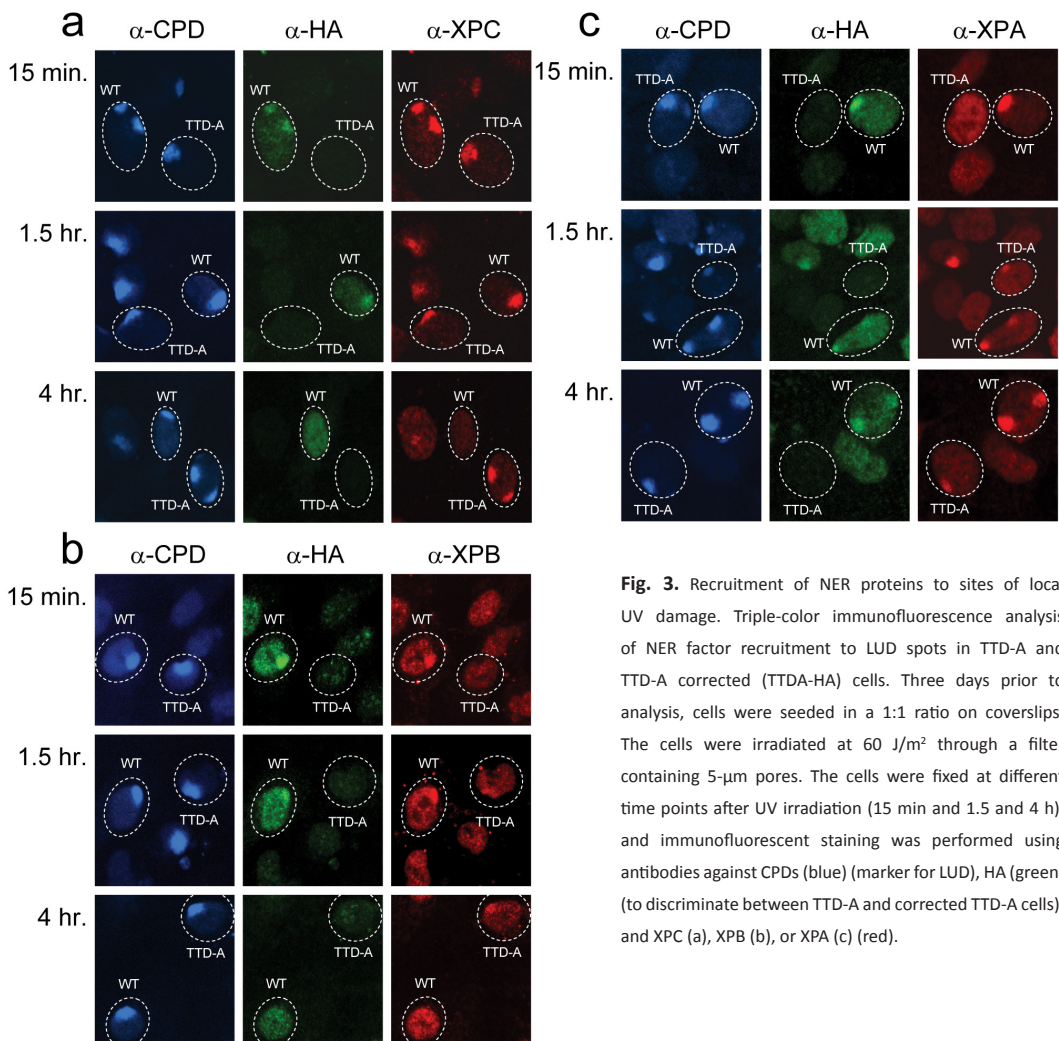


Fig. 3. Recruitment of NER proteins to sites of local UV damage. Triple-color immunofluorescence analysis of NER factor recruitment to LUD spots in TTD-A and TTD-A corrected (TTDA-HA) cells. Three days prior to analysis, cells were seeded in a 1:1 ratio on coverslips. The cells were irradiated at 60 J/m^2 through a filter containing $5\text{-}\mu\text{m}$ pores. The cells were fixed at different time points after UV irradiation (15 min and 1.5 and 4 h), and immunofluorescent staining was performed using antibodies against CPDs (blue) (marker for LUD), HA (green) (to discriminate between TTD-A and corrected TTD-A cells), and XPC (a), XPB (b), or XPA (c) (red).

Table 1. Recruitment of NER proteins to chromatin after UV irradiation

Protein	Recruitment ^a					
	WT			TTD-A		
	15 min	1.5 h	4 h	15 min	1.5 h	4 h
XPC	+	+	–	+	+	+
XPB	+	+	–	–	+	+
XPA	+	+	+	–	+	+

^aAt the indicated time points, the recruitment of different NER proteins to LUD sites was scored. Accumulations are scored with a minus for no accumulation or a plus for accumulation.

proteins that recognized the UV-damaged DNA, and its binding to lesions is responsible for the subsequent recruitment of TFIIH to the emerging chromatin-bound NER complex. As expected, XPC was able to rapidly accumulate at the sites of lesions in both wild-type and TTD-A cells, since the accumulation of XPC is independent of TFIIH status (45, 57, 59). However, 4 h after UV irradiation, when the 6-4PP lesions are mostly repaired in wild-type cells and XPC is undetectable at LUD in these cells, XPC remains clearly visible at LUD in TTD-A cells, showing that UV lesions are still not fully repaired in these cells. We next tested the binding of TFIIH to NER complexes by visualizing the XPB helicase subunit at the LUD with an XPB-specific antibody (Fig. 3b). While in wild-type cells XPB accumulates very rapidly at LUD, TFIIH recruitment in TTD-A cells is severely delayed but persists at these sites at least up to 4 h after UV irradiation (Fig. 3b and Table 1). After TFIIH binding to damaged DNA, XPA is recruited to the growing NER complex (57), and this recruitment was found to be completely abolished in TTD-A cells (7). However, we found that XPA accumulated at LUD with the same slower kinetics in TTD-A cells as TFIIH (Fig. 3c, Table 1), showing that as soon as sufficient TFIIH is loaded, XPA also becomes visible at LUD. It is surprising to note that XPA remains visible even 4 h post-UV irradiation in wild-type (TTDA-HA corrected) cells, in contrast to the other tested preincision NER factors, XPC and TFIIH. Although this sustained XPA binding at LUD was previously also observed in live-cell microscopy using green fluorescent protein (GFP)-tagged XPA (27), thereby excluding an artifact introduced by the immunofluorescence procedure, we currently do not have a satisfactory mechanistic explanation for this prolonged XPA binding to LUD other than that XPA has an additional unknown function(s) in NER beyond damage verification. Next to XPA, other downstream NER factors (whose incorporation into NER complexes was also dependent on functional TFIIH), such as ERCC1 and XPF, also slowly accumulate at LUD (data not shown).

Inefficient chromatin-bound NER complex formation in TTD-A cells.

The delayed or inefficient NER complex assembly in TTD-A cells could in theory also be derived from the reduced TFIIH steady-state level observed in TTD-A cell lines (51). To investigate whether the reduced NER complex formation is derived from an improperly structured TFIIH complex or could be attributed to a reduced amount of TFIIH, we directly analyzed the interactions between TFIIH and the other NER factors within chromatin-bound NER complexes by performing a variant of ChIP (15). In this assay, immunoprecipitation and sample preparation were performed as in classical ChIP, though rather than analyzing the coprecipitating genomic DNA, we analyzed the chromatin-bound interacting proteins

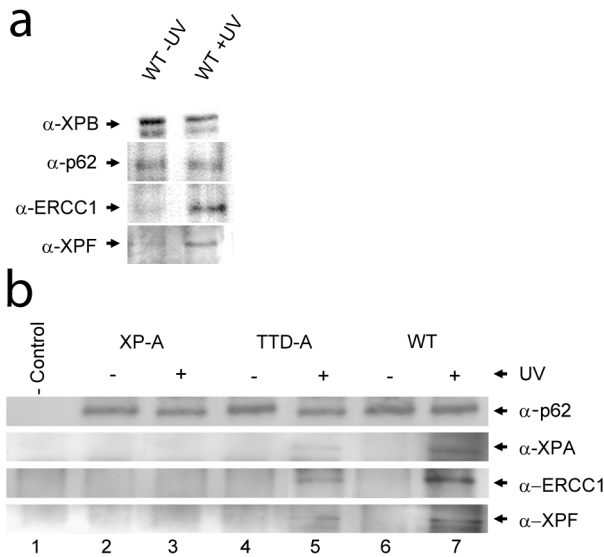


Fig. 4. Recruitment of NER proteins to chromatin after UV irradiation. (a) Western on ChIP was performed on extracts isolated after formaldehyde cross-linking of wild-type (MRC5-SV) cells (with and without 25 J/m² UV irradiation; 1 h after irradiation) using an XPB-specific rabbit polyclonal antibody. Equal amounts of precipitated TFIIH were loaded (analyzed by anti-XPB and anti-p62 immunostaining [top two rows]). Under these conditions, a strong increase in the NER endonuclease complex ERCC1-XPF (bottom two rows) was observed to coprecipitate with chromatin-bound TFIIH after UV irradiation. (b) Western on ChIP analysis of XP-A (XP2OS-SV, lanes 2 and 3), TTD-A (TTD1BR-SV, lanes 4 and 5), and wild-type (MRC5-SV, lanes 6 and 7) cells from UV-treated (+) or mock-treated (-) cells, as in panel a. Equal amounts

of precipitated TFIIH (anti-p62 signal) were loaded. The immunoprecipitated material was probed for XPA, ERCC1, and XPF and compared to nonspecific precipitated material (lane 1) from preimmune rabbit IgG. In XP-A cells, XPA, ERCC1, and XPF do not coprecipitate after UV irradiation, whereas in TTD-A cells, strongly reduced amounts of these proteins were coprecipitated with TFIIH after UV irradiation.

(ChIP on Western) that coprecipitated with an XPB antibody (TFIIH subunit) (see Materials and Methods). As expected, chromatin-bound association between TFIIH and the ERCC1-XPF complex was dependent on UV irradiation (Fig. 4a). Next, we analyzed the chromatin-bound and UV-induced TFIIH-interacting proteins in wild-type (MRC5-SV) and TTD-A cells and compared them to completely NER-deficient cells (XP-A). To exclude the possibility that the inefficient recruitment of XPA and ERCC1-XPF to the NER complex could be a consequence of the low TFIIH steady state, we normalized TFIIH quantities (on the basis of anti-p62 staining, another core component of TFIIH) by loading equal amounts of precipitated TFIIH (Fig. 4b). We were able to visualize a significant UV-induced increase in the loading of XPA and ERCC1-XPF to the chromatin in NER-proficient cells. As expected, XPA and ERCC1-XPF binding to chromatin was abolished in XP-A cells. Importantly, clearly less efficient XPA and ERCC1-XPF were also coprecipitated in TTD-A cells compared to wild-type cells. These data suggest that it is not the amount of TFIIH but the physical and chemical constitution of TFIIH in the absence of TTDA that does not allow proper loading of downstream NER factors.

In addition, this ChIP on Western analysis provided independent evidence that in TTD-A cells NER complex formation can occur, though only in a very inefficient manner, and thus confirmed the conclusion obtained from the immunofluorescence studies.

Discussion

Mutations in the TFIIH subunits XPB, XPD, and TTDA are associated with a surprising clinical variation ranging from cancer-prone XP to the severe neurodevelopmental and premature-ageing syndromes TTD, cranio-oculo-facial syndrome (COFS), and XP combined with CS or TTD (3, 5, 16, 19, 25, 41, 42, 53).

Thus far, only patients expressing the TTD phenotype have been found to be

associated with inherited mutations in the *TTDA* gene (17, 40). Among TTD patients, the spectrum of clinical features is very broad and stretches from very mild forms of the disease (with normal development and only the brittle-hair phenotype) to very severe cases (characterized by high mortality at a young age and severe developmental defects) (12). TTD-A patients present in general a relatively mild form of TTD, including moderate UV hypersensitivity (17, 42, 47). It is remarkable to note that the repair properties of TTD-A primary fibroblasts present a puzzling picture, as the mild UV sensitivity is accompanied by very low UV-induced UDS (17, 51). In other NER-deficient XP cells, such as XP-D, XP-A, or XP-G, that present similar low levels of UDS, UV sensitivity appeared much more pronounced. This apparent discrepancy has drawn our attention to thoroughly analyzing the repair properties of TTD-A cells. NER-induced DNA synthesis measurements are generally conducted within the first 2 h after UV irradiation, whereas UV survival measurements extend over a few days after the initial damaging event. Based on these two entirely different time scales of monitoring DNA repair endpoints, we hypothesize that the repair activity in TTD-A cells is not completely deficient but progresses slowly. When repair continues at a slower pace, the UV-induced lesions that are mainly responsible for cytotoxicity (6-4PP) could be gradually removed during the extended time between irradiation and colony survival measurement. Indeed, in our time-resolved UDS experiments, we showed that the low level of UDS in TTD-A cells progresses at more or less the same rate to at least 8 h after UV irradiation. Within this time frame, the UDS gradually declines in NER-proficient cells assayed in parallel. In addition, the actual 6-4PP removal is not completely absent in TTD-A cells, though it is severely retarded (Fig. 2a). The continuous slow removal of 6-4PP still repairs most of these lesions within a reasonable time (75% within 6 h, whereas 85% is removed within 3 h in WT cells [Fig. 2a]), thus explaining the only moderate UV sensitivity, in line with our hypothesis. Surprisingly, CPD removal was not retarded in TTD-A primary fibroblasts but showed repair kinetics similar to those of a NER-proficient cell line (Fig. 2b). This observation supports the hypothesis that 6-4PP lesions are the main lesions that are repaired with slower repair kinetics in TTD-A primary fibroblasts. Apparently, for the repair of CPD lesions, other NER-associated factors are more important for determining the rate of NER complex formation and actual removal of CPD lesions. This observation is remarkably different from the repair parameters measured in other non-*TTDA* mutated TTD (XP-B or XP-D) cells. In fact, it has been shown that, in XP-D mutated TTD primary fibroblasts, the 6-4PP repair capacity is highly variable and depends on the mutation in the *XPD* gene: 6-4PPs are either repaired normally, as in TTD1VI cells (R722W), or not repaired at all in TTD9VI (R112H) cells (6). In addition, in XP-B/TTD primary fibroblasts, TTD6VI (amino acid [aa] 355 mutated [58]) 6-4PPs are efficiently repaired (36). Although 6-4PP removal appeared highly variable throughout the different NER-deficient TTD cells, delayed repair, as in TTD-A cells, was never observed. In conclusion, the retarded repair of 6-4PP observed in TTD-A cells appeared to be a specific feature of this complementation group.

Previously, it was found that the absence of *TTDA* inhibits the ATPase activity of *XPB*, thereby hindering the opening of the DNA, and it was suggested that this defect precludes the subsequent loading of *XPA* (7). In contrast to these observations, we were able to show that, in TTD-A cells, *XPA* can still be loaded on damaged DNA, although with much lower efficiency and slower kinetics than in wild-type cells. As a matter of fact, *XPA* binding to LUD followed almost the same kinetics as *TFIIH*, suggesting a scenario in which *XPA* is recruited once sufficient mutated *TFIIH* is properly loaded on the damaged sites. The discrepancy between the present study and the work of Coin and collaborators (7) can be explained by different detection thresholds of the antibodies used in the two studies

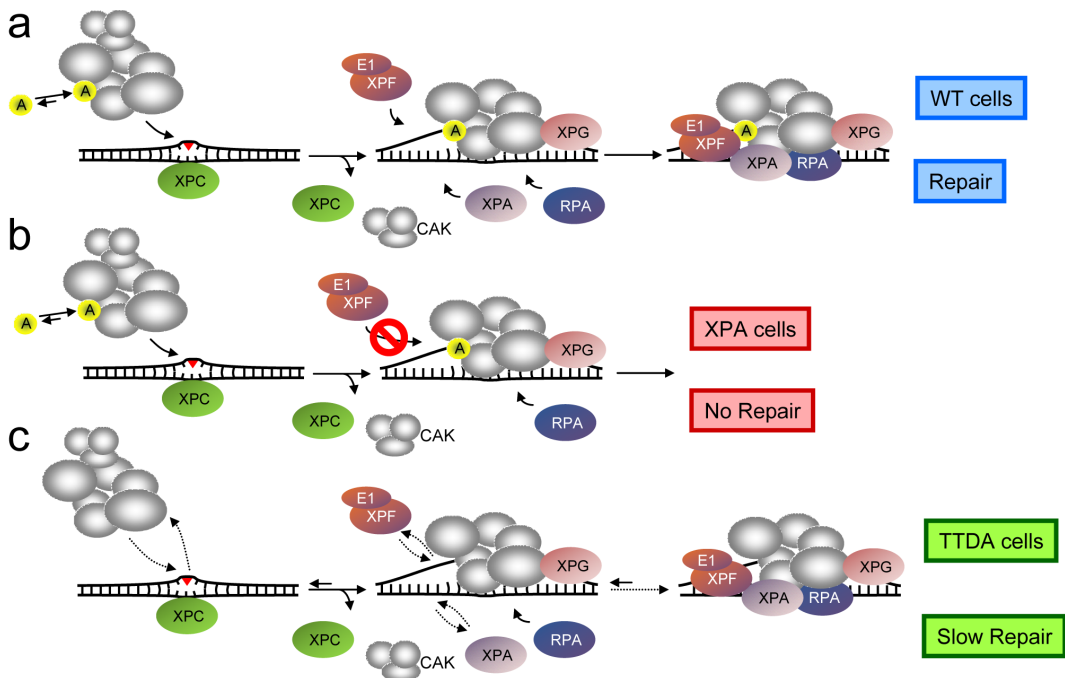


Fig. 5. Model for TTD function in NER and proposed model for lesion-bound NER complex formation in wild-type, XP-A, and TTD-A cells. (a) In wild-type cells, XPC binds to UV lesions and recruits TFIIH and XPG, followed by XPA binding via its interaction with TFIIH. Under these conditions, TTD-A (p8) is more stably bound to TFIIH and promotes the subsequent steps in NER complex formation and possibly stimulates the helicase activity of TFIIH. The unwound DNA structure is stabilized by the presence of TFIIH, XPA, and RPA; together, these proteins are required for recruiting the ERCC1-XPF complex via XPA interaction. After assembling the complete NER machinery, dual incision can occur, and these intermediates are further processed by gap-filling synthesis and ligation. (b) In XP-A cells, recruitment of XPC, TFIIH, and XPG occurs normally, including stable association of TTD-A. Nevertheless, due to the absence of XPA, downstream NER factors were not assembled, and thus NER activity is completely abolished. (c) In TTD-A cells, TFIIH stability and probably protein conformation have been altered because of the complete absence or the presence of a truncated TTD-A protein. Efficient binding of mutated TFIIH is affected and reduces its affinity for the NER complex. Retarded binding of mutated TFIIH attracts XPA to the site of damage to stabilize the NER complex. Furthermore, incorporation of ERCC1-XPF into the NER complex is also retarded similarly to XPA. Nevertheless, although retarded, the assembly of the different NER factors takes place, and finally, DNA lesions are repaired.

and the single time point (30 min post-UV irradiation) analyzed in the Coin study. Based on our data, we favor a different scenario, in which the recruitment of the downstream NER factors of XPC is affected in TTD-A cells (Fig. 5) rather than only XPA. Importantly, the absence of TTD-A seems to influence the assembly kinetics of TFIIH, XPA, and ERCC1-XPF (Fig. 3). This finding was further corroborated by ChIP experiments, showing that the binding capacity of XPA and ERCC1-XPF on damaged DNA in TTD-A cells is strongly reduced. We propose a model (Fig. 5) in which the absence of TTD-A causes improperly folded/structured TFIIH that affects not only the stability of TFIIH (51), but also efficient recruitment of subsequent NER factors. Nevertheless, although retarded, the assembly of the different NER factors still occurs, though with strongly decreased efficiency, and finally, DNA lesions are removed. From our previous studies, we know that the transient binding of TTD-A to TFIIH is stabilized during active NER (18). We do not know, however, how this binding influences TFIIH structure when bound to lesions. It is possible that the

2

observed interaction between TTDA, p52 (TFIIH core subunit), and XPD (22, 56) both modifies the XPB ATPase activity (7) of TFIIH and favors the affinity of downstream NER factors for the lesion-bound complex. Together, these actions create a more NER-efficient TFIIH complex that allows the incision step to occur (this paper). Previously, it was shown that overexpression of TTDA can partly rescue the UV sensitivity and NER defect in *D. melanogaster* p52 mutants (Dmp52) (1) and also suggested that the presence of TTDA renders TFIIH a NER-competent complex. In summary, our study sheds new light on the peculiar repair parameters of TTD-A cells and provides an explanation for the mild UV sensitivity in combination with a low UDS.

Acknowledgment

We thank K. Tanaka for kindly providing XPA antibody, M. Fousteri for help with the ChIP experiments, J. H. J. Hoeijmakers for helpful discussions, and A. Raams for technical assistance.

This study was financed by the Dutch Organization for Scientific Research (grants ZonMW 917-46-364 and 912-08-031; EU-FP6, IP DNA repair, and LSHG-CT-2005-512113; EU-FP6; and MRTN-CT-2003-503618 to W.V.), the Centre National de la Recherche Scientifique (CNRS contract no. 039438 to G.G.-M.), and the Institut National du Cancer (InCa contract no. 2009-001 to G.G.-M.).

References

1. **Aguilar-Fuentes, J., M. Fregoso, M. Herrera, E. Reynaud, C. Braun, J. M. Egly, and M. Zurita.** 2008. p8/TTDA overexpression enhances UV-irradiation resistance and suppresses TFIIH mutations in a *Drosophila* trichothiodystrophy model. *PLoS Genet* **4**:e1000253.
2. **Bergmann, E., and J. M. Egly.** 2001. Trichothiodystrophy, a transcription syndrome. *Trends Genet* **17**:279-86.
3. **Broughton, B. C., M. Berneburg, H. Fawcett, E. M. Taylor, C. F. Arlett, T. Nardo, M. Stefanini, E. Menefee, V. H. Price, S. Queille, A. Sarasin, E. Bohnert, J. Krutmann, R. Davidson, K. H. Kraemer, and A. R. Lehmann.** 2001. Two individuals with features of both xeroderma pigmentosum and trichothiodystrophy highlight the complexity of the clinical outcomes of mutations in the XPD gene. *Hum Mol Genet* **10**:2539-47.
4. **Broughton, B. C., H. Steingrimsdottir, C. A. Weber, and A. R. Lehmann.** 1994. Mutations in the xeroderma pigmentosum group D DNA repair/transcription gene in patients with trichothiodystrophy. *Nat Genet* **7**:189-94.
5. **Broughton, B. C., A. F. Thompson, S. A. Harcourt, W. Vermeulen, J. H. Hoeijmakers, E. Botta, M. Stefanini, M. D. King, C. A. Weber, J. Cole, and et al.** 1995. Molecular and cellular analysis of the DNA repair defect in a patient in xeroderma pigmentosum complementation group D who has the clinical features of xeroderma pigmentosum and Cockayne syndrome. *Am J Hum Genet* **56**:167-74.
6. **Chigancas, V., K. M. Lima-Bessa, A. Stary, C. F. Menck, and A. Sarasin.** 2008. Defective transcription/repair factor IIH recruitment to specific UV lesions in trichothiodystrophy syndrome. *Cancer Res* **68**:6074-83.
7. **Coin, F., L. P. De Santis, T. Nardo, O. Zlobinskaya, M. Stefanini, and J. M. Egly.** 2006. p8/TTD-A as a repair-specific TFIIH subunit. *Mol Cell* **21**:215-26.
8. **Conaway, R. C., and J. W. Conaway.** 1993. General initiation factors for RNA polymerase II. *Annu Rev Biochem* **62**:161-90.
9. **Egly, J. M.** 2001. The 14th Datta Lecture. TFIIH: from transcription to clinic. *FEBS Lett* **498**:124-8.
10. **Evans, E., J. G. Moggs, J. R. Hwang, J. M. Egly, and R. D. Wood.** 1997. Mechanism of open complex and dual incision formation by human nucleotide excision repair factors. *Embo J* **16**:6559-73.
11. **Eveno, E., F. Bourre, X. Quilliet, O. Chevallier-Lagente, L. Roza, A. P. Eker, W. J. Kleijer, O. Nikaido, M. Stefanini, J. H. Hoeijmakers, and et al.** 1995. Different removal of ultraviolet photoproducts in genetically related xeroderma pigmentosum and trichothiodystrophy diseases. *Cancer Res* **55**:4325-32.

12. **Faghri, S., D. Tamura, K. H. Kraemer, and J. J. Digiovanna.** 2008. Trichothiodystrophy: a systematic review of 112 published cases characterises a wide spectrum of clinical manifestations. *J Med Genet* **45**:609-21.
13. **Fisher, R. P., and D. O. Morgan.** 1994. A novel cyclin associates with MO15/CDK7 to form the CDK-activating kinase. *Cell* **78**:713-24.
14. **Fousteri, M., and L. H. Mullenders.** 2008. Transcription-coupled nucleotide excision repair in mammalian cells: molecular mechanisms and biological effects. *Cell Res* **18**:73-84.
15. **Fousteri, M., W. Vermeulen, A. A. van Zeeland, and L. H. Mullenders.** 2006. Cockayne syndrome A and B proteins differentially regulate recruitment of chromatin remodeling and repair factors to stalled RNA polymerase II in vivo. *Mol Cell* **23**:471-82.
16. **Fujimoto, M., S. N. Leech, T. Theron, M. Mori, H. Fawcett, E. Botta, Y. Nozaki, T. Yamagata, S. Moriwaki, M. Stefanini, M. Y. Momoi, H. Nakagawa, S. Shuster, C. Moss, and A. R. Lehmann.** 2005. Two new XPD patients compound heterozygous for the same mutation demonstrate diverse clinical features. *J Invest Dermatol* **125**:86-92.
17. **Giglia-Mari, G., F. Coin, J. A. Ranish, D. Hoogstraten, A. Theil, N. Wijgers, N. G. Jaspers, A. Raams, M. Argentini, P. J. van der Spek, E. Botta, M. Stefanini, J. M. Egly, R. Aebersold, J. H. Hoeijmakers, and W. Vermeulen.** 2004. A new, tenth subunit of TFIIH is responsible for the DNA repair syndrome trichothiodystrophy group A. *Nat Genet* **36**:714-9.
18. **Giglia-Mari, G., C. Miquel, A. F. Theil, P. O. Mari, D. Hoogstraten, J. M. Ng, C. Dinant, J. H. Hoeijmakers, and W. Vermeulen.** 2006. Dynamic interaction of TTDA with TFIIH is stabilized by nucleotide excision repair in living cells. *PLoS Biol* **4**:e156.
19. **Graham, J. M., Jr., K. Anyane-Yeboah, A. Raams, E. Appeldoorn, W. J. Kleijer, V. H. Garritsen, D. Busch, T. G. Ederheim, and N. G. Jaspers.** 2001. Cerebro-oculo-facio-skeletal syndrome with a nucleotide excision-repair defect and a mutated XPD gene, with prenatal diagnosis in a triplet pregnancy. *Am J Hum Genet* **69**:291-300.
20. **Guzder, S. N., H. Qiu, C. H. Sommers, P. Sung, L. Prakash, and S. Prakash.** 1994. DNA repair gene RAD3 of *S. cerevisiae* is essential for transcription by RNA polymerase II. *Nature* **367**:91-4.
21. **Hanawalt, P. C.** 2002. Subpathways of nucleotide excision repair and their regulation. *Oncogene* **21**:8949-56.
22. **Kainov, D. E., M. Vitorino, J. Cavarelli, A. Poterszman, and J. M. Egly.** 2008. Structural basis for group A trichothiodystrophy. *Nat Struct Mol Biol* **15**:980-4.
23. **Kaldis, P., A. A. Russo, H. S. Chou, N. P. Pavletich, and M. J. Solomon.** 1998. Human and yeast cdk-activating kinases (CAKs) display distinct substrate specificities. *Mol Biol Cell* **9**:2545-60.
24. **Kraemer, K. H., D. D. Levy, C. N. Parris, E. M. Gozokara, S. Moriwaki, S. Adelberg, and M. M. Seidman.** 1994. Xeroderma pigmentosum and related disorders: examining the linkage between defective DNA repair and cancer. *J Invest Dermatol* **103**:965-1015.
25. **Lafforet, D., and J. M. Dupuy.** 1978. Photosensibilite et reparation de l'ADN. *Arch. franc. Pediat.* **35**:65-74.
26. **Lehmann, A. R.** 2003. DNA repair-deficient diseases, xeroderma pigmentosum, Cockayne syndrome and trichothiodystrophy. *Biochimie* **85**:1101-11.
27. **Luijsterburg, M. S., G. von Bornstaedt, A. M. Gourdin, A. Z. Politi, M. J. Mone, D. O. Warmerdam, J. Goedhart, W. Vermeulen, R. van Driel, and T. Hofer.** 2010. Stochastic and reversible assembly of a multiprotein DNA repair complex ensures accurate target site recognition and efficient repair. *J Cell Biol* **189**:445-63.
28. **Mathieu, N., N. Kaczmarek, and H. Naegeli.** 2010. Strand- and site-specific DNA lesion demarcation by the xeroderma pigmentosum group D helicase. *Proc Natl Acad Sci U S A* **107**:17545-50.
29. **Mitchell, D. L., C. A. Haipek, and J. M. Clarkson.** 1985. (6-4)Photoproducts are removed from the DNA of UV-irradiated mammalian cells more efficiently than cyclobutane pyrimidine dimers. *Mutat Res* **143**:109-12.
30. **Moser, J., H. Kool, I. Giakzidis, K. Caldecott, L. H. Mullenders, and M. I. Fousteri.** 2007. Sealing of chromosomal DNA nicks during nucleotide excision repair requires XRCC1 and DNA ligase III alpha in a cell-cycle-specific manner. *Mol Cell* **27**:311-23.
31. **Nishiwaki, Y., N. Kobayashi, K. Imoto, T. A. Iwamoto, A. Yamamoto, S. Katsumi, T. Shirai, S. Sugiura, Y. Nakamura, A. Sarasin, S. Miyagawa, and T. Mori.** 2004. Trichothiodystrophy fibroblasts are deficient in the repair of ultraviolet-induced cyclobutane pyrimidine dimers and (6-4)photoproducts. *J Invest Dermatol* **122**:526-32.

32. **Nouspikel, T.** 2009. DNA repair in mammalian cells : Nucleotide excision repair: variations on versatility. *Cell Mol Life Sci* **66**:994-1009.
33. **O'Donovan, A., A. A. Davies, J. G. Moggs, S. C. West, and R. D. Wood.** 1994. XPG endonuclease makes the 3' incision in human DNA nucleotide excision repair. *Nature* **371**:432-5.
34. **Ogi, T., S. Limsirichaikul, R. M. Overmeer, M. Volker, K. Takenaka, R. Cloney, Y. Nakazawa, A. Niimi, Y. Miki, N. G. Jaspers, L. H. Mullenders, S. Yamashita, M. I. Fousteri, and A. R. Lehmann.** 2010. Three DNA polymerases, recruited by different mechanisms, carry out NER repair synthesis in human cells. *Mol Cell* **37**:714-27.
35. **Ranish, J. A., S. Hahn, Y. Lu, E. C. Yi, X. J. Li, J. Eng, and R. Aebersold.** 2004. Identification of TFB5, a new component of general transcription and DNA repair factor IIH. *Nat Genet* **36**:707-13.
36. **Riou, L., L. Zeng, O. Chevallier-Lagente, A. Stary, O. Nikaido, A. Taieb, G. Weeda, M. Mezzina, and A. Sarasin.** 1999. The relative expression of mutated XPB genes results in xeroderma pigmentosum/Cockayne's syndrome or trichothiodystrophy cellular phenotypes. *Hum Mol Genet* **8**:1125-33.
37. **Roza, L., W. Vermeulen, J. B. Bergen Henegouwen, A. P. Eker, N. G. Jaspers, P. H. Lohman, and J. H. Hoeijmakers.** 1990. Effects of microinjected photoreactivating enzyme on thymine dimer removal and DNA repair synthesis in normal human and xeroderma pigmentosum fibroblasts. *Cancer Res.* **50**:1905-10.
38. **Sijbers, A. M., W. L. de Laat, R. R. Ariza, M. Biggerstaff, Y. F. Wei, J. G. Moggs, K. C. Carter, B. K. Shell, E. Evans, M. C. de Jong, S. Rademakers, J. de Rooij, N. G. Jaspers, J. H. Hoeijmakers, and R. D. Wood.** 1996. Xeroderma pigmentosum group F caused by a defect in a structure-specific DNA repair endonuclease. *Cell* **86**:811-22.
39. **Staresincic, L., A. F. Fagbemi, J. H. Enzlin, A. M. Gourdin, N. Wijgers, I. Dunand-Sauthier, G. Giglia-Mari, S. G. Clarkson, W. Vermeulen, and O. D. Scharer.** 2009. Coordination of dual incision and repair synthesis in human nucleotide excision repair. *Embo J* **28**:1111-20.
40. **Stefanini, M., P. Lagomarsini, S. Giliani, T. Nardo, E. Botta, A. Peserico, W. J. Kleijer, A. R. Lehmann, and A. Sarasin.** 1993. Genetic heterogeneity of the excision repair defect associated with trichothiodystrophy. *Carcinogenesis* **14**:1101-5.
41. **Stefanini, M., G. Orecchia, G. Rabbiosi, and F. Nuzzo.** 1986. Altered cellular response to UV irradiation in a patient affected by premature ageing. *Hum Genet* **73**:189-92.
42. **Stefanini, M., W. Vermeulen, G. Weeda, S. Giliani, T. Nardo, M. Mezzina, A. Sarasin, J. I. Harper, C. F. Arlett, J. H. Hoeijmakers, and et al.** 1993. A new nucleotide-excision-repair gene associated with the disorder trichothiodystrophy. *Am J Hum Genet* **53**:817-21.
43. **Sugasawa, K.** 2010. Regulation of damage recognition in mammalian global genomic nucleotide excision repair. *Mutat Res* **685**:29-37.
44. **Sugasawa, K., J. Akagi, R. Nishi, S. Iwai, and F. Hanaoka.** 2009. Two-step recognition of DNA damage for mammalian nucleotide excision repair: Directional binding of the XPC complex and DNA strand scanning. *Mol Cell* **36**:642-53.
45. **Sugasawa, K., J. M. Ng, C. Masutani, S. Iwai, P. J. van der Spek, A. P. Eker, F. Hanaoka, D. Bootsma, and J. H. Hoeijmakers.** 1998. Xeroderma pigmentosum group C protein complex is the initiator of global genome nucleotide excision repair. *Mol Cell* **2**:223-32.
46. **Tirode, F., D. Busso, F. Coin, and J. M. Egly.** 1999. Reconstitution of the transcription factor TFIIH: assignment of functions for the three enzymatic subunits, XPB, XPD, and cdk7. *Mol Cell* **3**:87-95.
47. **van der Spek, P. J., A. Eker, S. Rademakers, C. Visser, K. Sugawara, C. Masutani, F. Hanaoka, D. Bootsma, and J. H. Hoeijmakers.** 1996. XPC and human homologs of RAD23: intracellular localization and relationship to other nucleotide excision repair complexes. *Nucleic Acids Res* **24**:2551-9.
48. **van Hoffen, A., J. Venema, R. Meschini, A. A. van Zeeland, and L. H. Mullenders.** 1995. Transcription-coupled repair removes both cyclobutane pyrimidine dimers and 6-4 photoproducts with equal efficiency and in a sequential way from transcribed DNA in xeroderma pigmentosum group C fibroblasts. *Embo J* **14**:360-7.
49. **van Vuuren, A. J., E. Appeldoorn, H. Odijk, A. Yasui, N. G. Jaspers, D. Bootsma, and J. H. Hoeijmakers.** 1993. Evidence for a repair enzyme complex involving ERCC1 and complementing activities of ERCC4, ERCC11 and xeroderma pigmentosum group F. *Embo J* **12**:3693-701.
50. **Vandenbergh, K., I. Casteels, E. Vandenbussche, F. De Zegher, and K. De Boeck.** 2001. Bilateral cataract and high myopia in a child with trichothiodystrophy: a case report. *Bull Soc Belge Ophthalmol*:15-8.

51. **Vermeulen, W., E. Bergmann, J. Auriol, S. Rademakers, P. Frit, E. Appeldoorn, J. H. Hoeijmakers, and J. M. Egly.** 2000. Sublimiting concentration of TFIIH transcription/DNA repair factor causes TTD-A trichothiodystrophy disorder. *Nat Genet* **26**:307-13.
52. **Vermeulen, W., P. Osseweijer, A. J. de Jonge, and J. H. Hoeijmakers.** 1986. Transient correction of excision repair defects in fibroblasts of 9 xeroderma pigmentosum complementation groups by microinjection of crude human cell extracts. *Mutat Res* **165**:199-206.
53. **Vermeulen, W., R. J. Scott, S. Rodgers, H. J. Muller, J. Cole, C. F. Arlett, W. J. Kleijer, D. Bootsma, J. H. Hoeijmakers, and G. Weeda.** 1994. Clinical heterogeneity within xeroderma pigmentosum associated with mutations in the DNA repair and transcription gene ERCC3. *Am J Hum Genet* **54**:191-200.
54. **Vermeulen, W., M. Stefanini, S. Giliani, J. H. Hoeijmakers, and D. Bootsma.** 1991. Xeroderma pigmentosum complementation group H falls into complementation group D. *Mutat Res* **255**:201-8.
55. **Vermeulen, W., A. J. van Vuuren, M. Chipoulet, L. Schaeffer, E. Appeldoorn, G. Weeda, N. G. Jaspers, A. Priestley, C. F. Arlett, A. R. Lehmann, and et al.** 1994. Three unusual repair deficiencies associated with transcription factor BTF2(TFIIH): evidence for the existence of a transcription syndrome. *Cold Spring Harb Symp Quant Biol* **59**:317-29.
56. **Vitorino, M., F. Coin, O. Zlobinskaya, R. A. Atkinson, D. Moras, J. M. Egly, A. Poterszman, and B. Kieffer.** 2007. Solution structure and self-association properties of the p8 TFIIH subunit responsible for trichothiodystrophy. *J Mol Biol* **368**:473-80.
57. **Volker, M., M. J. Mone, P. Karmakar, A. van Hoffen, W. Schul, W. Vermeulen, J. H. Hoeijmakers, R. van Driel, A. A. van Zeeland, and L. H. Mullenders.** 2001. Sequential assembly of the nucleotide excision repair factors in vivo. *Mol Cell* **8**:213-24.
58. **Weeda, G., E. Eveno, I. Donker, W. Vermeulen, O. Chevallier-Lagente, A. Taieb, A. Stary, J. H. Hoeijmakers, M. Mezzina, and A. Sarasin.** 1997. A mutation in the XPB/ERCC3 DNA repair transcription gene, associated with trichothiodystrophy. *Am J Hum Genet* **60**:320-9.
59. **Yokoi, M., C. Masutani, T. Maekawa, K. Sugawara, Y. Ohkuma, and F. Hanaoka.** 2000. The xeroderma pigmentosum group C protein complex XPC-HR23B plays an important role in the recruitment of transcription factor IIH to damaged DNA. *J Biol Chem* **275**:9870-5.
60. **Zhou, Y., H. Kou, and Z. Wang.** 2007. Tfb5 interacts with Tfb2 and facilitates nucleotide excision repair in yeast. *Nucleic Acids Res* **35**:861-71.
61. **Zotter, A., M. S. Luijsterburg, D. O. Warmerdam, S. Ibrahim, A. Nigg, W. A. van Cappellen, J. H. Hoeijmakers, R. van Driel, W. Vermeulen, and A. B. Houtsmuller.** 2006. Recruitment of the nucleotide excision repair endonuclease XPG to sites of UV-induced dna damage depends on functional TFIIH. *Mol Cell Biol* **26**:8868-79.
62. **Zurita, M., and C. Merino.** 2003. The transcriptional complexity of the TFIIH complex. *Trends Genet* **19**:578-84.

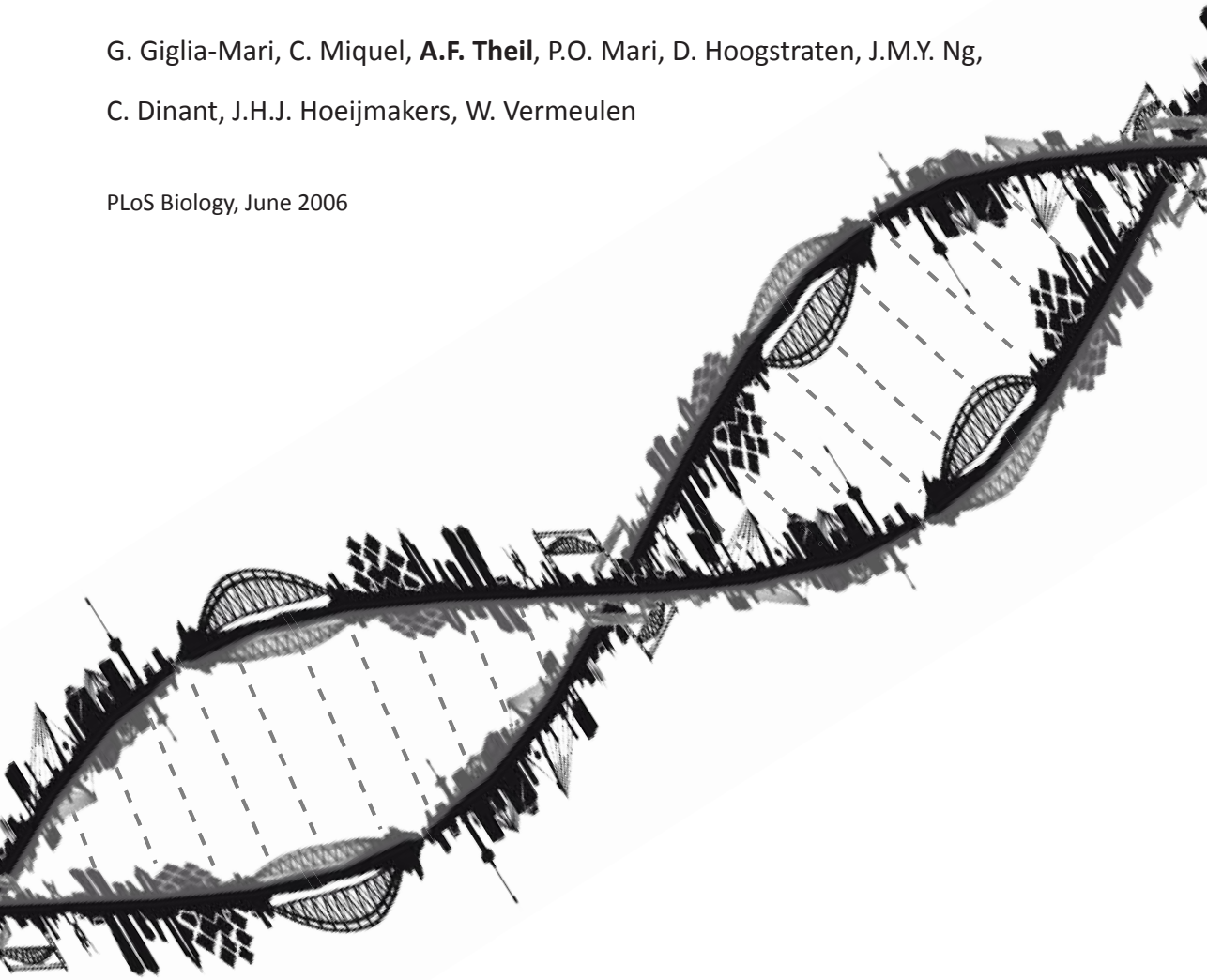


CHAPTER 3

Dynamic Interaction of TTDA with TFIIH is Stabilized by Nucleotide Excision Repair in Living Cells

G. Giglia-Mari, C. Miquel, **A.F. Theil**, P.O. Mari, D. Hoogstraten, J.M.Y. Ng,
C. Dinant, J.H.J. Hoeijmakers, W. Vermeulen

PLoS Biology, June 2006



Abstract

Transcription/repair factor IIH (TFIIH) is essential for RNA polymerase II transcription and nucleotide excision repair (NER). This multi-subunit complex consists of ten polypeptides, including the recently identified small 8-kDa trichothiodystrophy group A (TTDA)/ hTFB5 protein. Patients belonging to the rare neurodevelopmental repair syndrome TTD-A carry inactivating mutations in the TTDA/hTFB5 gene. One of these mutations completely inactivates the protein, whereas other TFIIH genes only tolerate point mutations that do not compromise the essential role in transcription. Nevertheless, the severe NER-deficiency in TTD-A suggests that the TTDA protein is critical for repair. Using a fluorescently tagged and biologically active version of TTDA, we have investigated the involvement of TTDA in repair and transcription in living cells. Under non-challenging conditions, TTDA is present in two distinct kinetic pools: one bound to TFIIH, and a free fraction that shuttles between the cytoplasm and nucleus. After induction of NER-specific DNA lesions, the equilibrium between these two pools dramatically shifts towards a more stable association of TTDA to TFIIH. Modulating transcriptional activity in cells did not induce a similar shift in this equilibrium. Surprisingly, DNA conformations that only provoke an abortive-type of NER reaction do not result into a more stable incorporation of TTDA into TFIIH. These findings identify TTDA as the first TFIIH subunit with a primarily NER-dedicated role in vivo and indicate that its interaction with TFIIH reflects productive NER.

Introduction

DNA-damaging agents constantly challenge the integrity of DNA. A network of distinct DNA-repair systems collectively removes most injuries and safeguards the stability of the genome [1]. Nucleotide excision repair (NER) is a DNA repair mechanism capable of removing different structurally unrelated DNA helix-distorting lesions, including ultraviolet light (UV)-induced lesions and bulky chemical adducts. NER requires the concerted action of 25 proteins in a coordinated multi-step process [2]. After initial damage recognition, the DNA helix is opened by the bi-directional helicase function of TFIIH. Subsequently, four proteins (xeroderma pigmentosum complementation group G protein [XPG], xeroderma pigmentosum complementation group A protein [XPA], replication protein A, and excision repair cross complementing group 1 protein [ERCC1] in complex with xeroderma pigmentosum group F [XPF]) are recruited to stabilize the open intermediate, verify the damage, and incise the damaged strand 3' and 5' at some distance from the injury [3]. Finally, the resulting gap is filled by repair replication and sealed by ligation. Within NER, two lesion recognition pathways are operational: transcription-coupled NER (TC-NER) and global genome NER (GG-NER) [4]. TC-NER is dedicated to lesions that block RNA polymerase II elongation. Within TC-NER, the stalled RNA polymerase likely first detects lesions whereas also the Cockayne syndrome A and B proteins play roles in the early steps of this process. The GG-NER-specific complexes (xeroderma pigmentosum complementation group C [XPC] in complex with the human homologue of Rad23 [hHR23B/A], and xeroderma pigmentosum complementation group E [XPE/DDB2] in complex with the UV-damaged DNA binding protein 1, [UV-DDB1]) recognize lesions at any position in the genome [5]. GG-NER mainly protects against damage-induced mutagenesis and can thus be considered as a cancer-preventing process, whereas TC-NER primarily promotes cellular survival, and therefore may prevent aging [6]. Hereditary NER deficiency is associated with severe clinical features as presented by three photo-sensitive disorders: the cancer-prone syndrome xeroderma pigmentosum (XP) and the neurodevelopmental

conditions Cockayne syndrome and trichothiodystrophy (TTD)[7]. TTD is a premature aging syndrome, with the hallmark feature of brittle hair and nails, ichthyosis, and progressive mental and physical retardation also seen in Cockayne syndrome. Within photo-sensitive TTD, three TFIIH coding genes are implicated: xeroderma pigmentosum complementation group B (XPB) [8], xeroderma pigmentosum complementation group D (XPD) [9, 10], and the newly identified protein termed “TTD group A” (TTDA) [11, 12].

Besides GG-NER and TC-NER, TFIIH is also engaged in RNA polymerase II transcription initiation, RNA polymerase I transcription, activated transcription, and cell cycle regulation [13–20]. TFIIH consists of ten subunits, five of which (XPB, p62, p52, p44, and p34) form a tight core-complex, and the trimeric cyclin activating kinase-subcomplex (CDK7, MAT1, and cyclin H) is linked to the core via the XPD protein [21]. The recently identified 8-kDa TTDA protein [11, 12] connects to the core via interactions with p52 and XPD [29]. TFIIH harbors different enzymatic activities: two DNA-dependent ATPases, XPB and XPD, required for the helicase function [22, 23], a protein kinase displayed by CDK7 [24], and the recently uncovered ubiquitin ligase activity of p44 [25]. Currently, the functions or possible enzymatic properties of the other TFIIH subunits including that of TTDA remain enigmatic.

Cells from patients with TTD-A have reduced steady-state levels of TFIIH, due to mutated TTDA gene [26], suggesting that an important role of TTDA is to stabilize the entire TFIIH complex. The most striking feature of TTD-A cells is their reduced DNA repair activity. Intriguingly, the identified mutations, within the TTDA gene of three non-related patients with TTD-A, lead either to the complete absence of the protein (mutation on the first ATG), or to non-functional truncated peptides, making TTDA the first TFIIH subunit for which a complete absence is compatible with life [12]. Despite these rather diverse mutations, a surprisingly similar expression of the clinical features is observed amongst the patients.

In order to investigate the participation of TTDA in DNA repair and transcription, we measured the differences in mobility of TTDA during repair and transcription in living cells by confocal imaging of a functional green fluorescent protein (GFP)-tagged TTDA (TTDA-GFP) expressed in TTDA-deficient transformed fibroblasts. To compare the mobility of TTDA with others TFIIH subunits, we also measured kinetic parameters of XPB-GFP and XPD-GFP in each of these processes.

Results

Expression and Functionality of TTDA-GFP and XPD-GFP

To investigate the localization, behavior and dynamic properties of TTDA in the most relevant biologically context—the living cell, and under different conditions, such as transcriptional interference and introduction of DNA lesions, we have generated a GFP-tagged TTD A (Figure 1). To compare the behavior of TTDA-GFP with other TFIIH components, we also produced an XPD-GFP fusion (Figure 1A) and used a cell line stably expressing XPB-GFP [14]. The cDNAs encoding TTDA-GFP and XPD-GFP were expressed in TTD-A and XP-D SV40-immortalized human fibroblasts, respectively. Functionality of the fusion proteins was tested, in stably expressing clones, by determining the UV sensitivity (Figure 1B) and recovery of RNA synthesis after UV irradiation (unpublished data). Both TTDA-GFP and XPD-GFP restored both NER-deficient parameters in TTD-A and XP-D cells, respectively, showing that both fluorescently marked proteins are completely functional in repair.

Immunoprecipitation assays showed that the TFIIH core factor, XPB, co-precipitates with both fusion proteins, using anti-GFP cross-linked sepharose beads and

extracts of TTDA-GFP (Figure 1C, left panel) and XPD-GFP-expressing cells (Figure 1D). In addition, TTDA-GFP co-precipitated with anti-p44 (Figure 1C, right panel). These results showed that XPD-GFP and TTDA-GFP were incorporated into TFIIH, despite the relatively large GFP tag, particularly considering the very small size of the TTDA subunit. Moreover, the severely reduced amount of TFIIH in TTD-A cells [26] was restored to wild-type (wt) levels (Figure 1E) by TTDA-GFP expression, as was previously observed for Hemagglutinin peptide-tagged TTDA (TTDA-HA)-expressing cells [12]. Interestingly, the stable expression of TTDA-GFP does not induce higher levels of TFIIH than in wt cells (Figure 1F). We conclude from these data that we have generated two cell lines that stably express biological active fluorescently tagged subunits of TFIIH, which are bona fide tools to study the spatiotemporal distribution and protein dynamics of TFIIH during repair and transcription.

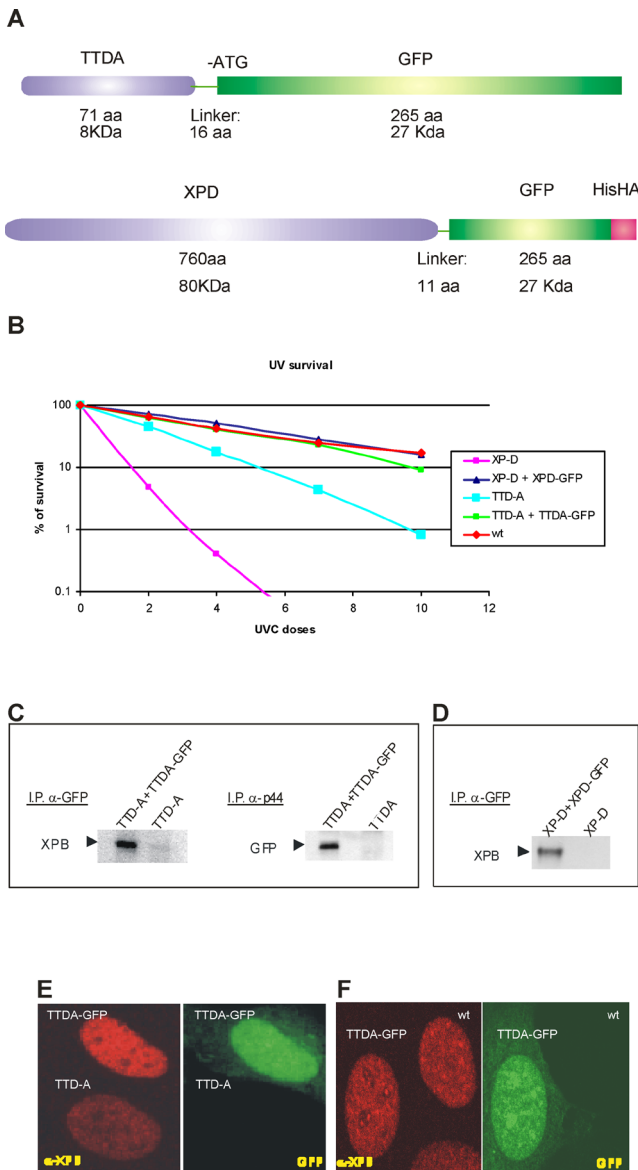


Figure 1. Constructs and Functionality Assays

(A) Scheme of the TTD-A-GFP and XPD-GFP fusion proteins.

(B) UV survival using wt VH10 cells (red diamonds), TTD1BRSV (TTD-A) cells (light blue squares), XP6BESV (XP-D) cells (pink squares), TTD1BRSV-expressing TTDA-GFP cells (green squares), and XP6BESV-expressing XPD-GFP cells (blue triangles). The percentage of surviving cells is plotted against the applied UV-C dose (J/m^2).

(C) Immunoprecipitation: Left panel shows that the XPB TFIIH subunit (by monoclonal anti-XPB detection) co-precipitates with anti-GFP from extracts of TTDA-GFP-expressing fibroblasts (lane 1) and not from TTD1BRSV (TTD-A) fibroblast whole-cell extracts (lane 2). Right panel shows that TTDA-GFP (detected with anti-GFP monoclonal) co-precipitates with the core TFIIH component p44 from extracts from TTDA-GFP-expressing fibroblasts (lane 1) and not in whole-cell extracts from TTD1BRSV (TTD-A) fibroblasts (lane 2). (D) Immunoprecipitation using polyclonal anti-GFP. Also the XPB TFIIH subunit co-precipitated with XPD-GFP (using anti-GFP) in extracts from XPD-GFP-expressing fibroblasts (lane 1), but not from XP6BESV (XP-D) fibroblasts (lane 2).

(E) Immunofluorescence of a mixed population of TTD-A cells (label 2) and TTDA-GFP-expressing TTD-A cells. Cells expressing TTDA-GFP (right panel) showed an increased level of XPB (left panel), compared to TTD-A cells.

(F) Immunofluorescence of a mixed population of VH10 (wt) cells and TTDA-GFP-expressing TTD-A cells. Cells expressing TTDA-GFP (right panel) exhibit a similar expression level of XPB (left panel) as wt cells.

doi:10.1371/journal.pbio.0040156.g001

Cellular Localization of TTDA-GFP and XPD-GFP

High-resolution confocal imaging (Figure 2) of TTDA-GFP- and XPD-GFP-expressing cells revealed a strikingly similar localization. Both present a cytoplasmic and nuclear localization (Figure 2A and 2B), sharply contrasting to XPB-GFP that is strictly nuclear [14] (Figure 2C). Cytoplasmic expression of XPD-GFP is not unexpected since it was previously observed [27] and endogenously expressed XPD was found in both cytoplasmic and nuclear fractions after subcellular fractionation (unpublished data). Cytoplasmic expression is not due to alternative translation starts or fusion protein breakdown products, because immunoblot analysis using an antibody against GFP revealed the presence of only intact XPD-GFP and TTDA-GFP (Figure 2D). Previous immunofluorescent analysis revealed that TTDA-HA was predominantly localized in the nucleus [12]; however, this technique includes permeabilization, which will wash out the cytoplasmic pool of TTDA-HA. In addition, both TTDA-GFP and XPD-GFP accumulate in nucleolar foci, previously also observed in fixed TTDA-HA-expressing fibroblasts [12] and in living cells expressing XPB-GFP [14].

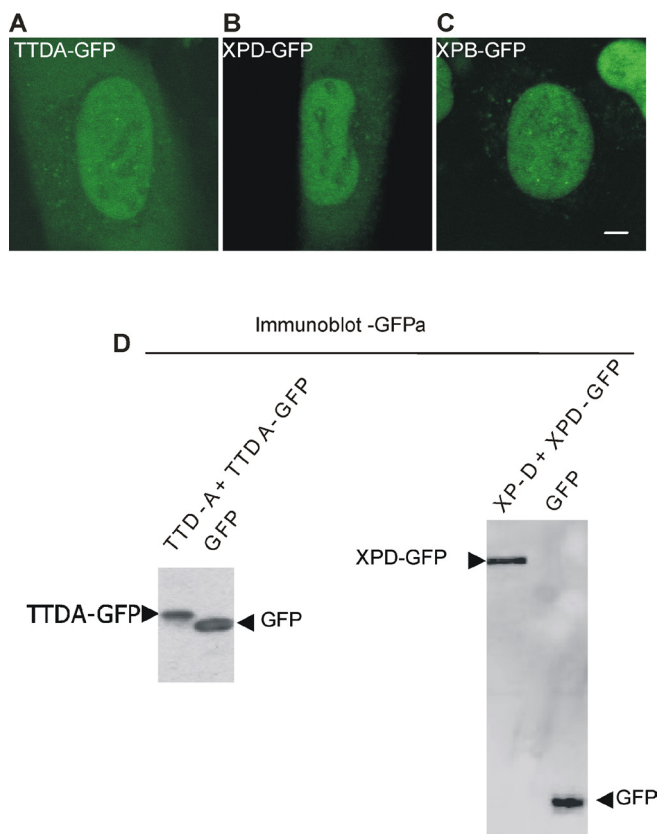


Figure 2. Localization of TTDA-GFP and XPD-GFP

(A) Confocal image of a TTDA-GFP-expressing cell.

(B) Confocal image of a XPD-GFP-expressing cell.

(C) Confocal image of a XPB-GFP-expressing cell.

(D) Immunoblot probed with anti-GFP monoclonal antibody of TTD1BRSV (TTD-A) fibroblasts stably expressing TTDA-GFP (lane 1), XP6BESV (XP-D) transformed fibroblasts stably expressing XPD-GFP (lane 3), and MRC5SV (wt) transformed fibroblasts expressing free GFP (lane 2 and 4).

doi:10.1371/journal.pbio.0040156.g002

Mobility of TTDA-GFP and XPD-GFP in Different Cellular Compartments

The cytoplasmic localization of both XPD-GFP and TTDA-GFP argues for a possible assembly of TFIIH-related subcomplexes within the cytoplasm. In order to investigate this, we measured the mobility of TTDA-GFP, XPB-GFP, XPD-GFP, and GFP in both the cytoplasm and the nucleus by photo-bleaching experiments. We applied a tailor-made variant of fluorescence recovery after photo-bleaching (FRAP) [28] in which fluorescent molecules are photo-bleached in a small strip by a high intensity laser pulse, the subsequent fluorescence recovery in time is monitored and is a measure for the protein mobility (Figure 3).

Within the cytoplasm (Figure 3A), the mobility curve of TTDA-GFP virtually overlaps with that of non-tagged GFP and both show a significant faster fluorescence recovery than cytoplasmic XPD-GFP. These results suggest that the majority of TTDA-GFP and XPD-GFP do not interact with each other in the cytoplasm of living cells, despite the fact that these proteins do interact in the context of TFIIH [29]. Furthermore, the similar mobility rate of GFP and TTDA-GFP argued for a mobility of TTDA-GFP that is mainly determined by passive diffusion on its own, very comparable to GFP [30]. In the nucleus (Figure 3B), TTDA-GFP and XPD-GFP exhibit a slower mobility than in the cytosol (Figure 3A and 3B). In addition, the overall nuclear mobility of TTDA-GFP is slower than that of free GFP. Surprisingly however, even in the nucleus both XPD-GFP and TTDA-GFP move much faster than XPB-GFP (Figure 3B). The relative slow mobility of XPB-GFP was previously explained by its incorporation into the large TFIIH complex with a predicted molecular size of 500 kDa which is even more retarded by its "stop and go" interactions with the transcriptional machinery at promoter sites [14]. Immunoprecipitation experiments showed however that both TTDA-GFP and XPD-GFP are also associated with TFIIH (Figure 1C and 1D). A possible explanation for this unexpected high motility and apparent discrepancy is that the determined mobility reflects the mean of two (or more) components: a slow one, representing the fraction of molecules incorporated in TFIIH, and a fast one, representing the unbound pool of TTDA-GFP and XPD-GFP molecules.

In order to eliminate the fluorescence of this non-incorporated fraction, we modified the FRAP procedure by pre-bleaching the cytoplasmic fraction (see Materials and Methods and Figure 4). Assuming protein exchange between the nucleoplasm and the cytoplasm this procedure will photo-bleach both cytosolic and nuclear free fractions (Figure 4A). Subsequent FRAP analysis in the nucleus, which for simplicity we have called FRAP after bleaching the cytoplasm (FRAP_abc) allowed us to measure the mobility of possibly incorporated TTDA-GFP and XPD-GFP into nuclear complexes. When we applied FRAP_abc, we observed a striking reduction of TTDA-GFP (Figure 4B) and XPD-GFP (Figure 4C) mobility that was very similar to XPB-GFP assayed in parallel and significantly slower than GFP (Figure 4D). However, only the initial recovery of TTDA-GFP (i.e., the early time points after photo-bleaching) was similar to XPB-GFP. At later time points a surprising decline of the initial recovery of TTDA-GFP was observed, whereas the XPD-GFP recovery-curve remained stable and indistinguishable from XPB-GFP (Figure 4D). The remarkable downward slope of the recovery curve was also detected, though much more pronounced, with free GFP (Figure 4D) and only occurred after FRAP_abc (when cytoplasmic GFP molecules were bleached), implying that exchange occurred of bleached and non-bleached GFP molecules with the cytoplasm through the nuclear pores and vice-versa. This is consistent with increased fluorescence in the bleached cytoplasm (unpublished data). The reciprocal experiment i.e. bleaching of the nuclear pool of TTDA-GFP (Figure S1), confirmed that the mobility of the cytoplasmic pool of TTDA-GFP mainly represents

freely mobile, non-complexed TTDA-GFP. The similar early fluorescence recovery profile of all TFIIH components tested, suggested that the initial recovery is mainly determined by the molecules moving through the nuclear space. As argued above the subsequent loss of fluorescence at later time points can be explained by exchange through the nuclear membrane. This latter process has a slower kinetics due to spatial restrictions (change of diffusion through a nuclear pore), explaining its minute contribution to the relatively fast initial recovery. Because this fluorescence decline did not occur with the XPB and XPD TFIIH components, but only with TTDA-GFP, we hypothesized that TTDA is not stably associated to TFIIH. This implies that in these non-challenged cells, equilibrium exists between two kinetic pools of TTDA-GFP molecules, i.e. a free fraction and a TFIIH-bound pool. The fact that free GFP exchanges much faster than TTDA-GFP, though both are almost identical in size, supports the idea that TTDA-GFP exchange over the nuclear membrane is retarded by its incorporation into TFIIH.

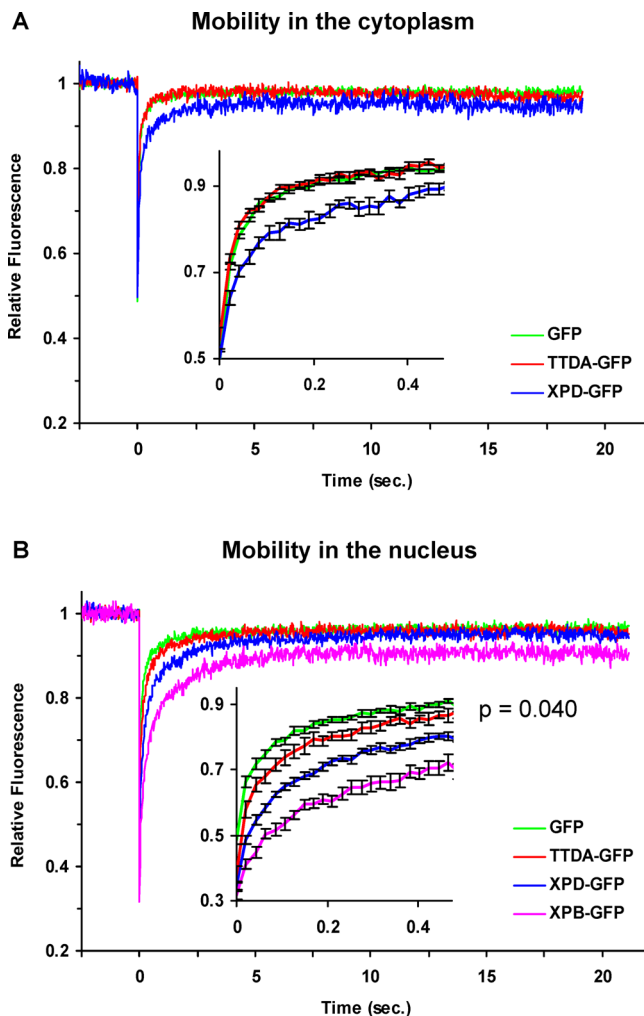


Figure 3. Mobility of TTDA-GFP and XPD-GFP in the Cytoplasm and in the Nucleus Determined by FRAP

(A) FRAP analysis of XPD-GFP (blue line), TTDA-GFP (red line), and free GFP (green line) residing in the cytoplasm. Inset shows increased time resolution of the curves with error bars.

(B) FRAP analysis of XPB-GFP (pink line), XPD-GFP (blue line), TTDA-GFP (red line), and free GFP (green line) in the nucleus. Relative fluorescence (fluorescence post-bleach divided by fluorescence pre-bleach) plotted against time in seconds. Inset shows increased time resolution of the curves with error bars. The p-value has been calculated for GFP and TTDA-GFP datasets.

doi:10.1371/journal.pbio.0040156.g003

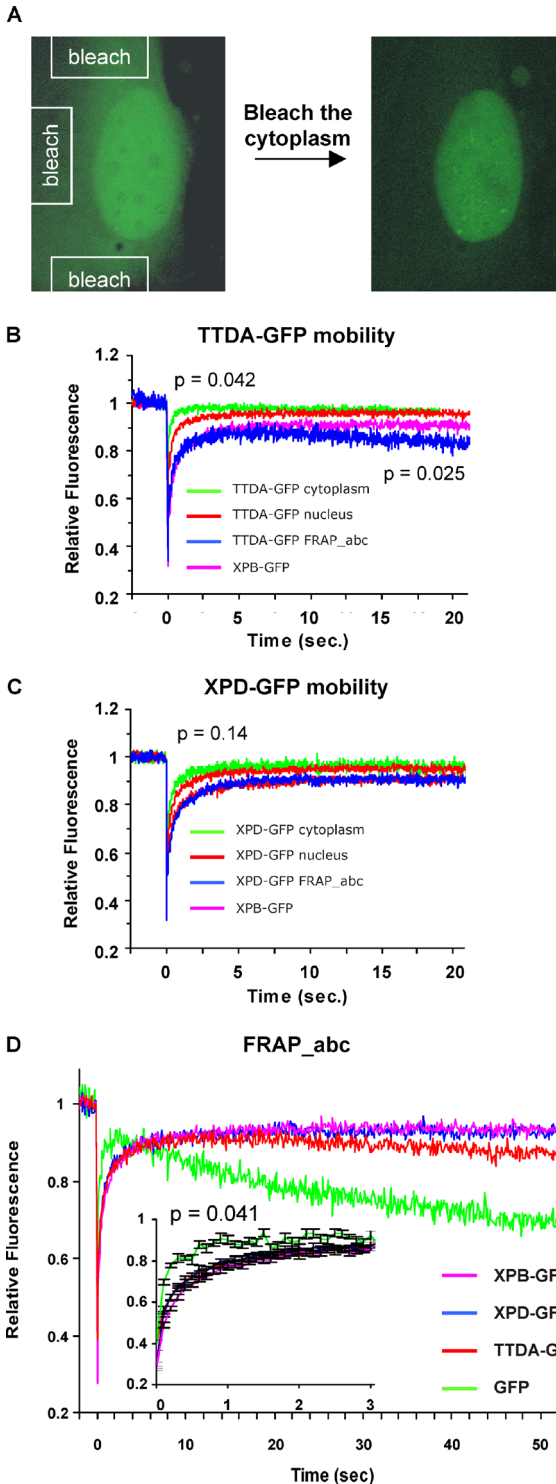


Figure 4. FRAP_abc

(A) TTDA-GFP-expressing fibroblast without treatment (left panel) and after (right panel) applying several high laser pulses in the cytoplasmic compartment (see Materials and Methods for details).

(B) TTDA-GFP mobility in the cytoplasm (green line), in the nucleus without bleaching the cytoplasm (red line), in the nucleus after bleaching the cytoplasmic fraction (blue line), and XPB-GFP mobility in the nucleus (pink line). The p-value has been calculated for cytoplasmic and nuclear mobility curves of TTDA-GFP.

(C) XPD-GFP mobility in the cytoplasm (green line), in the nucleus without bleaching the cytoplasm (red line), in the nucleus after bleaching the cytoplasmic fraction (blue line), and XPB-GFP mobility in the nucleus (pink line). The p-value has been calculated for cytoplasmic and nuclear mobility curves of XPD-GFP.

(D) FRAP_abc on XPB-GFP (pink line), XPD-GFP (blue line), TTDA-GFP (red line), and free GFP (green line). Inset shows increased time resolution of the curves with error bars.

doi:10.1371/journal.pbio.0040156.g004

Mobility of TTDA-GFP after UV Irradiation

To investigate whether the presence of DNA damage influences the equilibrium between the various TTDA-GFP pools, we compared the dynamic behavior of TTDA-GFP before and after UV irradiation (measured between 5 to 30 min after exposure) (Figure 5). FRAP_{abc} revealed that after UV both XPD-GFP and TTDA-GFP exhibit an incomplete recovery, indicative for a relatively long immobilization (Figure 5A and 5B), previously explained by the physical participation in the repair reaction [14, 28, 31, 32]. Surprisingly, the downward slope, as observed in the mobility curve of untreated TTDA-GFP-expressing cells, is significantly reduced when cells are treated with UV. This observation can be explained as a reduction of the pool size of free TTDA-GFP, thus attenuating the effect of exchange with the cytoplasmic bleached pool. This phenomenon argues for a more stable integration of TTDA into TFIIH when the complex is engaged in the NER reaction. In order to show that the stabilized association of TTDA to TFIIH is derived from actual participation in NER, we reduced the XPC concentration by RNA interference. Because XPC is the initiator of GG-NER, its depletion would prevent the formation of NER complexes on damaged DNA and thus should not induce damage-dependent immobilization of subsequent NER factors. When we transfected our cells that stably express TTDA-GFP with a mixture of two small interference RNA constructs against XPC (Figure S2), a reduction of the immobile fraction can be observed in irradiated TTDA-GFP-expressing cells (Figure S2C), showing that indeed the integration of TTDA in TFIIH is dependent on NER.

We further explored the participation of the three TFIIH components in NER by determining the binding time of each of the components when actively engaged in NER. To that aim, we applied FRAP on locally UV-damaged cells (Figure 5C), as was previously determined for XPB-GFP [14]. As shown in Figure 5D, both TTDA-GFP and XPD-GFP have a similar average turnover time as XPB-GFP on locally damaged areas (time at which the equilibrium between damaged area and the rest of the nucleoplasm is re-established). These data argue for a similar dynamic behavior of the three measured TFIIH components within NER and furthermore imply that the association between TTDA-GFP and TFIIH is stronger or longer after UV damage.

Mobility of TTDA-GFP after Transcription Inhibition

This tighter association of TTDA-GFP to TFIIH during repair can be explained in two ways: TTDA is more tightly anchored to TFIIH when (non-specifically) bound to DNA or TTDA is indeed a NER-specific subunit of TFIIH docking with higher affinity to the complex when actively repairing. A standard not NER-related DNA interaction of TFIIH is of course its transient interaction with promoter sequences during transcription initiation. Varying the transcriptional competence of the cells would thus also affect the equilibrium of TFIIH-bound versus free TTDA. To verify this hypothesis, we measure the mobility of TTDA-GFP during inhibition of transcription by DRB (5,6-dichloro-1-beta-D-ribofuranosylbenzimidazole), known to increase overall mobility of XPB-GFP by the reduced number of interactions with transcription initiation complexes [14]. As shown in Figure 6, both TTDA-GFP and XPB-GFP exhibit a similar sensitivity towards DRB in terms of the effect that this drug has on mobility. However, the rate of exchange of molecules over the nuclear pores is not very much changed as could be inferred from the similar fluorescence decline after the initial recovery, suggesting that the equilibrium is not significantly affected by transcriptional interference. Thus, TFIIH binding per se does not affect TTDA pool equilibrium and suggests a more stable association of TTDA to TFIIH, when TFIIH is bound specifically in a NER-dependent reaction.

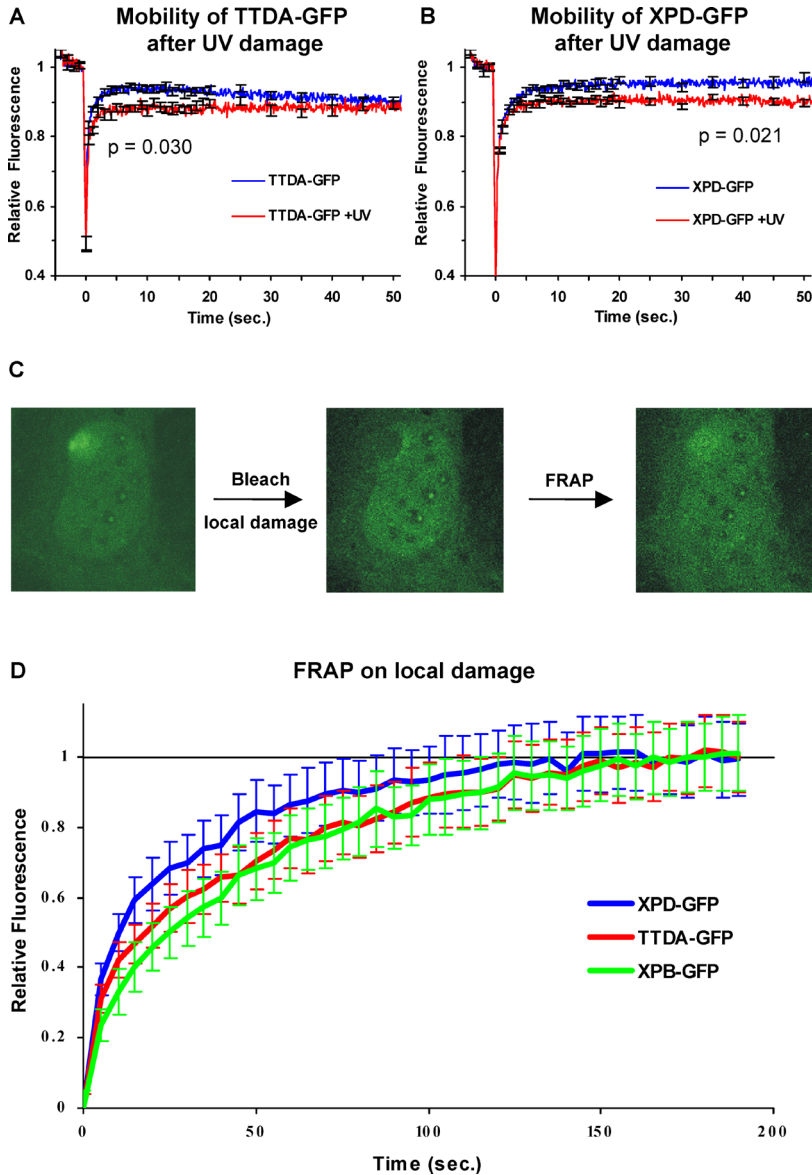


Figure 5. Mobility of TTDA-GFP and XPD-GFP after UV Irradiation

(A) FRAP_abc of TTDA-GFP expressing cells untreated (blue line) and treated with $8\text{J}/\text{m}^2$ UV-C (red line). Error bars are included in the curves, and the p-value has been calculated for the two distinct datasets.

(B) FRAP_abc of XPD-GFP-expressing cells untreated (blue line) and treated with $8\text{J}/\text{m}^2$ UV-C (red line). For each line at least 20 different cells were measured. Error bars are included in the curves, and the p-value has been calculated for the two distinct datasets.

(C) Example of FRAP on local damage. A TTDA-GFP-expressing cell (left panel) containing a locally inflicted UV-damaged spot (shown by the white arrow). The locally damaged area is bleached by applying a high-pulse laser beam (middle panel), and the subsequent recovery of fluorescence is followed in time (right panel).

(D) Curves of FRAP on local damage of TTDA-GFP- (red line), XPD-GFP- (blue line), and XPB-GFP- (green line) expressing cells. FLD, fluorescence measured on local damage; FNLD, fluorescence measured on untreated areas. Error bars are included in the curves.

doi:10.1371/journal.pbio.0040156.g005

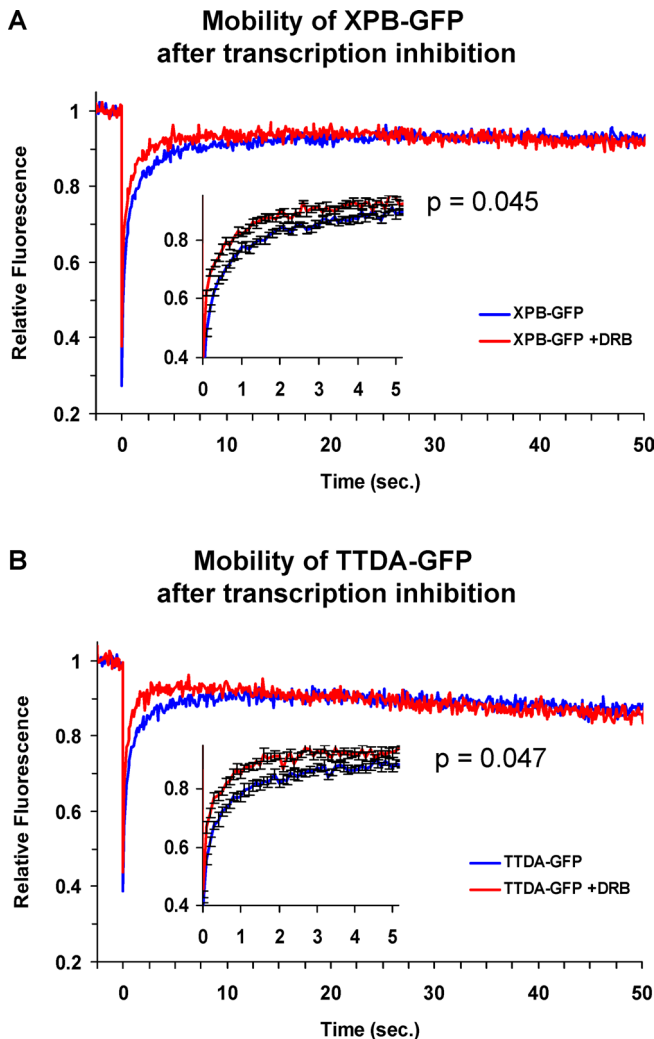


Figure 6. Mobility of XPB-GFP, TTDA-GFP after Transcription Inhibition

(A) FRAP_abc of XPB-GFP-expressing cells untreated (blue line) and treated with dRB (see Materials and Methods) (red line). Inset shows increased time resolution of the curves with error bars. The p-value has been calculated for the two distinct datasets.

(B) FRAP_abc of TTDA-GFP-expressing cells untreated (blue line) and treated with dRB (red line). Inset shows increased time resolution of the curves with error bars. The p-value has been calculated for the two distinct datasets.

doi:10.1371/journal.pbio.0040156.g006

Accumulation of TTDA-GFP on Actinomycin D/488 nm Laser-Induced Damage

Next we tested the effect of actinomycin D (ActD), classically used as a transcription elongation inhibitor but also known to interfere with other DNA transactions [33–35]. In contrast to transcriptional inhibition by DRB, ActD induces an apparent increase of immobilized XPB-GFP (unpublished data), similar to previous observations with RNA polymerase II [36] and the TC-NER specific factor CSB [32]. Upon closer inspection of XPB-GFP mobility after ActD treatment and following fluorescence recovery over a longer time we noticed a surprising increase of fluorescence in the bleached strip, reaching even a higher level than in the non-bleached areas of the nucleus, arguing for locally accumulated TFIIF molecules in the region that was bleached. It is known that photo-activation of intercalated ActD by exposure to blue light (>400 nm), induces a variety of DNA lesions, such as single-strand breaks, oxidative damages, and probably also bulky lesions [37]. It is therefore likely that treatment of cells with ActD and subsequent illumination by 488

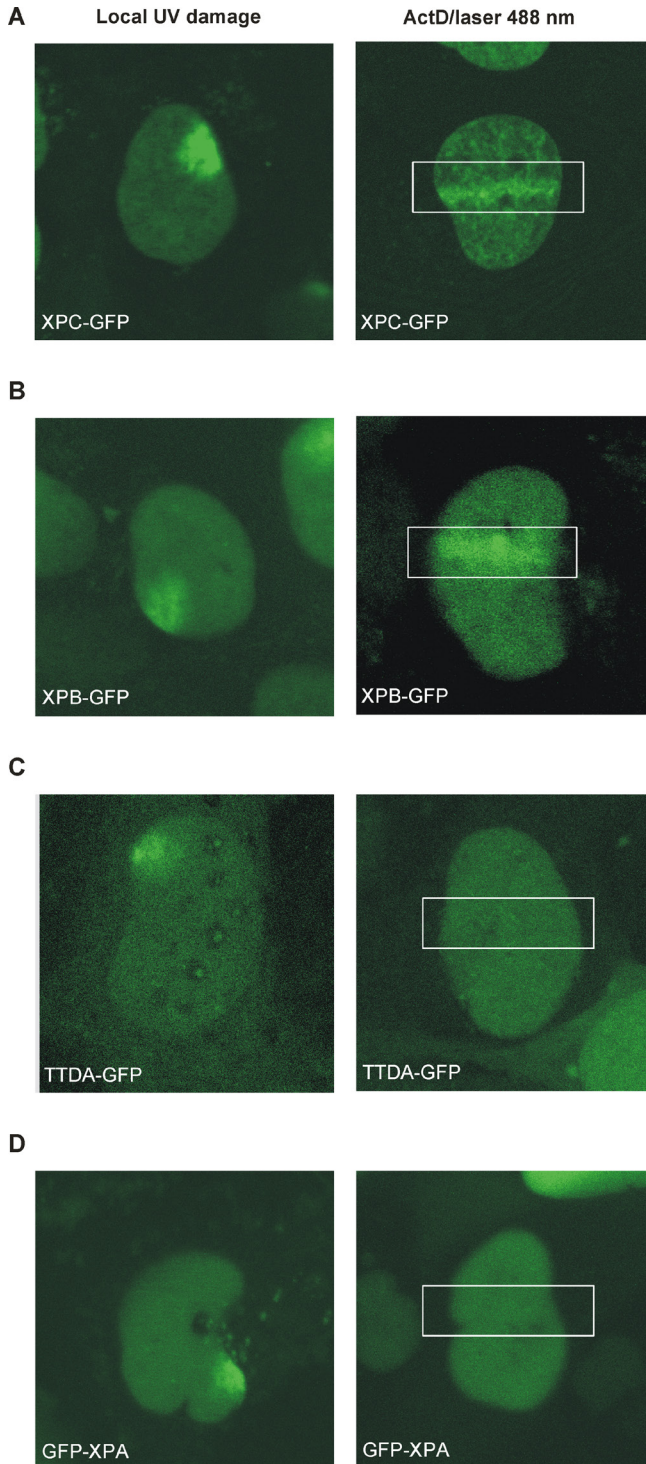


Figure 7. Comparison of Accumulation of NER Proteins on Local UV Damage and on Localized ActD-Photosensitized Laser Damage

(A–D) Left panel, local DNA damage inflicted by UV-C irradiation through a micro-porous filter. Right panel, local laser-induced (488 nm) DNA lesions by photo-sensitization of ActD.

(A) XPC-GFP-expressing cells showing accumulation at local UV-damaged area (left panel) and laser induced ActD-damaged area (right panel).

(B) XPB-GFP expressing cells showing accumulation at local UV-damaged area (left panel) and laser induced ActD-damaged area (right panel).

(C) TTDA-GFP expressing cells showing only accumulation on local UV-damaged area (left panel) but not on laser induced ActD-damaged area (right panel); drawn rectangle corresponds with the irradiated area.

(D) GFP-XPA expressing cells showing only accumulation on local UV-damaged area (left panel) but not on laser induced ActD-damaged area (right panel); drawn rectangle corresponds with the irradiated area.

doi:10.1371/journal.pbio.0040156.g007

nm (i.e. the excitation wavelength of GFP) causes DNA lesions that recruit NER factors. To test this possibility in addition to TTDA-GFP- and XPB-GFP-expressing cells, we also treated XPC-GFP- and GFP-XPA-expressing cells with ActD and locally photo-sensitize the intercalated drug by 488-nm exposure (Figure 7). As shown in Figure 7A (right panel), this treatment induced local accumulation of the GG-NER damage recognizer XPC-GFP in the photo-sensitized area similarly to local UV-damage infliction (by irradiation through a micro-porous filter) (Figure 7A, left panel). XPB-GFP exhibited the same behavior as XPC-GFP (Figure 7B). This indicates that indeed ActD-sensitized DNA is a substrate for XPC binding and the subsequent recruitment of core TFIIH. Remarkably however, TTDA-GFP did not accumulate on this sensitized ActD (Figure 7C, right panel), whereas it was able to accumulate on a more defined NER-inducing lesion introduced by filter UV irradiation (Figure 7C, left panel) [12]. In addition, also GFP-XPA that accumulates on UV-C (Ultraviolet-C) damaged subnuclear regions (Figure 7D, left panel) [31] was not detectably recruited to photo-sensitized ActD-injured DNA (Figure 7D, right panel). These data suggest that only NER factors that act early in the sequential assembly process of NER complexes are recruited to these type of lesions, but do not lead to a complete functional complex. Previously, we have found that also the late factor ERCC1-GFP was not immobilized in ActD-treated cells [32]. To exclude that ActD per se would specifically reduce the overall mobility of TTDA-GFP, impairing the capability of TTDA to assemble at the sites of DNA damage, we performed strip-FRAP_{abc} in ActD-treated TTDA-GFP expressing cells (Figure S3). Although ActD induces partial immobilization of TTDA-GFP (due to transient binding of TFIIH to ActD lesions), the obvious loss of fluorescence at later monitoring time points is indicative for movement of fluorescent molecules over the nuclear membrane. The fact that exchange over the nuclear membrane occurs with the same kinetics as in untreated cells (Figure S3) suggests that binding to TFIIH is not stabilized in sharp contrast to what was observed with UV light. Apparently, this tethering of TTDA to ActD-bound TFIIH is too short to be visualized as a microscopically visible accumulation. Most importantly, these experiments further showed that increased immobilization of core TFIIH on a non-NER lesion did not change TTDA binding to TFIIH, suggesting that lesions that provoke an abortive NER reaction did not induce a more stable association of TTDA to core TFIIH and exclude the option that simply binding of TFIIH to DNA-induced stabilized anchorage of TTDA.

Discussion

TFIIH is implicated in a multitude of DNA-transactions, ranging from basal and activated RNA polymerase II transcription, to ribosomal RNA gene expression, participation in GG-NER and TC-NER, and possibly cell-cycle regulation. The complexity of this factor is also reflected by the dynamic composition of distinct subcomplexes, as well as its multiple enzymatic activities: DNA-dependent ATPases and helicases, kinase, and ubiquitin ligase. Participation in multiple reactions complicates the analysis of specific functions when studied in standard *in vitro* assays. Dynamic regulation of the activity in either one or another process and the existence of different kinetic pools usually escape scrutiny by test tube analysis. Moreover, thermodynamic parameters within mammalian cell nuclei, critical for regulating activity (such as physiologically relevant milieu, high local variations of protein concentrations, and conformation of the DNA substrate), cannot be fully mimicked *in vitro*. Recent developments in cell biology have opened new opportunities for studying complex processes in the most relevant context, i.e. the living cell.

Prior to in depth live cell analysis of protein dynamics, the biological activity

should be carefully checked. In this study we thoroughly analyzed the function of GFP-tagged TTDA. The most pertinent cellular phenotype of TTDA-insufficiency is the NER defect. Remarkably, despite the 4-fold larger size of the tag compared to TTDA itself and the fact that it has to fit in a complex with nine other subunits, that should have numerous interaction partners, TTDA-GFP appeared normally incorporated into TFIIH (Figure 1C), able to restore normal levels of TFIIH in TTD-A cells (Figure 1E and 1F), and to correct the UV-sensitivity (Figure 1B) and RSS after UV irradiation (unpublished data). We conclude that the generated cell line expressing this fluorescently tagged TTDA is a bona fide source to study the actions of this protein.

Subcellular Localization of TFIIH Subunits

In our live cell studies we have shown that TTDA-GFP and XPD-GFP reside both in the cytoplasm and in the nucleus, contrasting to the strictly nuclear localization of XPB. Photobleaching experiments indicated that both proteins do not interact in the cytoplasm. However, application of a newly developed variant of FRAP, FRAP_abc, revealed that TTDA and XPD do interact with TFIIH in the nucleus. In striking contrast to XPB, the association of TTDA to TFIIH (and to a lesser extent also of XPD) is much more dynamic. Previously we found by subcellular fractionation (unpublished data) and others found, by GFP-tagging [27], that endogenous XPD is found in both cytoplasm and nucleus. Santagati and colleagues also find p44 to exist in both cytoplasmic and nuclear fractions [27]. Thus, it is not unprecedented that some of the TFIIH subunits can exist outside of the context of the complex. Assuming that TTDA is not tightly bound to TFIIH (as our results suggest), a small-sized protein, such as free TTDA (8 kDa for the endogenous and 35 kDa for the tagged version), is expected to exchange between nucleus and cytoplasm through the nuclear pores. Hence a cytoplasmic fraction can be observed.

Both TTDA-GFP and XPD-GFP accumulate in nucleolar foci (previously observed in fixed TTDA-HA-expressing fibroblasts [12]). Nucleolar foci co-localize with XPB and p62 in fixed cells and translocate when cells are treated with DRB (unpublished data). This co-localization with the fibrillar nucleolar structure was previously also shown with the other TFIIH component, XPB [13, 14].

TTDA Is Primarily a NER-Specific Factor

Reduced steady-state levels of TFIIH in TTD-A cultured fibroblasts appeared to be a critical determinant in NER efficiency [26], but this lower concentration of the crucial basal transcription factor in cultured cells does not seem to largely affect the transcriptional competence. This suggests that NER requires higher concentrations of TFIIH or that the altered structure of the complex mainly affects the NER function rather than the transcription function. Previous live cell kinetic studies [14] revealed that a relatively large proportion of the resident TFIIH molecules are recruited to NER sites at which they are bound significantly longer (4–5 min) than when bound for an average transcription initiation event (2–10 s). This difference in kinetic behavior of TFIIH when engaged in either transcription or DNA repair provides an explanation why one process is more sensitive to relative enzyme concentrations than the other. Evaluating the cellular UV-response in TTD-A cells presented an apparent discrepancy between the observed severely reduced levels of DNA repair synthesis (reflecting the rate of NER) and the relatively moderate UV sensitivity [9, 26]. Because UV survival reflects a late outcome of UV exposure, whereas DNA repair synthesis provides a snapshot of repair activity, but not its total impact over time these endpoints are not always directly comparable. A low but long-lasting repair activity (as expected when TFIIH concentrations in TTD-A fibroblasts are low) would still in

the end be able to eliminate a substantial fraction of the cytotoxic gene damage, explaining the relatively high UV survival.

The *in vitro* NER studies [29] showed that not only the concentration but also the composition of TFIIH is critical for its function in NER. In the absence of TTDA, only background levels of repair are detected, suggesting that association of TTDA to TFIIH renders this complex more competent for NER at least *in vitro*. A simple model to explain the NER specificity is that TTDA is required for recruiting subsequent NER factors after the loading of core TFIIH at a lesion. A likely NER-specific role for TTDA could thus be that this subunit specifically interacts with subsequent NER factors. However, considering its very small size and that it interacts already with TFIIH it is hard to imagine that there is much space left for additional interactions. Another possibility is that anchorage of TTDA into TFIIH triggers a conformational change that enables recruitment of other NER factors. This latter alternative may also fit with the observation that lack of TTDA makes TFIIH less stable. Improperly folded proteins are usually vulnerable to degradation. Interaction with TTDA might stabilize the complex either by aiding folding (as a chaperone-like function) or by maintaining tertiary structure. Thus this option would bring reduced repair and instability under the same heading.

TTDA Is Not Essential for Cell Viability

The complete absence of TTDA in patients, as deduced from the mutation abolishing the start codon, shows that cell viability is not critically depending on TTDA and on high amounts of TFIIH. This is in striking contrast with deletion mutants of each of the previously known TFIIH subunits, which are not viable in yeast and mammals. Incompatibility with life associated with deletions of TFIIH encoding genes was explained by the vital transcriptional role of TFIIH [38]. Extrapolation of this hypothesis thus argues that TTDA is not essential for the transcription reaction. Coin and coworkers [29] indeed show that *in vitro* TTDA appeared not to stimulate transcription, whereas it was shown to aid NER. However, part of the non-NER-related features observed in patients with TTD-A (such as the brittle hair) are thought to be derived from an effect on the transcription function [39]. This apparent contradiction can be explained by the differential transcriptional program and faith of specific tissues and cell types that are involved in TTD pathology. Previously, it was shown [26] that TTDA mutations do not only affect the NER-function but also affect the stability of TFIIH, thereby reducing the steady-state levels of this complex. Decreased stability of TFIIH will mainly affect steady-state levels in cells in which TFIIH *de novo* synthesis is reduced. Within terminally differentiated cells such as keratinocytes in the hair shaft, a large part of the genome is transcriptionally silent (heterochromatin), except for the final group of abundantly transcribed specialized genes. In these cells, transcription relies on stable TFIIH from earlier differentiation steps. In the absence of TTDA, TFIIH appears unstable, thus this complex may be depleted before the specialized transcription program is finished. Within terminally differentiated keratinocytes, cysteine-rich matrix protein genes are abundantly transcribed. These gene products cross-link keratin filaments and make hair strong. Reduced transcription of this group of genes that are the last to be expressed explains the hallmark feature of TTD, brittle hair. Evidence supporting this model was obtained using a TTD-mutant mouse [40]. Further evidence came from studies revealing decreased β -globin expression in precursor erythrocytes (prior to enucleation a large proportion of the genome is transcriptional silent, except the globin genes) causing thalassemia [41]. Thus, although TTDA may not be essential for *in vitro* transcription [29], reduced stability of TFIIH by TTDA mutations will indirectly affect transcription in highly specialized or terminally differentiated cells. The affected transcription function is

however compatible with sustaining life, though severely affected. Further analysis, by the future generation of a TTDA mouse-model will help to elucidate the molecular basis for the enigmatic clinical features.

Model of Dynamic TTDA Regulation

TTDA can be considered as integral component of TFIIH in biochemical terms ([12] and Figure 1C and 1D), however its association to TFIIH in live cells appeared not as firm as some other components. Under normal culture conditions (relatively low presence of genomic injuries) a dynamic equilibrium between TFIIH-associated and free TTDA is present (Figure 8, schematic cell on the left). In addition, the non-TFIIH bound TTDA molecules can rapidly exchange over the nuclear membrane. Due to its small size this nuclear/cytoplasmic shuttling is likely not an active process but driven by random diffusion. However, exchange over the nuclear membrane is slower than diffusion since it is limited by spatial restrictions (chance of diffusion through a nuclear pore). The fact that a sudden high concentration of DNA lesions by UV-irradiation causes a quick shift in the equilibrium of free versus TFIIH-bound TTDA (Fig 8, right top cell), suggests that this protein is stronger associated or trapped when the complex is actively engaged in NER. The surprising absence of an effect on TTDA when a non-NER photo-sensitized ActD lesion is introduced is remarkable (Figure 8, right bottom cell). We showed that early steps of the NER reaction occur on these 'fake' NER lesions by the efficient loading of the GG-NER initiating factors XPC followed by TFIIH. However, TTDA is not loaded, providing evidence that increased association of TTDA to TFIIH is selective for the presence of NER-specific lesions. Moreover, also subsequent factors as XPA (Figure 7) and ERCC1 [32] were not targeted to these pre-NER complexes. These observations identify TTDA as a primarily NER-dedicated factor, but also provide interesting insight into the NER mechanism. It is tempting to speculate that such lesions trigger the binding of early NER factors, because they induce a DNA conformation resembling a stable helix-distortion and thereby mislead XPC that primarily screens for local distortions. In subsequent steps other aspects of true NER lesions are verified. In the case of photo-sensitized ActD sites, core TFIIH appears to act as a "go or no-go" decision maker in NER. It is possible that the helix-unwinding catalyzed by TFIIH constitutes at least one of the lesion verification steps in normal NER, e.g. when the actual lesion arrests the local unwinding. The extremely high lesion specificity that NER has to achieve (one damage of very wide spectrum of structurally unrelated lesions in more than 106 normal nucleotides) cannot be accomplished in one step [5]. In the case of ActD intercalation no damage in either of the two strands may be present to stop TFIIH unwinding (or ActD may dissociate when the DNA is opened by TFIIH). This lack of a restriction point may destabilize the early NER complex that will be disassembled.

Taken as a whole, our data show that bona fide NER-lesions selectively trigger an increased stability of TTDA within the TFIIH complex in living cells. This behavior highlights a dynamic, NER-dedicated role of TTDA in relation to lesion-specific function of TFIIH. Our work also underscores the highly versatile and surprisingly diverse nature of TFIIH activities enabling it to participate in a remarkable variety of processes.

Materials and Methods

Construction and expression of TTD-A-GFP fusion protein.

Full length TTDA cDNA [12] was cloned in-frame into a pEGFP-N1 vector (Clontech, Heidelberg, Germany), at which the first ATG was mutated, to exclude alternative translation start of GFP itself. In addition, full-length human XPD cDNA was cloned in-frame

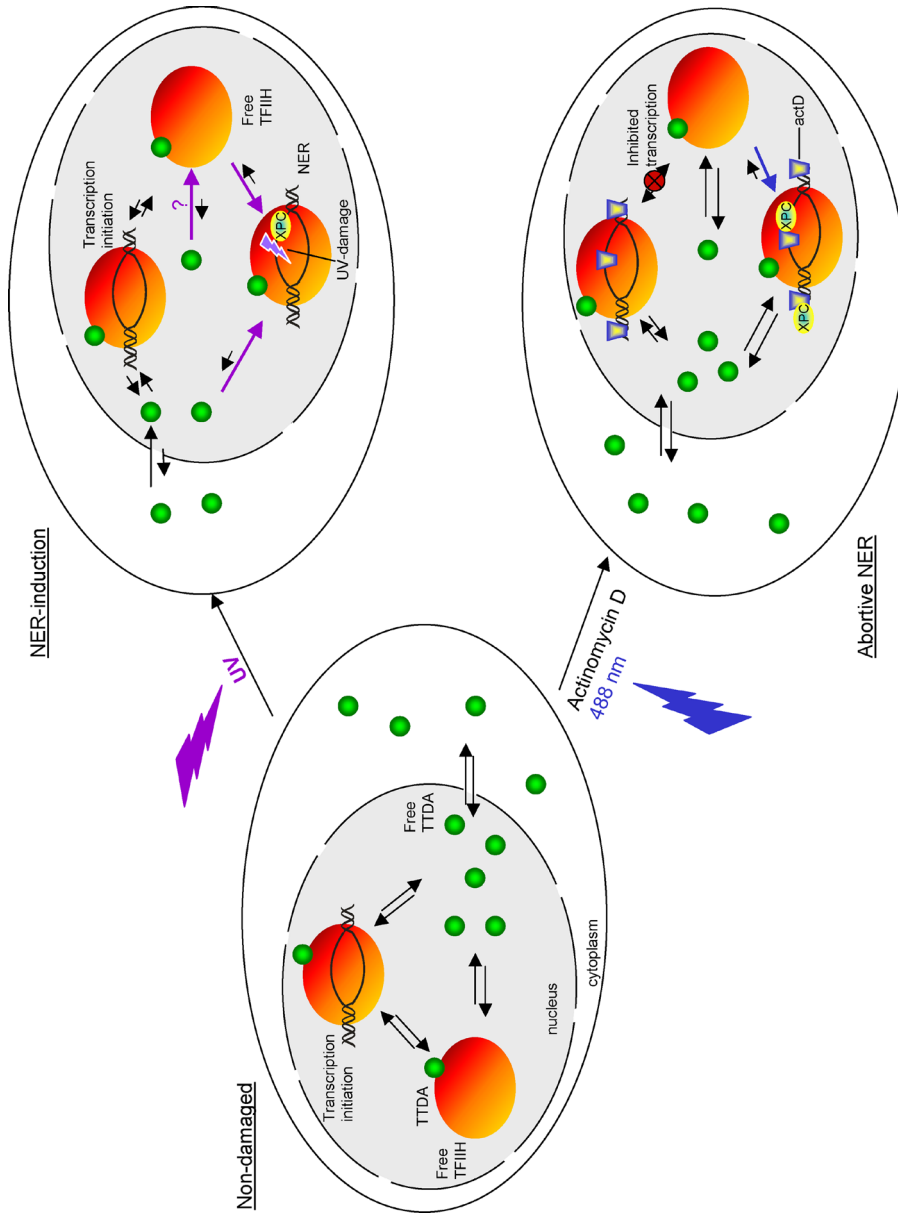


Figure 8. Model of TTDA Binding to TFIIH during Transcription, NER, and Abortive NER

Schematic representation of a mammalian cell with the nucleus in gray and nuclear pores simplified by holes in the membrane. TTDA is represented as a green sphere, TFIIH is depicted as an orange ellipse, and XPC is illustrated as a yellow ellipse. Arrows indicate equilibrium (passage through) over the nuclear pores and equilibrium between different TTDA and/or TFIIH molecules. Colored arrows show the changes in the equilibrium after DNA-damage induction or ActD treatment. In "NER-induction" (right, upper), the UV lesion is depicted as a lightning-sign, in "Abortive NER" (right, bottom), ActD is depicted as a blue trapezoid, and the red cross represents the inhibition of transcription. doi:10.1371/journal.pbio.0040156.g008

into pEGFP-N2 vector (Clontech). Both constructs were sequenced prior to transfection, using Eugene 6 transfection reagent (Roche, Basel, Switzerland), into respectively TTD-A-deficient human fibroblasts (TTD1BR-Sv) and XP-D-deficient human fibroblasts (XP6BE-Sv).

Stably expressing cells were isolated after subsequent rounds of selection; first Neomycin-dominant marker selection using G418, followed by selection on UV-resistance by exposing them three times to a dose of 6 J/m² of UV-C light (254 nm) with 2-d intervals. Next, from these mass populations, stably expressing GFP-fusion protein clones were isolated after single cell sorting using the FACS Vantage (FACS Vantage, Becton Dickinson, Palo Alto, California, United States). Single-cell sorted clones were further analyzed for GFP expression by microscopic evaluation and immunoblot analysis.

Cell culture and specific treatments.

Cell strains used were SV40-immortalized human fibroblasts: TTD1BR-Sv (TTD-A), with and without stably expressing TTDA-GFP; XPCS2B-Sv (XP-B) stably expressing XPB-GFP [14]; XP6BE-Sv (XP-D), with and without stably expressing XPD-GFP; and the NER-proficient cell line (VH10). Cell lines were cultured in a 1:1 mixture of Ham's F10 and DMEM (Gibco, San Diego, California, United States), supplemented with antibiotics and 10% fetal calf serum, at 37 °C, 20% O₂ and 5% CO₂.

Treatment with UV-C was performed using a Philips germicidal lamp. A dose of 8 J/m² was used for total irradiation, and 40 J/m² for local irradiation, through a micro-porous filter [42]. Transcription inhibition was performed by treating the cultured cells with 5,6-dichloro-1-beta-D-ribofuranosylbenzimidazole (DRB, 100 mM) for 3 h. Localized laser-induced damage was achieved by treating the cells with 2 µg/ml of ActD for 1 h. Subsequently, a narrow band across the nucleus was irradiated with 600 pulses of a 488-nm Argon laser at 0.5% laser power (laser power 6.1 A) applied every 100 ms for 1 min. For UV-induced local damage, an isopore polycarbonate filter (Millipore, Billerica, Massachusetts, United States) containing 8-µm diameter pores was used to cover the cells before UV irradiation.

For UV-survival experiments, cells were exposed to different UV-C doses, 2 d after plating. Survival was determined 3 d after UV irradiation by incubation at 37 °C with ³H-thymidine, as described previously [43].

Immunoprecipitations and Western blot analysis.

We prepared whole-cell extracts by isolating cells from six petri dishes (14 cm) per cell line. Cells were washed with phosphate-buffered saline (PBS) before lysing them by douncing (20 strokes using a 12.61-mm dounce homogenizer, Bellco Glass) in 2 ml of buffer A (50 mM Tris [pH 7.9], 150 mM NaCl, 20% glycerol, 0.1% Nonidet-P40, and 5 mM β-mercaptoethanol), supplemented with anti-proteases. Cellular extracts were incubated overnight at 4 °C in buffer A with Rabbit polyclonal antibodies to GFP (Abcam, Cambridge, Massachusetts, United States) and mouse monoclonal p44 (1H5), cross-linked to protein A-sepharose beads (Amersham Biosciences, Little Chalfont, United Kingdom). Before immunoprecipitations, cross-linked beads were washed three times with buffer A. After incubation with the extracts, the cross-linked beads were washed extensively with buffer A. Subsequently, beads were boiled in Laemli SDS-PAGE sample buffer, separated on 11% SDS-PAGE, blotted onto nitrocellulose and analyzed using the following antibodies: anti-XPB (1B3) and monoclonal anti-GFP (Roche).

To analyze expression levels of the fusion proteins we prepared whole-cell extracts by sonication. These were separated on an 11% SDS-PAGE and transferred to 0.45 µm nitrocellulose membranes (Millipore). Expression of the fusion proteins was analyzed by

hybridizing the membranes with a monoclonal anti-GFP (Roche), followed by a secondary antibody (rabbit anti-mouse) conjugated with horseradish peroxidase (Biosource International, Camarillo, California, United States) and detected using enhanced chemoluminescence (ECL+ Detection Kit) (Amersham).

Immunofluorescence assays.

Cells were grown on glass coverslips and fixed with 2% paraformaldehyde at 37 °C. Coverslips were washed with PBS containing 0.1% Triton X-100, three times for 5 min, and subsequently washed with PBS+ (PBS containing 0.15 % glycine and 0.5 % BSA). Cells were incubated at room temperature with primary antibodies (mouse monoclonal anti-XPB, 1:1000, IB3) for 2 h in a moist chamber. Subsequently, coverslips were washed three times with PBS/TritonX-100 and PBS+, incubated 1 h with secondary antibodies, (Cy3-conjugated goat anti-mouse antiserum, Jackson ImmunoResearch Laboratories, Bar Harbor, Maine, United States) at room temperature and again washed three times in PBS/TritonX-100. Samples were embedded in Vectashield mounting medium (Vector Laboratories, Burlingame, California, United States) containing 0.1 mg/ml DAPI (4'-6-diamino-2-phenylindole). Images were obtained by confocal laser scanning microscopy imaging, carried out with a LSM 510 microscope (Zeiss, Oberkochen, Germany).

FRAP procedures.

3 d prior to microscopy experiments, cells were seeded onto 24-mm-diameter coverslips. Imaging and FRAP were performed on a Zeiss LSM 510 meta confocal laser scanning microscope (Zeiss, Oberkochen, Germany).

FRAP analysis was performed at high time resolution [44]. Briefly, a strip spanning the nucleus was photo-bleached for 20 ms at 100% laser intensity (laser current set at 6.1Å). Recovery of fluorescence in the strip was monitored either every 20 ms for 25 s, or every 100 ms for 1 min at 0.5% of laser intensity. Average values from 20 independent measurements were used for every mobility curve. Mobility curves are plotted as relative fluorescence (fluorescence post-bleach divided by fluorescence pre-bleach) measured against time [14, 28, 44]. To determine mobility parameters of only TFIIF-bound TTDA-GFP, we developed a novel adaptation of FRAP, designated FRAP_abc. Mobility measurements were obtained after intense bleach pulses (100% laser intensity) were applied to the cytoplasm for about 2 min for TTD-A-GFP and 4 min for XPD-GFP.

To determine residence times of the different TFIIF components at locally damaged areas, we applied FRAP on local damage. After local irradiation of TTDA-GFP, XPB-GFP, and XPD-GFP fibroblasts with UV-C light, locally damaged areas were photo-bleached during 3 s with 100% laser intensity. Monitoring of the fluorescence recovery was followed by imaging the cell every 5 s for 200 s. A single image was taken prior to the photo-bleaching. Results are expressed by the ratio between damaged area and undamaged area. The first data point after photo-bleaching is set to 0, while final recovery is normalized to 1. Error bars, in the inset of the curves, represent the standard error of the mean. Statistical significance was checked, whenever two distinct curves were not easily dissociable, by using Student's t-test (two-sample, two-tailed) within an appropriate time window: right after the photo-bleaching when evaluating mobility differences or after complete recovery when immobile fractions are being compared.

Supporting Information

Figure S1. Mobility of TTDA-GFP

Mobility of TTDA-GFP in the cytoplasm after bleaching the nuclear pool (red line) compared to the mobility of TTDA-GFP in the cytoplasm without bleaching the nuclear pool (green line). The relative fluorescence (fluorescence post-bleach divided by fluorescence pre-bleach) is plotted against time in seconds.

Figure S2. Mobility of TTDA-GFP after Knocking Down XPC

(A) Scheme of the plasmid used to transfect TTD-A-GFP expressing cells. The construct expresses small-interference RNA against XPC (sequence available upon request), under the control of an H1 (RNA polymerase III) promoter. The plasmid also contains a Mito DsRED_IRES_Hygro transcriptional unit, allowing the selection of transfected clones by the Hygromycin resistance and the mitochondrial DsRED signal.

(B) Example of a TTDA-GFP expressing cell transfected with a mixture of two different XPC small-interference RNA-expressing constructs.

(C) Strip-FRAP_abc of UV-irradiated TTDA-GFP expressing cells knocked-down for XPC (green curve), compared with untreated TTDA-GFP expressing cells (blue curve) and UV-treated TTDA-GFP expressing cells (red curve). Relative fluorescence (fluorescence post-bleach divided by fluorescence pre-bleach) plotted against time in seconds.

Figure S3. Mobility of TTDA-GFP after ActD Treatment

FRAP curve of TTDA-GFP expressing cells untreated (green line) and treated (see Materials and Methods) with ActD (red line). Relative fluorescence (fluorescence post-bleach divided by fluorescence pre-bleach) plotted against time in seconds.

Acknowledgments

We thank Dr. J. M. Egly for kindly providing TFIIH antibodies. We wish to thank Drs. W. van Cappellen and A. Houtsmuller (Optical Image Centre, Erasmus MC, Rotterdam) for help in confocal live cell imaging. We are grateful to Dr. C. Baldeyron for critical reading of the manuscript.

Author Contributions. GGM and WV conceived and designed the experiments. GGM, CM, and AFT performed the experiments. GGM, CM, and POM analyzed the data. DH, JMYN, and CD contributed reagents/materials/analysis tools. GGM, JHJH, and WV wrote the paper.

Funding. This work was supported by NWO (VIDI 917.46.364), ZonMW (project 912.03.012), and ALW/NOW (EMCR-2002–2701). GGM holds an EUR fellowship (Erasmus MC, Rotterdam), and CM holds a fellowship from the Fondation pour la Recherche Médicale (France).

Competing interests. The authors have declared that no competing interests exist.

References

1. Hoeijmakers JH (2001) Genome maintenance mechanisms for preventing cancer. *Nature* 411: 366–374.
2. Wood RD, Mitchell M, Sgouros J, Lindahl T (2001) Human DNA repair genes. *Science* 291: 1284–1289.
3. Riedl T, Hanaoka F, Egly JM (2003) The comings and goings of nucleotide excision repair factors on damaged DNA. *Embo J* 22: 5293–5303.
4. Hanawalt PC (2002) Subpathways of nucleotide excision repair and their regulation. *Oncogene* 21: 8949–8956.
5. Sugasawa K, Ng JM, Masutani C, Iwai S, van der Spek PJ, et al. (1998) Xeroderma pigmentosum group C protein complex is the initiator of global genome nucleotide excision repair. *Mol Cell* 2: 223–232.
6. Mitchell JR, Hoeijmakers JH, Niedernhofer LJ (2003) Divide and conquer: Nucleotide excision repair battles

cancer and ageing. *Curr Opin Cell Biol* 15: 232–240.

7. Lehmann AR (2003) DNA repair-deficient diseases, xeroderma pigmentosum, Cockayne syndrome, and trichothiodystrophy. *Biochimie* 85: 1101–1111.
8. Weeda G, Eveno E, Donker I, Vermeulen W, Chevallier-Lagente O, et al. (1997) A mutation in the XPB/ERCC3 DNA repair transcription gene, associated with trichothiodystrophy. *Am J Hum Genet* 60: 320–329.
9. Stefanini M, Vermeulen W, Weeda G, Giliani S, Nardo T, et al. (1993) A new nucleotide-excision-repair gene associated with the disorder trichothiodystrophy. *Am J Hum Genet* 53: 817–821.
10. Broughton BC, Steingrimsdottir H, Weber CA, Lehmann AR (1994) Mutations in the xeroderma pigmentosum group D DNA repair/transcription gene in patients with trichothiodystrophy. *Nat Genet* 7: 189–194.
11. Ranish JA, Hahn S, Lu H, Yi EC, Li X-J, et al. (2004) Quantitative proteomics analysis of an RNA polymerase II transcription complex identifies TFB5, a new component of general transcription/DNA repair factor IIH. *Nat Genet* 7: 707–713.
12. Giglia-Mari G, Coin F, Ranish JA, Hoogstraten D, Theil A, et al. (2004) A new, tenth subunit of TFIIH is responsible for the DNA repair syndrome trichothiodystrophy group A. *Nat Genet* 36: 714–719.
13. Iben S, Tschochner H, Bier M, Hoogstraten D, Hozak P, et al. (2002) TFIIH plays an essential role in RNA polymerase I transcription. *Cell* 109: 297–306.
14. Hoogstraten D, Nigg AL, Heath H, Mullenders LH, van Driel R, et al. (2002) Rapid switching of TFIIH between RNA polymerase I and II transcription and DNA repair in vivo. *Mol Cell* 10: 1163–1174.
15. Egly JM (2001) The 14th Datta Lecture. TFIIH: From transcription to clinic. *FEBS Lett* 498: 124–128.
16. Rochette-Egly C, Adam S, Rossignol M, Egly JM, Chambon P (1997) Stimulation of RAR alpha activation function AF-1 through binding to the general transcription factor TFIIH and phosphorylation by CDK7. *Cell* 90: 97–107.
17. Wallenfang MR, Seydoux G (2002) cdk-7 Is required for mRNA transcription and cell cycle progression in *Caenorhabditis elegans* embryos. *Proc Natl Acad Sci U S A* 99: 5527–5532.
18. Lee KM, Miklos I, Du H, Watt S, Szilagy Z, et al. (2005) Impairment of the TFIIH-associated CDK-activating kinase selectively affects cell cycle-regulated gene expression in fission yeast. *Mol Biol Cell* 16: 2734–2745.
19. Drane P, Compe E, Catez P, Chymkowitz P, Egly JM (2004) Selective regulation of vitamin D receptor-responsive genes by TFIIH. *Mol Cell* 16: 187–197.
20. Chen D, Riedl T, Washbrook E, Pace PE, Coombes RC, et al. (2000) Activation of estrogen receptor alpha by S118 phosphorylation involves a ligand-dependent interaction with TFIIH and participation of CDK7. *Mol Cell* 6: 127–137.
21. Tirode F, Busso D, Coin F, Egly JM (1999) Reconstitution of the transcription factor TFIIH: Assignment of functions for the three enzymatic subunits, XPB, XPD, and cdk7. *Mol Cell* 3: 87–95.
22. Evans E, Moggs JG, Hwang JR, Egly JM, Wood RD (1997) Mechanism of open complex and dual incision formation by human nucleotide excision repair factors. *Embo J* 16: 6559–6573.
23. Coin F, Marinoni JC, Rodolfo C, Fribourg S, Pedrini AM, et al. (1998) Mutations in the XPD helicase gene result in XP and TTD phenotypes, preventing interaction between XPD and the p44 subunit of TFIIH. *Nat Genet* 20: 184–188.
24. Roy R, Adamczewski JP, Seroz T, Vermeulen W, Tassan JP, et al. (1994) The MO15 cell cycle kinase is associated with the TFIIH transcription-DNA repair factor. *Cell* 79: 1093–1101.
25. Takagi Y, Masuda CA, Chang WH, Komori H, Wang D, et al. (2005) Ubiquitin ligase activity of TFIIH and the transcriptional response to DNA damage. *Mol Cell* 18: 237–243.
26. Vermeulen W, Bergmann E, Auriol J, Rademakers S, Frit P, et al. (2000) Sublimiting concentration of TFIIH transcription/DNA repair factor causes TTD-A trichothiodystrophy disorder. *Nat Genet* 26: 307–313.
27. Santagati F, Botta E, Stefanini M, Pedrini AM (2001) Different dynamics in nuclear entry of subunits of the repair/transcription factor TFIIH. *Nucleic Acids Res* 29: 1574–1581.
28. Houtsmuller AB, Rademakers S, Nigg AL, Hoogstraten D, Hoeijmakers JH, et al. (1999) Action of DNA repair endonuclease ERCC1/XPF in living cells. *Science* 284: 958–961.
29. Coin F, De Santis LP, Nardo T, Zlobinskaya O, Stefanini M, et al. (2006) p8/TTD-A as a repair-specific TFIIH subunit. *Mol Cell* 21: 215–226.
30. Dittrich P, Malvezzi-Campeggi F, Jahnz M, Schwille P (2001) Accessing molecular dynamics in cells by fluorescence

correlation spectroscopy. *Biol Chem* 382: 491–494.

31. Rademakers S, Volker M, Hoogstraten D, Nigg AL, Mone MJ, et al. (2003) Xeroderma pigmentosum group A protein loads as a separate factor onto DNA lesions. *Mol Cell Biol* 23: 5755–5767.
32. Van den Boom V, Citterio E, Hoogstraten D, Zotter A, Egly JM, et al. (2004) DNA damage stabilizes interaction of CSB with the transcription elongation machinery. *J Cell Biol* 166: 27–36.
33. Horwitz KB, McGuire WL (1978) Actinomycin D prevents nuclear processing of estrogen receptor. *J Biol Chem* 253: 6319–6322.
34. Haaf T, Ward DC (1996) Inhibition of RNA polymerase II transcription causes chromatin decondensation, loss of nucleolar structure, and dispersion of chromosomal domains. *Exp Cell Res* 224: 163–173.
35. Casse C, Giannoni F, Nguyen VT, Dubois MF, Bensaude O (1999) The transcriptional inhibitors, actinomycin D, and alpha-amanitin, activate the HIV-1 promoter and favor phosphorylation of the RNA polymerase II C-terminal domain. *J Biol Chem* 274: 16097–16106.
36. Kimura H, Sugaya K, Cook PR (2002) The transcription cycle of RNA polymerase II in living cells. *J Cell Biol* 159: 777–782.
37. Pan JX, Liu Y, Zhang SP, Tu TC, Yao SD, et al. (2001) Photodynamic action of actinomycin D: an EPR spin trapping study. *Biochim Biophys Acta* 1527: 1–3.
38. de Boer J, Donker I, de Wit J, Hoeijmakers JH, Weeda G (1998) Disruption of the mouse xeroderma pigmentosum group D DNA repair/basal transcription gene results in preimplantation lethality. *Cancer Res* 58: 89–94.
39. Dubaele S, Proietti De Santis L, Bienstock RJ, Keriell A, Stefanini M, et al. (2003) Basal transcription defect discriminates between xeroderma pigmentosum and trichothiodystrophy in XPD patients. *Mol Cell* 11: 1635–1646.
40. de Boer J, Andressoo JO, de Wit J, Huijman J, Beems RB, et al. (2002) Premature aging in mice deficient in DNA repair and transcription. *Science* 296: 1276–1279.
41. Viprakasit V, Gibbons RJ, Broughton BC, Tolmie JL, Brown D, et al. (2001) Mutations in the general transcription factor TFIIH result in beta-thalassaemia in individuals with trichothiodystrophy. *Hum Mol Genet* 10: 2797–2802.
42. Mone MJ, Volker M, Nikaido O, Mullenders LH, van Zeeland AA, et al. (2001) Local UV-induced DNA damage in cell nuclei results in local transcription inhibition. *EMBO Rep* 2: 1013–1017.
43. Sijbers AM, van der Spek PJ, Odijk H, van den Berg J, van Duin M, et al. (1996) Mutational analysis of the human nucleotide excision repair gene ERCC1. *Nucleic Acids Res* 24: 3370–3380.
44. Houtsmuller AB, Vermeulen W (2001) Macromolecular dynamics in living cell nuclei revealed by fluorescence redistribution after photobleaching. *Histochem Cell Biol* 115: 13–21.

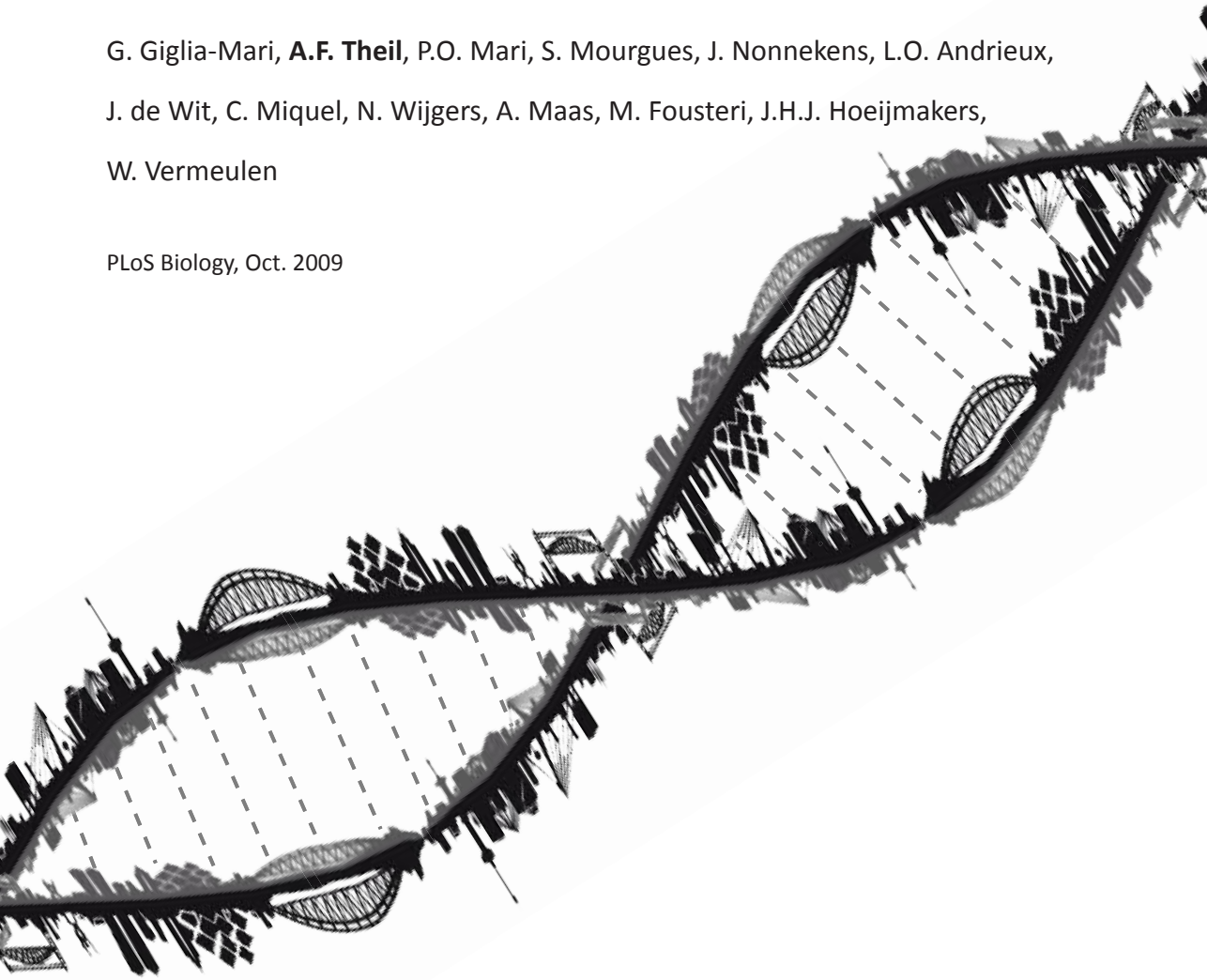


CHAPTER 4

Differentiation Driven Changes in the Dynamic Organization of Basal Transcription Initiation

G. Giglia-Mari, **A.F. Theil**, P.O. Mari, S. Mourgues, J. Nonnekens, L.O. Andrieux,
J. de Wit, C. Miquel, N. Wijgers, A. Maas, M. Fousteri, J.H.J. Hoeijmakers,
W. Vermeulen

PLoS Biology, Oct. 2009



Abstract

Studies based on cell-free systems and on *in vitro*–cultured living cells support the concept that many cellular processes, such as transcription initiation, are highly dynamic: individual proteins stochastically bind to their substrates and disassemble after reaction completion. This dynamic nature allows quick adaptation of transcription to changing conditions. However, it is unknown to what extent this dynamic transcription organization holds for postmitotic cells embedded in mammalian tissue. To allow analysis of transcription initiation dynamics directly into living mammalian tissues, we created a knock-in mouse model expressing fluorescently tagged TFIID. Surprisingly and in contrast to what has been observed in cultured and proliferating cells, postmitotic murine cells embedded in their tissue exhibit a strong and long-lasting transcription-dependent immobilization of TFIID. This immobilization is both differentiation driven and development dependent. Furthermore, although very statically bound, TFIID can be remobilized to respond to new transcriptional needs. This divergent spatiotemporal transcriptional organization in different cells of the soma revisits the generally accepted highly dynamic concept of the kinetic framework of transcription and shows how basic processes, such as transcription, can be organized in a fundamentally different fashion in intact organisms as previously deduced from *in vitro* studies.

Author Summary

The accepted model of eukaryotic mRNA production is that transcription factors spend most of their time diffusing throughout the cell nucleus, encountering gene promoters (their substrate) in a random fashion and binding to them for a very short time. A similar *modus operandi* has been accepted as a paradigm for interactions within most of the chromatin-associated enzymatic processes (transcription, replication, DNA damage response). However, it is not known whether such behavior is indeed a common characteristic for all cells in the organism. To answer this question, we generated a knock-in mouse that expresses in all cells a fluorescently tagged transcription factor (TFIID) that functions in both transcription initiation and DNA repair. This new tool, when combined with quantitative imaging techniques, allowed us to monitor the mobility of this transcription factor in virtually all living tissues. In this study, we show that, in contrast to the aforementioned paradigm, in highly differentiated postmitotic cells such as neurons, hepatocytes, and cardiac myocytes, TFIID is effectively immobilized on the chromatin during transcription, whereas in proliferative cells, TFIID has the same dynamic behavior as in cultured cells. Our study also points out that results obtained from *in vitro* or cultured cell systems cannot always be directly extrapolated to the whole organism. More importantly, this raises a question for researchers in the transcription field: why do some cells opt for a dynamic framework for transcription, whereas others exhibit a static one?

Introduction

Basal transcription/repair factor IID (TFIID) is a ten-subunit complex [1], essential for both RNA polymerase I and II (RNAP1 and 2) transcription initiation and nucleotide excision repair (NER) [2]. NER is an important DNA repair process, which is able to remove a broad spectrum of different DNA lesions. Inherited defects in NER cause severe cancer predisposition and/or premature aging, illustrating its biological significance [3]. In RNAP2

transcription and DNA repair, TFIIH acts as a DNA helix opener, required for transition of initiation to early elongation of RNAP2 and establishment of the preincision NER complex [4],[5]. Mutations in this complex are associated with a surprising phenotypic heterogeneity, ranging from the (skin) cancer-prone disorder xeroderma pigmentosum (XP) to the severe progeroid conditions Cockayne syndrome (CS) and trichothiodystrophy (TTD), the latter additionally characterized by brittle hair and nails [1],[6]–[8]. Since TFIIH is considered to be a general or basal transcription factor and essential NER component, it is surprising to note that TFIIH-associated syndromes present different pathologically affected tissues. For instance, within TTD, primarily differentiated cells appear to be affected. TTD-specific scaly skin and brittle hair features derive from defects in the latest stage of differentiating keratinocytes [9],[10]. In addition, reduced β -globin expression and subsequent anemia in TTD originates from a defective terminal differentiation of precursor erythrocytes [11]. Furthermore, both TTD and XP/CS patients and mice express neurological features caused by defects in final-stage differentiated postmitotic neuronal cells [9],[12]. Nevertheless, many other tissues/organs and cell types appear to be relatively unaffected. This observation can be partly explained by the hypothesis that some tissues are more susceptible than others to endogenous DNA damage [13],[14] and/or that TFIIH transcriptional function is differentially regulated in distinct cell types [15].

Most transcription factors, including basal factors and transcription activators, are only very transiently bound, on the order of a few seconds, to their substrate [16],[17]. This uniformly emerging concept of dynamic transient machineries, with the exception of components of the actual RNAP2 [18], is thought to have a number of advantages over previous proposed models based on stable preassembled large MW “holo” complexes. Live-cell protein mobility studies have culminated in unprecedented, novel insights into the spatial and dynamic organization of macromolecule machines within the context of the complex mammalian cell nucleus with a general, but not universal, modus operandi of dynamic exchange of reaction constituents (proteins). Exceptions to this general mechanism of action have been described for transcriptional activators, such as Gal4 [19] and hypoxia-inducible factor 1 (HIF) [20], and for molecular chaperones such as heat-shock protein 70 [21]. It was found that upon transcription activation these factors reside longer at the transcription sites. Interestingly, the basal transcription factor RNAP2 (GFP-RPB3) was also shown to be longer bound at transcribed regions when transcription was induced [22],[23]. However, it is currently not known whether the generally observed dynamic kinetic framework in *in situ*-cultured cell types for transcription initiation factors, such as TFIIH [24], can be extrapolated to other cell types in the organisms, under ground-state transcriptional conditions.

To study the consequences of different transcriptional programs on the kinetic behavior of TFIIH and further understand the complex phenotypic expression of mutated TFIIH, we created a knock-in mouse model (*Xpb^{y/y}*) that expresses homozygously a YFP (yellow fluorescent protein, a variant of the green fluorescent protein)-tagged TFIIH subunit under control of the endogenous transcriptional regulatory elements. Using this tool, we explored TFIIH binding kinetics directly in different cells and tissues of the organism.

Results

Generation of the XPB-YFP Knock-In Mouse Model

In order to visualize and quantitatively determine dynamic interactions of transcription initiation factor TFIIH within different postmitotic and differentiated cells and living tissues,

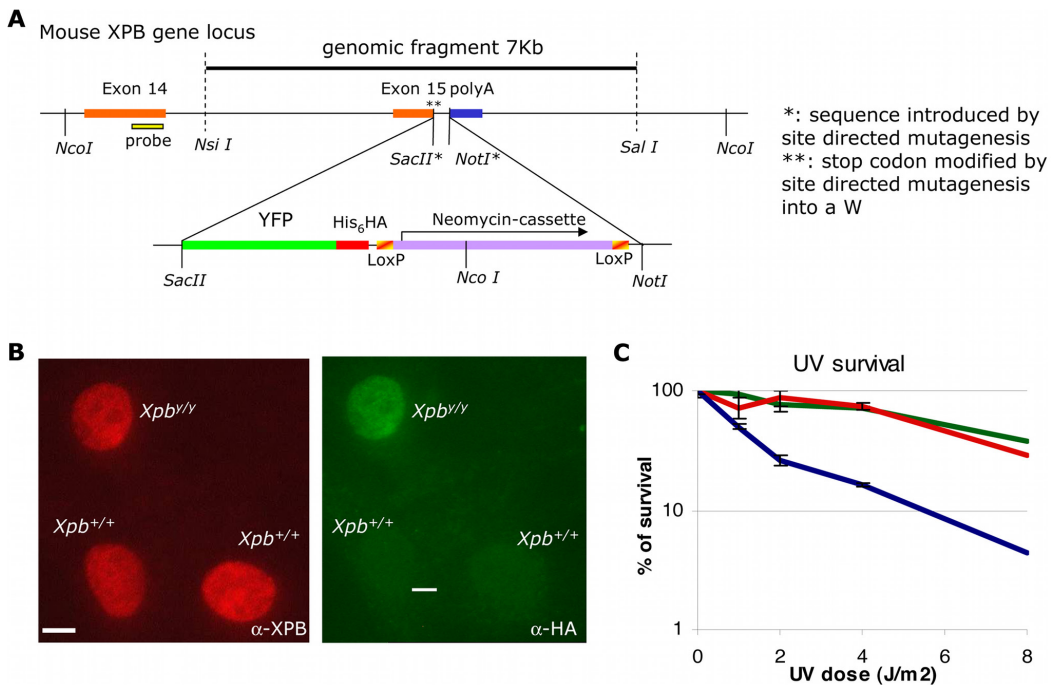


Figure 1. Generation and characterization of a mouse model expressing XPB-YFPHis-HA fused protein.

(A) Schematic presentation of the 3' part of the mouse *Xpb* gene locus, including the last exons 14 and 15. The dotted line indicates the 7-kb mouse genomic DNA fragment used for gene targeting. The translational stop codon (in exon 15) was mutated to allow in-frame fusion with the modified fluorescent marker, YFP (i.e., ATG-less YFP, with an additional stretch of six histidines and an HA epitope tags). As a dominant selectable marker, a neomycin cassette (flanked by two LoxP sites) was introduced downstream the YFP sequence. Details of the targeting strategy are presented in Materials and Methods. (B) Percentage of surviving cells, 48 h after UV irradiation at the indicated doses of dermal fibroblasts isolated from *Xpb*^{+/y} mice (wild-type [wt], green), *Xpb*^{+/y} mice (red), and *Xpb*^{+/y} mice crossed with *Xpc* (NER-deficient) mice (blue). (C) Comparative immunofluorescence of a mixed population of dermal fibroblasts isolated from an untargeted mouse (*Xpb*^{+/+}, HA negative) and a targeted mouse (*Xpb*^{+/y}, HA positive), stained with anti-XPB (red, left) or anti-HA (green, right), which recognizes the XPB-YFP-His6HA protein. Bar: 10 μ m.

doi:10.1371/journal.pbio.1000220.g001

we created a mouse knock-in model that expresses the XPB protein (largest subunit and helicase of the ten-subunit TFIIH complex) tagged at its C-terminus with the yellow GFP variant (YFP). Gene-targeting constructs and strategy are schematically depicted in Figure 1A (see Materials and Methods and Figure S1A for details). Briefly, the targeting strategy was designed in such a way that interference of the genomic organization of the *Xpb* locus was kept to a minimum, keeping the integrity of the promoter, all the intron-exon boundaries, and the 3' UTR (including the endogenous poly A signals) of the *Xpb* gene intact. The XPB-YFP fusion protein further contains additional convenient C-terminal His6- and HA-tags. Embryonic stem (ES) cells transfected with the targeting fusion construct were selected for proper targeting (by homologous recombination) by Southern blotting (Figure S1A). Immunoblotting of whole-cell extracts revealed that an intact XPB-YFP fusion protein was produced in recombinant ES cells (Figure S1B). Selected ES cells were introduced in C57Bl/6 blastocysts and transplanted into foster mothers. Chimeric offspring were further crossed for germ-line transmission of the targeted allele (Figure S1D and S1E).

To avoid any possible interference with expression of the fusion gene by the presence of the dominant selectable NeoMarker in the 3' UTR, heterozygous *Xpb^{y-Neo/+}* mice were crossed with a ubiquitous Cre-Recombinase-expressing mouse model [25] (Figure S1D). The subsequent “floxed” heterozygous offspring (*Xpb^{y/+}*) were intercrossed to generate homozygous knock-in mice (*Xpb^{y/y}*) (Figure S1E). Homozygous *Xpb^{y/y}*, heterozygous *Xpb^{y/+}*, and wild-type (*Xpb^{+/+}*) progeny were obtained in a Mendelian ratio (32 homozygous knock-in mice out of 125 offspring), indicating that homozygosity for the knock-in fusion gene does not impair embryonic development. A small cohort of homozygous (males and females) and heterozygous (six of each) littermates was allowed to age, until natural death, which occurred around 2 years for both *Xpb^{y/y}* and *Xpb^{y/+}* mice. No obvious features of premature aging or spontaneous carcinogenesis of the *Xpb^{y/y}* other than those occurring in *Xpb^{+/+}* mice were observed. Knock-in *Xpb^{y/y}* mice appeared healthy and fertile, indicating that the presence of the fluorescent tag does not significantly interfere with the vital functions (transcription initiation) of the *Xpb* gene.

Most viable, naturally occurring TFIIH mutations cause an overall reduction of the steady-state levels of TFIIH [26]–[28]. However, comparative immunofluorescence revealed that the intracellular concentration of p62 (Figure S2A) (another nontagged TFIIH subunit) and XPB were not altered by the presence of the tagged XPB subunit (Figure 1B) [26]–[28], suggesting that neither the expression nor the stability was affected by the presence of the YFP-His6_HA tag on the XPB protein. Unscheduled DNA repair synthesis capacity (UDS, a measure of NER activity) after UV damage (Figure S2B) and UV-survival of *Xpb^{y/y}* dermal fibroblasts were similar to wild-type (*Xpb^{+/+}*) cells assayed in parallel (Figure 1C), indicating that the tagged XPB protein remains normally active in NER. Immunoprecipitation experiments also showed that the tagged XPB protein was incorporated into TFIIH (unpublished data), consistent with our previous observations that exogenously expressed GFP-tagged XPB is properly incorporated into TFIIH complexes [24].

In conclusion, the addition of the 27-kDa fluorescent tag to the strongly conserved XPB protein does not detectably affect the multiple functions of TFIIH in transcription and NER even at the critical level of an intact organism, whereas single amino acid substitutions in XPB patients give rise to severe skin cancer predisposition and dramatic premature aging [29],[30]. This demonstrates that the *Xpb^{y/y}* knock-in mouse model is a bona fide source to obtain relevant information on the spatial and dynamic organization of transcription and DNA repair in vivo in an intact organism. Fluorescence of TFIIH was detectable in all primary cultures of different cell types isolated from these mice, e.g., ES cells, dermal fibroblasts, and keratinocytes (Figure S2C). Note that the level and subnuclear distribution of fluorescence throughout the cell population is homogeneous (Figure S2C), in striking contrast to the heterogeneous expression characteristic of stably transfected cell cultures.

TFIIH Mobility Is Different in Distinct Living Tissues

To study the spatiotemporal distribution of TFIIH and to determine its kinetic engagements in different cell types within intact tissues, we established organotypic cultures of several organs and tissues. Within organotypic slices of cerebral cortex, isolated and maintained according to established procedures [31], the different cortex layers and the neurons are easily recognizable (Figure S3A). We determined live-cell protein mobility of TFIIH by fluorescence recovery after photobleaching (FRAP) (see Figure 2A, top panel, and Materials and Methods). Using exogenously expressed XPB-GFP, we previously demonstrated that TFIIH in SV40-immortalized human fibroblasts is highly dynamic: the majority moves freely through the nucleus, and a fraction transiently interacts with promoters for only a

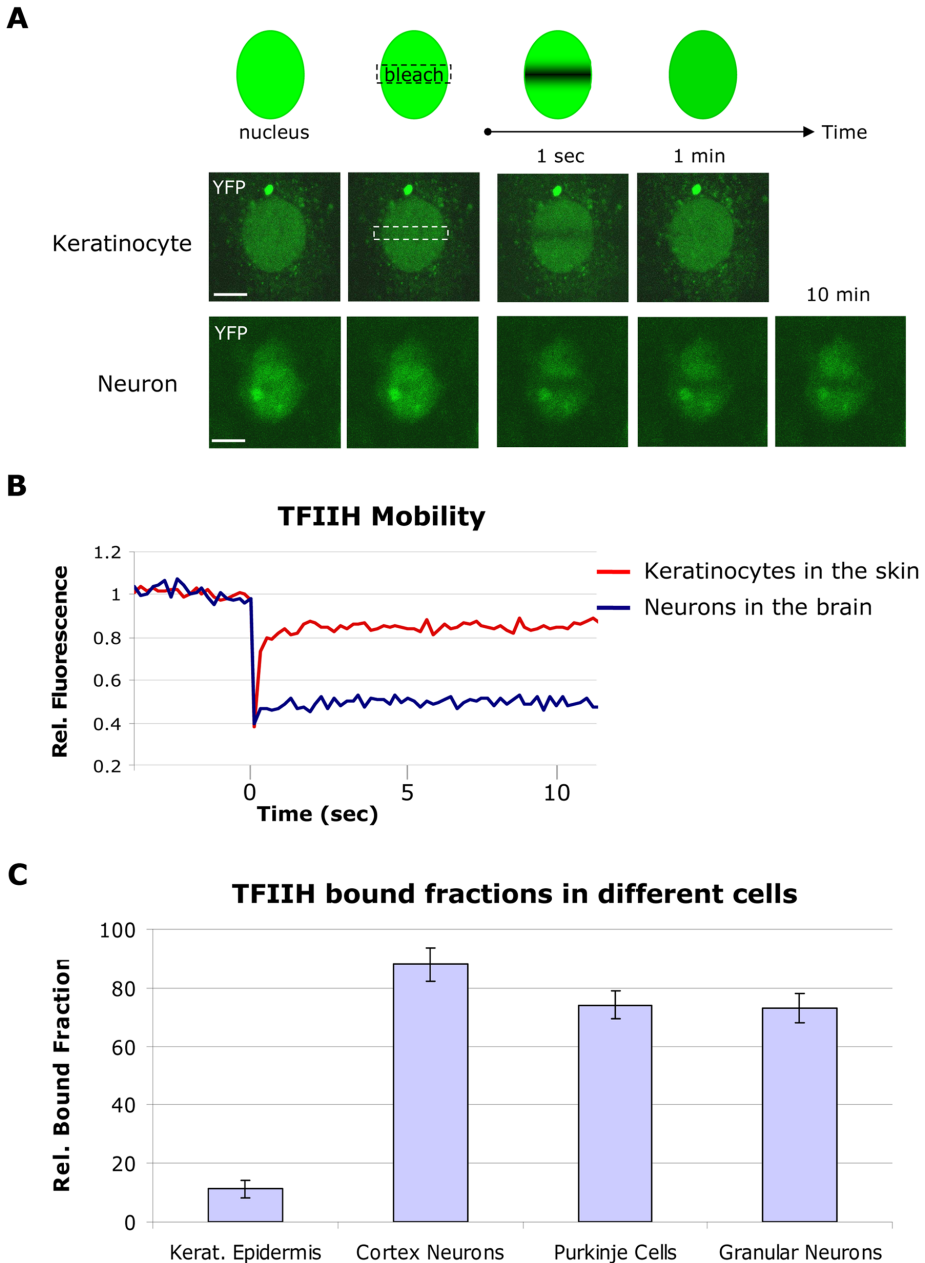


Figure 2. Mobility of TFIIH in cultured cells and in living tissues.

(A) FRAP assay (upper panel) and confocal images of keratinocytes (middle panel) and cortex neurons (lower panel) within tissue sections during FRAP analysis. A small region in the middle of the nucleus is bleached; the subsequent recovery is followed in time for 10 min. Fluorescence is quickly recovered in keratinocytes (less than 10 s; see Figure 2B), whereas in neurons after 10 min, fluorescence in the bleached area is still not fully recovered. Bar: 20 μ m. (B) FRAP graph in which the relative fluorescence (Rel. Fluorescence) recovery after bleaching is plotted against time (seconds). The recovery curve of keratinocytes is shown in red and the curve from cortex neurons in blue. (C) TFIIH bound fractions in different cells, calculated as described in Materials and Methods. Amount of immobilized TFIIH is indicated as percentage of the total amount of TFIIH. Error bars represent the standard error of the mean. Rel.: relative.

doi:10.1371/journal.pbio.1000220.g002

few seconds (2–6 s) [24]. We found a similar high mobility in primary keratinocytes when monitored within the epidermis of skin explants from *Xpb^{y/y}* mice (Figure 2A, middle panel), where fluorescence fully recovered in the bleached strip within a few seconds. In sharp contrast, FRAP on neurons within cerebral cortex slices revealed a striking incomplete fluorescence recovery, even after 60 min postbleaching (Figure 2A, lower panel, and Figure S3B), indicating an unprecedented large (>80%) immobile pool of TFIID (Figure 2B) stably bound to static nuclear structures, most likely chromatin. This unexpected static behavior of a transcription initiation factor, which can be compared to the static behavior of H2B in cultured cells [32], was also observed in Purkinje cells and cerebellar granular neurons in organotypic slices (Figure 2C and Figure S4) suggesting that this behavior is a common feature in various neurons, despite their different functions, chromatin compaction, and different TFIID expression levels (Figure S5A). Moreover, computation of the (squared) Pearson product moment correlation coefficient between measured immobile fractions and single-cell TFIID expression levels showed no significant linear relation between these parameters ($r^2 = 0.062$). We also measured the mobility of nonfused GFP in neurons within organotypic cerebellar slices derived from a mouse that expressed GFP under the control of actin promoter [33]. In contrast to TFIID mobility, GFP itself diffuses very rapidly in neurons (Figure S5B), as was previously found in cultured cells [34],[35]. These results indicate that this static behavior is specific for TFIID and not a common phenomenon of nuclear protein mobility in neurons.

Mobility of TFIID in Neurons Reflects TFIID Cellular Engagement in Transcription

How does TFIID immobilization relate to its multiple biological activities? Obviously, the engagement of TFIID in transcription is most relevant in tissue sections not treated with DNA-damaging agents. However, to exclude that an eventual NER-dependent binding activity could account for the immobilized TFIID in neurons, initiated by a possible high load of endogenously produced lesions, we measured TFIID mobility in NER-deficient mice. For this purpose, we crossed *Xpb^{y/y}* mice with *Xpc^{-/-}*, to generate *Xpb^{y/y}•Xpc^{-/-}* mice. In the absence of XPC, TFIID does not bind damaged DNA [36]. TFIID mobility in neurons from *Xpb^{y/y}•Xpc^{-/-}* mice appeared identical as in neurons derived from NER-proficient mice (Figure 3A and Figure S6), showing that the DNA repair function of TFIID is not responsible for the protracted binding of TFIID. To demonstrate that the transcription function is responsible for TFIID immobilization, we inhibited transcription by treating organotypic brain slices with the RNAP2-specific transcription inhibitor α -amanitin [37]. α -Amanitin blocks the catalytic domain of RNAP2 [38], inhibiting both transcription initiation and elongation. Treatment of organotypic tissues with α -amanitin resulted in a release of immobilized TFIID (Figure 3A and Figure S7), suggesting that the immobilization is due to the transcriptional function of TFIID [17],[24]. In parallel, we verified that the condition used (incubation time and drug concentration) for transcription inhibition in tissues blocked transcription in cultured cells by measuring the BrU incorporation (Figure S8A and S8B). To further prove that the transcriptional engagement of TFIID causes its high immobilization in neurons, we modulated transcription by inducing a cold shock (4°C or 27°C). As with the heat-shock response, cold shock generally induces a reduction in basal transcription and translation and a growth arrest [39]. This response is temporary, since after an adaptation period, cellular metabolism is resumed, although at a lower rate compared to growth at 37°C [40]. Moreover, after cold shock, a change in global expression of genes is observed [41] to allow adaptation to this environmental stress. As shown in Figure 3A and Figure S7, reducing the temperature of organotypic slices to extreme (4°C) and moderate hypothermia values (27°C) for 30 to 60 min fully remobilized

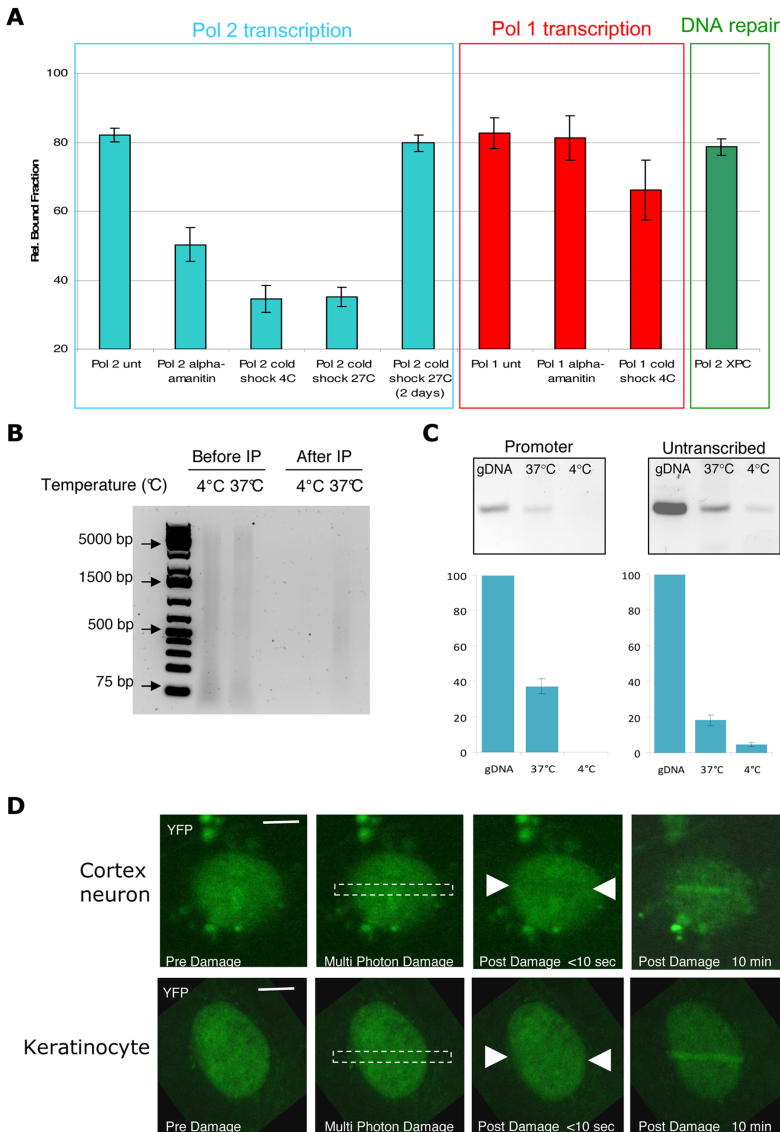


Figure 3. Mobility of TFIID in cortex neurons during transcription and repair.

(A) TFIID bound fractions in cortex neurons from *Xpb^{+/+}* mice treated with α -amanitin (transcription inhibition) or submitted to a cold-shock treatment (4°C or 27°C) for 1 h and 2 d (27°C); the effect on TFIID mobility was compared to the untreated samples (unt). To measure TFIID dynamics during Pol 2 transcription, measurements were conducted in the nucleoplasm (blue square); to measure TFIID dynamics during Pol 1 transcription, measurements were conducted in the nucleoli (red square). TFIID bound fractions were measured in cortex neurons from *Xpb^{+/+}Xpc^{-/-}* (NER-deficient) mice (green square). Error bars represent the standard error of the mean. Rel.: relative. (B) Equal amounts of sonicated chromatin solution were analyzed on SYBR Green-stained agarose gel after proteinase K treatment and reversal of the cross-links (lane 1 and 2). Following sonication, HA-antibody was added to the chromatin solution for immunoprecipitation of TFIID complex. Equal volume of

immunoprecipitated DNA fraction complex was loaded on gel (lane 3 and 4). (C) Semiquantitative PCR on 200 ng of genomic DNA (gDNA) and 200 ng of HA-precipitated chromatin from cortex slice incubated at 37°C and 4°C. Promoter sequence from the *XPB* gene (-143/-274) and untranscribed region adjacent to the *XPB* gene (chr 18: 32479000–32478600) were amplified. PCR products were quantified and plotted on a bar graph: the y-axis represents the percentage of amplified sequences from the HA-precipitated chromatin versus amplified sequences from gDNA. Asterisk (*): undetectable. Error bars have been calculated for three biological replicates. (D) TFIID accumulation after multiphoton laser induction of DNA damage in cortex neurons (upper panel) versus cultured keratinocytes (lower panel). Images are taken before and after the damage at different indicated time points. Bar: 10 μ m.

doi:10.1371/journal.pbio.1000220.g003

TFIIH in neurons. To check whether this is a temporary stress response, we also measured the mobility of TFIIH in neurons embedded in organotypic slices kept at 27°C for 48 h. Under these conditions, TFIIH was found to bind as in untreated organotypic slices (37°C), demonstrating that the remobilization of TFIIH at low temperatures is a rapid (60 minutes at 4°C or 27°C) temporary response, likely reflecting a change in the transcriptional engagement (Figure 3A and Figure S7).

Additionally to RNAP2 transcription, TFIIH has been found to accumulate in nucleoli and participate in RNAP1 transcription [24],[42]. Although the clear TFIIH function in RNAP1 transcription has not been elucidated yet, dynamic studies showed that TFIIH residence time in RNAP2 transcription (2–10 s) is different from RNAP1 transcription (~25 s), suggesting that the role played by TFIIH in these two cellular functions could be slightly different [24]. Cortex neurons and Purkinje cells show a strong localization of TFIIH in nucleoli (Figure S9A), allowing local FRAP analysis in this subnuclear compartment. Similarly to nucleoplasmic TFIIH immobilization (RNAP2 transcription), nucleolar TFIIH immobilization (RNAP1 transcription) was also very high (Figure 3A and Figure S10). In contrast, however, this immobilization is partly resistant to cold shock and resistant to α -amanitin treatment, in line with the expectation, as α -amanitin is known to exclusively inhibit RNAP2 transcription (Figure 3A and Figure S8). To determine that moderate cold shock would indeed inhibit RNAP1 transcription, we measured the amount of pre-rRNA 45S in cold shock-treated cells and tissues (organotypic brain cultures). Surprisingly, cold shock did not alter the amount of 45S, either in cultured cells or in organotypic cortex slices (Figure S9B). The absence of a reduction of the steady-state-levels of 45S rRNA by either a severe (4°C) or a mild (27°C) cold shock is likely explained by the fact that cold shock also interferes with pre-rRNA maturation or degradation. In fact, some proteins, induced by cold shock, have been showed to play a role in preventing the degradation of RNA molecules (reviewed in [43]). In contrast, RNAP1 transcription inhibition induced by actinomycin D (0.1 μ g/ml) led to a clear reduction of the amount of pre-rRNA in cultured cells. In conclusion, our results suggest that TFIIH is highly immobilized in neurons in both RNAP2 and RNAP1 transcription.

As TFIIH is known to be involved in RNAP2 transcription initiation, its transcription-dependent immobilization in neurons predicts a favored binding of TFIIH at promoter sequences. To verify that indeed TFIIH in cortex neurons was bound to promoters of active genes, we performed chromatin immunoprecipitation (ChIP) on adult cortex tissues slices under normal conditions and after cold shock, and measured the proportion of active housekeeping genes (*xpb*, *RnaPolII*) promoter sequences versus adjacent untranscribed areas by semiquantitative PCR (Figure 3C and Figure S9D). As shown by the FRAP experiments (Figure 3A and Figure S7), during cold shock, TFIIH is released from chromatin (Figure 3B). Importantly, we found that TFIIH in cortex slices is more strongly bound to promoter sequences (40% of the input genomic DNA) than to untranscribed areas (19%) (see Materials and Methods for details, Figure 3C and Figure S9D). However, after cold shock, TFIIH is less bound to promoters, clearly showing that cold shock-induced transcription inhibition is associated with remobilization of TFIIH from housekeeping gene promoters.

In view of the notion that the majority of TFIIH is immobilized to chromatin, we wondered whether TFIIH would be available to act in NER after a sudden high dose of genotoxic stress. Since neurons located in the slice are inaccessible to UV-C light, we used multiphoton laser irradiation to locally induce DNA damage [44],[45] in cerebral neurons and compared the accumulation of TFIIH to that observed in skin keratinocytes damaged by the same procedure. Surprisingly, despite the large fraction of immobilized TFIIH,

significant amounts of TFIIH were still recruited to damaged DNA (Figure 3D).

Transcription Organization Varies during Development

Since the observed high TFIIH immobilization is not found in all cell types (Figure 2C), we exploited the availability of an entire organism to analyze the dynamic distribution of TFIIH in different cell types within the context of living tissues (Figure 4A and Figure S11). Specifically in postmitotic and nonproliferative cells (neurons, myocytes, and hepatocytes), we identified a large pool of immobilized TFIIH, whereas in proliferating cells and/or cells that have the capacity to proliferate (intestine epithelium, epidermal keratinocytes, and dermal fibroblasts), TFIIH was found to be highly mobile (Figure 4A and Figure S11). This would suggest that the kinetic organization of this essential transcription factor would be determined by the proliferative capacity of cells. However cultured chondrocytes maintained in a confluent state under low serum were shown to become quiescent (as shown by the absence of the Ki67 marker, Figure S12A) and did not show a difference in TFIIH mobility when compared with proliferative chondrocytes (Figure S12B), suggesting that absence of proliferation is not a condition sufficient to cause a reduction in TFIIH mobility. In view of this result, we investigated whether TFIIH mobility is affected during the establishment of a differentiation-dependent specific transcriptional program. We measured TFIIH mobility during postnatal development of cerebral cortex and liver. Brain and liver were isolated from pups at different postnatal days (PN_d), and TFIIH mobility was measured in cortex neurons and hepatocytes. Remarkably, we observed a progressive TFIIH immobilization during development (Figure 4B and Figure S13) (Figure 4C and Figure S14), which appeared time- and organ-specific. In cortex neurons, TFIIH bound fractions are gradually increasing from PN_d 10 (Figure 4B and Figure S13). TFIIH mobility in neurons is very homogeneous throughout the tested population of cells at each different developmental stage, whereas in liver during development at, e.g., PN_d 6, the kinetic pools differ over the population (see inset, Figure 4C) and becomes homogeneous at later stages. Our results demonstrate that the strong TFIIH binding is a physiological event that takes place during normal development of organs and suggests the establishment of a more fixed transcriptional program than in rapidly growing cells.

Mobility of TFIIH in Differentiated Cells In Vivo and In Vitro

To further investigate differentiation-dependent mobility of TFIIH, we used an in vivo keratinocyte differentiation model. Within the hair shaft, highly differentiated nonproliferative keratinocytes, known as trichocytes [46], can be found. These cells produce the keratins and keratin-associated proteins that form the structure of hairs. Trichocytes are easily recognizable because of their position in the hair and of the melanin inclusions in their cytoplasm (Figure 5A, left panel). Indeed, in trichocytes (Figure 5B and Figure S15), TFIIH mobility is greatly reduced, almost to the same extent as in neurons and myocytes, whereas in other keratinocytes of the hair follicle (bulb) (Figure 5A, right panel), TFIIH is highly mobile (Figure 5B and Figure S15). To substantiate that indeed differentiation is an important determinant for the observed shift in TFIIH mobility, we measured TFIIH mobility during in vitro differentiation. ES cells were nonspecifically differentiated using the hanging drop technique [47]. Through the use of this method, several differentiated cell types can be obtained, organized in morphologically different areas of a developing clone. We measured different cells in several morphologically distinct regions of the differentiated ES clones. In these clones, three distinct TFIIH mobility groups were observed (Figure 5C and Figure S16). The vast majority of cells (~70%) presented a high TFIIH mobility, a second group (~20%) presented an intermediate (~40%) bound fraction

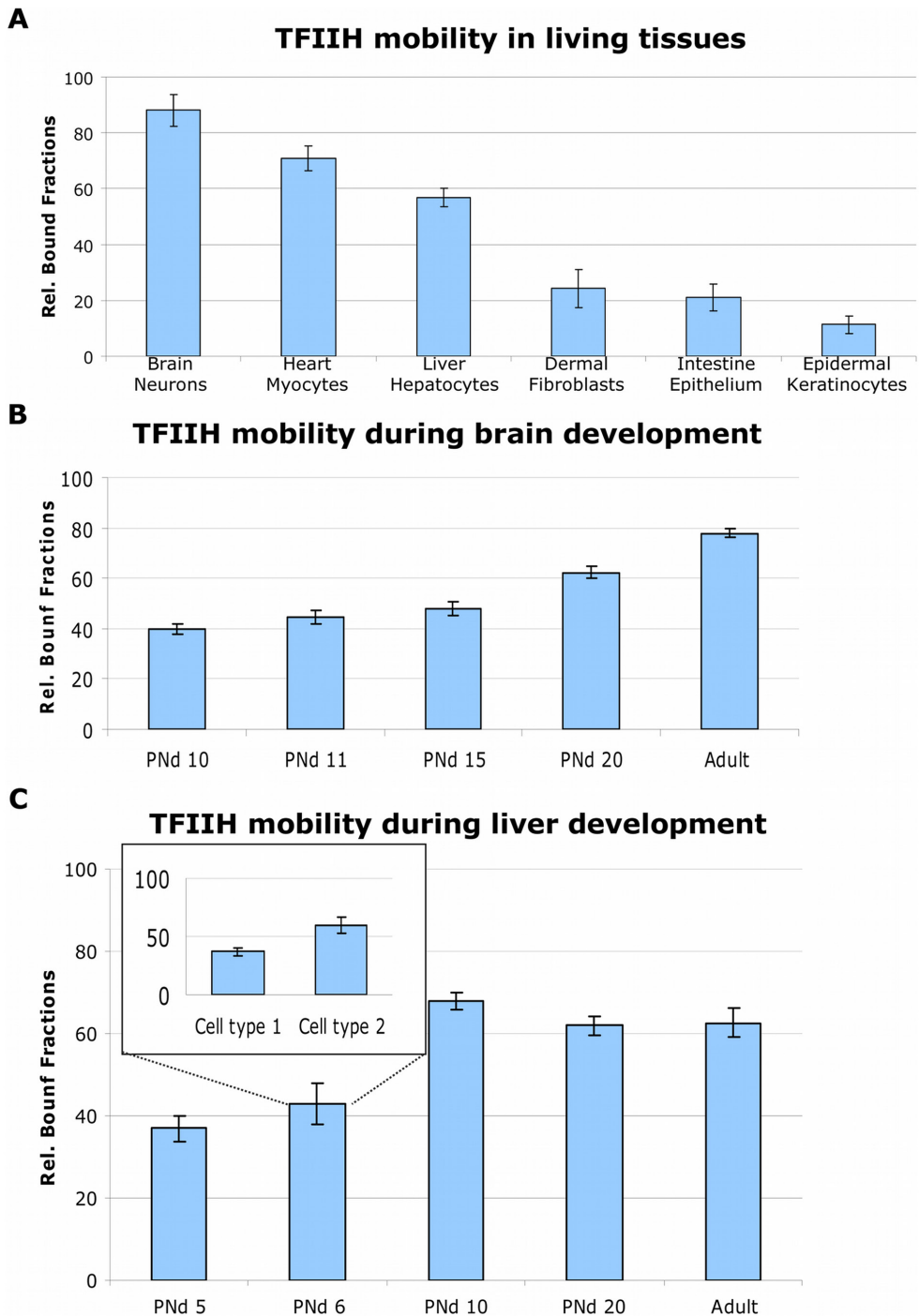


Figure 4. Mobility of TFIIH in different cell types and during development.

(A) TFIIH bound fractions are determined in different (indicated) cell types in their tissue. Rel.: relative. (B) TFIIH bound fractions determined at different stages of brain development. PN_d, postnatal day. (C) TFIIH bound fractions during different stages of liver development. The insert shows two distinct groups of cells having two different levels of TFIIH immobilization. The error bars represent the standard error of the mean. doi:10.1371/journal.pbio.1000220.g004

4

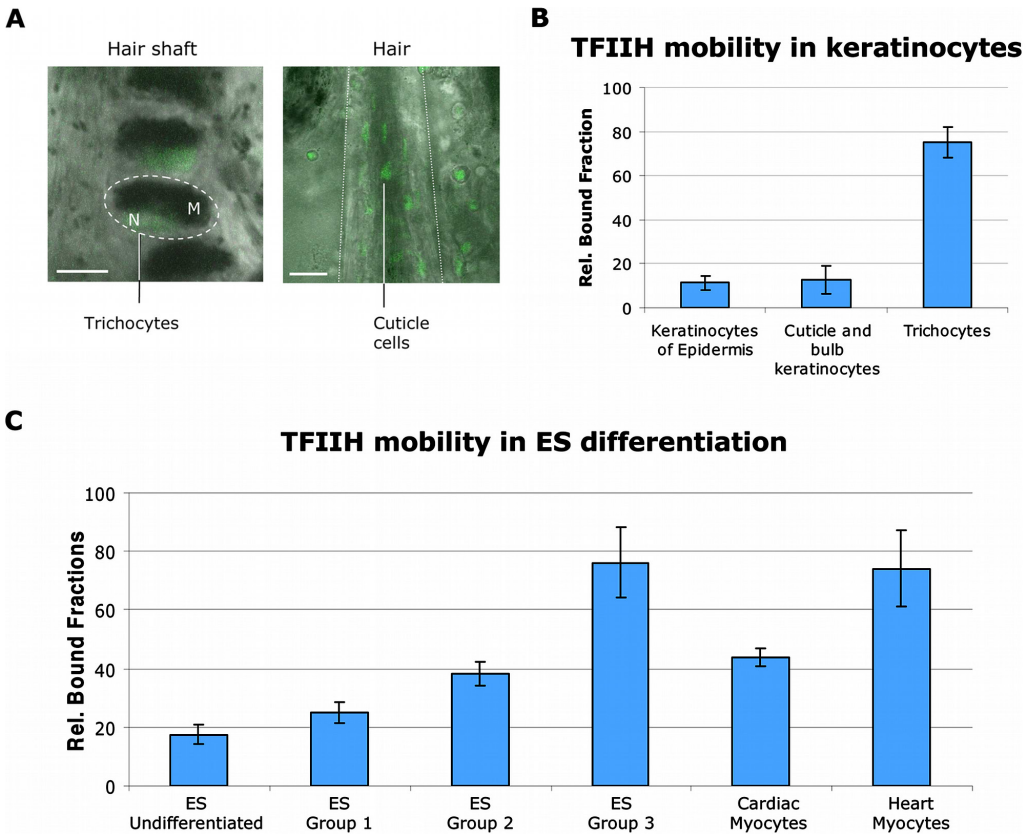


Figure 5. Mobility of TFIIH during in vivo and in vitro differentiation.

(A) Left panel: image (bar: 10 μm) of the hair shaft with trichocytes; the dotted circle indicate the body of a trichocyte. Right panel: image of a hair bulb; the dotted line indicates the limit of the hair (bar: 50 μm). Within the hair shaft, cuticle cells are recognizable. M, cytoplasmic melanin inclusions; N, nucleus. (B) TFIIH bound fractions determined in proliferative and differentiated keratinocytes in the tissue. Rel.: relative. (C) TFIIH bound fractions within different populations of in vitro differentiated ES cells and mature heart myocytes within the heart muscle. The error bars represent the standard error of the mean.

doi:10.1371/journal.pbio.1000220.g005

of TFIIH, and a small fraction of cells (~10%) presented a high TFIIH binding capacity (> than 70%). Postlabeling showed that cells with high TFIIH binding were mainly osteocytes (Figure S17A and S17B). During ES hanging drop differentiation, cardiac myocytes were produced in culture. Morphologically indistinguishable from other cell types, however, cardiac myocytes have the property to beat in vitro, making them easily recognizable, but not easily measurable. Addition of Ca^{2+} -free medium impedes cardiac myocytes beating, allowing measuring of TFIIH mobility in these differentiated cells. In these cells, we measured a TFIIH bound fraction of 43%, an intermediate fraction between the mobility observed in cardiac myocytes in situ and the undifferentiated ES cells. All together, our results show that during cellular differentiation of some cell types (neurons, hepatocytes, osteocytes, thricocytes, and myocytes), the dynamic organization of the basal transcription machinery is radically changed, whereas in other cell types (keratinocytes, fibroblasts, and chondrocytes), the dynamic framework of TFIIH activity is maintained.

Discussion

Previous live-cell studies on complex multifactorial chromatin-associated processes that take place in mammalian cell nuclei, such as transcription, replication, and various DNA repair processes, have disclosed a general model in which highly mobile proteins (process factors) interact with sites of activity (e.g., promoters or DNA lesions) on the basis of stochastic collisions to form transient local machineries in an ordered but highly versatile manner [16],[48],[49]. These biologically relevant novel concepts, however, have been obtained mainly by exogenous expression of tagged factors within highly replicative cells in culture.

In an attempt to study the essential basal transcription initiation factor TFIID within cells embedded in their natural environment (tissue), we designed a mouse model that allows quantitative determination of TFIID dynamics. Using carefully designed targeted integration of the live-cell marker YFP at the *Xpb* locus (expressing the TFIID subunit XPB), we obtained expression of functional YFP-tagged XPB protein under control of the endogenous promoter (guaranteeing physiological expression); we now find evidence for a fundamentally different scenario for the organization of basic transcription initiation in some cell types in the organism. Postmitotic cells (neurons, myocytes, and hepatocytes, etc.) appear to apply a largely static organization of transcription initiation with components being stably bound to chromatin that otherwise in other cell types (fibroblasts, chondrocytes, and keratinocytes, etc.) exchange constantly in a highly dynamic manner. In postmitotic cells, TFIID is bound to promoters with a much longer residence time than in proliferative cells. A possible explanation for this static behavior is that in these postmitotic terminally differentiated cells, a large part of the transcription program is dedicated to a specific subset of genes defining cellular specialty and housekeeping functions, without the need to continuously switch to transcribed genes that are involved in proliferation (cell cycle, replication, and mitosis, etc.). It is possible that regular replication of the genome in proliferating (cultured) cells and tissues causes a continuous resetting of the transcription regulation machinery after each round of cell division and, in parallel, would involve a more open and accessible chromatin conformation.

It is generally accepted that differentiation requires and causes a resetting of the transcriptional program by activating and down-regulating specific genes in response to internal and external stimuli, thereby utilizing lineage-specific transcription activators and/or repressors. However, here, we have identified a novel concept of differentiation-dependent spatio-temporal organization of transcription initiation. This concept implies that transcription initiation factors, such as TFIID, will be bound to promoters much longer in certain cell types than in others (Figure 6). Previously, differences in dynamic associations of lineage-specific transcriptional activators [50],[51] and elongation factors [21],[52] have been linked to activation of transcription. However, the herein described dynamic association of the basal initiation factor TFIID in neurons, hepatocytes, and myocytes is likely not linked to a higher level of transcription than in, for example, keratinocytes, fibroblasts, or ES cells. We propose a model that the observed low mobility of TFIID in highly differentiated postmitotic cells is derived from the establishment of a differentiation- and lineage-specific transcriptional program. However, slow mobility of TFIID is not a general differentiation-dependent phenomenon because in, e.g., fibroblasts, chondrocytes, and keratinocytes, although differentiated, a much higher mobility of TFIID is present. This observation excludes that this phenomenon is caused by a general change in mobility of histones during ES differentiation, as was previously described [53].

The fast TFIID remobilization observed in neurons after a cold shock or the induction

of local DNA damage demonstrates that, within neurons, TFIIH is still able to respond promptly to a “stress situation” that requires a rapid adaptation of the transcriptional program (in the case of the cold-shock response) or to be implicated in DNA repair. Thus remarkably, the static involvement of TFIIH in transcription initiation does not interfere with the flexibility of cells to change the nuclear organization in response to changing conditions. It is of interest to know how multifunctional factors such as TFIIH are still able to switch from one functional role to another and to relocate to other activity sites despite their virtually immobile nature. Further analysis is required to identify which subroute of NER (global genome NER, transcription-coupled NER, or differentiation-associated repair [DAR] [54]) is employed to repair genomic injuries in differentiated cells or whether lesions in permanently inactive sequences are repaired at all. The strategy outlined here has allowed us to address how transcription is organized in fully differentiated tissues or organs and during differentiation and development. Insights into these processes at the level of an intact organism are also relevant for a better understanding of the molecular basis of cancer and aging-related pathology. Importantly, our mouse model can be crossed into different genetic backgrounds, including existing TFIIH mutated mouse models [12],[55], mutated in another TFIIH subunit, i.e., XPD. These mice are associated with a puzzling clinical heterogeneity ranging from cancer predisposition to dramatically accelerated aging [1],[6]–[8],[12]. For instance, investigating TFIIH engagements directly in affected cells (neurons) in living tissues of XP/CS or TTD mice, which harbor a mutation in one of the other TFIIH components (XPD) [56], will help to elucidate the peculiar phenotype observed in these syndromes.

4

Materials and Methods

Ethics Statement

All animal work have been conducted according to Federation of European Laboratory Animal Science Associations (FELASA) ethical requirements and according to the respect of the 3R animal welfare rules.

Generation of the Targeting Construct

The knock-in targeting vector (backbone pGEM5ZF) consisted of an approximately 7 Kb (NsiI/SalI fragment) mouse genomic DNA (isogenic to 129 OLA), which contains the 3' part of the *Xpb* locus. The locus was modified by site-directed mutagenesis (SDM) to transform the stop codon into a coding amino acid (tryptophan) and two unique restriction sites were inserted for cloning purposes (i.e., SacII at the stop codon and NotI at a distance of 20 bp downstream of the SacII site). Between the SacII and NotI, a modified YFP was cloned, the YFP start was modified into a valine to avoid undesired translation of nonfused YFP. The *YFP* gene was further tagged at the C-terminus with a stretch of six histidines and an HA epitope sequence. A unique ClaI site was created 10 bp downstream of the stop codon of the modified YFP to introduce a neomycin gene-expression cassette, flanked by two LoxP sites [57], used as a dominant selectable marker. The dominant marker was inserted in the same transcriptional orientation as the *Xpb* gene.

ES Cell Culture and Gene Targeting

ES cells (129 Ola, subclone IB10) were cultured in BRL-conditioned medium supplemented with 1,000 U/ml leukemia inhibitory factor. A total of 20 µg of the PmeI linearized targeting vector was electroporated into approximately 10⁷ ES cells in 500 µl. Selection with 0.2 µg/ml G418 was started 24 h after electroporation. After 8–10 d, G418 resistant clones were

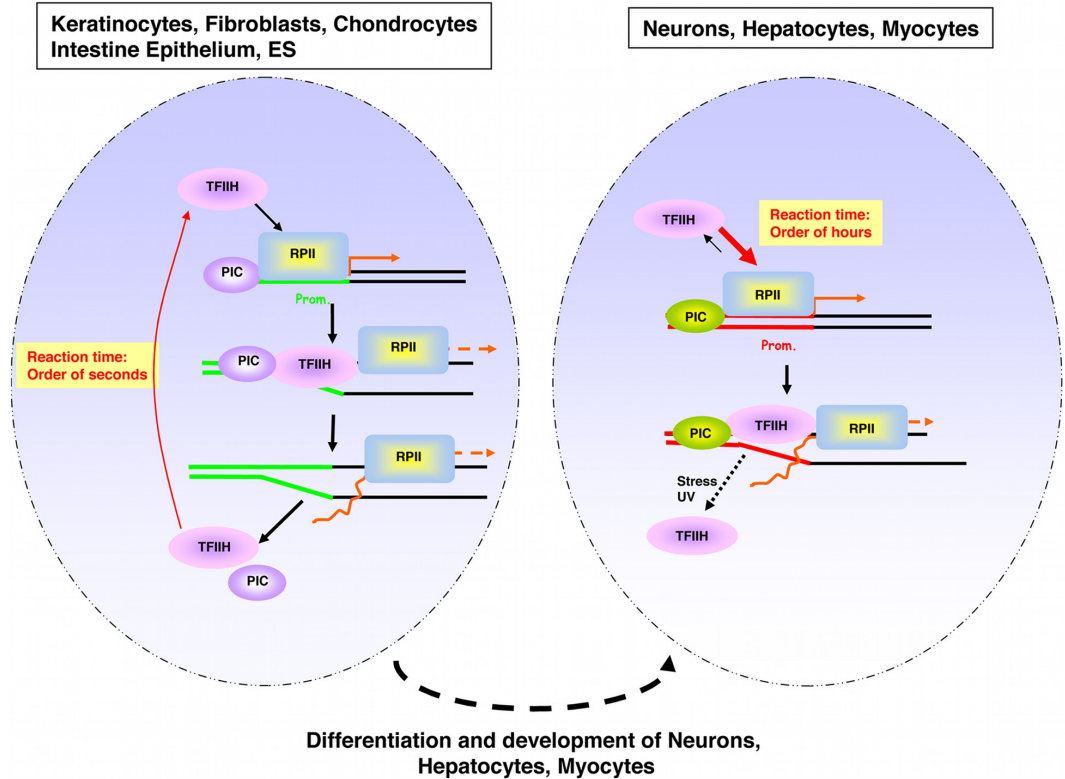


Figure 6. Schematic model of TFIIF switch in mobility during differentiation.

Schematic illustration of the nucleus of a proliferative (left) and a postmitotic (right) cell. Green lines (left) and red lines (right) identify the promoter regions. Orange arrows depict the transcriptional start. PIC represents the preinitiation complex. RPII represents the RNA polymerase II. The arrow width indicates the preferential direction of the equilibrium.

doi:10.1371/journal.pbio.1000220.g006

isolated. Screening for homologous recombinants was performed using DNA blot analyses of *Nco*I-digested DNA with a 400-bp 5' external probe (see Figure 1A and Figure S1A). Out of 128 G418 resistant clones, 12 ES clones had a correctly targeted *Xpb* allele. Two out of the 12 correctly targeted ES clones, checked for proper karyotype, were injected into blastocysts of C57Bl/6 mice and transplanted into B10/CBA foster mothers. Chimeric mice were further crossed, and germline transmission of the targeted allele to offspring was genotyped by PCR using primer sets (as described in Figure S1) and genotyping of offspring was done by PCR (see Figure S1). Primers sequences are available on request.

Mice

The knock-in *Xpb^y* (resulting fusion gene between *Xpb* and *YFP*, coding for XPB-YFP) allele was maintained in both FVB and C57BL/6 backgrounds. We thank P. Vassalli for pCAGGSCre plasmid used to generate the transgenic CAG-Cre recombinase-expressing mice. EGFP-expressing mice were kindly provided by Dr. Okabe [33] and Dr. R. Torensma (Nijmegen).

Cell Culture and Specific Treatments

Murine dermal fibroblasts (MDF) were extracted from *Xpb^{+/+}*, *Xpb^{y/y}*, and *Xpb^{y/y}•Xpc^{-/-}*

mice, following established procedures [58] and cultured in a 1:1 mixture of Ham's F10 and DMEM (Gibco) supplemented with antibiotics and 10% fetal calf serum at 37°C, 3% O₂, and 5% CO₂. To induce in vitro differentiation of XPB-YFP-expressing ES cells, we applied the hanging drop method [47]. Briefly, 20 µl of ES cell suspension (2×10⁵/ml in DMEM [Lonza] with 20% fetal calf serum [Lonza], 50 U penicillin/ml, and 50 µg streptomycin/ml [Lonza], 1% nonessential amino acids [Lonza], 0.1 mM B-mercaptoethanol [Sigma]) were placed on the lids of Petri dishes filled with PBS. After culturing for 3 d, the aggregates were transferred into bacteriological Petri dishes. Two days later, embryoid bodies were placed in Costar six-well plates with gelatin-coated coverslips for further development into different cell tissues. From day 3 on, retinoic acid (10⁻⁸ M) was added to induce skeletal muscle differentiation. Treatment with ultraviolet (UV) light at 254 nm (UV-C) was performed using a Philips germicidal lamp. For UV-survival experiments, cells were exposed to different UV-C doses, 2 d after plating. Survival was determined 3 d after UV irradiation by incubation at 37°C with ³H-thymidine, as described previously [59]. For unscheduled DNA synthesis (UDS), cells were exposed to 8 J/m² of UV-C and processed as described previously [28].

Organotypic Cultures

Organotypic explants of cerebral cortex and cerebellum were produced as previously described [31],[60]. Tissues were analyzed on the same day of extraction in Neurobasal-A (GIBCO) medium, supplemented with antibiotics and B-27 at 37°C, 3% O₂, and 5% CO₂. FRAP analysis on cells within organotypic slices, maintained in culture for 1 wk, gave the same results as when performed on freshly extracted slices. Organotypic slices of heart, liver, and intestine were produced by cutting 300 µm of the organ with a Tissue Chopper (McIlwain). Slices were analyzed within 2 h following preparation, unless differently specified in the text. Skin tissues (epidermis and dermis) were prepared as described [10]. Before imaging, the two layers were mechanically separated and mounted on a coverslip for imaging and analysis.

Immunoblot Analysis

Whole-cell extracts (WCE) of *Xpb*^{+/+} and *Xpb*^{y/y} ES cells were prepared by isolating cells from a semiconfluent Petri dish (10 cm). Cells were washed with phosphate-buffered saline (PBS) and homogenized by sonication. Western blot analysis was performed as previously described [1].

Comparative Immunofluorescence Assays

A mixture of *Xpb*^{+/+} and *Xpb*^{y/y} cells were grown on glass coverslips and fixed with 2% paraformaldehyde at 37°C for 15 min. Immunofluorescence analysis was carried out as previously described [1]. Antibodies used were a rabbit polyclonal anti XPB (1:500, S-19, Santa Cruz Biotechnology), a mouse monoclonal anti-p62 (1:1,000, 3C9, kindly provided by Dr. J. M. Egly), and a rat monoclonal anti-HA (1:1,000, 3F10, Roche).

Fluorescence Recovery after Photobleaching (FRAP) and Calculation of TFIID Bound Fractions

FRAP experiments were performed as described before [24],[61] at high time resolution on a Zeiss LSM 510 meta confocal laser scanning microscope (Zeiss). Briefly, a narrow strip spanning the nucleus of a cell was monitored every 200 ms at 1% laser intensity (30 mW argon laser, current set at 6.5 A, 514-nm line) until the fluorescence signal reached a steady level (after circa 4 s). The same strip was then photobleached for 60 ms at the

maximum laser intensity. Recovery of fluorescence in the strip was then monitored every 200 ms for about 30 s (1% laser intensity). All FRAP data was normalized to the average prebleached fluorescence after removal of the background signal. Every plotted FRAP curve is an average of at least ten measured cells.

To estimate the relative TFIIH bound fractions (BF) from the FRAP measurements, we used the first data point after photobleaching (F_{\min}) as an approximation of the baseline fluorescence recovery (BF = 1), i.e., the fluorescence level in the absence of recovery, when all proteins are considered immobile. We calculated the time-average fluorescence signal taken between 2 and 3.9 s prior to the photobleaching step to obtain the average prebleach fluorescence (F_{pre}), and then between 10 and 15 s to estimate the final fluorescence recovery level (F_{max}). The bound fraction is then given by:

$$\text{BF} = 1 - (F_{\text{max}} - F_{\min}) / (F_{\text{pre}} - F_{\min})$$

We corrected for the photobleached fraction, i.e., the incomplete recovery of fluorescence due to irreversible YFP bleaching during the FRAP procedure, as follows: whole nuclei of cultured keratinocytes were first imaged, subsequently strip-bleached (60-ms photobleach at maximum laser intensity), then imaged immediately after the bleach pulse and again 1 min later when no traces of the bleached strip were observed. The photobleached fraction (PBF) relative to the baseline fluorescence recovery (F_{\min}) was estimated as the average fluorescence intensity loss between the prebleached image ($F_{\text{nucleus}}(\text{pre})$) and the last image of the nucleus ($F_{\text{nucleus}}(\text{last})$):

$$\text{PBF} = 1 - (F_{\text{nucleus}}(\text{last}) - F_{\min}) / (F_{\text{nucleus}}(\text{pre}) - F_{\min}).$$

The corrected bound fraction is then given by:

$$\text{BF}_{\text{corr}} = (\text{BF} - \text{PBF}) / (1 - \text{PBF}).$$

Note: Measuring conditions were designed solely to measure immobile fractions, not diffusion or dissociation constants.

Multiphoton Laser-Induced DNA Damage

Laser-induced DNA damage was conducted as previously described [45]. Briefly, a Coherent Verdi pump laser with a Mira 900 mode locked Ti:Sapphire laser system (Coherent) was directly coupled to a LSM 510 NLO microscope (Zeiss) to obtain an 800-nm pulsed output (200-fs pulse width at 76 MHz, 10 mW output at the sample). Single nuclei targeted with the multiphoton laser received an approximately 250-ms exposure restricted to a 1- μm -wide strip.

Chromatin Immunoprecipitation (ChIP)

The applied ChIP protocol was adapted from previously described methods [62],[63]. Briefly, brain fragments were fixed by adding 11% formaldehyde solution containing 50 mM Hepes (pH 8), 1 mM EDTA, 0.5 mM EGTA, and 0.1 M NaCl to a final concentration of 1% and incubated for 15 min at room temperature and 1 h at 4°C. Cross-linking was stopped by addition of glycine to a final concentration of 0.125 M. Fragments were washed twice with cold phosphate-buffered saline and treated with lysis buffer (50 mM Hepes [pH 8], 140 mM NaCl, 1 mM EDTA, 0.5 mM EGTA, 10% glycerol, 0.5% NP-40, 0.25% Triton X-100) containing 1 mM PMSF and a mixture of protease inhibitors.

Fragments were homogenized (Ultra turrax, T25 basic), and ground on ice with an A-type and B-type glass pestle (20 strokes each) to allow nuclei release. Nuclear suspension was then sheared extensively by sonication on ice to obtain fragments of 200 to 600 bp (as revealed by ethidium bromide staining of aliquots run on agarose gels). For each ChIP reaction, 100 μg of cross-linked chromatin was immunoprecipitated with 0.5 μg of HA-antibody in RIPA buffer (10 mM Tris-HCl [pH 8], 1 mM EDTA, 0.5 mM EGTA, 140 mM NaCl, 1% Triton X-100, 0.1% Na-deoxycholate, 0.1% sodium dodecyl, 1 mM PMSF, and a mixture of protease inhibitors) overnight. The immunocomplexes were collected by adsorption (3 h) to precleared protein G sepharose beads (Upstate) precoated in RIPA containing 0.1 mg/ml sonicated salmon sperm DNA (ssDNA). The beads were then washed twice with 20 volumes of RIPA and once with RIPA containing ssDNA (Sigma), and twice with RIPA containing ssDNA and 0.3 M NaCl. Finally, the beads were washed with 20 volumes of LiCl buffer (10 mM Tris-HCl [pH 8], 1 mM EDTA, 0.5 mM EGTA, 0.25 M LiCl, 0.5% triton X-100, 0.5% Na-deoxycholate, 1 mM PMSF, and a mixture of protease inhibitors), resuspended in RIPA buffer, and divided into two equal parts to analyze coprecipitating proteins and DNA sequences.

DNA Extraction after ChIP and PCR Reaction

For DNA analysis, the immunocomplexes were treated with RNase (5 $\mu\text{g}/\mu\text{l}$) for 30 min at 37°C and by proteinase K (200 $\mu\text{g}/\mu\text{l}$) 3 h at 55°C in 50 mM Tris-HCl (pH 8), 1 mM EDTA, 100 mM NaCl, 0.5% SDS. Formaldehyde cross-links were reverted by heating the samples at 65°C for 6 h. The cross-linked DNA was extracted with phenol:chloroform and precipitated with ethanol in the presence of carrier glycogen. Pellets were resuspended in 30 μl of distilled water. Chromatin-immunoprecipitated DNA was subjected to PCR amplification. PCR was performed using 200 ng (for promoter *XPB* gene amplification) and 100 ng (for untranscribed sequences) of the chromatin immunoprecipitate and 400 nM concentration of both sense and antisense primers (primer sequence available upon request) in a final volume of 25 μl using the PureTaq Ready-to-go PCR beads (GE Healthcare). PCR products were analyzed on 2% agarose7 gels by SYBR Green reagent. Data were analyzed and quantified using Quantity One program (Bio-Rad). For adjustment of amplification efficiency of each primer set, PCR signal intensities from chromatin-immunoprecipitated DNA were normalized to those from the input genomic DNA and expressed as a percentage of the input (gDNA).

RNA Extraction and Reverse Transcriptase PCR Reaction

Brain slices and cultured cells were incubated at 37°C and 4°C. Additionally, cultured cells were incubated with 0.1 $\mu\text{g}/\text{ml}$ of actinomycin D for 2 h. Samples were homogenized in Trizol using the TissueLyser (Qiagen) for 90 s. RNA isolation was performed using the RNeasy Mini Kit (Qiagen). cDNA was produced using 2 μg of RNA with a Reverse Transcription Kit (Invitrogen), random primers (Invitrogen), 1 μg of cDNA, and 400 nM concentration of both sense and antisense primers (primer sequence and PCR cycle available upon request) in a final volume of 25 μl using the PureTaq Ready-to-go PCR beads (GE Healthcare). PCR products were analyzed on 2.5% agarose gels.

Supporting Information

Figure S1. Analysis of the *Xpb* gene targeting. (A) Southern blot analysis of genomic DNA (NcoI digest) from IB10 ES cells (OLA 129) electroporated with the targeting construct (Figure 1A and Materials and Methods) to identify clones with proper gene targeting

by homologous recombination, using a part of exon 14 (*Xpb*) as an external probe (not included in the targeting construct), indicated as a yellow bar. The genomic organization, including relevant restriction sites of both the wild-type (wt) allele and the homologous targeted allele were indicated: exons in orange, *YFP* coding sequence in green, LoxP_Neo_LoxP cassette in purple, and sizes of *NcoI* restriction fragments in red. Untargeted genomic DNA from IB10 ES cells (lane 1) and chromosomal DNA of tails from 129 mouse strain (lane 2) were loaded as control. Twelve homologous recombinant ES cell lines (e.g., in lane 3) out of 128 analyzed G418-resistant transformants were obtained (9% targeting frequency). (B) Immunoblot of total cellular protein extracts from three targeted ES clones (lanes 2–4) and a nontargeted ES clone (lane 1) as negative control was performed using an antibody against the HA tag (3F10, Roche). (C) Scheme of the amplification strategy to identify wt, heterozygous, and homozygous animals. Two sets of primers: set A ($I_{\text{forward}} [I_f] + I_{\text{reverse}} [I_r]$) and set B ($I_{\text{forward}} [I_f] + I_{\text{reverse}} [II_r]$) amplify the untargeted allele (set A) or the targeted allele (set A and B). The size of the fragment amplified by primer set A discriminates the untargeted allele (*Xpb*⁺ allele: 470 bp amplification, upper scheme) from the targeted allele containing the neomycin-resistant marker (*Xpb*^{Neo} allele: >2,500 bp amplification, middle scheme), and from the targeted allele without the NeoMarker (*Xpb*^Y allele: 1,180 bp amplification, lower scheme). (D) Amplification of genomic DNA from untargeted *Xpb*^{+/+} (lane 1), heterozygous *Xpb*^{+/+} (lane 2), and homozygous *Xpb*^{Y/Y} mice (lane 3) after recombining out the LoxP_Neo_LoxP cassette. Lane M: marker. (E) Amplification of genomic DNA from *Xpb*^{+/+} (lane 1 and 2), *Xpb*^{Y-Neo/+} (lane 3 and 4), and *Xpb*^{Y/+} mice (lane 5 and 6). Lane M: marker.

doi:10.1371/journal.pbio.1000220.s001

Figure S2. Characterization of cell expressing fluorescently tagged TFIH (XPB-YFP). (A) Comparative immunofluorescence of a mixed population of dermal fibroblasts isolated from an untargeted mouse (*Xpb*^{+/+}, HA negative) and a targeted mouse (*Xpb*^{Y/Y}, HA positive), stained with anti-p62 (red, left) or anti-HA (green, right), which recognizes the XPB-YFP-His6HA protein. Bar: 10 μm. (B) DNA repair or unscheduled DNA synthesis (UDS); expressed as percentage of wild-type (wt) UDS (NER-proficient cells assayed in parallel) of dermal fibroblasts isolated from *Xpb*^{+/+} mice (wt, green), *Xpb*^{Y/Y} mice (red), and *Xpb*^{Y/Y} mice crossed with *Xpc*^{-/-} (NER-deficient) mice (blue). UDS in *Xpb*^{+/+} was set at 100%. (C) Cultured cells derived from the *Xpb*^{Y/Y} mouse model. The YFP signal and transmission image were merged from a primary cultures of dermal fibroblasts (left panel) and keratinocytes (right panel). Note the uniform expression of TFIH in both cell types. Bar: 20 μm.

doi:10.1371/journal.pbio.1000220.s002

Figure S3. TFIH expression and mobility in neurons. (A) Image of an organotypic tissue slice of cortex brain from *Xpb*^{Y/Y}. Bar: 50 μm. (B) Prolonged time-lapse imaging of a cortex neuron after strip-FRAP. Time scale is expressed in minutes.

doi:10.1371/journal.pbio.1000220.s003

Figure S4. Strip-FRAP graphs used to calculate TFIH bound fractions indicated in Figure 2C. The dotted square indicates the approximate time frame used to calculate the immobile fractions. Mean SEM is the average standard error of the mean calculated over the entire time range of each FRAP curve.

doi:10.1371/journal.pbio.1000220.s004

Figure S5. Mobility of TFIH and free-GFP in neurons from the cerebellum. (A) TFIH

mobility in Purkinje cells and granular neurons in cerebellar organotypic slices. Left upper panel: immunohistochemistry of a cerebellum paraffin-embedded section stained with an HA antibody (brown). Left bottom panel: image of DAPI-stained Purkinje cell and a granular neuron, bar: 10 μm . Right panel: FRAP curve of Purkinje cells (red) and granular neurons (blue), showing the same TFIID in these two different neuron types having different TFIID concentrations and chromatin make-ups. (B) Mobility of free GFP in granular neurons (GN) of the cerebellum from mice that ubiquitously express nontagged GFP. Left panel: image of GFP-expressing GN, the dotted circle indicates the nuclear contour, bar: 5 μm . Right panel: FRAP curve of free GFP (red), indicating that nonfused GFP is freely mobile in GN. doi:10.1371/journal.pbio.1000220.s005

Figure S6. Strip-FRAP graphs used to calculate TFIID bound fractions indicated in Figure 3A, section DNA repair. In blue is TFIID mobility from cortex neurons of *XPBYFP* mice and in red, TFIID mobility from cortex neurons of *XPBYFP* mice crossed into the *XPC* background. The dotted square indicates the approximate time frame used to calculate the immobile fractions. Mean SEM is the average standard error of the mean calculated over the entire time range of each FRAP curve. doi:10.1371/journal.pbio.1000220.s006

Figure S7. Strip-FRAP graphs used to calculate TFIID bound fractions indicated in Figure 3A, section Pol 2 transcription. The dotted square indicates the approximate time frame used to calculate the immobile fractions. Mean SEM is the average standard error of the mean calculated over the entire time range of each FRAP curve. doi:10.1371/journal.pbio.1000220.s007

Figure S8. α -Amanitin transcription inhibition. (A) Confocal imaging of chondrocytes isolated from *Xpb^{yy}* mice, untreated (left panel) and (B) treated (right panel) with α -amanitin. Transcription activity has been measured by incorporating BrU into nascent m-RNA. Anti-BrU (red), YFP (green), and Dapi (Blue). doi:10.1371/journal.pbio.1000220.s008

Figure S9. RNAP1 and RNAP2 transcription in neurons. (A) Image of a cortex neuron within organotypic slice in transmitted light (TL) (left panel) and fluorescent light (middle panel). Bar: 10 μm . Left panel: image shows a cortex neuron within an organotypic brain slice 10 min after bleaching part of the nucleolus. (B) Semiquantitative reverse transcriptase (RT)-PCR of pre-rRNA extracted from organotypic cortex slices and cultured chondrocytes (left panel) and Hela cells (right panel), incubated at different temperatures and treated with actinomycin D. (C) Nuclear extract from the brain was immunoprecipitated with HA-antibodies and subjected to Western blot analysis with the indicated antibodies. The input lanes represent Immunoprecipitation fraction (IP), cleared chromatin (CC) cross-linked extract before IP, supernatant (S) of cross-linked extract after IP. (D) Bar graphs representing the quantification of a semiquantitative PCR on 200 ng of genomic DNA (gDNA) and 200 ng of HA-precipitated chromatin from cortex slice incubated at 37°C and 4°C. Promoter sequence from *Po1* gene (-119/+7) and untranscribed region adjacent to the *Po1* gene (Chr 6: 71937600–71938000). The y-axis represents the percentage of amplified sequences from the HA-precipitated chromatin versus amplified sequences from gDNA, set to 100%. Error bars have been calculated for three biological replicates. doi:10.1371/journal.pbio.1000220.s009

Figure S10. Strip-FRAP graphs used to calculate TFIIH bound fractions indicated in Figure 3A, section Pol 1 transcription. The dotted square indicates the approximate time frame used to calculate the immobile fractions. Mean SEM is the average standard error of the mean calculated over the entire time range of each FRAP curve.

doi:10.1371/journal.pbio.1000220.s010

Figure S11. Strip-FRAP graphs used to calculate TFIIH bound fractions indicated in Figure 4A. The dotted square indicates the approximate time frame used to calculate the immobile fractions. Mean SEM is the average standard error of the mean calculated over the entire time range of each FRAP curve.

doi:10.1371/journal.pbio.1000220.s011

Figure S12. TFIIH mobility in chondrocytes. (A) Confocal imaging of chondrocytes isolated from *Xpb^{+/+}* mice proliferating (left panels) and confluent (right panels). Ki67 immunostaining (in red) was used to confirm the proliferative state of the cells. (B) TFIIH mobility in proliferating (blue) and confluent (red) chondrocytes.

doi:10.1371/journal.pbio.1000220.s012

Figure S13. Strip-FRAP graphs used to calculate TFIIH bound fractions indicated in Figure 4B. The dotted square indicates the approximate time frame used to calculate the immobile fractions. Mean SEM is the average standard error of the mean calculated over the entire time range of each FRAP curve.

doi:10.1371/journal.pbio.1000220.s013

Figure S14. Strip-FRAP graphs used to calculate TFIIH bound fractions indicated in Figure 4C. The dotted square indicates the approximate time frame used to calculate the immobile fractions. Mean SEM is the average standard error of the mean calculated over the entire time range of each FRAP curve.

doi:10.1371/journal.pbio.1000220.s014

Figure S15. Strip-FRAP graphs used to calculate TFIIH bound fractions indicated in Figure 5B. The dotted square indicates the approximate time frame used to calculate the immobile fractions. Mean SEM is the average standard error of the mean calculated over the entire time range of each FRAP curve.

doi:10.1371/journal.pbio.1000220.s015

Figure S16. Strip-FRAP graphs used to calculate TFIIH bound fractions indicated in Figure 5C. The dotted square indicates the approximate time frame used to calculate the immobile fractions. Mean SEM is the average standard error of the mean calculated over the entire time range of each FRAP curve.

doi:10.1371/journal.pbio.1000220.s016

Figure S17. Differentiation markers in ES clones. (A) Transmission light image of a differentiated ES clone stained with Alizarin Red. Red-stained cells and inclusion are characteristically highly mineralized (Ca^{2+} -containing) cells. (B) Transmission light image of a differentiated ES clone stained with alkaline phosphatase. Violet-stained cells are osteocytes producing the enzyme.

doi:10.1371/journal.pbio.1000220.s017

Acknowledgments

We thank Drs. K. Kwikkers, J. M. Y. Ng, C. Andrieu-Soler, X. Bonnefont, N. G. J. Jaspers, and J. Essers for technical assistance and helpful suggestions, and Drs. A. B. Houtsmuller and W. A. van Cappellen (Applied Optical Image Center, Erasmus MC, Rotterdam) for providing confocal live-cell imaging facility.

Author Contributions

The author(s) have made the following declarations about their contributions: Conceived and designed the experiments: GGM WV. Performed the experiments: GGM AFT POM SM LOA JdW NW AM. Analyzed the data: GGM POM. Contributed reagents/materials/analysis tools: POM CM. Wrote the paper: GGM POM JHJH WV.

References

1. Giglia-Mari G, Coin F, Ranish J. A, Hoogstraten D, Theil A, et al. (2004) A new, tenth subunit of TFIIH is responsible for the DNA repair syndrome trichothiodystrophy group A *Nat Genet* 36: 714–719.
2. Egly J. M (2001) The 14th Datta Lecture. TFIIH: from transcription to clinic. *FEBS Lett* 498: 124–128.
3. Mitchell J. R, Hoeijmakers J. H, Niedernhofer L. J (2003) Divide and conquer: nucleotide excision repair battles cancer and ageing. *Curr Opin Cell Biol* 15: 232–240.
4. Dvir A, Conaway R. C, Conaway J. W (1997) A role for TFIIH in controlling the activity of early RNA polymerase II elongation complexes. *Proc Natl Acad Sci U S A* 94: 9006–9010.
5. Hoeijmakers J. H, Egly J. M, Vermeulen W (1996) TFIIH: a key component in multiple DNA transactions. *Curr Opin Genet Dev* 6: 26–33.
6. Bergmann E, Egly J. M (2001) Trichothiodystrophy, a transcription syndrome. *Trends Genet* 17: 279–286.
7. Lehmann A. R (2003) DNA repair-deficient diseases, xeroderma pigmentosum, Cockayne syndrome and trichothiodystrophy. *Biochimie* 85: 1101–1111.
8. Bootsma D, Hoeijmakers J. H (1993) DNA repair. Engagement with transcription. *Nature* 363: 114–115.
9. de Boer J, Andressoo J. O, de Wit J, Huijmans J, Beems R. B, et al. (2002) Premature aging in mice deficient in DNA repair and transcription. *Science* 296: 1276–1279.
10. Backendorf C, de Wit J, van Oosten M, Stout G. J, Mitchell J. R, et al. (2005) Repair characteristics and differentiation propensity of long-term cultures of epidermal keratinocytes derived from normal and NER-deficient mice. *DNA Repair (Amst)* 4: 1325–1336.
11. Viprakasit V, Gibbons R. J, Broughton B. C, Tolmie J. L, Brown D, et al. (2001) Mutations in the general transcription factor TFIIH result in beta-thalassaemia in individuals with trichothiodystrophy. *Hum Mol Genet* 10: 2797–2802.
12. Andressoo J. O, Mitchell J. R, de Wit J, Hoogstraten D, Volker M, et al. (2006) An Xpd mouse model for the combined xeroderma pigmentosum/Cockayne syndrome exhibiting both cancer predisposition and segmental progeria. *Cancer Cell* 10: 121–132.
13. Wijnhoven S. W, Hoogervorst E. M, de Waard H, van der Horst G. T, van Steeg H (2007) Tissue specific mutagenic and carcinogenic responses in NER defective mouse models. *Mutat Res* 614: 77–94.
14. van de Ven M, Andressoo J. O, Holcomb V. B, Hasty P, Suh Y, et al. (2007) Extended longevity mechanisms in short-lived progeroid mice: identification of a preservative stress response associated with successful aging. *Mech Ageing Dev* 128: 58–63.
15. Vermeulen W, Rademakers S, Jaspers N. G, Appeldoorn E, Raams A, et al. (2001) A temperature-sensitive disorder in basal transcription and DNA repair in humans. *Nat Genet* 27: 299–303.
16. Vermeulen W, Houtsmuller A. B (2002) The transcription cycle in vivo. A blind watchmaker at work. *Mol Cell* 10: 1264–1266.
17. Misteli T (2007) Beyond the sequence: cellular organization of genome function. *Cell* 128: 787–800.

18. Kimura H, Sugaya K, Cook P. R (2002) The transcription cycle of RNA polymerase II in living cells. *J Cell Biol* 159: 777–782.
19. Nalley K, Johnston S. A, Kodadek T (2006) Proteolytic turnover of the Gal4 transcription factor is not required for function in vivo. *Nature* 442: 1054–1057.
20. Yu P, Kodadek T (2007) Dynamics of the hypoxia-inducible factor-1-vascular endothelial growth factor promoter complex. *J Biol Chem* 282: 35035–35045.
21. Yao J, Munson K. M, Webb W. W, Lis J. T (2006) Dynamics of heat shock factor association with native gene loci in living cells. *Nature* 442: 1050–1053.
22. Ardehali M. B, Yao J, Adelman K, Fuda N. J, Petesch S. J, et al. (2009) Spt6 enhances the elongation rate of RNA polymerase II in vivo. *EMBO J*.
23. Yao J, Ardehali M. B, Fecko C. J, Webb W. W, Lis J. T (2007) Intranuclear distribution and local dynamics of RNA polymerase II during transcription activation. *Mol Cell* 28: 978–990.
24. Hoogstraten D, Nigg A. L, Heath H, Mullenders L. H, van Driel R, et al. (2002) Rapid switching of TFIIF between RNA polymerase I and II transcription and DNA repair in vivo. *Mol Cell* 10: 1163–1174.
25. Sakai K, Miyazaki J (1997) A transgenic mouse line that retains Cre recombinase activity in mature oocytes irrespective of the cre transgene transmission. *Biochem Biophys Res Commun* 237: 318–324.
26. Andressoo J. O, Jans J, de Wit J, Coin F, Hoogstraten D, et al. (2006) Rescue of progeria in trichothiodystrophy by homozygous lethal Xpd alleles. *PLoS Biol* 4: e322. doi:10.1371/journal.pbio.0040322.
27. Botta E, Nardo T, Lehmann A. R, Egly J. M, Pedrini A. M, et al. (2002) Reduced level of the repair/transcription factor TFIIF in trichothiodystrophy. *Hum Mol Genet* 11: 2919–2928.
28. Vermeulen W, Bergmann E, Auriol J, Rademakers S, Frit P, et al. (2000) Sublimiting concentration of TFIIF transcription/DNA repair factor causes TTD-A trichothiodystrophy disorder. *Nat Genet* 26: 307–313.
29. Weeda G, van Ham R. C, Vermeulen W, Bootsma D, van der Eb A. J, et al. (1990) A presumed DNA helicase encoded by ERCC-3 is involved in the human repair disorders xeroderma pigmentosum and Cockayne's syndrome. *Cell* 62: 777–791.
30. Weeda G, Eveno E, Donker I, Vermeulen W, Chevallier-Lagente O, et al. (1997) A mutation in the XPB/ERCC3 DNA repair transcription gene, associated with trichothiodystrophy. *Am J Hum Genet* 60: 320–329.
31. Stoppini L, Buchs P. A, Muller D (1991) A simple method for organotypic cultures of nervous tissue. *J Neurosci Methods* 37: 173–182.
32. Lever M. A, Th'ng J. P, Sun X, Hendzel M. J (2000) Rapid exchange of histone H1.1 on chromatin in living human cells. *Nature* 408: 873–876.
33. Okabe M, Ikawa M, Kominami K, Nakanishi T, Nishimune Y (1997) 'Green mice' as a source of ubiquitous green cells. *FEBS Lett* 407: 313–319.
34. Yokoe H, Meyer T (1996) Spatial dynamics of GFP-tagged proteins investigated by local fluorescence enhancement. *Nat Biotechnol* 14: 1252–1256.
35. Houtsmuller A. B, Rademakers S, Nigg A. L, Hoogstraten D, Hoeijmakers J. H, et al. (1999) Action of DNA repair endonuclease ERCC1/XPF in living cells. *Science* 284: 958–961.
36. Volker M, Mone M. J, Karmakar P, van Hoffen A, Schul W, et al. (2001) Sequential assembly of the nucleotide excision repair factors in vivo. *Mol Cell* 8: 213–224.
37. Chafin D. R, Guo H, Price D. H (1995) Action of alpha-amanitin during pyrophosphorolysis and elongation by RNA polymerase II. *J Biol Chem* 270: 19114–19119.
38. Bushnell D. A, Cramer P, Kornberg R. D (2002) Structural basis of transcription: alpha-amanitin-RNA polymerase II cocrystal at 2.8 Å resolution. *Proc Natl Acad Sci U S A* 99: 1218–1222.
39. Al-Fageeh M. B, Smales C. M (2006) Control and regulation of the cellular responses to cold shock: the responses in yeast and mammalian systems. *Biochem J* 397: 247–259.
40. Rieder C. L, Cole R. W (2002) Cold-shock and the mammalian cell cycle. *Cell Cycle* 1: 169–175.
41. Sahara T, Goda T, Ohgiya S (2002) Comprehensive expression analysis of time-dependent genetic responses in yeast cells to low temperature. *J Biol Chem* 277: 50015–50021.
42. Iben S, Tschochner H, Bier M, Hoogstraten D, Hozak P, et al. (2002) TFIIF plays an essential role in RNA polymerase I transcription. *Cell* 109: 297–306.

43. Gualerzi C. O, Giuliodori A. M, Pon C. L (2003) Transcriptional and post-transcriptional control of cold-shock genes. *J Mol Biol* 331: 527–539.
44. Meldrum R. A, Botchway S. W, Wharton C. W, Hirst G. J (2003) Nanoscale spatial induction of ultraviolet photoproducts in cellular DNA by three-photon near-infrared absorption. *EMBO Rep* 4: 1144–1149.
45. Mari P. O, Florea B. I, Persengiev S. P, Verkaik N. S, Bruggenwirth H. T, et al. (2006) Dynamic assembly of end-joining complexes requires interaction between Ku70/80 and XRCC4. *Proc Natl Acad Sci U S A* 103: 18597–18602.
46. Bernard B. A (2005) [The biology of hair follicle]. *J Soc Biol* 199: 343–348.
47. Kim C, Lee I. H, Lee K, Ryu S. S, Lee S. H, et al. (2007) Multi-well chip for forming a uniform embryoid body in a tiny droplet with mouse embryonic stem cells. *Biosci Biotechnol Biochem* 71: 2985–2991.
48. Dunder M, Hoffmann-Rohrer U, Hu Q, Grummt I, Rothblum L. I, et al. (2002) A kinetic framework for a mammalian RNA polymerase in vivo. *Science* 298: 1623–1626.
49. Lukas C, Falck J, Bartkova J, Bartek J, Lukas J (2003) Distinct spatiotemporal dynamics of mammalian checkpoint regulators induced by DNA damage. *Nat Cell Biol* 5: 255–260.
50. Laricchia-Robbio L, Tamura T, Karpova T, Sprague B. L, McNally J. G, et al. (2005) Partner-regulated interaction of IFN regulatory factor 8 with chromatin visualized in live macrophages. *Proc Natl Acad Sci U S A* 102: 14368–14373.
51. Ficz G, Heintzmann R, Arndt-Jovin D. J (2005) Polycomb group protein complexes exchange rapidly in living *Drosophila*. *Development* 132: 3963–3976.
52. Yao J, Zobeck K. L, Lis J. T, Webb W. W (2008) Imaging transcription dynamics at endogenous genes in living *Drosophila* tissues. *Methods* 45: 233–241.
53. Meshorer E, Yellajoshula D, George E, Scambler P. J, Brown D. T, et al. (2006) Hyperdynamic plasticity of chromatin proteins in pluripotent embryonic stem cells. *Dev Cell* 10: 105–116.
54. Nospikel T, Hanawalt P. C (2000) Terminally differentiated human neurons repair transcribed genes but display attenuated global DNA repair and modulation of repair gene expression. *Mol Cell Biol* 20: 1562–1570.
55. de Boer J, de Wit J, van Steeg H, Berg R. J, Morreau H, et al. (1998) A mouse model for the basal transcription/DNA repair syndrome trichothiodystrophy. *Mol Cell* 1: 981–990.
56. Broughton B. C, Steingrimsdottir H, Weber C. A, Lehmann A. R (1994) Mutations in the xeroderma pigmentosum group D DNA repair/transcription gene in patients with trichothiodystrophy. *Nat Genet* 7: 189–194.
57. Pluck A (1996) Conditional mutagenesis in mice: the Cre/loxP recombination system. *Int J Exp Pathol* 77: 269–278.
58. Schul W, Jans J, Rijksen Y. M, Klemann K. H, Eker A. P, et al. (2002) Enhanced repair of cyclobutane pyrimidine dimers and improved UV resistance in photolyase transgenic mice. *EMBO J* 21: 4719–4729.
59. Sijbers A. M, van der Spek P. J, Odijk H, van den Berg J, van Duin M, et al. (1996) Mutational analysis of the human nucleotide excision repair gene ERCC1. *Nucleic Acids Res* 24: 3370–3380.
60. Tanaka M, Tomita A, Yoshida S, Yano M, Shimizu H (1994) Observation of the highly organized development of granule cells in rat cerebellar organotypic cultures. *Brain Res* 641: 319–327.
61. Giglia-Mari G, Miquel C, Theil A. F, Mari P. O, Hoogstraten D, et al. (2006) Dynamic interaction of TTDA with TFIIH is stabilized by nucleotide excision repair in living cells. *PLoS Biol* 4: e156. doi:10.1371/journal.pbio.0040156.
62. Compe E, Drane P, Laurent C, Diderich K, Braun C, et al. (2005) Dysregulation of the peroxisome proliferator-activated receptor target genes by XPD mutations. *Mol Cell Biol* 25: 6065–6076.
63. Fousteri M, Vermeulen W, van Zeeland A. A, Mullenders L. H (2006) Cockayne syndrome A and B proteins differentially regulate recruitment of chromatin remodeling and repair factors to stalled RNA polymerase II in vivo. *Mol Cell* 23: 471–482.

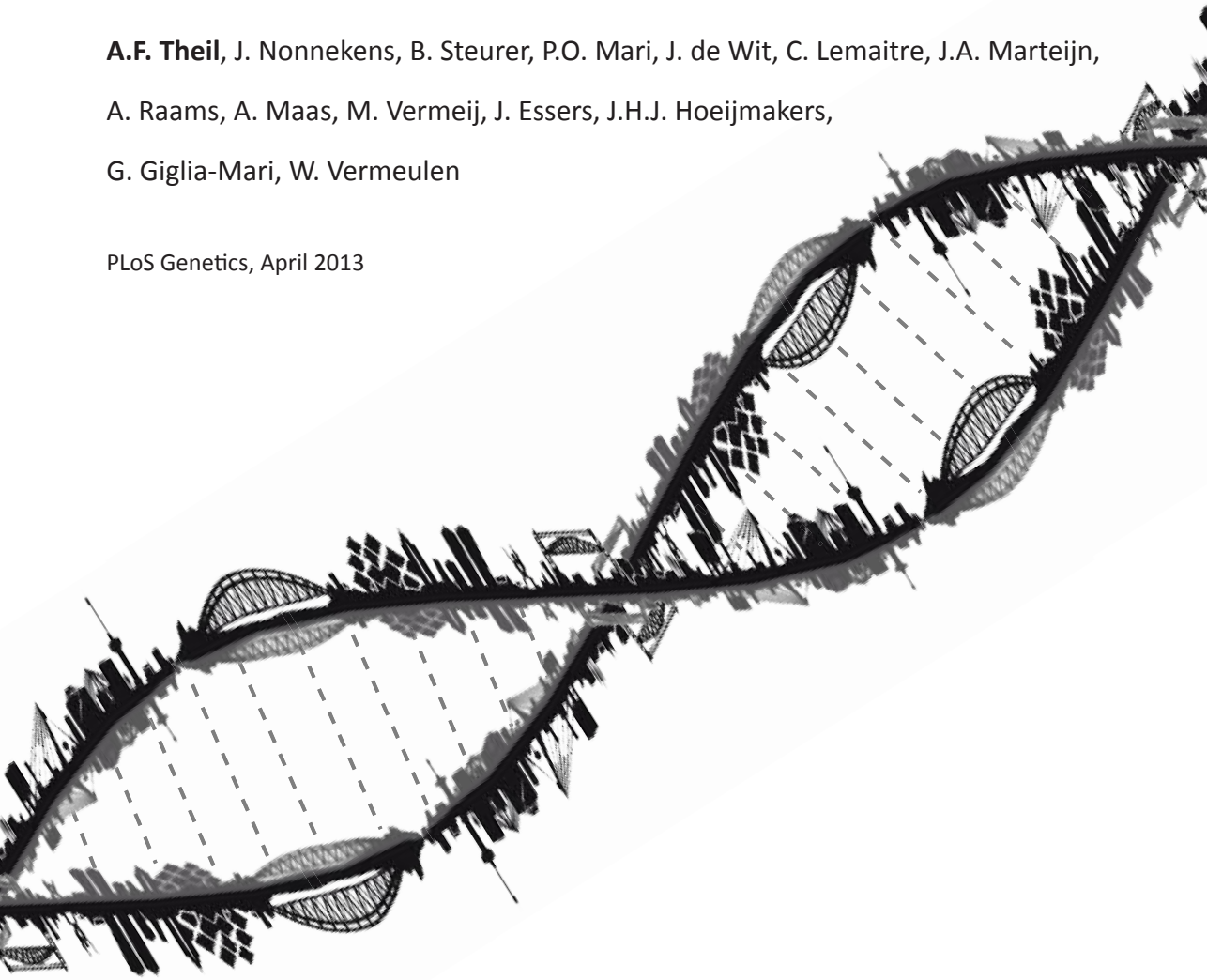


CHAPTER 5

Disruption of TTDA Results in Complete Nucleotide Excision Repair Deficiency and Embryonic Lethality

A.F. Theil, J. Nonnekens, B. Steurer, P.O. Mari, J. de Wit, C. Lemaitre, J.A. Marteijn,
A. Raams, A. Maas, M. Vermeij, J. Essers, J.H.J. Hoeijmakers,
G. Giglia-Mari, W. Vermeulen

PLoS Genetics, April 2013



Abstract

The ten-subunit transcription factor IIH (TFIIH) plays a crucial role in transcription and nucleotide excision repair (NER). Inactivating mutations in the smallest 8-kDa TFB5/TTDA subunit cause the neurodevelopmental progeroid repair syndrome trichothiodystrophy A (TTD-A). Previous studies have shown that TTDA is the only TFIIH subunit that appears not to be essential for NER, transcription, or viability. We studied the consequences of TTDA inactivation by generating a *Ttda* knock-out (*Ttda*^{-/-}) mouse-model resembling TTD-A patients. Unexpectedly, *Ttda*^{-/-} mice were embryonic lethal. However, in contrast to full disruption of all other TFIIH subunits, viability of *Ttda*^{-/-} cells was not affected. Surprisingly, *Ttda*^{-/-} cells were completely NER deficient, contrary to the incomplete NER deficiency of TTD-A patient-derived cells. We further showed that TTD-A patient mutations only partially inactivate TTDA function, explaining the relatively mild repair phenotype of TTD-A cells. Moreover, *Ttda*^{-/-} cells were also highly sensitive to oxidizing agents. These findings reveal an essential role of TTDA for life, nucleotide excision repair, and oxidative DNA damage repair and identify *Ttda*^{-/-} cells as a unique class of TFIIH mutants.

Author Summary

DNA is under constant attack of various environmental and cellular produced DNA damaging agents. DNA damage hampers normal cell function; however, different DNA repair mechanisms protect our genetic information. Nucleotide Excision Repair is one of the most versatile repair processes, as it removes a large variety of DNA helix-distorting lesions induced by UV light and various chemicals. To remove these lesions, the DNA helix needs to be opened by the transcription/repair factor II H (TFIIH). TFIIH is a multifunctional complex that consists of 10 subunits and plays a fundamental role in opening the DNA helix in both NER and transcription. TTDA, the smallest subunit of TFIIH, was thought to be dispensable for both NER and transcription. However, in this paper, we show for the first time that TTDA is in fact a crucial component of TFIIH for NER. We demonstrate that *Ttda*^{-/-} mice are embryonic lethal. We also show that *Ttda*^{-/-} mouse cells are the first known viable TFIIH subunit knock-out cells, which are completely NER deficient and sensitive to oxidative agents (showing a new role for TFIIH outside NER and transcription).

Introduction

DNA-damaging agents are a constant challenge to DNA integrity. A network of DNA-repair systems collectively removes most lesions and safeguards the stability of the genome [1]. Nucleotide excision repair (NER) is one such DNA-repair mechanism capable of removing a wide variety of structurally unrelated DNA helix-distorting lesions, including ultraviolet light (UV)-induced lesions and bulky chemical adducts. Two sub-pathways have been identified: global genome NER (GG-NER), eliminating distorting lesions anywhere in the genome and transcription-coupled NER (TC-NER), focusing only on lesions physically blocking ongoing transcription to permit resumption of gene expression.

DNA repair of helix-distorting lesions requires the helix to be opened at the site of the lesion for efficient incision of the damaged strand [2]. A protein complex essential to this process is basal transcription factor II H (TFIIH). Although TFIIH was initially identified as a general RNA polymerase II transcription initiation factor [3], this multi-subunit complex was subsequently found to have multiple functions: including RNA polymerase I transcription and, activated transcription and cell cycle control [4]–[6]. TFIIH

is composed of two sub-complexes: the 7-subunit core complex comprised of xeroderma pigmentosum group B (XPB), xeroderma pigmentosum group D (XPD), p62, p52, p44, p34 and trichothiodystrophy group A (TTDA), and the associated trimeric CDK-activating kinase (CAK) complex involving CDK7, MAT1 and cyclin H.

Mutations in genes encoding for TFIIH subunits (XPB, XPD and TTDA) are associated with a surprisingly heterogeneous range of UV-sensitive clinical syndromes [7], [8], consistent with its diverse cellular functions. These syndromes include the (skin) cancer prone disorder xeroderma pigmentosum (XP); the severe neurodevelopmental and premature-aging conditions Cockayne syndrome (CS) and trichothiodystrophy (TTD) and combined forms of these syndromes, XP-CS [9] and XP-TTD [10].

TTD is a multi-systemic premature-ageing condition, characterized by brittle hair and nails, ichthyosis, and progressive mental and physical retardation [11]. Within the disease subtype known as photosensitive TTD, three TFIIH-coding genes have been found to be mutated: XPB [12], XPD [13], [14] and TTDA [15].

Cells isolated from TTD-A patients present a reduced amount of TFIIH, suggesting that TTDA plays an important role in stabilizing the whole TFIIH complex [15], [16]. TTDA encodes for an 8 kDa protein that binds to the TFIIH core components XPD and p52 [17], [18]. Although TTDA appears to be the only core TFIIH subunit that is dispensable for mammalian *in vitro* transcription, its presence stimulates RNA synthesis in a reconstituted transcription assay [19]. Moreover, TTDA was originally identified as a component of the yeast transcription pre-incision complex and appeared to have a role in transcription initiation in the presence of an activator [20]. TTDA resides in two cellular fractions: a TFIIH-bound fraction and a free fraction [21]. During engagement in NER, TTDA binds more tightly to TFIIH and possibly plays a role in stabilizing TFIIH on lesions, thereby facilitating the transition between subsequent NER intermediates [21]. The NER-dependent TFIIH-stabilization role can also partly restore the DNA repair deficiency seen in p52 D. melanogaster mutants (Dmp52), when an excess of TTDA molecules are available [19]. TTDA has been thought to be required only to stimulate the helix opening during NER [17]. Up to now, the function of TTDA has been presumed not to be essential for NER but only to make it more efficient [22].

Three mutations within the TTDA gene of three non-related patients with TTD have been identified [15]. Patient TTD99RO carries a homozygous transition mutation at codon 56, converting an Arginine to a stop codon, thereby truncating the C-terminal 15 amino acids (i.e. more than 20%) of the protein. Patient TTD1BR is heterozygous for this allele, the other allele encodes for a transition mutation at codon 21 that converts a conserved Leucine to a Proline. Siblings TTD13PV and TTD14PV carry a homozygous mutation in the ATG start codon, aborting TTDA protein synthesis. Intriguingly, despite the rather diverse clearly severe mutations, these patients are surprisingly similar in their expression of the clinical features [15], [23], [24], consistent with the idea that they all represent null-alleles. Yeast strains with a complete *Ttda* deletion are viable [20], whereas complete absence of the TFIIH subunits XPB and XPD is incompatible with life in both mammals and yeast [25]–[27], likely due to their indispensable role in transcription. Together, this suggests that TTDA is not a vital TFIIH component [15].

Primary fibroblasts from the TTD-A patients described above have been extensively examined. Although these studies have provided valuable information on the NER function of TTDA, they do not provide an accurate explanation for all the observed clinical symptoms observed in the patients. This can be explained by the fact that most disease-specific symptoms are not apparent in fibroblasts but in neuronal tissue and epithelial cells (ichthyosis and brittle hair). Existing mouse models with mutations in TFIIH

components strikingly mimic the clinical symptoms seen in humans [26]–[28] and have provided important information towards our understanding of the molecular and genetic bases of TFIIF-related diseases. Here we describe the generation and analysis of a *Ttda* knock-out (KO) mouse-model to investigate the molecular mechanism that leads to the TTD-specific phenotype. This investigation has shown in fact that TTDA is an essential protein for repair and embryonic development, arguing previous conclusions that needs to be modified.

Results

***Ttda* knock-out mouse model is lethal**

To study the etiology of TTD and the cell-type-specific consequences of TTDA-deficiency, we developed a *Ttda*^{-/-} mouse model. A full KO approach was considered valid, since previous evidence has indicated that TTDA is the sole core TFIIF subunit that is dispensable for viability in yeast [20] and likely also in man [15]. The targeting strategy was designed such that exon 3 (which contains 83% of the *Ttda* coding sequence) was removed and replaced by a neomycin expression cassette, driven by a PGK promoter and flanked by two LoxP sites (referred to as LNL) (Figure 1A).

Following electroporation of the linearized targeting construct into embryonic stem (ES) cells and G418 selection, resistant clones were screened for correct targeting by DNA blotting of *Nhe*I-digested genomic DNA with the indicated 5'probe (Figure 1B). We selected two independent ES clones that had undergone homologous recombination and correct 5' integration and presented a correct karyotype (#J4 and #O8). These clones were injected into C57bl/6 blastocysts to produce chimeric mice with germ-line transmission of the targeted *Ttda* allele (referred to as *Ttda*^{+/-LNL}). Male chimeras were mated to C57bl/6 females to produce *Ttda*^{+/-LNL} heterozygous offspring. Consistent with the autosomal, recessive nature of the human syndrome the *Ttda*^{+/-LNL} mice did not exhibit any obvious phenotype up to the age of 2 years. Both independent mouse lines were used for the generation of *Ttda*^{-/-} mice. Since the *Ttda*^{+/-LNL} mice still harbored the dominant selectable Neo marker which may interfere with the transcriptional expression of neighboring genes, the *Ttda*^{+/-LNL} were crossed with the ubiquitous Cre-recombinase-expressing mouse model [29] to obtain *Ttda*^{-/-} offspring. Subsequently, heterozygous mice were inter-crossed to obtain *Ttda*^{-/-} mice. Genotyping of offspring was performed by PCR analysis using the sequence-specific primers shown in Figure 1A, and as indicated in Figure 1C. Surprisingly however, *Ttda*^{-/-} mice were absent from the large numbers of offspring analyzed (Table 1 and Table S1). It is thus likely that homozygous loss of *Ttda* resulted in embryonic lethality. Additionally, the average litter size observed — when two *Ttda*^{+/-} animals were intercrossed — was much lower than the litter size obtained after crossing of *Ttda*^{+/-} and wild-type (*Ttda*^{+/+}) mice (Table 2), which again points to embryonic loss prior to full gestation. This unexpected lethality seems to contradict with the alleged non-vital function of TTDA in the human situation [15]. Moreover, this lethality is independent of the genetic background of the mouse strain used, since matings of *Ttda*^{+/-} neither in C57bl/6 or in FVB background produced viable offspring. Isolated embryos from early pregnancy revealed a normal Mendelian distribution. We observed a progressive loss of phenotypically normal homozygous *Ttda*-deficient embryos during later stages of gestation. *Ttda*^{-/-} embryos that do survive up to 19.5 days of gestation show delay in development and have a reduction in size and body-weight (data not shown). Since we were unable to obtain *Ttda*^{-/-} mice we attempted to isolate viable *Ttda*^{-/-} ES cells and mouse embryo fibroblasts (MEF) lines. We succeeded in establishing both types of cells ruling out that the *Ttda* KO allele causes

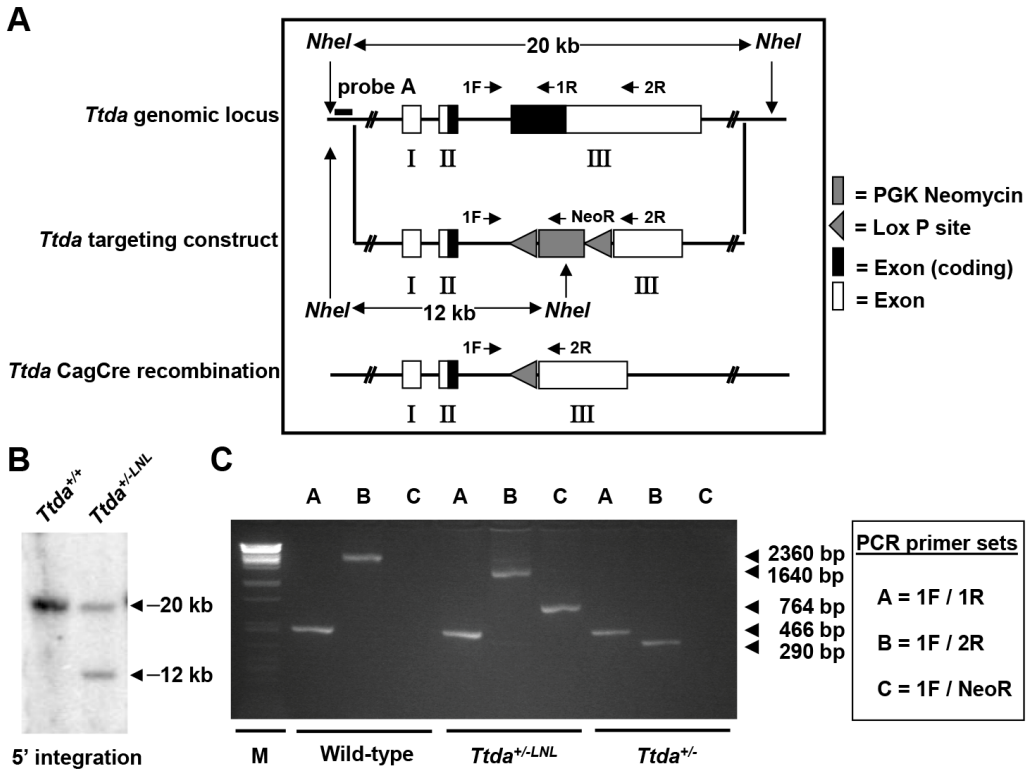


Figure 1. Generation of *Ttda* knock-out mice. (A) Schematic presentation of the mouse *Ttda* genomic locus, *Ttda* targeting construct and *Ttda* locus after CagCre recombination. Roman numbered boxes represent exons: white boxes are non-coding exon (parts) and black boxes are coding exon (parts). In the targeting construct *LoxP* sites are indicated with gray arrows and the dashed box represents the Neomycin selectable marker driven by a PGK promoter. The positions of *NheI* restriction sites, size of the *NheI* restriction fragments and the position of probe A used for DNA blot screening of digested ES cell DNA are indicated. The short arrows indicate the position and direction of primers used for genotyping. (B) DNA blot analysis of *NheI*-digested ES cell DNA using the probe A. (C) Genotype analysis with diagnostic PCR using primers 1F, 1R, 2R and NeoR in the different combinations (A, B and C).

Table 1. Genotyping and offspring from *Ttda*^{+/-} mice matings.

	Female	Male	Total expected	Total found	Expected % of total	Found % of total
Wild-type	58	60	78	118	25%	35%
<i>Ttda</i> ^{+/-}	90	102	154	192	50%	65%
<i>Ttda</i> ^{-/-}	0	0	78	0	25%	0%
Total	148	162	310	310	100%	100%

Genotyping of offspring from matings of *Ttda*^{+/-} mice, distributed over male and females, obtained number and percentage of offspring compared to the theoretical expected figures assuming a Mendelian inheritance pattern.

Table 2. Average litter size.

Breeding	Average litter size	SEM	SD
Wild-type × <i>Ttda</i> ^{+/-}	6.3 (n = 17)	0.60	2.40
<i>Ttda</i> ^{+/-} × <i>Ttda</i> ^{+/-}	5.1 (n = 19)	0.36	1.54

Average litter size of matings between two *Ttda*^{+/-} animals compared to matings between *Ttda*^{+/-} and wild-type mice.

cellular lethality, as observed with the other TFIIH subunits XPB and XPD due to their indispensable function in basal transcription initiation.

***Ttda* knock-out cells are NER deficient**

Since homozygous *Ttda*^{-/-} mice were not viable, we further analyzed cells derived from *Ttda*^{-/-} embryos. We determined the UV sensitivities of ES cells using a clonogenic survival assay. Surprisingly, as shown in Figure 2A, all *Ttda*^{-/-} ES clones exhibit a strong UV sensitivity, to the same extent as completely NER-deficient (*Xpa*^{-/-}) ES cells [30]. This severe UV-hypersensitivity was unexpected, since we have shown previously that TTD-A human primary fibroblasts only exhibit an intermediate UV sensitivity, caused by slow but persistent repair of UV-induced DNA lesions [22]. To find out whether this remarkable UV sensitivity in *Ttda*^{-/-} ES cells is not cell type specific, we also determined the UV sensitivity of *Ttda*^{-/-} mouse embryonal fibroblasts (MEFs). As shown in Figure 2B, *Ttda*^{-/-} MEFs were also extremely UV-sensitive to the same extent as *Xpa*^{-/-} MEFs.

Next, we investigated NER capacity in the *Ttda*^{-/-} MEFs, by measuring: UV-induced unscheduled DNA repair synthesis (UDS), i.e. a measure for GG-NER; and recovery of RNA synthesis after UV-irradiation (RRS), i.e. a measure for TC-NER (Figure 2C). UDS and RRS were both severely affected similar to completely NER-deficient (*Xpa*^{-/-}) MEFs, in line with the strong UV-hypersensitivity. In addition, *Ttda*^{-/-} MEFs were fully deficient in repair of 6-4 pyrimidine-pyrimidone (6-4PP) photoproducts as measured by ELISA, even 16 hours after UV irradiation (Figure 2D). This eliminates the option of slow but persisting repair as observed in the human TTD-A fibroblasts corroborating the complete NER-deficiency in these cells.

***Ttda* is required for TFIIH loading in NER complexes**

To further dissect the stage at which this unexpected complete NER deficiency occurs in *Ttda*^{-/-} MEFs, we first checked whether damage recognition is affected by *Ttda* ablation. As shown in Figure 2E, the damage recognizing protein Xpc is efficiently loaded to local UV-damage (LUD) similar as in wild-type cells. These results suggests that *Ttda* functions at the stage of TFIIH-loading onto XPC-bound lesions, downstream of damage recognition. To determine whether the TFIIH complex lacking *Ttda* was still capable of assembling at UV-induced DNA lesions — as shown in human TTD-A cells [17], [22] — we measured the binding kinetics of TFIIH to damaged regions. In these experiments either a Multi-photon (MP) laser or a UV-laser was used to locally induce (UV) DNA damage in the nuclei of living cells [31]. To monitor TFIIH loading we used a recently developed knock-in mouse model which expresses homozygously a fluorescently-tagged (YFP, for yellow fluorescent protein) Xpb (largest subunit of TFIIH) [32]. We crossed the *Ttda* KO allele into this *XpbYFP*^{+/+} background and isolated E10.5 MEFs from *XpbYFP*^{+/+} *Ttda*^{+/-} matings, each expressing the Xpb-YFP fusion protein. In contrast to the fast accumulation kinetics of Xpb-YFP to UV-laser damaged spots in the wild-type background (Figure 2F and 2G), this protein was unable to accumulate in *Ttda*^{-/-} background. Wild-type and *Ttda*^{+/-} MEFs showed similar accumulation kinetics for the multi-photon (MP) damaged area, which induces among other lesions also UV photoproducts [31] (Figure S1). However, Xpb-YFP is incapable of accumulating to DNA damaged regions in *Ttda*^{-/-} MEFs, even 15 minutes after DNA damage induction.

The absence of TFIIH binding to Xpc bound DNA lesions suggests that downstream processing of UV-lesions by the NER machinery is abrogated, since the helicase function of TFIIH is required for further assembly of the pre-incision NER complex and sequential dual incision [2], [33]. Repair intermediates produced by NER incision induces

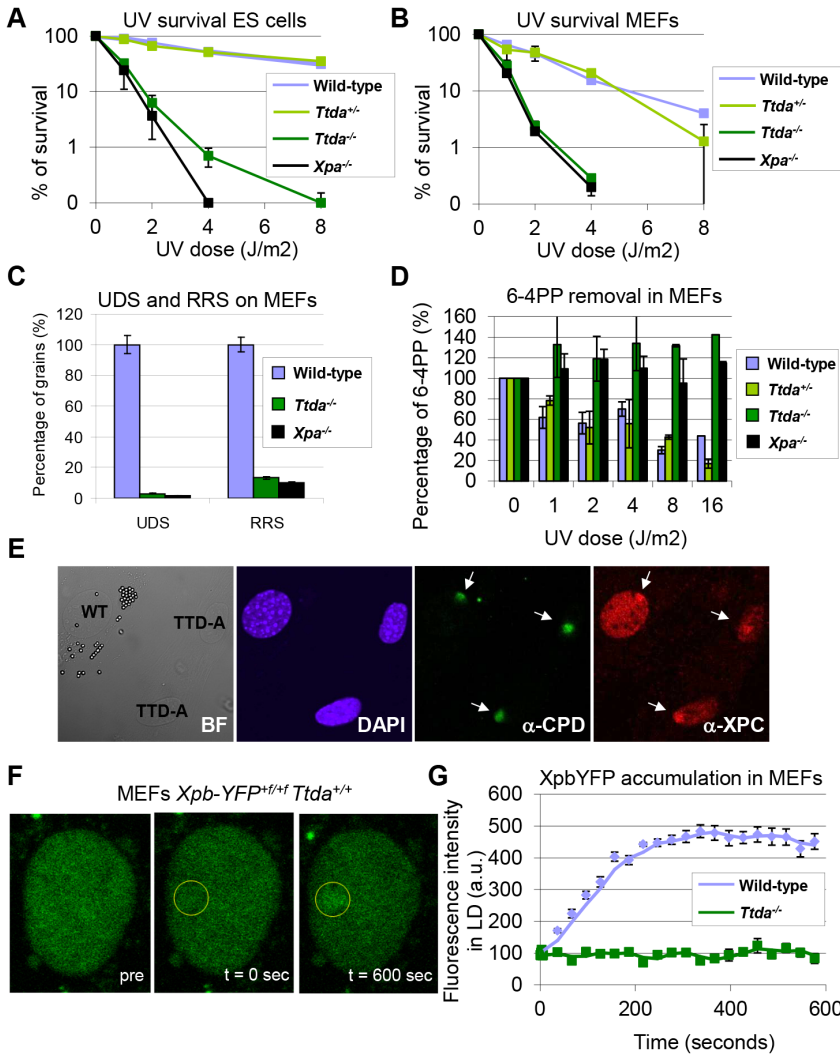


Figure 2. Repair capacity of *Ttda*^{-/-} cells.

(A) Colony forming ability after different doses of UV of wild-type, *Ttda*^{-/-}, *Ttda*^{-/-} and *Xpa*^{-/-} ES cells. The percentage of surviving cells was plotted against the applied UV-dose, measured by counting surviving colonies of two independent experiments and at least 2 different clones per genotype. The error bars indicate the SEM. (B) Survival assay after different doses of UV of wild-type, *Ttda*^{+/+}, *Ttda*^{-/-} and *Xpa*^{-/-} MEFs. The percentage of surviving cells was plotted against the applied UV-dose, measured by [3H]-thymidine incorporation of two independent experiments and at least 2 different clones per genotype. The error bars indicate the SEM. (C) DNA repair synthesis (UDS) and recovery of RNA synthesis (RRS) was measured by autoradiography. For the UDS assay, directly after

exposure to 16 J/m² UV-C MEFs were pulse labeled with medium containing [methyl-3H] Thymidine, washed with PBS and fixed. For the RRS assay, 16 hours after exposure to 16 J/m² MEFs were pulse labeled with medium containing [3H] Uridine, washed with PBS and fixed. UDS and RRS are expressed as the percentage of autoradiographic grains above wild-type, which was set at 100%. (D) 6-4PP removal assayed by ELISA using a 6-4PP specific antibody of wild-type, *Ttda*^{+/+}, *Ttda*^{-/-} and *Xpa*^{-/-} MEFs irradiated with 5 J/m² (UV-light). DNA was isolated at different time-points after UV irradiation (0, 1, 2, 4, 8, and 16 hrs post UV). The amount of 6-4PP measured directly after UV was set at 100%. (E) Immunofluorescent analysis of XPC recruitment to local UV-damage in wild-type (labeled with 2 μm latex beads) and *Ttda*^{-/-} MEFs. Cells were seeded in a 1:1 ratio on cover slips and the next day irradiated with 60 J/m² through a filter containing 5 μm pores. Cells were fixed 1 hour after UV and immunofluorescent staining was performed using antibodies against CPDs (damage marker, green) and XPC (green). (F) Representative series of confocal images of *XpbYFP*^{+/+/+} MEFs before (left; pre), directly after (middle; t=0 sec) and 600 seconds after (right; t=600 sec) local UV-damage infliction, the yellow circle marks the area irradiated with the UV-laser. (G) Accumulation kinetics of XpbYFP to local UV-C (laser-induced) DNA damage in a wild-type and *Ttda*^{-/-} background. Graphs represents the mean YFP-derived fluorescence intensity at the damaged spot at the indicated time points from approximately 12 cells.

H2AX phosphorylation (γ H2AX) in a cell-cycle independent manner [34], [35]. Local γ H2AX after filter irradiation can be used as a sensitive marker for dual incision during NER [36]. In non-S-phase cells, since γ H2AX signaling in S-phase cells is both triggered by stalled replication forks and NER. A clear local γ H2AX signaling is observed in wild-type non-S-phase MEFs 1 hr after LUD, which is however absent in both *Xpa*^{-/-} and *Ttda*^{-/-} MEFs (Figure 3). Together these data show that *Ttda* is pivotal for TFIIH loading on UV lesions and that in its absence no NER-dependent dual incision occurs. We therefore consider *Ttda* as an essential NER factor.

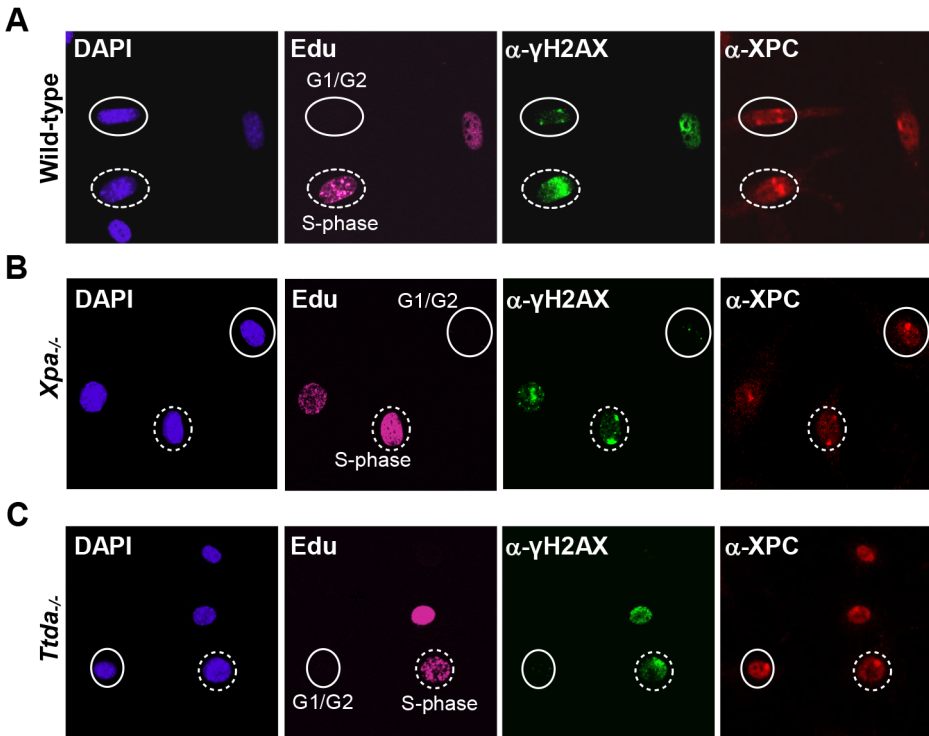


Figure 3. γ H2AX signaling is abolished in *Ttda*^{-/-} MEFs. Cell cycle dependent analysis of XPC and γ H2AX recruitment to local UV-damage in wild-type (A), *Xpa*^{-/-} (B) and *Ttda*^{-/-} (C) MEFs. Cells were seeded on cover slips and the next day irradiated with 60 J/m² through a filter containing 5 μ m pores and subsequently labeled with EdU for 1 hour. After fixation cells were assayed for DNA synthesis using EdU and Alexa Fluor 647 azide (cell cycle marker, pink) and by immuno-fluorescent staining using antibodies against γ H2AX (green) and XPC (red). Dashed circles indicate typical examples of cells in S-phase, closed circles indicate typical examples of G1/G2 cells.

Knock-down of mutant *hTTDA* results in complete NER deficiency

The absence of residual NER activity in *Ttda*^{-/-} MEFs and ES cells is in contrast with the partial NER activity in TTD-A human primary fibroblasts [22]. A possible explanation for this apparent discrepancy could be derived from a human-mouse difference in NER efficiency. This could be caused by the virtual absence of CPD removal by GG-NER in rodent cells, which still occurs albeit with a slow rate in human cells [37]. Alternatively, it is not formally excluded that a mutated TTDA protein with partial biological activity is still present in the patient cells. To investigate this latter option we attempted to further reduce TTDA in human patient cells (TTD1BR-SV) by shRNA interference of the resident mutant *TTDA* transcript. The knock-down efficiency of the different shRNAs targeting the *TTDA* transcript

was verified by RT-qPCR (Figure 4A). We selected two shRNAs (#3398 and #3402) that were most efficient in reducing the resident TTDA transcript to approximately 5% of the initial amount. Next, we determined the UV-sensitivity by performing a clonogenic survival assay (Figure 4B). Surprisingly, depleting mutant *TTDA* mRNA in TTD-A human patient cells severely aggravated the UV-sensitivity, whereas a control non-targeting shRNA did not have any effect. These results suggest that the mutated human TTDA proteins still harbor residual NER activity and that the severe NER-deficient phenotype observed in *Ttda*^{-/-} cells is not specific for mouse cells. To find out whether this strong NER deficiency upon TTDA depletion by shRNA in the human cells was due to a further reduction in cellular TFIIH content below a critical threshold, we determined TFIIH levels in the parental TTD-A cells and their cognate shRNA-TTDA-depleted cells. As shown by the immunofluorescence staining of the XPB subunit of TFIIH in Figure 4C and Figure S2 there was no further decline of the already low TFIIH levels upon TTDA depletion by shRNA in TTD-A cells.

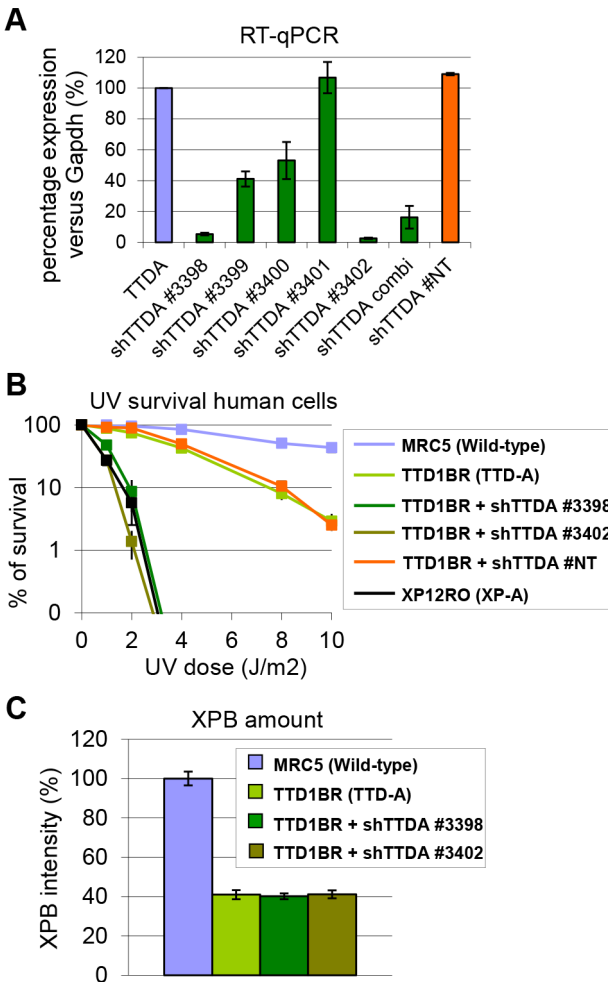


Figure 4. Knock-down of mutant hTTDA results in complete NER-deficiency. (A) Relative expression levels of TTDA mRNA as determined by quantitative RT-PCR in TTD1BR-sv cells (TTD-A) and TTD1BR-sv cells stably expressing shRNAs for respectively: #non-targeting (NT), #3398, #3399, #3400, #3401 or #3402. The levels were normalized to *Tubulin* and the error bars indicate SEM between two independent experiments. (B) Colony forming ability after different doses of UV irradiation of MRC5-sv (wild-type), XP12RO-sv (XP-A), TTD1BR-sv and TTD1BR-sv cells stably expressing shRNA: #non-targeting (NT), #3398, #3399, #3400, #3401 and #3402. The percentage of surviving cells was plotted against the applied UV-dose, measured by counting surviving colonies of two independent experiments. The error bars indicate the SEM. (C) Quantitative immuno-fluorescence to determine the relative amount of XPB (TFIIH) in MRC5-sv (wild-type), TTD1BR-sv (TTD-A) and TTD1BR-sv cells stably expressing shRNA (#3398 or #3402). Confocal microscope pictures were used to quantify the average intensity of XPB and MDC1 (internal control) in >100 cells and error bars indicate SEM.

TTDA mutant proteins accumulate at UV-induced damaged regions

Since depletion of mutant TTDA aggravated UV-sensitivity, we further investigated the functionality of the mutant human proteins (schematically depicted in Figure 5A). Because TTDA seems to be required for efficient loading of additional NER factors, the ability of TTDA to localize to LUD is indicative of its function in NER. To determine the binding of mutant TTDA to laser-induced LUD in living cells, we transduced *Ttda*^{-/-} MEFs with lentiviruses encoding for GFP-tagged TTDA: TTDA^{WT}-GFP (wild type), TTDA^{M1T}-GFP (start site mutation, using the first downstream Methionine codon (M16)), TTDA^{R56X}-GFP (premature stop mutation) or TTDA^{L21P}-GFP (transition mutation). The latter three mimic mutations found in TTD-A patients. TTDA-GFP fully complements the UV-sensitivity of *Ttda*^{-/-} MEFs (Figure S3A and [21]) and shows that the tagged TTDA is biologically active. As shown in Figure 5B and 5C, TTDA^{R56X}-GFP and TTDA^{L21P}-GFP accumulated with similar initial kinetics as TTDA^{WT}-GFP to LUD, though prior to steady-state less TTDA^{L21P}-GFP accumulated compared to TTDA^{WT}-GFP. This would suggest that the binding time of this mutant protein is reduced compared to the wild-type protein. The ability to accumulate at DNA damaged regions was also confirmed by an immunofluorescence experiment, using a 5 μm filter and a UV-C lamp to apply local UV damage (Figure S3B). However, we did not find accumulation of TTDA^{M1T}-GFP, despite the fact that patient cells carrying this mutation display only a mild NER-deficient phenotype [15]. This apparent discrepancy could be explained by a possible combinational functional interference of both the 16 amino acid N-terminal truncation and the C-terminal GFP-tag, despite the notion that over expression of a full length TTDA-GFP rescues the UV-sensitivity of *Ttda*^{-/-} MEFs (Figure S3A). To further investigate a possible partial function of the translational start-site mutant, we over expressed non-tagged mutant *TTDA* cDNA — mimicking the translation start mutation found in TTD13 PV and TTD14 PV patients — and the other mutants in *Ttda*^{-/-} MEFs and assayed for UDS. Co-transfected GFP served as a marker to identify transfected cells. Over expression of all *TTDA* mutant cDNAs clearly corrected the DNA repair synthesis deficiency of *Ttda*^{-/-} MEFs to almost wild-type levels, including the translational start-site (M1T) mutant (Figure 5D, 5E). Together these results strongly suggest that TTD-A patients do express a partially functional mutant protein and confirms that also in human cells TTDA is an essential NER component, rather than only an NER accessory factor.

Lethal phenotype caused by *Ttda* absence

The new finding of TTDA's essential role in NER has far-reaching biological significance. However, the complete NER deficiency cannot explain the embryonic lethality, since other mice with fully compromised NER function (such as *Xpa*^{-/-} mice) do not display similar developmental abnormalities and are viable [38], [39]. To gain further insight into the nature of this lethal phenotype, we analyzed whether the altered genomic locus of the *Ttda* KO allele interferes with the expression of neighboring genes. The deletion of genomic sequences in the *Ttda* gene may include cryptic or unrecognized transcriptional enhancers or insulators which may create hypomorphic expression of adjacent genes (see [40] for a typical example). To investigate possible transcriptional interference, we analyzed the expression levels of the 3 most proximal neighboring genes to the *Ttda* gene in *Ttda*^{-/-} ES cells by quantitative real-time PCR (RT-qPCR): Synaptojanin 2 (*Synj2*, 35.5 Kb upstream), Serine active site containing 1 (*Serac1*, 89 bp upstream) and Tubby-like protein 4 (*Tulp4*, 21.3 Kb downstream). The expression of these genes was not reduced when compared with expression in their heterozygous and wild-type cognates (Figure 6A). Two of these genes showed increased expression in the *Ttda*^{-/-} cells. This likely does not cause embryonic lethality, since cells from heterozygous animals, which also had this increased

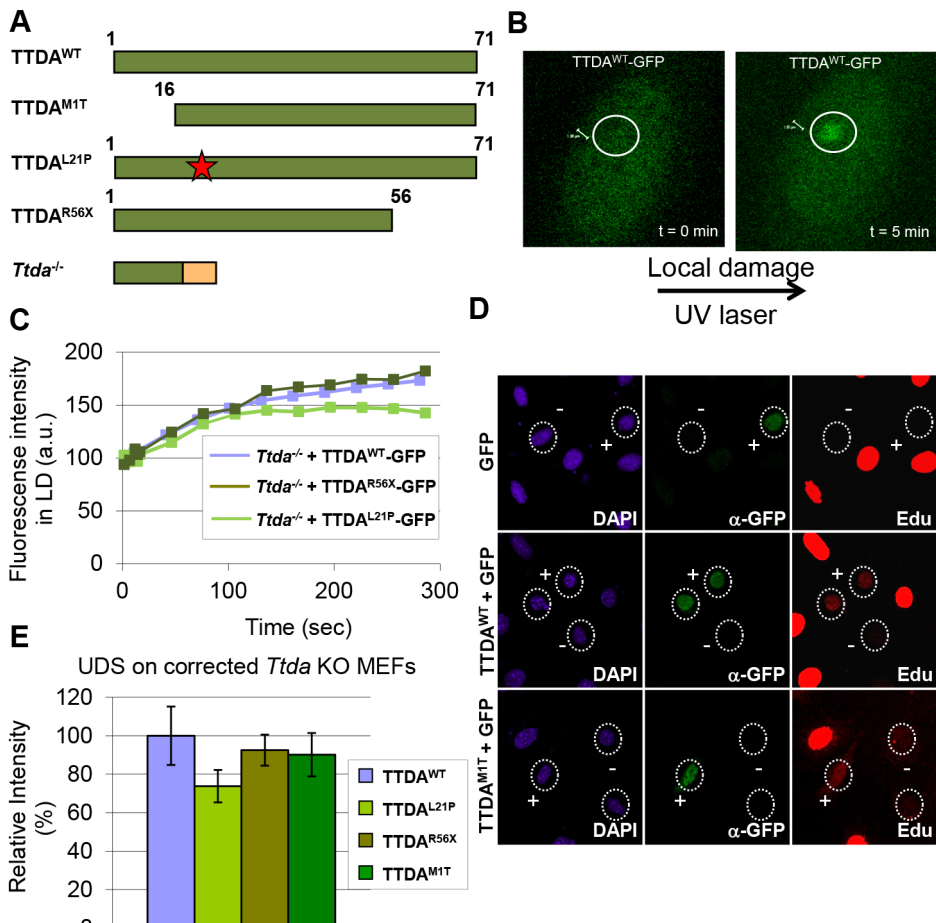


Figure 5. Mutant TTDA protein accumulation at local UV damage. (A) Schematically representation of the predicted TTDA polypeptide length (in amino acids) in human wild-type cells (TTDA^{WT}), TTDA-A patient cells (TTDA^{M1T}, TTDA^{L21P} and TTDA^{R56X}) and the *Ttda* knock-out cells (*Ttda*^{-/-}). The red star represents the mutation found in TTDA^{L21P} and the red part of the *Ttda*^{-/-} bar represents intronic encoded non-sense amino acids. (B) Representative confocal images of *Ttda*^{-/-} MEFs expressing TTDA^{WT}-GFP before (t = 0 min) and after local UV-damage infliction (t = 5 min) in a selected area inside the nucleus (dashed circle). (C) Accumulation kinetics of TTDA^{WT}-GFP, TTDA^{L21P}-GFP and TTDA^{R56X}-GFP to local UV-C (laser-induced) DNA damage expressed in *Ttda*^{-/-} MEFs. Graphs represents the mean GFP-derived fluorescence intensity at the damaged spot at the indicated time points from approximately 12 cells. (D) Representative confocal microscope images of UV-induced UDS of *Ttda*^{-/-} MEFs transiently co-transfected with an empty GFP vector (as a marker for transfected cells) in combination with a vector containing TTDA^{WT} or TTDA^{M1T}. Cells were seeded on cover slips and transfected 2 days before the experiment. Cells were irradiated with 16 J/m² and subsequently labeled for 2 hours with EdU. Cells were fixed and stained for EdU incorporation (UDS and S-phase DNA synthesis, red) and GFP using antibodies against GFP (transfected cells, green). The intense red labeled cells are cells in S-phase. (E) The percentage of UDS signal in the nucleus was quantified by measuring the average fluorescence intensity from at least 25 cells positively transfected (containing GFP) and non-S-phase cells with TTDA^{WT}, TTDA^{M1T}, TTDA^{R56X} or TTDA^{L21P}. The error bars indicate the SEM.

expression do not display any obvious phenotype. Expression analysis of the *Ttda* allele neighboring genes at a later stage of development (E11.5) (Figure S4) confirmed the absence of a clear correlation between aberrant gene expression and lethality in *Ttda*^{-/-} embryos.

It has been suggested that the TTDA protein is a repair-specific TFIIH-subunit, which is not strictly required for basal transcription as the other TFIIH components are [17]. However, mutated *TTDA* causes an overall reduction of TFIIH protein abundance in human fibroblasts [16]. This sub-limiting amount of TFIIH does not cause a significant reduction of basal transcription within cultured TTD-A patient fibroblasts [16]. On the other hand, in the developing mouse embryo a decreased amount of TFIIH might reduce the transcription capacity which is needed to produce a fully developed animal. To directly monitor the quantity of TFIIH in living cells, we isolated ES cells and E10.5 MEFs from *XpbYFP^{+/+} Ttda^{+/-}* matings (see above), each expressing the XPB-YFP fusion protein. A clear reduction in the quantity of TFIIH (as deduced from the strong reduction of the YFP signal) was easily observed in the live cell images of both *Ttda* KO ES cells and MEFs (Figure 6B–6C). We determined by direct fluorescence measurements the YFP signal emitted from the nuclei of ES cells and MEFs, which was respectively 22% and 33% in the KO cells as compared to wild-type cells isolated from litter mates. These levels are for the MEFs comparable to the amounts measured in human cells (approximately 30%) [16] and appeared even lower in ES cells.

Next we analyzed the transcription capacity in these murine cells by pulse labeling de novo RNA synthesis for either 30 minutes or 2 hours with fluorescent based 5-ethynyl-uridine (EU). The average fluorescence intensity, which is a measure for the total amount of transcription in these cells, was evaluated (Figure 6D). In accordance with the reduced steady-state level of TFIIH, measured in ES cells and MEFs, the overall transcription appeared to be significantly reduced in *Ttda*^{-/-} cells as well.

***Ttda* knock-out cells are sensitive to oxidative DNA damage**

Despite the severely reduced amount of TFIIH in *Ttda*^{-/-} cells, which also attenuated overall transcription, the proliferative capacity of the embryonic cells was not affected (Figure S5A). It is thus not likely that reduced overall transcription would be the sole cause to the observed embryonic lethality. Detailed analysis of different mutant TFIIH mouse models revealed a correlation between sensitivity to oxidative DNA damage and severity of the phenotype of the different models. These observations argued for a unknown function of TFIIH in oxidative lesion removal [27]. To investigate whether *Ttda*^{-/-} cells are also defective in repairing other (non NER-type) DNA lesions, we measured their sensitivity to several oxidizing agents. Clonogenic survival assays performed on *Ttda*^{-/-} ES cells revealed hyper-sensitivity to gamma irradiation (Figure 7A) and potassium bromate (Figure 7B), similar to *Csb*^{-/-} ES cells (known to be sensitive to oxidative DNA damage) [30]. Since the *Xpa*^{-/-} ES cells assayed in parallel were not sensitive to any of these agents, this sensitivity is not a general effect of NER-deficiency. This phenomenon is also not cell-type specific, since *Ttda*^{-/-} MEFs are also hyper-sensitive to gamma irradiation (Figure 7C). To exclude the possibility that *Ttda*^{-/-} cells have a general low tolerance to DNA damage, we also measured their sensitivity to mitomycin C (MMC). MMC induces inter-strand cross-linking that is specifically repaired by the inter-strand cross-link repair pathway — a pathway which specifically involves the NER protein complex XPF-ERCC1 (other NER factors are not required to remove this class of lesions) [41]. As shown in Figure 7D, *Ercc1*^{-/-} cells are highly sensitive to MMC treatment. All the other NER mutant cells, including the *Ttda*^{-/-} cells, are not sensitive. Since most oxidative DNA lesions are removed by the

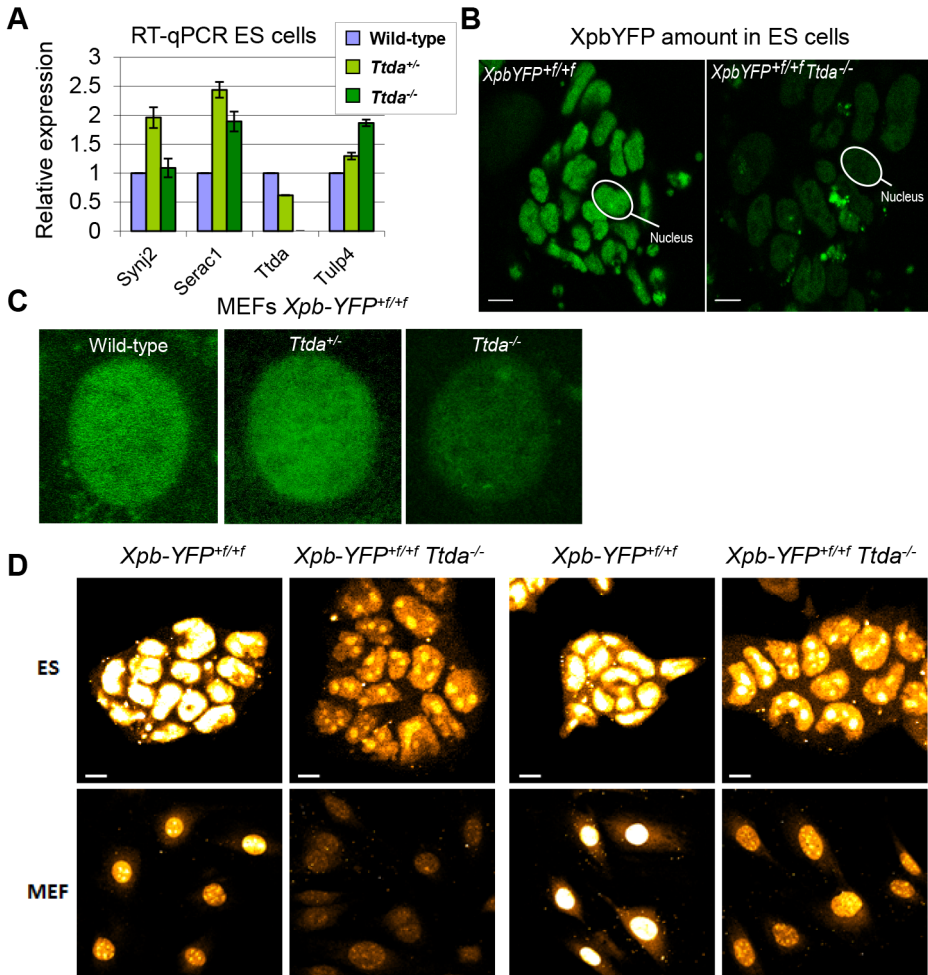


Figure 6. Gene expression levels and TFIIH amount in *Ttda*^{-/-} ES cells. (A) Relative expression levels of mRNAs neighboring genes encoding Synaptojanin 2 (*Synj2*), Serine active site containing 1 (*Serac1*), Trichothiodystrophy group A (*Ttda*) and Tubby like protein 4 (*Tulp4*) in *Ttda*^{-/-} (n=2), *Ttda*^{+/-} (n=2) and wild-type (n=2) ES cells as determined by quantitative RT-PCR. The levels were normalized to *Gapdh* and the error bars indicate SEM between experiments. (B) Representative confocal microscope pictures of *XpbYFP*^{+/+} *Ttda*^{-/-}, *XpbYFP*^{+/+} *Ttda*^{+/-} and *XpbYFP*^{+/+} MEFs isolated from 10.5-day-old embryos. (C) Confocal images of ES cells isolated from *XpbYFP*^{+/+} mouse model (left panel) and from *XpbYFP*^{+/+} *Ttda*^{-/-} mouse (right panel). The green signal is the direct fluorescence of the YFP tagged protein. The white bar measures 10 mm. (D) Confocal images of EU incorporation into ES cells isolated from *XpbYFP*^{+/+} mouse model and from *XpbYFP*^{+/+} *Ttda*^{-/-} mouse (upper panel) and MEF's isolated from the same mouse models (lower panel). Two EU incubation times have been performed: 30 minutes (left panels) and 120 minutes (right panels). The white bar measures 10 mm.

base excision repair (BER) genes [42], we wondered whether the oxidative DNA damage hypersensitivity could be due to reduced expression of BER genes, as a consequence of the low TFIIH level in *Ttda*^{-/-} cells. To that aim we analyzed the expression of the core BER genes by RT-qPCR, since the absence of single oxidative damage-specific glycosylases does not cause cellular hyper-sensitivity due to (partial) redundant glycosylases [43]. As shown in Figure S5B, none of the BER genes were lower expressed in the *Ttda*^{-/-} cells. To further investigate a possible general BER defect in *Ttda*^{-/-} cells, we tested for alkylating DNA damage sensitivity. Apart from the initial recognizing glycosylases, further processing of these lesions follows the same route as for oxidative DNA damage. To that aim we treated the cells with varying concentrations of Methyl methanesulfonate (MMS). In contrast to oxidative DNA damage, *Ttda*^{-/-} appeared not hypersensitive to this agent (Figure 7E). Together our data unambiguously establish a function for TTDA and likely for the entire TFIIH complex in the tolerance to oxidative DNA damage.

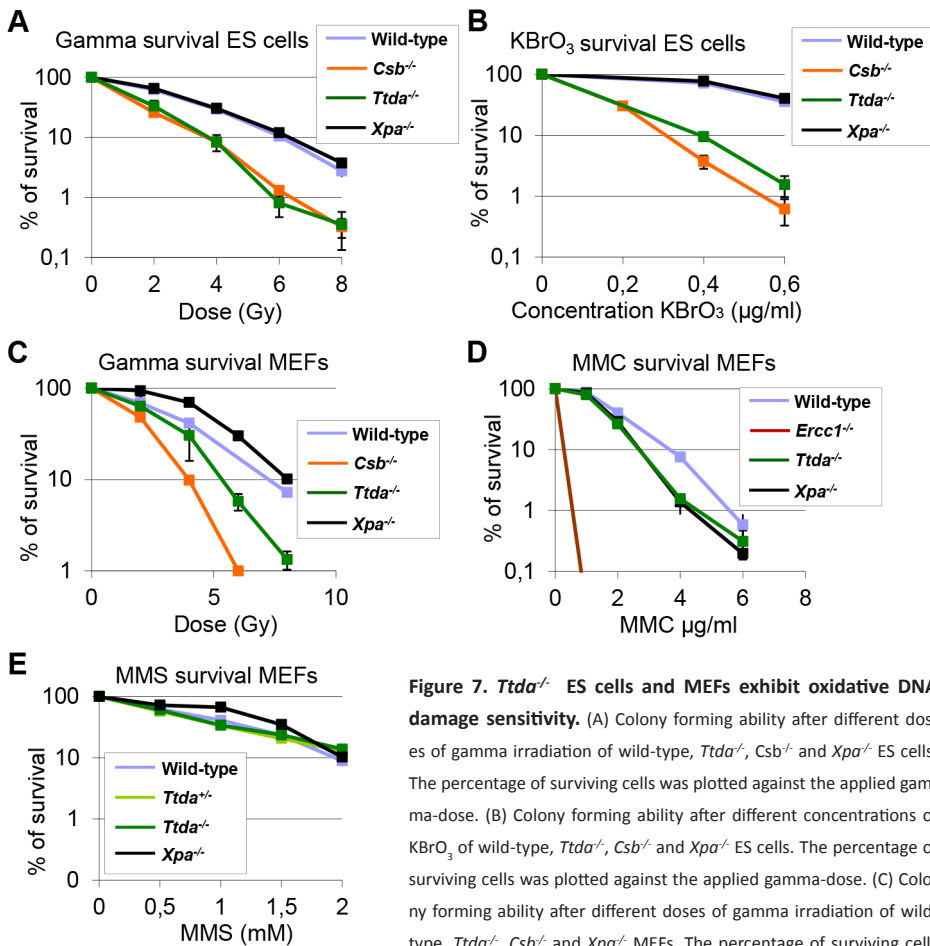


Figure 7. *Ttda*^{-/-} ES cells and MEFs exhibit oxidative DNA damage sensitivity. (A) Colony forming ability after different doses of gamma irradiation of wild-type, *Ttda*^{-/-}, *Csb*^{-/-} and *Xpa*^{-/-} ES cells. The percentage of surviving cells was plotted against the applied gamma-dose. (B) Colony forming ability after different concentrations of KBrO₃ of wild-type, *Ttda*^{-/-}, *Csb*^{-/-} and *Xpa*^{-/-} ES cells. The percentage of surviving cells was plotted against the applied gamma-dose. (C) Colony forming ability after different doses of gamma irradiation of wild-type, *Ttda*^{-/-}, *Csb*^{-/-} and *Xpa*^{-/-} MEFs. The percentage of surviving cells was plotted against the applied gamma-dose. (D) Colony forming ability after different doses of 1 hour MMC treatment of wild-type, *Ttda*^{-/-}, *Ercc1*^{-/-} and *Xpa*^{-/-} MEFs. The percentage of surviving cells was plotted against the applied gamma-dose. (E) Colony forming ability after different doses of 1 hour MMS treatment of wild-type, *Ttda*^{-/-}, *Ttda*^{-/-} and *Xpa*^{-/-} MEFs. The percentage of surviving cells was plotted against the applied gamma-dose. For each survival plot (A - E) at least 2 different clones per genotype were measured in two independent experiments. The error bars indicate the SEM.

Discussion

In an attempt to create a *Ttda* knock-out mouse model, we have shown that this gene is essential for embryonic development. Contrary to expectations, *Ttda*^{-/-} mice die in utero between 10.5 days of gestation and birth. The lethality observed in *Ttda*^{-/-} embryos obviously differs from the phenotype observed in TTD-A patients, whom have relatively mild TTD features. The fact that differential expression levels of neighboring genes did not correlate with lethality demonstrates that this lethality was not due to any inadvertent effect of the targeting strategy. Surprisingly, viable cells derived from *Ttda*^{-/-} embryos are completely NER deficient, again in contrast to the mild NER defect observed in TTD-A patient cells. These findings indicate that TTDA's role in NER is in fact essential, and not auxiliary as previously suggested. Finally, *Ttda*^{-/-} cells appeared hyper-sensitive to oxidative DNA damage, a finding not commonly associated with NER-deficiency. Both the requirement of *Ttda* for embryonic development and its function in oxidative DNA damage defense suggest that *Ttda* not only has a function in NER but also in several other processes, thereby challenging the NER-specific role of TTDA previously postulated.

TTDA has a pivotal role in NER

Analysis of NER parameters in embryonic *Ttda*^{-/-} cells revealed a remarkably severe NER-deficiency and includes extreme UV-hypersensitivity, absence of UV-induced UDS and defective in removing UV-induced lesion (comparable to *Xpa*^{-/-} cells). This complete NER-deficient phenotype is in striking contrast to the only mild NER defect seen in human TTD-A cells. The NER-deficiency observed cannot be explained by a cell-type specific UV-response, since MEFs and ES cells are equally UV-sensitive. In a previous study we noted very low levels of all subunits of TFIIH in human TTD-A patient cells and suggested that this contributes to the associated partial NER defect [16]. MEFs derived from a previously generated TTD mouse model [26] — mimicking a known human TTD-causative point mutation (R722W) in the mouse *Xpd* locus — are only slightly sensitive to UV irradiation and exhibit a mild UDS defect and have decreased TFIIH levels [28]. Therefore, complete NER-deficiency appears to be specific to the *Ttda*^{-/-} cells and not a general TTD-associated phenotype caused by a lower level of TFIIH. Since the NER-phenotype of *Xpd* TTD mice closely mimics the partial repair deficiency features in human XP-D TTD cells, it is thus unlikely that this discrepancy in the severity of the NER-phenotype between man and mice is a species-specific phenomenon of increased NER-deficiency in murine cells. Our dynamic in vivo studies have revealed that the TTDA defect is located at a stage prior to stable association of TFIIH with the NER initiation complex, containing XPC (Figure 2E). However, in contrast to NER, TTDA seems dispensable for loading TFIIH onto promoter sequences for transcription initiation of RNA pol I and II, in view of the fact that *Ttda*^{-/-} cells are viable and do not show a proliferation defect.

TTD-A patients express partially functional TTDA protein

Knock-down of the resident *TTDA* transcripts in TTD-A patient cells rendered these cells extremely UV-sensitive, with the same level of sensitivity as completely NER-deficient XP-A cells and similar to the *Ttda*^{-/-} MEFs. From these data we conclude that in humans the mutant TTDA protein are partially functional. This hypothesis is further substantiated by the finding that the GFP-tagged TTDA^{R56X} protein (homozygous mutation in patient TTD99RO) was able to accumulate at sites of UV-induced damages, in line with the suggested presence of residual activity of mutant TTDA proteins in patient TTD-A cells.

Our data suggest that the TTDA protein in TTD13/14PV cells is partially functional.

This observation is particularly intriguing, since it has been suggested that no TTDA protein is expressed in these cells, due to the homozygous translational start-site mutation [15]. However, the fact that depletion of the mutant *TTDA* mRNA by targeted shRNA interference further enhanced UV sensitivity, suggests that this mutant mRNA is still able to generate a partially functional TTDA protein. One way to explain this phenomenon is by assuming that despite this ATG mutation, some TTDA protein is still being produced by initiating from an in-frame downstream ATG (codon 16). The usage of such alternative start site may produce low levels of an N-terminally truncated TTDA protein, sufficient to rescue lethality and complete NER-deficiency. Indeed, over expression of a 16 amino-acid N-terminally truncated mutant TTDA, rescued the UDS defect of *Ttda*^{-/-} cells (Figure 5D, 5E) and argues for partial functional production of N-terminally truncated TTDA in TTD13/14PV patient cells. Interestingly, it has been shown (both in yeast and humans) that the N-terminal domain of TTDA is important for binding to the TFIIH subunits XPD and p52 [17], [44] and for stimulating the ATPase-activity of the XPB subunit [17]. Furthermore, this interaction is also critical for the TFIIH stability. Apparently, the truncated *Ttda* protein is nevertheless able to carry out part of its function to permit residual NER.

Ttda functions in oxidative DNA damage defense

Defects in multiple DNA repair systems may cause synergistic effects or even synthetic lethality [45]. For example, severe developmental and premature aging problems have been seen in KO mouse models of DNA repair factors that function in independent repair pathways, such as ERCC1 (which functions in NER and inter-strand cross-link repair) and *Xpa*^{-/-} *Csb*^{m/m} double KOs (which is defective in GG-NER, and presumably also in the broad TCR pathway) [46], [47]. It has been suggested that endogenously produced DNA lesions (e.g. from reactive oxygen species (ROS) or lipid peroxidation byproducts) that cannot be removed because of the repair defect, are in part responsible for the phenotype observed. Here we have shown that *Ttda*^{-/-} cells are sensitive to several oxidizing agents to the same extent as *Csb*^{-/-} ES cells [30]. Based on these results, we suggest that *Ttda*^{-/-} embryos are confronted with unrepaired endogenous oxidative lesions, possibly generated by low but continuous exposure to ROS during development. This compromised repair of oxidative DNA lesions may contribute to the observed lethal phenotype observed in the *Ttda*^{-/-} embryos. Importantly, this reduced resistance to oxidative DNA damage is likely not caused by a general (core) BER defect. Previously, it was suggested that TFIIH is implicated in coordinating incision of lesion-stalled transcription complexes [48] and that some oxidative DNA lesions are processed by transcription-coupled repair [49]. It is thus possible that TTDA (TFIIH) is involved in a specific — thus far uncharacterized — transcription-coupled repair process of oxidative DNA damage.

Lethal phenotype of *Ttda* knock-out mice

The fact that TTDA has a pivotal role not only in NER but also in oxidative DNA damage defense and transcription, argues for a function of TTDA in various DNA metabolizing processes, causing synergistic effects when inactivated. However, full NER-deficiency in combination with defects in oxidative DNA damage repair — as in *Xpa*^{-/-} *Csb*^{-/-} double KO mice — does not lead to embryonic lethality. In this mouse model pups are born, but they progressively develop very severe neurologic symptoms and premature aging features. It is thus likely that not only the repair functions contribute to the lethal phenotype of *Ttda*^{-/-} animals, but that also its function in transcription is involved. Nevertheless, human TTD-A patient derived cells also express low levels of TFIIH, but have only limited post-natal developmental problems [23]. It is possible that transcription is more demanding during

mouse embryogenesis than in the human embryo, due to its more rapid development. In this respect it should be noted that TTD-causing mutations in the human XPD gene are associated with impaired placental development and other gestational complications [50].

It has been shown that TTDA is dispensable for mammalian *in vitro* transcription [17]. Nevertheless, TTDA was originally found to be present in the pre-initiation complex [20] and reconstituted transcription assays have demonstrated that TTDA stimulates this reaction [19]. It has been hypothesized that mutations affecting XPD's function in DNA repair cause the disorder XP — associated with a 1000-fold increased risk of skin cancer — while mutations affecting XPD's role in RNA Polymerase II-mediated transcription lead to TTD-specific features: brittle hair and nails, and scaly skin [51]. TTD features in TTD-A patients are relatively mild compared to those seen in XPD-associated TTD patients. The mild TTD-phenotype suggests that the role of TTDA in transcription is plausible, but also that it is not the only cause for embryonic lethality. We have demonstrated that *Ttda* KO cells have a low steady state level of TFIID and accordingly have a lower transcriptional activity (Figure 6C and 6D). The low TFIID quantity does not seem to be the sole cause of embryonic lethality, since similar low levels of TFIID are observed in TTD-A patient cell lines, which are compatible with life. However, the notion of reduced transcriptional activity in *Ttda*^{-/-} cells argues that this feature may contribute to embryonic lethality. For instance, during certain stages of embryonic development which requires high transcriptional capacity, normal embryogenesis may be compromised. Moreover, it cannot be excluded that mutations in *TTDA* affect the transcription of a subset of specific genes, as shown in cells with XPD-associated TTD mutations defective in activated-transcription of nuclear receptors [52]. In this scenario, the expression of specific genes, essential for development of the embryo might be disturbed hindering proper embryogenesis and finally inducing *in utero* death. In both cases, TTDA function appears to extend beyond the previously suggested main function in NER, as it is also important for both development and viability.

Our data clearly show that TTDA has an essential function in NER. The rather mild TTD-phenotype observed in TTD-A patients is due to the presence of partly functional mutant proteins. The sensitivity to endogenously produced oxidative DNA lesions in *Ttda*^{-/-} cells suggests that TTDA (and likely the entire TFIID) has additional functions in DNA repair extending beyond NER. The lethal phenotype observed in *Ttda*^{-/-} embryos is possibly the result of several defects, such as insufficient levels of TFIID needed for transcription in highly proliferative tissues, impairment in the activated transcription of specific genes, and unrepaired lesions — induced either by UV or endogenously by oxidizing agents which are relevant for cancer as well as aging.

Materials and Methods

Ethics statement

All animal work was conducted according to the Federation of European Laboratory Animal Science Associations (FELASA) ethical requirements and with respect of the 3R animal welfare rules.

Construction of the *mTtda* targeting construct

The knock-out targeting vector (backbone Puc18) contained a 12.5 Kb XbaI fragment of mouse genomic DNA (isogenic to 129Ola) harboring the entire *Ttda* locus. The complete exon 3 (i.e. most of the protein coding sequence) was excised, using Ball digestion, and replaced with a neomycin gene-expression cassette, flanked by two LoxP sites [53] and used as a dominant selectable marker. The dominant marker was inserted in the same

transcriptional orientation as the *Ttda* gene.

Gene targeting

ES cells (129Ola, subclone IB10) were cultured in BRL-conditioned medium supplemented with 1,000 U/ml leukemia inhibitory factor (LIF). A total of 20 μg of the *Sall* linearized targeting vector was electroporated into approximately 107 ES cells in 500 μl . Selection with 0.2 $\mu\text{g}/\text{ml}$ G418 was started 24 h after electroporation. G418 resistant clones were isolated after 8–10 days. Screening for homologous recombinants was performed using DNA blot analyses of *NheI* digested DNA with a 1000 bp 5' external probe A (see Figure 1A). 13 ES clones out of 130 G418-resistant clones, had a correctly targeted *Ttda* allele. Two of the 13 correctly targeted ES clones were checked for proper karyotype and injected into blastocysts from C57bl/6 mice and then transplanted into B10/CBA foster mothers. Chimeric mice were further crossed, and germ line transmission of the targeted allele to offspring was genotyped by PCR (Figure 1). Primer sequences are available on request.

Cell culture and treatments

Cell culture

ES cells: IB10 (wild-type), *Xpb-YFP^{+/+}*, *Xpb-YFP^{+/+} Ttda^{+/-}*, *Xpb-YFP^{+/+} Ttda^{-/-}*, *Ttda^{+/-}*, *Ttda^{-/-}*, *Xpa^{-/-}*, *Csb^{-/-}* and *Ercc1^{-/-}*. They were cultured in a 1:1 mixture of DMEM (Lonza) and BRL conditioned medium with 10% foetal calf serum (FCS), 1% penicillin-streptomycin (pen-strep; Gibco), 1% non-essential amino acids, 0.1% β -mercaptoethanol (Invitrogen) and 0.01% leukemia inhibitor factor (home-made) at 37°C, 20% O₂ and 5% CO₂. The dishes were pre-coated with a 0.1% gelatine solution in water.

MEFs: wild-type, *Xpb-YFP^{+/+}*, *Xpb-YFP^{+/+} Ttda^{+/-}*, *Xpb-YFP^{+/+} Ttda^{-/-}*, *Ttda^{+/-}*, *Ttda^{-/-}*, *Ttda^{-/-}* expressing TTDA^{WT}-GFP; TTDA^{L21P}-GFP or TTDA^{R56X}-GFP, *Xpa^{-/-}*, *Csb^{-/-}* and *Ercc1^{-/-}*, were cultured in a 1:1 mixture of DMEM and Ham's F10 (Lonza) with 10% FCS and 1% pen-strep at 37°C, 20% O₂ and 5% CO₂.

SV40-immortalized human fibroblasts: TTD1BR-sv (TTD-A), TTD1BR-sv stably expressing shRNA (#non-targeting (NT), #3398, #3399, #3400, #3401 and #3402) and TTD1BR-sv stably expressing either TTDA^{WT}-GFP or TTDA^{R56X}-GFP, were cultured in a 1:1 mixture of DMEM and Ham's F10 with 10% FCS and 1% pen-strep at 37°C, 20% O₂ and 5% CO₂.

Treatments

For the local UV irradiation, cells were treated with a UV-C germicidal lamp (254 nm; Phillips) through a 5- μm microporous filter at 60 J/m².

For transiently expression of DNA construct in MEFs, transfections were performed using jetPEITM (Polyplus transfections) according to the manufacturer's protocols.

To determine the cell cycle stage, cells were incubated for 1 hour (prior to immuno fluorescence) with culture medium containing 0.1 μM 5-ethynyl-2'-deoxyuridine (EdU; Invitrogen). After labelling with EdU, an UDS experiment (fluorescently labelled) was performed followed by an immuno fluorescence experiment (described below).

Embryo isolation

3.5-day-old embryos to generate ES cells

Blastocysts were isolated 3.5 days after fertilization and grown in a 24 wells plate using irradiated MEFs (20 Gy) as a feeder layer in Knock-out ES medium (Invitrogen) with 20% knock-out serum replacement (Invitrogen), 100 U/ml penicillin/streptomycin, non-essential amino acids (Invitrogen) 0.1 mM β -mercaptoethanol (Invitrogen), 5000 U/ml

Leukaemia inhibitory factor (LIF) and 50 μM MEK1 inhibitor (Cell Signaling Technology). Colonies originated from blastocysts were trypsinized and cultured further on gelatine pre-coated culture dishes at 37°C, 20% O₂ and 5% CO₂.

10.5-day-old embryos to generate MEFs

Embryos were isolated 10.5 days after fertilization, sheared using a pipette to detach the different cells and cultured in MEF medium at 37°C, 5% O₂ and 5% CO₂. Cells were cultured further under high oxygen conditions (20%) until an established cell line was formed.

RNA isolation and real-time quantitative PCR

Total RNA was purified from ES cells and 11.5-day-old embryos using the RNeasy Mini Kit (Qiagen). cDNA was created from 2 μg of RNA using an RT kit (Invitrogen) and random primers (Invitrogen). 5 μl of this cDNA was used in the following reaction with 29 nM sense and antisense primer (primer sequences available on request). The cDNA was amplified by real-time quantitative PCR (RT-qPCR) in 25 μl reactions using platinum Taq polymerase and SYBR green according to manufacturer's protocol (Invitrogen) with the c1000 Thermal Cycler (Bio-Rad). Reaction conditions were: 95°C for 3 min, followed by 40 cycles of 95°C for 15 sec, 60°C for 30 s and 72°C for 30 sec and ending with 95°C for 1 min. Expression levels were normalized to *Gapdh* using the method described by Pfaffl [54]. Specificity of the reactions was confirmed by analysis of the RT-qPCR melt curves.

Cell survival

Colony survival

Sensitivity of ES cells, MEFs and human cells to increasing doses of DNA damaging agents was determined as described previously [55]. Briefly, cells were plated in 6 cm dishes, in quadruplicate (untreated) or triplicate (treated). After 12–16 hours, cells were irradiated with a single dose ranging between 0 and 8 Gy using a ¹³⁷Cs source or UV irradiation (0–8 J/m²; 254 nm; Philips TUV lamp) or treated for 1 hour with MMC (0–0.6 $\mu\text{g}/\text{ml}$; Kyowa), or treated for 1 hour with MMS (0–2 mM; Sigma) or KBrO₃ (0–0.8 $\mu\text{g}/\text{ml}$; Sigma). After approximately 7 days, the colonies were fixed and stained with 0.1% Brilliant Blue R (Sigma) and were counted. The survival was plotted as the percentage of colonies obtained after treatment compared to the mean number of colonies from the non-treated samples (set at 100%).

[methyl-³H]-thymidine survival

MEFs were plated in 6-well culture dishes (1 \times 10⁴ cells per well) in quadruplicate (0 J/m²) or triplicate (others) in 3 ml medium. Two days after seeding, cells were washed with PBS and UV irradiated (0–8 J/m²). Five days after irradiation cells were pulse-labeled with [methyl-³H]-thymidine (40–60 Ci/mmol; 5 $\mu\text{Ci}/\text{ml}$; Amersham Biosciences), chased for 30 minutes in unlabeled medium, washed with PBS, lysed in 0.25 M NaOH and harvested. Cell lysates were transferred into scintillation flasks and supplemented with 7.5 ml Hionic Fluor scintillation fluid (Packard). Each sample was counted in the scintillation counter for 10 minutes and results were expressed as the percentage of counts obtained from the non-treated dishes (set as 100%).

UV-induced UDS and RRS

Autoradiography

For the UDS and RRS assay [56] 1 \times 10⁶ cells were seeded onto 24 mm cover slips and after 2 days UV irradiated with 16 J/m². For UDS; cells were incubated (directly after UV

irradiation) for 2 hours in culture medium containing 10 $\mu\text{Ci/ml}$ [methyl- ^3H] Thymidine (110 Ci/mmol; Amersham Biosciences), washed with PBS and fixed. For RRS, 16 hours after UV irradiation cells were incubated for 2 hours in culture medium containing 10 $\mu\text{Ci/ml}$ [^3H] Uridine (110 Ci/mmol; Amersham Biosciences), washed with PBS and fixed. In both assays the cover slips with radioactively labeled cells were mounted onto slides and dipped in a photosensitive emulsion (Ilford K2). After 2 to 7 days exposure, slides were developed and stained. Repair capacity was quantified by the number of auto-radiographic grains above the nuclei of at least 25 cells. UDS or RRS levels were expressed as the percentage of the number of grains above wild-type cells (set at 100%), assayed in parallel.

Fluorescent assay

For UDS 1×10^6 cells were seeded onto 24 mm cover slips and after 2 days UV irradiated with 16 J/m^2 . The cells were washed once with PBS and incubated for 2 h in culture medium containing $0.1 \mu\text{M}$ 5-ethynyl-2'-deoxyuridine (EdU; Invitrogen). After EdU incorporation, cells were washed twice with PBS followed by fixation in 1 ml of 4% formaldehyde in PBS. Cells were washed twice with 3% BSA in PBS and permeabilized for 20 minutes in 0.5% Triton in PBS and washed once with PBS. Cells were incubated for 30 minutes with fluorescent dye coupling buffer containing 10 mM CuSO_4 and Alexa Fluor 594 azide (Qlick-iTTM, Invitrogen). After washing with PBS, cells were mounted in vectashield. UDS levels were expressed as the average fluorescence intensity in the nucleus of wild-type cells, which was set at 100%. The mean fluorescence is determined from at least 25 cells.

Transcription measured by EU incorporation

ES cells and MEFs were grown in a 6 cm dish and cultured for 2 days prior to the experiments. The cells were washed once with PBS and incubated for 30 minutes or 2 hours in culture medium containing $0.1 \mu\text{M}$ 5-ethynyl-uridine (EU). After EU incorporation, cells were treated in the same way as described above (UDS; fluorescent assay).

Quantification of 6-4 PP and CPD UV-photoproducts by ELISA

70–80% confluent cultures of MEFs to be analyzed were washed with PBS, UV irradiated (8 J/m^2) and incubated for various time points (1 to 16 hours). Cells were harvested in PBS and DNA was isolated using QIAamp DNA Blood Mini Kit (QIAGEN). DNA concentrations were determined by measuring the optical density at 260 nm. 96-well polyvinylchloride flat-bottom micro titer plates were precoated with 0.003% Protamine Sulfate, $50 \mu\text{l/well}$ and dried in the dark overnight at 37°C (Sigma). DNA samples were denatured for 10 minutes at 95°C and immediately cooled on ice for 20 min. $50 \mu\text{l/well}$ of vortexed DNA solution in H_2O was loaded in the precoated 96-well plate to a final concentration of $6 \mu\text{g/ml}$ for the detection of 6-4PP. The plate was dried overnight at 37°C , then washed 5 times with $\text{PBS}+0.05\%$ Tween-20 ($150 \mu\text{l/well}$). The wells were pre-absorbed with $\text{PBS}+2\%$ FCS for 30 minutes at 37°C and subsequently washed 5 times with PBS/Tween-20 prior to incubation for 30 min at 37°C with $100 \mu\text{l/well}$ of primary antibody: 6-4PP (1:1000; Bioconnect/MBL) diluted in PBS. After 5 washes with PBS/Tween-20 , samples were incubated for 30 minutes at 37°C with $100 \mu\text{l/well}$ of secondary antibody: goat anti-mouse IgG (H+L) conjugated to HRP (1:2000; Southern Biotech). After 5 washes with PBS/Tween-20 , samples were treated with $100 \mu\text{l/well}$ Citrate-phosphate buffer (24 mM $\text{C}_6\text{H}_8\text{O}_7 \cdot \text{H}_2\text{O}$ and 41 mM $\text{Na}_2\text{HPO}_4 \cdot 2\text{H}_2\text{O}$; Sigma). Samples were then incubated with $100 \mu\text{l/well}$ of freshly made ODP buffer (0.4% o-Phenylene diamine and 0.02% citrate-phosphate buffer; Sigma) at 37°C for 30 min. The reaction was stopped by adding $50 \mu\text{l/well}$ of 2 M H_2SO_4 and absorbance was immediately measured at 490 nm.

Confocal microscopy

Multiphoton laser-induced DNA damage

Laser-induced DNA damage on MEFs expressing the Xpb-YFP fusion protein was performed using a Chameleon Ultra II modelocked Ti:Sapphire laser system (Coherent Inc) that was directly coupled to an LSM 510 NLO microscope (Zeiss) to obtain an 800-nm, pulsed (80 MHz) output of 26 mW. Single nuclei targeted with the multiphoton laser were exposed for 56.6 ms (via 25 iterations) over a 2.6 micrometer diameter disc.

UV laser-induced DNA damage

For UV laser irradiation a 2 mW pulsed (7.8 kHz) diode pumped solid state laser emitting at 266 nm (Rapp OptoElectronic, Hamburg GmbH) was connected to a Leica SP5 confocal microscope. For local UV-C irradiation experiments cells were grown on 25 mm diameter quartz coverslips (010191T-AB, SPI supplies) and images were obtained using a 100× quartz objective. UV-C laser irradiation was performed as previously described [31].

Analysis

The accumulation of tagged proteins at locally induced damaged regions was obtained from a series of time-lapse images by measuring the average fluorescence within a circular region matching the laser-damaged area (F^{LD}). The average fluorescence of the nucleus and the background fluorescence levels were also measured. To calculate the fluorescence signal due to the accumulation of tagged proteins within the damaged area, the average fluorescence estimated outside of the damaged region ($F^{Nucleus}$) (but still within the nucleus) was subtracted from F^{LD} . The obtained fluorescence: $F^{LD \text{ true}}$ is derived from: $F^{LD \text{ true}} = F^{LD} - F^{Nucleus}$. Dividing $F^{LD \text{ true}}$ by the total nuclear fluorescence corrected for background, resulted in the normalized fluorescence signal at the local damage area: $F^{Norm. LD \text{ true}} = F^{LD \text{ true}}/F^N$.

Immunofluorescence

Cells were grown on glass cover slips (24 mm) for three days prior to the experiments and fixed with 2% paraformaldehyde (Sigma) at 37°C for 15 minutes. Cover slips were washed three times for 5 minutes with PBS containing 0.1% Triton X-100 (Sigma). To visualize the DNA photoproducts, nuclear DNA was denatured by incubation with 0.07 N NaOH (Sigma) at room temperature for 5 minutes and washed three times for 5 minutes with 0.1% Triton X-100 and subsequently for 5 minutes with PBS⁺ (PBS containing 0.15% glycine (Sigma) and 0.5% BSA (Sigma)). Cells were incubated at room temperature with primary antibodies for 2 hrs in a moist chamber. Subsequently, cover slips were washed three times with PBS/Triton X-100 and PBS⁺, incubated 1 hour with secondary antibodies at room temperature and again washed three times in PBS/Triton X-100. Samples were embedded in Vectashield mounting medium (Vector Laboratories). Images were obtained using a confocal laser scanning microscope (LSM 510; Zeiss). The primary antibodies used for this procedure were mouse anti-CPD (1:1000; TDM-2; BioConnect/MBL), rabbit anti-GFP (1:1000; ab290; Abcam), rabbit anti XPB (1:1000; S19; Santa Cruz), rabbit anti XPC (1:200; fraction 5; home-made), mouse anti γ H2AX (1:1000; 07-164; Millipore) and mouse anti-MDC1 (1:1000; MDC1-50; Abcam). The secondary antibodies used were Alexa Fluor 594 goat anti-mouse IgG (H+L) (1:1000; Molecular probes), Alexa Fluor 594 goat anti-rabbit IgG (H+L) (1:1000; Molecular probes), Alexa Fluor 488 goat anti-rabbit IgG (H+L) (1:1000; Molecular probes), Alexa Fluor 488 goat anti-mouse IgG (H+L) (1:1000; Molecular probes) and Alexa Fluor 647 azide (1:400; invitrogen).

Proliferation assay

To measure proliferation in MEFs, equal number of cells from early passages (p2) were plated in 6 cm culture dishes (approximately 1×10^4 cells per well) in triplicate in 3 ml medium (day 0). The medium was changed every 2 days cells and cells were counted 1, 3, 5 and 6 days after seeding, using a cell counter (Beckman Coulter Z2).

Supporting Information

Figure S1 Accumulation of XpbYFP and Xpc at locally induced DNA damaged regions. Accumulation kinetics of XpbYFP to local Multi Photon (MP) damage in a wild-type, *Ttda*^{+/-} and *Ttda*^{-/-} backgrounds. Graphs represents the mean YFP-derived fluorescence intensity at the damaged spot at the indicated time points from 12 cells.

Figure S2 Quantitative immune-fluorescence to determine the relative amount of TFIH. Representative confocal microscope pictures of MRC5-sv (wild-type), TTD1BR-sv (TTD-A) and TTD1BR-sv cells stably expressing shRNA (#3398 or #3402). Cells were stained with DAPI (left), anti-XPB (TFIIH subunit) (middle) and anti-MDC1 (internal control) (right).

Figure S3 Mutant TTDA-GFP accumulation at locally UV-induced regions. (A) Colony forming ability after different doses of UV of wild-type, *Ttda*^{+/-}, *Ttda*^{-/-}, *Ttda*^{-/-} stably transfected with TTDA^{WT}-GFP and *Xpa*^{-/-} ES cells. The percentage of surviving cells was plotted against the applied UV-dose, measured by counting surviving colonies of two independent experiments. The error bars indicate the SEM. (B) Immuno-fluorescent analysis on TTD1BR-sv cells stably expressing either TTDA^{WT}-GFP or TTDA^{R56X}-GFP. Cells were seeded on cover slips and the next day irradiated locally with 60 J/m² through a filter containing 5 μm pores. Cells were fixed 1 hour after UV and immuno-fluorescent staining was performed using antibodies against CPDs (damage marker, red) and GFP (green).

Figure S4 Gene expression levels of *Ttda*^{-/-} 11.5-day-old embryos. Relative expression levels of mRNAs neighboring genes encoding Synaptojamain 2 (*Synj2*), Serine active site containing 1 (*Serac1*) and Tubby like protein 4 (*Tulp4*) in *Ttda*^{-/-} (n=8), *Ttda*^{+/-} (n=8) and wild-type (n=8) in embryos as determined by quantitative RT-PCR. The levels were normalized to *Gapdh* and the error bars indicate SEM between experiments.

Figure S5 Proliferation assay and gene expression levels of BER genes. (A) Equal number of cells (1×10^4) were plated on 6 cm culture dishes in triplicate (day 0). The total number of cells was counted in wild-type (n=2), *Ttda*^{+/-} (n=2) and *Ttda*^{-/-} (n=2) MEFs at different days after seeding. The error bars indicate the SEM. (B) Relative expression levels of mRNAs encoding Apurinic-apyrimidinic endonuclease 1 (*Apex1*), Flap structure-specific endonuclease 1 (*Fen1*), Ligase III (Lig3), Poly [ADP-ribose] polymerase 1 (*PARP1*), DNA polymerase beta (*PolB*) and X-ray repair cross-complementing protein 1 (*Xrcc1*) in wild-type (n=8) and *Ttda*^{-/-} (n=8) 11.5-days-old embryos as determined by quantitative RT-PCR. The levels were normalized to *Gapdh* and the error bars indicate SEM between experiments.

Table S1 Genotyping of the offspring from matings of *Ttda*^{+/-LNL} mice. Genotyping of offspring from matings of *Ttda*^{+/-LNL} mice, distributed over male and females, obtained number and percentage of offspring compared to the theoretical expected figures

assuming a Mendelian inheritance pattern.

Acknowledgments.

We thank Applied Optical Image Center, Erasmus MC, Rotterdam, for providing the confocal live-cell imaging facility.

Author Contributions

Conceived and designed the experiments: AFT GG-M WV. Performed the experiments: AFT JN BS P-OM JdW CL AR AM MV GG-M. Analyzed the data: AFT GGM. Wrote the paper: AFT JHJH GG-M WV. Provided analysis tools and scientific input: JAM JE.

References

- Hoeijmakers JH (2001) Genome maintenance mechanisms for preventing cancer. *Nature* 411: 366-374.
- Sugasawa K, Akagi J, Nishi R, Iwai S, Hanaoka F (2009) Two-step recognition of DNA damage for mammalian nucleotide excision repair: Directional binding of the XPC complex and DNA strand scanning. *Mol Cell* 36: 642-653.
- Conaway RC, Conaway JW (1993) General initiation factors for RNA polymerase II. *Annu Rev Biochem* 62: 161-190.
- Egly JM (2001) The 14th Datta Lecture. TFIIH: from transcription to clinic. *FEBS Lett* 498: 124-128.
- Zurita M, Merino C (2003) The transcriptional complexity of the TFIIH complex. *Trends Genet* 19: 578-584.
- Schaeffer L, Roy R, Humbert S, Moncollin V, Vermeulen W, et al. (1993) DNA repair helicase: a component of BTF2 (TFIIH) basic transcription factor. *Science* 260: 58-63.
- Vermeulen W, Scott RJ, Rodgers S, Muller HJ, Cole J, et al. (1994) Clinical heterogeneity within xeroderma pigmentosum associated with mutations in the DNA repair and transcription gene ERCC3. *Am J Hum Genet* 54: 191-200.
- Lehmann AR (2003) DNA repair-deficient diseases, xeroderma pigmentosum, Cockayne syndrome and trichothiodystrophy. *Biochimie* 85: 1101-1111.
- Kraemer KH, Levy DD, Parris CN, Gozukara EM, Moriwaki S, et al. (1994) Xeroderma pigmentosum and related disorders: examining the linkage between defective DNA repair and cancer. *J Invest Dermatol* 103: 96S-101S.
- Broughton BC, Berneburg M, Fawcett H, Taylor EM, Arlett CF, et al. (2001) Two individuals with features of both xeroderma pigmentosum and trichothiodystrophy highlight the complexity of the clinical outcomes of mutations in the XPD gene. *Hum Mol Genet* 10: 2539-2547.
- Faghri S, Tamura D, Kraemer KH, Digiovanna JJ (2008) Trichothiodystrophy: a systematic review of 112 published cases characterises a wide spectrum of clinical manifestations. *J Med Genet* 45: 609-621.
- Weeda G, Eveno E, Donker I, Vermeulen W, Chevallier-Lagente O, et al. (1997) A mutation in the XPB/ERCC3 DNA repair transcription gene, associated with trichothiodystrophy. *Am J Hum Genet* 60: 320-329.
- Broughton BC, Steingrimsdottir H, Weber CA, Lehmann AR (1994) Mutations in the xeroderma pigmentosum group D DNA repair/transcription gene in patients with trichothiodystrophy. *Nat Genet* 7: 189-194.
- Stefanini M, Lagomarsini P, Giliani S, Nardo T, Botta E, et al. (1993) Genetic heterogeneity of the excision repair defect associated with trichothiodystrophy. *Carcinogenesis* 14: 1101-1105.
- Giglia-Mari G, Coin F, Ranish JA, Hoogstraten D, Theil A, et al. (2004) A new, tenth subunit of TFIIH is responsible for the DNA repair syndrome trichothiodystrophy group A. *Nat Genet* 36: 714-719.
- Vermeulen W, Bergmann E, Auriol J, Rademakers S, Frit P, et al. (2000) Sublimiting concentration of TFIIH transcription/DNA repair factor causes TTD-A trichothiodystrophy disorder. *Nat Genet* 26: 307-313.
- Coin F, De Santis LP, Nardo T, Zlobinskaya O, Stefanini M, et al. (2006) p8/TTD-A as a repair-specific TFIIH subunit. *Mol Cell* 21: 215-226.
- Kainov DE, Vitorino M, Cavarelli J, Poterszman A, Egly JM (2008) Structural basis for group A trichothiodystrophy. *Nat Struct Mol Biol* 15: 980-984.

19. Aguilar-Fuentes J, Fregoso M, Herrera M, Reynaud E, Braun C, et al. (2008) p8/TTDA overexpression enhances UV-irradiation resistance and suppresses TFIIH mutations in a *Drosophila* trichothiodystrophy model. *PLoS Genet* 4: e1000253.
20. Ranish JA, Hahn S, Lu Y, Yi EC, Li XJ, et al. (2004) Identification of TFB5, a new component of general transcription and DNA repair factor IIH. *Nat Genet* 36: 707-713.
21. Giglia-Mari G, Miquel C, Theil AF, Mari PO, Hoogstraten D, et al. (2006) Dynamic interaction of TTDA with TFIIH is stabilized by nucleotide excision repair in living cells. *PLoS Biol* 4: e156.
22. Theil AF, Nonnekens J, Wijgers N, Vermeulen W, Giglia-Mari G (2011) Slowly progressing nucleotide excision repair in trichothiodystrophy group A patient fibroblasts. *Mol Cell Biol* 31: 3630-3638.
23. Jorizzo JL, Atherton DJ, Crouse RG, Wells RS (1982) Ichthyosis, brittle hair, impaired intelligence, decreased fertility and short stature (IBIDS syndrome). *Br J Dermatol* 106: 705-710.
24. Brooks BP, Thompson AH, Clayton JA, Chan CC, Tamura D, et al. (2011) Ocular manifestations of trichothiodystrophy. *Ophthalmology* 118: 2335-2342.
25. Park E, Guzder SN, Koken MH, Jaspers-Dekker I, Weeda G, et al. (1992) RAD25 (SSL2), the yeast homolog of the human xeroderma pigmentosum group B DNA repair gene, is essential for viability. *Proc Natl Acad Sci U S A* 89: 11416-11420.
26. de Boer J, Donker I, de Wit J, Hoeijmakers JH, Weeda G (1998) Disruption of the mouse xeroderma pigmentosum group D DNA repair/basal transcription gene results in preimplantation lethality. *Cancer Res* 58: 89-94.
27. Andressoo JO, Weeda G, de Wit J, Mitchell JR, Beems RB, et al. (2009) An Xpb mouse model for combined xeroderma pigmentosum and cockayne syndrome reveals progeroid features upon further attenuation of DNA repair. *Mol Cell Biol* 29: 1276-1290.
28. Andressoo JO, Mitchell JR, de Wit J, Hoogstraten D, Volker M, et al. (2006) An Xpd mouse model for the combined xeroderma pigmentosum/Cockayne syndrome exhibiting both cancer predisposition and segmental progeria. *Cancer Cell* 10: 121-132.
29. Sakai K, Miyazaki J (1997) A transgenic mouse line that retains Cre recombinase activity in mature oocytes irrespective of the cre transgene transmission. *Biochem Biophys Res Commun* 237: 318-324.
30. de Waard H, de Wit J, Gorgels TG, van den Aardweg G, Andressoo JO, et al. (2003) Cell type-specific hypersensitivity to oxidative damage in CSB and XPA mice. *DNA Repair (Amst)* 2: 13-25.
31. Dinant C, de Jager M, Essers J, van Cappellen WA, Kanaar R, et al. (2007) Activation of multiple DNA repair pathways by sub-nuclear damage induction methods. *J Cell Sci* 120: 2731-2740.
32. Giglia-Mari G, Theil AF, Mari PO, Mourgues S, Nonnekens J, et al. (2009) Differentiation driven changes in the dynamic organization of Basal transcription initiation. *PLoS Biol* 7: e1000220.
33. Mocquet V, Laine JP, Riedl T, Yajin Z, Lee MY, et al. (2008) Sequential recruitment of the repair factors during NER: the role of XPG in initiating the resynthesis step. *EMBO J* 27: 155-167.
34. Hanasoge S, Ljungman M (2007) H2AX phosphorylation after UV irradiation is triggered by DNA repair intermediates and is mediated by the ATR kinase. *Carcinogenesis* 28: 2298-2304.
35. Matsumoto M, Yaginuma K, Igarashi A, Imura M, Hasegawa M, et al. (2007) Perturbed gap-filling synthesis in nucleotide excision repair causes histone H2AX phosphorylation in human quiescent cells. *J Cell Sci* 120: 1104-1112.
36. Marteiijn JA, Bekker-Jensen S, Mailand N, Lans H, Schwertman P, et al. (2009) Nucleotide excision repair-induced H2A ubiquitination is dependent on MDC1 and RNF8 and reveals a universal DNA damage response. *J Cell Biol* 186: 835-847.
37. Ruven HJ, Berg RJ, Seelen CM, Dekkers JA, Lohman PH, et al. (1993) Ultraviolet-induced cyclobutane pyrimidine dimers are selectively removed from transcriptionally active genes in the epidermis of the hairless mouse. *Cancer Res* 53: 1642-1645.
38. Nakane H, Takeuchi S, Yuba S, Saijo M, Nakatsu Y, et al. (1995) High incidence of ultraviolet-B-or chemical-carcinogen-induced skin tumours in mice lacking the xeroderma pigmentosum group A gene. *Nature* 377: 165-168.
39. de Vries A, van Oostrom CT, Hofhuis FM, Dortant PM, Berg RJ, et al. (1995) Increased susceptibility to ultraviolet-B and carcinogens of mice lacking the DNA excision repair gene XPA. *Nature* 377: 169-173.

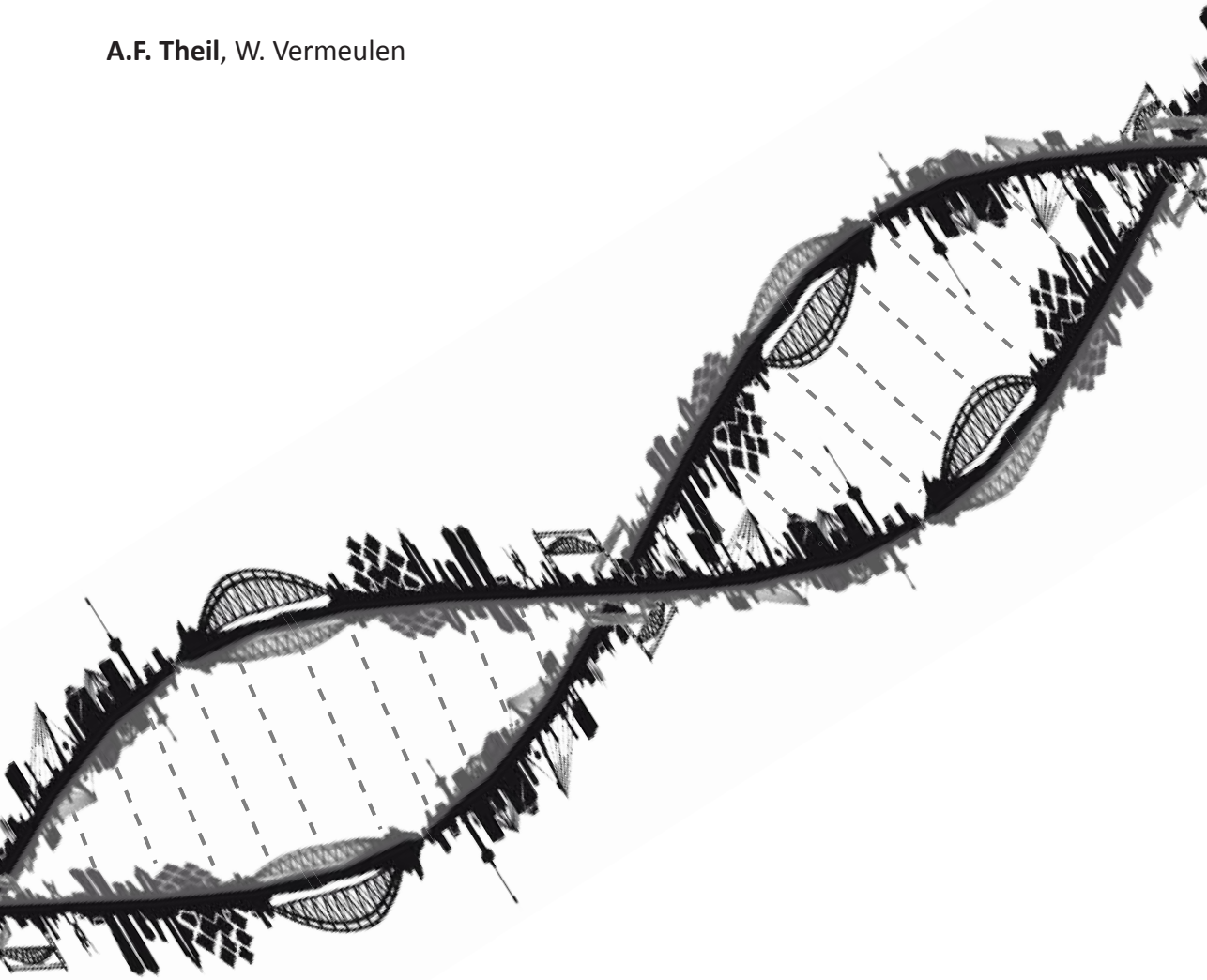
40. Hanada K, Vermeij M, Garinis GA, de Waard MC, Kunen MG, et al. (2007) Perturbations of vascular homeostasis and aortic valve abnormalities in fibulin-4 deficient mice. *Circ Res* 100: 738-746.
41. Niedernhofer LJ, Odijk H, Budzowska M, van Drunen E, Maas A, et al. (2004) The structure-specific endonuclease Ercc1-Xpf is required to resolve DNA interstrand cross-link-induced double-strand breaks. *Mol Cell Biol* 24: 5776-5787.
42. Hegde ML, Hazra TK, Mitra S (2008) Early steps in the DNA base excision/single-strand interruption repair pathway in mammalian cells. *Cell Res* 18: 27-47.
43. Hazra TK, Das A, Das S, Choudhury S, Kow YW, et al. (2007) Oxidative DNA damage repair in mammalian cells: a new perspective. *DNA Repair (Amst)* 6: 470-480.
44. Zhou Y, Kou H, Wang Z (2007) Tfb5 interacts with Tfb2 and facilitates nucleotide excision repair in yeast. *Nucleic Acids Res* 35: 861-871.
45. Helleday T, Petermann E, Lundin C, Hodgson B, Sharma RA (2008) DNA repair pathways as targets for cancer therapy. *Nat Rev Cancer* 8: 193-204.
46. Niedernhofer LJ, Garinis GA, Raams A, Lalai AS, Robinson AR, et al. (2006) A new progeroid syndrome reveals that genotoxic stress suppresses the somatotroph axis. *Nature* 444: 1038-1043.
47. van der Pluijm I, Garinis GA, Brandt RM, Gorgels TG, Wijnhoven SW, et al. (2007) Impaired genome maintenance suppresses the growth hormone--insulin-like growth factor 1 axis in mice with Cockayne syndrome. *PLoS Biol* 5: e2.
48. Sarker AH, Tsutakawa SE, Kostek S, Ng C, Shin DS, et al. (2005) Recognition of RNA polymerase II and transcription bubbles by XPG, CSB, and TFIIH: insights for transcription-coupled repair and Cockayne Syndrome. *Mol Cell* 20: 187-198.
49. Hanawalt PC, Spivak G (2008) Transcription-coupled DNA repair: two decades of progress and surprises. *Nat Rev Mol Cell Biol* 9: 958-970.
50. Moslehi R, Kumar A, Mills JL, Ambroggio X, Signore C, et al. (2012) Phenotype-specific adverse effects of XPD mutations on human prenatal development implicate impairment of TFIIH-mediated functions in placenta. *Eur J Hum Genet*.
51. de Boer J, Hoeijmakers JH (1999) Cancer from the outside, aging from the inside: mouse models to study the consequences of defective nucleotide excision repair. *Biochimie* 81: 127-137.
52. Keriell A, Stary A, Sarasin A, Rochette-Egly C, Egly JM (2002) XPD mutations prevent TFIIH-dependent transactivation by nuclear receptors and phosphorylation of RARalpha. *Cell* 109: 125-135.
53. Pluck A (1996) Conditional mutagenesis in mice: the Cre/loxP recombination system. *Int J Exp Pathol* 77: 269-278.
54. Pfaffl MW (2001) A new mathematical model for relative quantification in real-time RT-PCR. *Nucleic Acids Res* 29: e45.
55. Essers J, Hendriks RW, Swagemakers SM, Troelstra C, de Wit J, et al. (1997) Disruption of mouse RAD54 reduces ionizing radiation resistance and homologous recombination. *Cell* 89: 195-204.
56. Vermeulen W, Osseweijer P, de Jonge AJ, Hoeijmakers JH (1986) Transient correction of excision repair defects in fibroblasts of 9 xeroderma pigmentosum complementation groups by microinjection of crude human cell extracts. *Mutat Res* 165: 199-206.



CHAPTER 6

| Discussion

A.F. Theil, W. Vermeulen



Discussion

The importance of nucleotide excision repair (NER) for the prevention of both aging and cancer is exemplified by the dramatic consequences associated with inherited NER defects [1-8]. Depending on the type of DNA repair defect, two of the major manifestations of these syndromes are cancer predisposition and/or segmental progeria. These UV-hypersensitive NER-deficient syndromes, include: the cancer-prone XP, and the progeroid and developmental syndromes; TTD and CS. Next to cancer, also age-related diseases and discomfort have become a major social and medical issue due to the still increasing life expectancy in developed countries. It is therefore highly relevant to understand the biological processes that counteract these phenomena. In this thesis we investigated the molecular mechanism and clinical implications of TTDA deficiency in patient derived cells and a whole organism. In general, TTD-A patients present a relatively mild form of TTD, including the moderate UV-hypersensitivity [4, 9, 10]. Although analysis of TTD-A patient cells have provided valuable information on the NER function of TTDA, they do not deliver an accurate explanation for their clinical symptoms. To get a better understanding of the molecular mechanisms underlying this phenotype, we have investigated the function of TTDA in human derived cell lines and created a *Ttda* knock-out (*Ttda*^{-/-}) mouse-model.

TTDA localization

Basal transcription factor II H (TFIIH) is a ten-subunit complex that is implicated in multiple cellular processes: basal and activated RNA polymerase II transcription, ribosomal RNA gene expression (RNA polymerase I transcription), participation in GG-NER and TC-NER, and cell-cycle regulation [11, 12]. The complexity of this factor is also reflected by the dynamic composition of distinct sub-complexes, as well as its multiple enzymatic activities: DNA-dependent ATPases and helicases, kinase, and ubiquitin ligase. The existence of these multiple activities clearly complicates the analysis of specific functions, when studied in standard *in vitro* assays. Both the dynamic regulation of activities and the existence of different kinetic pools are usually not measured by *in vitro* analysis. The thermodynamic parameters within the mammalian cell nuclei are also critical for regulating these activities (such as physiologically relevant environment, high local variations of protein concentrations, and conformation of the DNA substrate) and cannot be fully mimicked *in vitro*.

Using subcellular fractionation (unpublished data) and GFP-tagging [13], we and others have shown that endogenous XPD is found in both the cytoplasm and the nucleus. Santagati and colleagues also find p44 to exist in both the cytoplasmic fraction and the nuclear fraction [13]. It was recently shown that XPD has a potential role in chromosome segregation [14, 15], functioning independently of TFIIH. It is thus not unprecedented that some of the subunits can exist outside the context of the TFIIH-complex. In our live cell studies we found that TTDA-GFP and XPD-GFP reside both in the cytoplasm and in the nucleus, contrasting to the strictly nuclear localization of XPB-GFP [16]. Photo-bleaching experiments also indicated that both proteins do not interact with TFIIH in the cytoplasm. However, we showed that both TTDA-GFP and XPD-GFP do interact with TFIIH in the nucleus. In striking contrast to XPB-GFP, the association of TTDA-GFP to TFIIH (and to a lesser extent also of XPD-GFP) is much more dynamic [16].

Although TTDA can be considered as integral component of TFIIH in biochemical terms [10], its association to TFIIH in live cells appeared not as firm as some other components. Under normal culture conditions (relatively low presence of genomic injuries) a dynamic equilibrium between TFIIH-associated and free TTDA is present. The

fact that a sudden high concentration of DNA lesions by UV-irradiation causes a quick shift in the equilibrium of free versus TFIIH-bound TTDA, suggests that this protein is stronger associated or trapped when the complex is actively engaged in NER [16, 17].

TTDA function in NER

Remarkable and puzzling repair properties are present in TTD-A primary fibroblasts, as a relatively mild UV-sensitivity is accompanied with a very low UV-induced unscheduled DNA synthesis (UDS) [10, 18]. In other NER-deficient XP cells that present similar low levels of UDS (such as XP-D, XP-A or XP-G), UV-sensitivity appeared much more pronounced. By thorough analysis of different NER properties in TTD-A cells, we were able to produce a possible explanation for this apparent discrepancy. NER-induced DNA synthesis measurements are generally conducted within the first two hours after UV irradiation, whereas UV-survival measurements extend over a few days after the initial damaging event. Based on these two entirely different time-scales of monitoring DNA repair endpoints, we hypothesized that the repair activity in TTD-A cells is not completely deficient, but progresses slowly in time. Indeed, UV-induced lesions that are mainly responsible for cytotoxicity (6-4PP) are gradually removed in TTD-A cells. The removal of 6-4PPs occurs at a much slower rate than in wild type cells and was not observed in complete NER-deficient XP-A cells (assayed in parallel). Surprisingly, CPD removal was not retarded in TTD-A primary fibroblasts but showed similar repair kinetics as a NER-proficient cell line. Apparently, for the repair of CPD lesions other NER associated factors are more important to determine the rate of NER-complex formation and actual removal of CPD lesions. This observation is remarkably different to the repair parameters measured in other non-*TTDA* mutated UV-hypersensitive TTD (XP-B or XP-D) cells. In fact, it has been shown that, in XP-D mutated TTD primary fibroblasts, the 6-4PP repair capacity is highly variable and depends on the mutation in the *XPD* gene: 6-4PPs are either repaired normally as in TTD1VI cells (R722W), or not repaired at all in TTD9VI (R112H) [19]. In addition, in XP-B/TTD primary fibroblasts TTD6VI (amino acid 355 affected) [20] 6-4PP are efficiently repaired [21]. Although 6-4PP removal appeared highly variable throughout the different NER-deficient TTD cells, a delayed repair as in TTD-A was never observed. In conclusion, the retarded repair of 6-4PP observed in TTD-A cells appeared a specific feature of this complementation group and explains the initial low UDS accompanied by moderate UV-hypersensitivity.

Reduced steady-state levels of TFIIH in TTD-A cultured fibroblasts appeared to be a critical determinant in NER efficiency [18], but this lower concentration of the crucial basal transcription factor in cultured cells does not seem to largely affect the transcriptional competence. This suggests that NER requires higher concentrations of TFIIH or that the altered structure of the complex in the absence of TTDA mainly affects the NER function rather than the transcription function. Previous live cell kinetic studies [22] revealed that a relatively large proportion of the resident TFIIH molecules are recruited to NER sites at which they are bound significantly longer (4–5 min) than when bound for an average transcription initiation event (2–10 s). This difference in kinetic behavior of TFIIH when engaged in either transcription or DNA repair provides an explanation why one process is more sensitive to relative enzyme concentrations than the other. The *in vitro* NER studies [23] showed that not only the concentration but also the composition of TFIIH is critical for its function in NER. In the absence of TTDA, only low levels of repair are detected, suggesting that association of TTDA to TFIIH renders this complex more competent for NER, at least *in vitro*.

Ttda knock-out mice

In an attempt to create a *Ttda* knock-out mouse model, we have shown that this gene is essential for embryonic development. Contrary to expectations, *Ttda*^{-/-} mice die *in utero* between 10.5 days of gestation and birth. This unexpected lethality contradicts with the alleged non-vital function of TTDA in TTD-A patients, who only express relatively mild TTD features. The possible origin of this lethality will be discussed later. Obviously, with this remarkable lethal phenotype detailed organismal analysis to the nature of the TTD etiology is not possible. However, early embryonic development was still possible that allowed the isolation of embryonic cells.

Analysis of NER parameters in embryonic *Ttda*^{-/-} cells revealed a remarkably severe NER-deficiency and includes extreme UV-hypersensitivity, absence of UV-induced UDS and complete absence of removing UV-induced lesions (comparable to *Xpa*^{-/-} cells). This complete NER-deficient phenotype is in striking contrast to the only mild NER defect seen in human TTD-A cells. The NER-deficiency observed cannot be explained by a cell-type specific UV-response, since MEFs and ES cells are equally UV-sensitive. This apparent discrepancy could be derived from a human-mouse difference in NER efficiency or that the mutated TTDA proteins in patient cells are partially biological active. Upon depletion of mutant *TTDA* mRNA in TTD-A human patient cells by short hairpin RNA interference, a strong aggravation of the UV-sensitivity was noticed. These results suggest that the mutated human TTDA proteins still harbor residual NER activity and that the severe NER-deficient phenotype observed in *Ttda*^{-/-} cells is not specific for mouse cells. From these data we conclude that in the currently known patients the mutant TTDA protein is partially functional. This hypothesis is further substantiated by the fact that all TTDA mutant proteins were able to partially correct the complete absence of NER of *Ttda*^{-/-} MEFs when overexpressed. The suggestion that in TTD13/14PV patient cells a partly functional protein is present is particularly intriguing, since it has been suggested that no TTDA protein is expressed in these cells due to the homozygous translational start-site mutation [10]. One way to explain this phenomenon is by assuming that despite this ATG mutation, some TTDA protein is still being produced by initiating from an in-frame downstream ATG (codon 16). The usage of this alternative start site may produce low levels of an N-terminally truncated TTDA protein, sufficient to partly correct the complete absence of NER in TTD-A patient cells. Interestingly, it has been shown (both in yeast and humans) that the N-terminal domain of TTDA is important for binding to the TFIIH subunits XPD and p52 [23, 24] and for its role in stimulating the ATPase-activity of the XPB subunit [23]. Furthermore, this interaction is also critical for the TFIIH stability. Apparently, the truncated *Ttda* protein is nevertheless able to carry out part of its function to permit residual NER. A possibility is that anchorage of TTDA into TFIIH triggers a conformational change that increases the residence time on NER-lesions and enables recruitment of subsequent NER factors. This may also fit with the observation that lack of TTDA makes TFIIH less stable. Improperly folded proteins are usually vulnerable to degradation. Interaction with TTDA might stabilize the complex either by aiding folding (as a chaperone-like function) or by maintaining tertiary structure. This model unites reduced repair with instability.

We propose a model in which the absence of functional TTDA causes improperly folded/structured TFIIH that not only affects the stability of TFIIH [18], but also efficient NER complex assembly [25, 26]. In the absence of TTDA we could not observe binding of TFIIH to local DNA damage, whereas its predecessor XPC is bound to lesions in *Ttda*^{+/-} MEFs. This notion further corroborates our model and suggests that TTDA is an essential NER factor for stable NER complex assembly [26].

TTDA and oxidative DNA repair

TTDA's essential role in NER has far-reaching biological significance. However, the complete NER deficiency cannot explain the embryonic lethality, since other mice with fully compromised NER function (e.g. *Xpa*^{-/-} mice) do not display similar developmental abnormalities and are viable [27]. Despite the severely reduced amount of TFIIH in *Ttda*^{-/-} cells, which also display attenuated overall transcription, the proliferative capacity of the embryonic cells was not affected. It is thus not likely that reduced overall transcription would be a major cause to the embryonic lethality. Detailed analysis of different mutant TFIIH mouse models revealed a correlation between sensitivity to oxidative DNA damage (oxidative DNA damage) and severity of the phenotype of the different models [28, 29]. These observations argued for a unknown function of TFIIH in oxidative DNA damage removal. To investigate whether *Ttda*^{-/-} cells are also defective in repairing other (non NER-type) DNA lesions, we measured their sensitivity to several oxidizing agents. Clonogenic survival assays performed on *Ttda*^{-/-} ESCs revealed hyper-sensitivity to gamma irradiation and potassium bromate, similar to *Csb*^{-/-} ESCs (known to be sensitive to oxidative DNA damage). Since *Xpa*^{-/-} ESCs assayed in parallel were not sensitive to any of these agents, this sensitivity is not a general effect of NER-deficiency. These clear sensitivities to oxidative DNA damage of *Ttda*^{-/-} cells, distinguishes these cells from the other TFIIH mutants which are only mildly (or even hardly detectable) sensitive.

Based on these results we suggest that *Ttda*^{-/-} embryos are confronted with unrepaired endogenous oxidative lesions, possibly generated by low but continuous exposure to ROS during development. Defects in multiple DNA repair systems may cause synergistic effects or even synthetic lethality [30]. For example, severe developmental and premature aging problems have been seen in KO mouse models of DNA repair factors that function in independent repair pathways, such as ERCC1 (which functions in NER and inter-strand cross-link repair) and *Xpa*^{-/-} *Csb*^{m/m} double KOs (which are defective in GG-NER, and presumably also in the broad TCR pathway) [31, 32]. Based on cellular sensitivity to oxidative DNA damage [29] it has been suggested that endogenously produced DNA lesions (e.g. from ROS side products of respiration or lipid peroxidation) that cannot be removed because of the repair defect are in part responsible for the phenotype observed. This compromised repair of oxidative DNA lesions may contribute to the observed lethal phenotype observed in the *Ttda*^{-/-} embryos. Importantly, this reduced resistance to oxidative DNA damage is likely not caused by a general (core) BER defect. Previously it was suggested that TFIIH is implicated in coordinating incision of lesion-stalled transcription complexes [33] and that some oxidative DNA lesions are processed by transcription-coupled repair [34]. It is thus possible that TTDA (TFIIH) is involved in a specific — thus far uncharacterized — transcription-coupled repair process of oxidative DNA damage.

The existence of a transcription-coupled repair (TCR) process for oxidative DNA damage, similar to TC-NER for bulky lesions, has long been a matter of debate within the DNA repair field, due to the lack of robust or sensitive assays. However, very recently the Spivak/Hanawalt laboratory has developed a very sensitive assay to monitor strand-specific repair of both bulky lesions and oxidative DNA lesions, by combining FISH (strand specific gene probes) with a Comet-assay [35]. This unique novel assay unequivocally proved the existence of TCR of oxidative lesions. We are currently investigating whether *Ttda*^{-/-} cells are defective in repairing other (non NER-type) DNA lesions. The technique described by the group of Spivak/Hanawalt would be ideally suited to determine whether TTDA (or TFIIH) is implicated in TCR of oxidative lesions.

Most oxidative DNA lesions however do not interfere with the RNAP2 elongation, although increasing evidence suggests that BER repair-intermediates do so. If repair of these lesions is initiated by RNAP2 stalling, it would be interesting to investigate if repair-intermediates of BER really block transcription (measured by a technique called Recovery after RNA Synthesis (RRS)) and which proteins are required to repair the damage.

TTDA and transcription

It is surprising to note that viability is not critically depending on TTDA and on high amounts of TFIIF, as embryos develop to almost birth. This is in striking contrast with deletion mutants of other tested TFIIF subunits, which are not viable in yeast and mammals. Incompatibility with life associated with deletions of TFIIF encoding genes was explained by the vital transcriptional role of TFIIF [36]. Extrapolation of this hypothesis thus argues that TTDA is not essential for the transcription reaction. Coin and coworkers [23] indeed show that *in vitro* TTDA appeared not to stimulate transcription, whereas it was shown to aid NER. However, part of the non-NER-related features observed in patients with TTD-A (such as the brittle hair) are thought to be derived from an effect on the transcription function [36, 37]. This apparent contradiction can be explained by the differential transcriptional program and fate of specific tissues and cell types that are involved in TTD pathology. We propose a model in which transcription in terminally differentiated keratinocytes that form hair is limited to a group of cysteine-rich matrix protein genes. These gene products cross-link keratin filaments and make hair strong. Due to the highly specialized nature (terminal differentiation) of these cells the majority of the genome is transcriptionally repressed, including genes coding for house-keeping transcription factors. Transcription of these cysteine-rich matrix protein genes thus relies on the resident transcription factors. However, in TTD patient keratinocytes, due to the reduced TFIIF stability, the amount of TFIIF will not be sufficient to support transcription by the time these cells have reached the final differentiation stage. Thus reduced transcription of this group of genes that are the last to be expressed explains the hallmark feature of TTD, brittle hair. From this model it is predicted that the reduced stability of TFIIF by TTD mutations will affect transcription in other highly specialized or terminally differentiated cells. Indeed anemic-features have been described in some TTD patients, likely due to reduced beta-globin expression [38]. Also in precursor erythrocytes (just prior to nuclear eviction) cells are highly specialized in producing hemoglobin and predominantly transcribe large amounts of globin genes. This observation further corroborates our hypothesis. In addition to the sub-limiting TFIIF concentrations, also the specific spatio-temporal organization of highly differentiated post-mitotic cells (e.g.: neurons, myocytes, and hepatocytes) may contribute to cell-specific expression of TTD features. We have shown that in post-mitotic cells, TFIIF is bound to promoters with a much longer residence time than in proliferative cells [39]. A possible explanation for this static behaviour is that in these post-mitotic terminally differentiated cells, a large part of the transcription program is dedicated to a specific subset of genes defining cellular specialty and housekeeping functions, without the need to continuously switch to transcribe genes that are needed for proliferation (cell cycle, replication, and mitosis, etc.). This reduced plasticity of transcription factors can be (partly) reversed by changing conditions such as sudden high doses of genomic insults [39], allowing adaptation to a changing environment. When, due to the TTD mutations, TFIIF function is affected or unstable, transcription adaptation is no longer possible and may make cells less responsive to external and internal cues, which may eventually lead to premature

cell death or senescence. We have demonstrated that *Ttda*^{-/-} cells have a low steady state level of TFIIH and accordingly have a lower transcriptional activity. The low TFIIH quantity does not seem to be the sole cause of embryonic lethality, since similar low levels of TFIIH are observed in TTD-A patient cell lines, which are compatible with life. It is however, possible that transcription is more affected in *Ttda*^{-/-} cells, since TTD-A patients still harbor a partial functional TTDA protein. The notion of reduced transcriptional activity in *Ttda*^{-/-} cells argues that this feature may contribute to embryonic lethality. For instance, during certain stages of embryonic development which requires high transcriptional capacity, normal embryogenesis may be compromised. Moreover, it cannot be excluded that completely lacking *Ttda* affect the transcription of a subset of specific genes as shown in cells with XPD-associated TTD mutations defective in activated-transcription of nuclear receptors [40]. In this scenario, the expression of specific genes, essential for development of the embryo might be disturbed hindering proper embryogenesis and finally inducing in utero death. In both cases, TTDA function appears to extend beyond the previously suggested main function in NER, as it is also important for both development and viability.

***Ttda*^{-/-} embryos**

It was surprising to note that the *Ttda* knock-out mice were not viable. The fact that differential expression levels of neighboring genes did not correlate with lethality demonstrates that this lethality was not due to any inadvertent effect of the targeting strategy. This lethality is also independent of the genetic background of the mouse strain used, since mating's of *Ttda*^{+/-} neither in C57bl/6 or in FVB background produced viable offspring. Isolated embryos from early pregnancy revealed a normal Mendelian distribution. However, we observed a progressive loss of phenotypically normal homozygous *Ttda*^{-/-} embryos during later stages of gestation. *Ttda*^{-/-} embryos that do survive up to 19.5 days of gestation show a delay in development and have a reduction in size and body-weight. On top of these common features, *Ttda*^{-/-} embryos also exhibit a rather heterogeneous spectrum of phenotypes. These additional features range from having a “pale” appearance to internal haemorrhages, most likely leading to embryonic lethality. Using next generation sequencing (NGS) we determined which genes were differentially expressed at a very early stage of gestation (unpublished data). Indeed, when we compared the transcriptional profile of *Ttda*^{-/-} ES cells with their wild type littermates, we found multiple genes being differentially expressed. By using Ingenuity Pathway Analysis (IPA) we found several networks differentially regulated, which included: embryonic development, cellular growth and proliferation, and hematological system development and function.

Our data clearly show that TTDA has an essential function in NER. The rather mild TTD-phenotype observed in TTD-A patients is due to the presence of partly functional mutant proteins. The sensitivity to endogenously produced oxidative DNA lesions in *Ttda*^{-/-} cells suggests that TTDA (and likely the entire TFIIH) has additional functions in DNA repair extending beyond NER, causing synergistic effects when inactivated. However, full NER-deficiency in combination with defects in oxidative DNA damage repair — as in *Xpa*^{-/-} *Csb*^{-/-} double KO mice — does not lead to embryonic lethality. In this mouse model pups are born, but they progressively develop very severe neurologic symptoms and premature aging features. Recently, it has been shown that the ribosome biogenesis in TTD patients is disturbed in *Ttda*^{-/-} ES cells [41]. Interestingly, neurological abnormality is a feature also found in a number of genetic diseases caused by mutations in ribosomal genes [42]. The lethal phenotype observed in *Ttda*^{-/-} embryos is possibly the result of several defects, such as insufficient levels of TFIIH needed for

transcription in highly proliferative tissues, ribosome biogenesis, impairment in the activated transcription of specific genes, and unrepaired lesions — induced either by UV or endogenously by oxidizing agents, both relevant for cancer as well as aging [43].

References

1. Lafforet, D. and J.M. Dupuy, [Photosensitization and DNA repair. Possible nosologic relationship between Xeroderma pigmentosum and Cockayne's syndrome] Arch Fr Pediatr, 1978. **35**(10 Suppl): p. 65-74.
2. Broughton, B.C., et al., Molecular and cellular analysis of the DNA repair defect in a patient in xeroderma pigmentosum complementation group D who has the clinical features of xeroderma pigmentosum and Cockayne syndrome. Am J Hum Genet, 1995. **56**(1): p. 167-74.
3. Stefanini, M., et al., Xeroderma pigmentosum (complementation group D) mutation is present in patients affected by trichothiodystrophy with photosensitivity. Hum Genet, 1986. **74**(2): p. 107-12.
4. Stefanini, M., et al., Genetic heterogeneity of the excision repair defect associated with trichothiodystrophy. Carcinogenesis, 1993. **14**(6): p. 1101-5.
5. Vermeulen, W., et al., Clinical heterogeneity within xeroderma pigmentosum associated with mutations in the DNA repair and transcription gene ERCC3. Am J Hum Genet, 1994. **54**(2): p. 191-200.
6. Graham, J.M., Jr., et al., Cerebro-oculo-facio-skeletal syndrome with a nucleotide excision-repair defect and a mutated XPD gene, with prenatal diagnosis in a triplet pregnancy. Am J Hum Genet, 2001. **69**(2): p. 291-300.
7. Broughton, B.C., et al., Two individuals with features of both xeroderma pigmentosum and trichothiodystrophy highlight the complexity of the clinical outcomes of mutations in the XPD gene. Hum Mol Genet, 2001. **10**(22): p. 2539-47.
8. Fujimoto, M., et al., Two new XPD patients compound heterozygous for the same mutation demonstrate diverse clinical features. J Invest Dermatol, 2005. **125**(1): p. 86-92.
9. Vandenberghe, K., et al., Bilateral cataract and high myopia in a child with trichothiodystrophy: a case report. Bull Soc Belge Ophtalmol, 2001(282): p. 15-8.
10. Giglia-Mari, G., et al., A new, tenth subunit of TFIIH is responsible for the DNA repair syndrome trichothiodystrophy group A. Nat Genet, 2004. **36**(7): p. 714-9.
11. Egly, J.M., The 14th Datta Lecture. TFIIH: from transcription to clinic. FEBS Lett, 2001. **498**(2-3): p. 124-8.
12. Zurita, M. and C. Merino, The transcriptional complexity of the TFIIH complex. Trends Genet, 2003. **19**(10): p. 578-84.
13. Santagati, F., et al., Different dynamics in nuclear entry of subunits of the repair/transcription factor TFIIH. Nucleic Acids Res, 2001. **29**(7): p. 1574-81.
14. Ito, S., et al., MMXD, a TFIIH-independent XPD-MMS19 protein complex involved in chromosome segregation. Mol Cell, 2010. **39**(4): p. 632-40.
15. Li, X., O. Urwyler, and B. Suter, Drosophila Xpd regulates Cdk7 localization, mitotic kinase activity, spindle dynamics, and chromosome segregation. PLoS Genet, 2010. **6**(3): p. e1000876.
16. Giglia-Mari, G., et al., Dynamic interaction of TTDA with TFIIH is stabilized by nucleotide excision repair in living cells. PLoS Biol, 2006. **4**(6): p. e156.
17. Nonnekens, J., et al., In vivo interactions of TTDA mutant proteins within TFIIH. J Cell Sci, 2013. **126**(Pt 15): p. 3278-83.
18. Vermeulen, W., et al., Sublimiting concentration of TFIIH transcription/DNA repair factor causes TTD-A trichothiodystrophy disorder. Nat Genet, 2000. **26**(3): p. 307-13.
19. Chigancas, V., et al., Defective transcription/repair factor IIH recruitment to specific UV lesions in trichothiodystrophy syndrome. Cancer Res, 2008. **68**(15): p. 6074-83.
20. Weeda, G., et al., A mutation in the XPB/ERCC3 DNA repair transcription gene, associated with trichothiodystrophy. Am J Hum Genet, 1997. **60**(2): p. 320-9.
21. Riou, L., et al., The relative expression of mutated XPB genes results in xeroderma pigmentosum/Cockayne's syndrome or trichothiodystrophy cellular phenotypes. Hum Mol Genet, 1999. **8**(6): p. 1125-33.

22. Hoogstraten, D., et al., *Rapid switching of TFIIH between RNA polymerase I and II transcription and DNA repair in vivo*. Mol Cell, 2002. **10**(5): p. 1163-74.
23. Coin, F., et al., *p8/TTD-A as a repair-specific TFIIH subunit*. Mol Cell, 2006. **21**(2): p. 215-26.
24. Zhou, Y., H. Kou, and Z. Wang, *Tfb5 interacts with Tfb2 and facilitates nucleotide excision repair in yeast*. Nucleic Acids Res, 2007. **35**(3): p. 861-71.
25. Theil, A.F., et al., *Slowly progressing nucleotide excision repair in trichothiodystrophy group A patient fibroblasts*. Mol Cell Biol, 2011. **31**(17): p. 3630-8.
26. Theil, A.F., et al., *Disruption of TTD results in complete nucleotide excision repair deficiency and embryonic lethality*. PLoS Genet, 2013. **9**(4): p. e1003431.
27. de Vries, A., et al., *Increased susceptibility to ultraviolet-B and carcinogens of mice lacking the DNA excision repair gene XPA*. Nature, 1995. **377**(6545): p. 169-73.
28. Andressoo, J.O., J.H. Hoeijmakers, and H. de Waard, *Nucleotide excision repair and its connection with cancer and ageing*. Adv Exp Med Biol, 2005. **570**: p. 45-83.
29. de Waard, H., et al., *Cell type-specific hypersensitivity to oxidative damage in CSB and XPA mice*. DNA Repair (Amst), 2003. **2**(1): p. 13-25.
30. Helleday, T., et al., *DNA repair pathways as targets for cancer therapy*. Nat Rev Cancer, 2008. **8**(3): p. 193-204.
31. Niedernhofer, L.J., et al., *A new progeroid syndrome reveals that genotoxic stress suppresses the somatotroph axis*. Nature, 2006. **444**(7122): p. 1038-43.
32. van der Pluijm, I., et al., *Impaired genome maintenance suppresses the growth hormone--insulin-like growth factor 1 axis in mice with Cockayne syndrome*. PLoS Biol, 2007. **5**(1): p. e2.
33. Sarker, A.H., et al., *Recognition of RNA polymerase II and transcription bubbles by XPG, CSB, and TFIIH: insights for transcription-coupled repair and Cockayne Syndrome*. Mol Cell, 2005. **20**(2): p. 187-98.
34. Hanawalt, P.C. and G. Spivak, *Transcription-coupled DNA repair: two decades of progress and surprises*. Nat Rev Mol Cell Biol, 2008. **9**(12): p. 958-70.
35. Guo, J., P.C. Hanawalt, and G. Spivak, *Comet-FISH with strand-specific probes reveals transcription-coupled repair of 8-oxoGuanine in human cells*. Nucleic Acids Res, 2013.
36. de Boer, J., et al., *A mouse model for the basal transcription/DNA repair syndrome trichothiodystrophy*. Mol Cell, 1998. **1**(7): p. 981-90.
37. Dubaele, S., et al., *Basal transcription defect discriminates between xeroderma pigmentosum and trichothiodystrophy in XPD patients*. Mol Cell, 2003. **11**(6): p. 1635-46.
38. Viprakasit, V., et al., *Mutations in the general transcription factor TFIIH result in beta-thalassaemia in individuals with trichothiodystrophy*. Hum Mol Genet, 2001. **10**(24): p. 2797-802.
39. Giglia-Mari, G., et al., *Differentiation driven changes in the dynamic organization of Basal transcription initiation*. PLoS Biol, 2009. **7**(10): p. e1000220.
40. Keriell, A., et al., *XPD mutations prevent TFIIH-dependent transactivation by nuclear receptors and phosphorylation of RARalpha*. Cell, 2002. **109**(1): p. 125-35.
41. Nonnekens, J., et al., *Mutations in TFIIH causing trichothiodystrophy are responsible for defects in ribosomal RNA production and processing*. Hum Mol Genet, 2013. **22**(14): p. 2881-93.
42. Freed, E.F., et al., *When ribosomes go bad: diseases of ribosome biogenesis*. Mol Biosyst, 2010. **6**(3): p. 481-93.
43. Hoeijmakers, J.H., *Genome maintenance mechanisms for preventing cancer*. Nature, 2001. **411**(6835): p. 366-74.



CHAPTER 7

Summary

Nederlandse samenvatting

List of Abbreviations

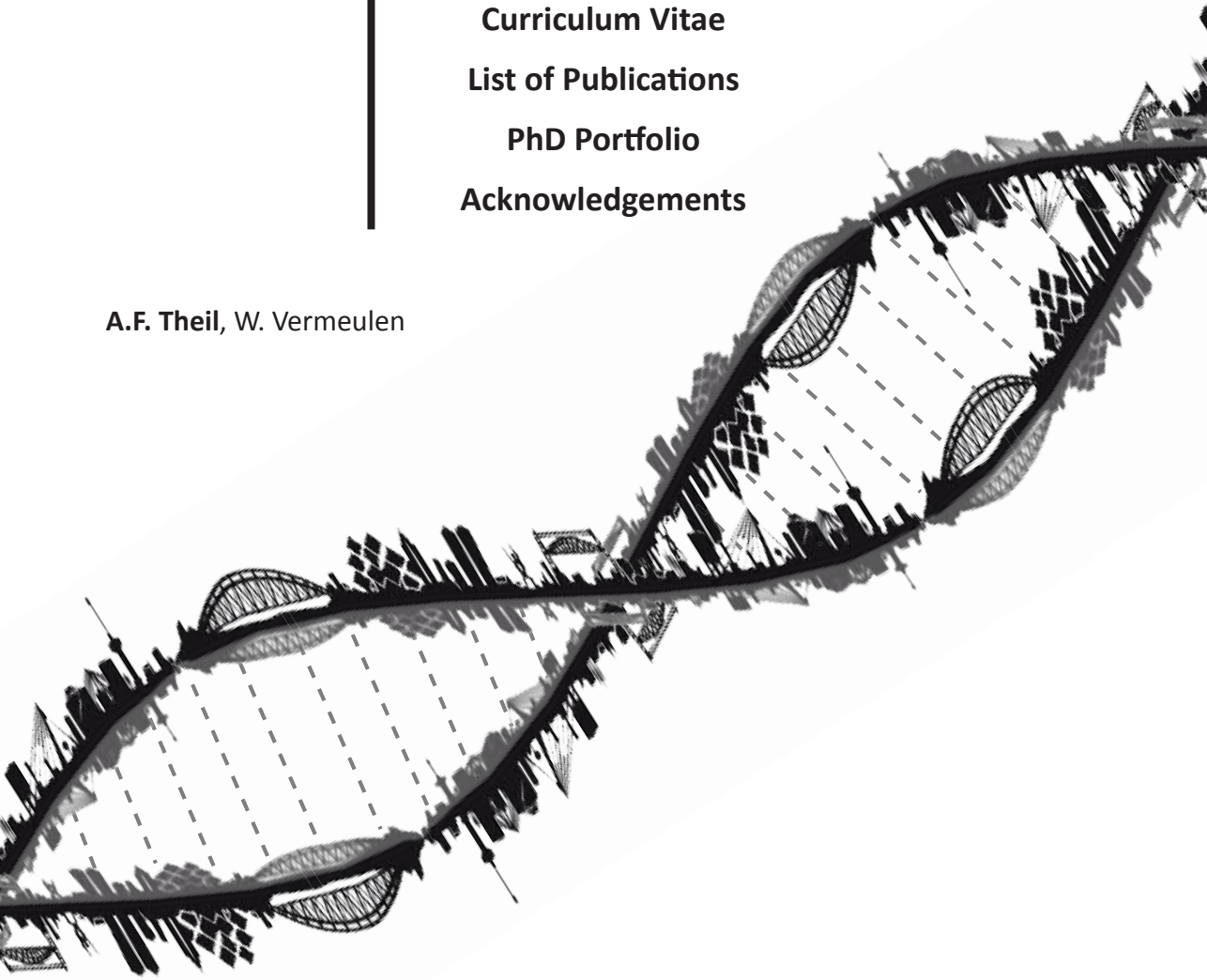
Curriculum Vitae

List of Publications

PhD Portfolio

Acknowledgements

A.F. Theil, W. Vermeulen



Summary

The integrity DNA in all living organisms is under constant attack by numerous processes and agents that damage DNA, either derived from by-products of cellular metabolism or from environmental agents and radiation. It has been estimated that in each cell of the human body approximately 10,000-50,000 lesions per day are induced. One of the most abundant internal sources of DNA damage is created by the group of Reactive Oxygen Species (ROS), which include oxygen ions, free radicals (such as the highly reactive hydroxyl radical ($\bullet\text{OH}$)) and peroxides. ROS can be formed as a by-product of normal cellular metabolism and respiration. Environmental sources of DNA damage include ionizing radiation, various chemicals in food and UV light (component of sunlight). Depending on its wavelength, UV irradiation has been divided into: UVA (320 to 400 nm), UVB (295 to 320 nm) and UVC (100 to 295 nm). Solar UV light, which reaches the Earth surface, consists mainly of UVA and UVB, since UVC is efficiently blocked by the ozone layer. UVA mainly induces oxygen radicals that can induce DNA damage, whereas the energy from UVB can be directly absorbed by DNA and induces harmful DNA lesions such as cyclobutane pyrimidine dimers (CPDs) or 6-4 photoproducts (6-4PPs). DNA damage can interfere with important processes in the cell, such as gene transcription and DNA replication—a process that copies all the DNA in the cell each time a cell divides into two new cells. Unrepaired lesions in genes interfere with the function of RNA polymerases during transcription, causing a physical block. This block may inactivate genes and could eventually result in permanent cell arrest or even cell death. If these cells are not replaced in the tissues or organs, it can result in premature ageing. Unrepaired lesions can also interfere with DNA replication, affecting the accuracy of the DNA replication machinery. These replication errors may result in irreversible mutations and can lead to cancer. To ensure preservation of genetic information, and to allow optimal progression of these vital cellular processes, the cell harbours multiple DNA repair mechanisms, each with their own lesion specificity and characteristics.

Nucleotide excision repair (NER) is responsible for removal of numerous structurally unrelated DNA lesions that destabilize the DNA double helix, including bulky chemical adducts and UV-induced 6-4PPs and CPDs. This mechanism consists of two DNA damage sensing sub-pathways: one that scans the entire genome for lesions (global genome NER, GG-NER) and one that targets lesions that physically block the RNA polymerase when engaged in transcription (transcription coupled NER, TC-NER). After initial damage recognition, both GG-NER and TC-NER funnel into a common process that involves the opening of the DNA double helix by the helicase function of the basal transcription factor II H (TFIIH). TFIIH consists of ten subunits and is essential for transcription and NER. In both these processes, TFIIH unwinds the DNA to allow gene transcription or lesion removal in NER.

Mutations in the TFIIH subunits XPB, XPD and TTDA are associated with UV-hypersensitivity and a surprising phenotypic heterogeneity, including features commonly seen in: cancer-prone xeroderma pigmentosum (XP), or in the severe neuro-developmental and premature ageing syndromes trichothiodystrophy (TTD) and Cockayne syndrome (CS), or even combinations of those, as in some rare cases with combined features of XP and (XP/CS) or XP and TTD (XP/TTD). Mutations that affect only the GG-NER pathway mainly cause XP features, as non-repaired lesions induced by e.g. exposure to UV-light can induce cell killing or can be converted into mutations. The former explains the severe sun-sensitivity, whereas increased mutagenesis in oncogenes and tumor-suppressor genes may explain the strong skin-cancer predisposition in XP. Contrary to GG-NER, mutations that affect the TC-NER pathway do not significantly contribute to mutagenesis, explaining

the absence of elevated cancer in CS and TTD. However, lesion-blocked RNA polymerases are extremely cytotoxic and mainly induce cell killing or senescence and may explain the segmental ageing features seen in CS and TTD. The spectrum of symptoms observed in TTD patients is very broad and stretches from very mild forms of the disease—characterized by normal development with only brittle hair and scaling skin (typical TTD-features)—to very severe cases—characterized by high mortality at young age combined with severe developmental defects. Both cancer-related and age-related diseases/discomforts have become a major social and medical issue due to the still increasing lifespan. It is therefore highly relevant to understand the biological processes that cause these phenomena.

The work presented in this thesis is aimed to better understand the etiology of the spectrum of symptoms presented in TTD patients. Mutations in the XPB and XPD subunits of TFIIH induce a broad spectrum of clinical features, however mutations in the TTDA subunit are thus far only found to be associated with TTD-specific symptoms. These patients belong to the rare neurodevelopment repair syndrome trichothiodystrophy group A (TTD-A). The small (8 kDa) TTDA protein is important for maintaining the stability of the entire TFIIH complex. The cellular concentration of TFIIH in TTD-A fibroblasts is reduced to only 30% of the amount found in wild-type cells. However, this low quantity cannot fully explain the remarkable or puzzling repair properties observed in TTD-A cells. TTD-A cells exhibit a very low DNA repair activity when measured shortly after inducing a high dose of DNA damage by e.g. UV-light. This low level of NER activity should render cells hyper-sensitive to UV. Strikingly however, in UV-colony survival assays, that measures the long term biological effect of UV-irradiation, TTD-A cells appeared only moderately UV-sensitive. By further analysis of different NER properties in TTD-A mutant cells (**Chapter 1**), we noticed that UV-lesions are repaired although with slow rate. Based on these data obtained from measurements with entirely different time-scales of monitoring DNA repair endpoints, we hypothesized that the repair activity in TTD-A mutant cells is not completely absent, but is most likely only slower, eventually removing most lesions and thus explaining moderate UV-sensitivity. The reduced resistance to UV-light is also observed at relative low UV-doses, suggesting that not only the limited amount of TFIIH causes the observed repair capacity but argues for an additional more direct role of TTDA in NER.

Although TTDA was identified as an associated TFIIH factor, its dynamic binding equilibrium to TFIIH is not known. In order to understand TTDA-binding to TFIIH and how this association is affected when engaged in DNA repair, we measured the mobility of TTDA in living cells using fluorescence recovery after photo-bleaching (FRAP). To that aim TTD-A cells that stably express a fluorescently labeled version of the TTDA protein (TTDA-GFP; TTDA fused to Green Fluorescent Protein or GFP) was generated (**Chapter 2**). Experiments performed in this chapter showed that TTDA is only transiently bound to TFIIH and dynamically switches between a TFIIH-bound and TFIIH-free form of TTDA. However, when cells are exposed to DNA damage, the balance is quickly shifted towards a TFIIH-bound form of TTDA that is actively engaged in NER.

Analysis of TTD-A patient derived fibroblasts in **Chapter 1** and of the dynamic properties of TTDA in living cells **Chapter 2** have provided valuable information on the function of TTDA in NER. The majority of the disease-specific symptoms of TTD-A patients are presented in either neuronal cells or skin cells (causative for either mental retardation, or brittle hair and scaly skin) rather than in fibroblasts. In order to provide important clues on the etiology and molecular basis of TFIIH-related diseases, we have generated two mouse models: an *XpbYFP* knock-in mouse model and TTDA knock-out mice (*Ttda*^{-/-}). The *XpbYFP* mice were generated by homologous targeting of a gene encoding for the yellow fluorescent protein (YFP, spectral variant of GFP) to the endogenous *Xpb* allele to create an

in-frame fusion gene between *Xpb* (coding for TFIIH subunit XPB) and *YFP* (XPBYFP). Inter crosses between heterozygous *XpbYFP/Xpb* mice resulted in mice that express from both alleles fluorescently-tagged *Xpb*. This allowed us to study the dynamics of XPbYFP and the entire TFIIH complex (as XPB is an essential and integral component of TFIIH) in different cell types in living tissue (**Chapter 3**). Time-lapse imaging and photobleaching experiments in living tissues derived from these mice has provided us with valuable novel insight into the dynamic organization of transcription in different cell types (post-mitotic cells: e.g. neuronal cells or liver cells). We observed a striking difference in the transcription-dependent dynamic behaviour between highly differentiated post-mitotic cells (e.g. neuronal, muscle or liver cells) and proliferating cells (e.g. keratinocytes). TFIIH is virtually immobilized on chromatin in a transcription-dependent fashion in the former cell types, whereas in proliferating cells most TFIIH freely diffuses and only transiently interacts with the transcription machinery. These differences in the temporal organization of TFIIH in transcription may also influence its repair function and might be a role in the tissue-specific phenotypic expression of the different TFIIH mutants. In addition, the fluorescent TFIIH was also used to study the fate of TFIIH in the absence of TTDA in *Ttda* knock-out mice (*Ttda*^{-/-}) (**Chapter 4**). In this chapter we describe the generation and analysis of the *Ttda*^{-/-} mouse model. Unexpectedly, and in striking contrast to TTD-A patients, embryos that lack *Ttda* die between embryonic day 10.5 and just before birth. We provide evidence that the difference between the lethal *Ttda*^{-/-} mouse and the rather mild TTD-phenotype observed in TTD-A patients is due to the presence of partly functional mutant TTDA proteins in patient cells. Because the cells isolated from the mouse embryos were completely lacking *Ttda*, we were able to study for the first time both transcription and DNA repair in the absence of *Ttda*. TTDA seems to play only a minor role in basal transcription, although its presence may be more critical during specific transcriptional programs. The severely reduced amount of TFIIH in the absence of TTDA may become insufficient to support high levels of transcription required in critical steps of embryogenesis.

Cells isolated from these mice present a complete inactivation of NER, also contrasting to the only mild NER defect in TTD-A patient cells (described in chapter 1) with partial functional mutant protein. These data indicate that TTDA is not only an NER accessory factor, as previously suggested, but appeared essential for NER. We also observed that *Ttda*-deficient cells were hyper-sensitive to oxidative DNA damaging agents, which induce lesions normally not repaired by the NER pathway. Oxidative DNA lesions are the most abundant lesions produced by endogenous cellular processes. The sensitivity to (endogenously produced) oxidative DNA lesions suggests that TTDA (and likely the entire TFIIH) has additional functions in DNA repair extending beyond NER, causing synergistic defects in genome preservation when inactivated. The synthetic consequences of partial defective transcription in combination with severe NER-deficiency and a reduced capacity to remove endogenously produced DNA lesions, may explain the lethal phenotype observed in *Ttda*^{-/-} embryos.

Nederlandse samenvatting

De integriteit van het DNA in alle levende organismen wordt continue bedreigd door verschillende interne (endogene) en externe processen en stoffen die het DNA beschadigen – als gevolg van bijproducten die vrijkomen bij de cellulaire stofwisseling (endogeen) of door stralingen uit het milieu (extern). Het aantal DNA beschadigingen die in elke cel in het menselijk lichaam worden gemaakt, wordt geschat op ongeveer 10.000 tot 50.000 per dag. Eén van de meest voorkomende bronnen van interne DNA beschadigingen wordt veroorzaakt door zuurstofradicalen (Reactive Oxygen Species of ook wel ROS genoemd): zuurstof ionen, vrije radicalen (zoals het zeer sterk reagerend hydroxylradicaal ($\bullet\text{OH}$)) en peroxiden. Zuurstofradicalen zijn bijproducten die gevormd worden door de stofwisseling van cellen en ademhaling. Stoffen uit het milieu die het DNA beschadigen zijn: ioniserende straling, verschillende chemicaliën in voedsel en UV-licht (bestandsdeel van zonlicht). UV-licht kan onderverdeeld worden in 3 groepen (afhankelijk van de golflengte): UVA (320 tot 400 nm), UVB (295 tot 320 nm) en UVC (100 tot 295 nm). Zonlicht dat de aarde bereikt bestaat voornamelijk uit UVA en UVB, aangezien UVC efficiënt wordt geblokkeerd door de ozonlaag. UVA produceert voornamelijk zuurstofradicalen die het DNA beschadigen. De energie van UVB wordt daarentegen direct geabsorbeerd door het DNA en veroorzaakt zeer schadelijke DNA beschadigingen zoals cyclobutane pyrimidine dimers (CPDs) en 6-4 photoproducts (6-4PPs). DNA beschadigingen kunnen belangrijke processen in de cel verstoren, bijvoorbeeld transcriptie – een proces dat instructies op het DNA doorgeeft aan de cel d.m.v. een kopie van het DNA (messenger RNA of mRNA) – en replicatie – een proces dat al het DNA in de cel kopieert voordat deze deelt in twee nieuwe “dochter” cellen. Niet gerepareerde beschadigingen in genen veroorzaken een fysieke blokkering en daardoor verstoring van het RNA polymerase complex tijdens transcriptie. Deze blokkeringen kunnen genen inactiveren, wat uiteindelijk kan resulteren in een permanente cel inactiviteit of zelfs celdood. Als deze cellen niet worden vervangen in het desbetreffende weefsel of orgaan, dan kan dit leiden tot vervroegde veroudering. Niet gerepareerde beschadigingen kunnen ook DNA replicatie verstoren, met als gevolg dat met name de nauwkeurigheid van het DNA replicatie mechanisme wordt aangetast. Deze replicatie-fouten leiden mogelijk tot permanente mutaties en kunnen uiteindelijk kanker veroorzaken. Om de genetische informatie intact te houden en voortgang van deze vitale cellulaire processen te waarborgen, is de cel uitgerust met een aantal reparatie mechanismen, elk met hun eigen schade-specificiteit en karakteristieken.

Nucleotide excision repair (NER) is verantwoordelijk voor het verwijderen van een groot aantal structureel niet-verwante DNA schades die de dubbele DNA-helix destabiliseren – waar omvangrijke chemische adducten, UV-geïnduceerde 6-4PPs en CPDs onder vallen. Dit mechanisme bestaat uit twee DNA-schade zoekende sub-routes: een route die het hele genoom op schades scant (global genome NER, GG-NER) en een die schades vindt die het RNA polymerase fysiek blokkeren tijdens actieve transcriptie (transcription coupled NER, TC-NER). Na de initiële schadeherkenning in zowel GG-NER en TC-NER voegen deze zich samen in een gemeenschappelijk proces, namelijk het openen van de DNA dubbele helix door de ontwindende functie van het basale transcriptiefactor II H (TFIIH). TFIIH bestaat uit tien componenten en is essentieel voor transcriptie en NER. TFIIH is in beide processen verantwoordelijk voor het openen van het DNA voor transcriptie initiatie of voor het verwijderen van een schade in NER.

Mutaties in TFIIH componenten *XPB*, *XPD* en *TTDA* worden geassocieerd met UV-overgevoeligheid en een verrassende fenotypische heterogeniteit. Symptomen die hieronder vallen worden vaak gezien in kanker gevoelige Xeroderma pigmentosum (XP),

ernstige neurologische ontwikkelingsstoornissen en vroegtijdige verouderings syndromen trichothiodystrophy (TTD) en Cockayne syndrome (CS), of zelfs in sommige zeldzame gevallen met gecombineerde symptomen van XP en CS (XP / CS) of XP en TTD (XP / TTD). Mutaties in genen die alleen een functie hebben in de GG-NER-route veroorzaken voornamelijk XP symptomen, doordat niet gerepareerde schades (veroorzaakt door bijvoorbeeld blootstelling aan UV-licht) celdood induceren of worden omgezet in mutaties. Celdood verklaart de aanwezigheid van extreme zongevoeligheid in XP patiënten, aan de andere kant zijn de verhoogde hoeveelheid mutaties verantwoordelijk voor de sterke vatbaarheid voor huidkanker bij XP. In tegenstelling tot GG-NER dragen mutaties in genen die alleen een functie hebben in de TC-NER-route niet significant bij aan mutagenese, dat de afwezigheid van een verhoogde kans op kanker in CS en TTD verklaart. Schades die het RNA polymerase blokkeren zijn daarentegen wel zeer cytotoxisch en induceren vooral celdood of veroudering – de segmentale verouderingssymptomen die te zien zijn in CS en TTD patiënten kunnen hierdoor verklaard worden. Het spectrum van symptomen waargenomen bij TTD patiënten is zeer breed en strekt zich uit van een zeer milde vorm van de ziekte – gekarakteriseerd door normale ontwikkeling en slechts broos haar en schilferende huid (typisch TTD symptomen) – tot zeer ernstige gevallen die worden gekarakteriseerd door een hoge sterfte op jonge leeftijd in combinatie met ernstige ontwikkelingsstoornissen. Als gevolg van de nog steeds toenemende levensverwachting zijn zowel kanker- als leeftijds-gerelateerde ziekten/ongemakken een belangrijke sociale en medische kwestie geworden. Het is daarom zeer relevant om de biologische processen die ten grondslag liggen aan deze verschijnselen beter te begrijpen.

Het werk, beschreven in dit proefschrift, is erop gericht een beter inzicht te krijgen hoe het spectrum van symptomen in TTD patiënten ontstaat. Mutaties in de *XPB* en *XPD* genen (componenten van TFIIH) veroorzaken een breed spectrum van klinische symptomen. Mutaties in het *TTDA* gen (kleinste component van TFIIH) zijn tot nu toe alleen in verband gebracht met TTD-specifieke symptomen. Deze patiënten behoren tot het zeldzame neurologische reparatie syndroom trichothiodystrophy groep A (TTD-A). Dit kleine TTDA eiwit (8 kDa) is belangrijk voor de stabiliteit van het gehele TFIIH complex. Vergeleken met normale cellen is de concentratie van TFIIH verminderd tot 30% in TTD-A fibroblasten. Deze lage hoeveelheid TFIIH kan echter de opmerkelijke en raadselachtige reparatie eigenschappen, waargenomen in TTD-A cellen, niet volledig verklaren. TTD-A cellen hebben een zeer lage DNA reparatie-activiteit – gemeten vlak na het geven van een hoge dosis DNA schade (door bijvoorbeeld UV-licht). Cellen met een lage NER reparatie-activiteit (korte termijn) zijn over het algemeen zeer gevoelig voor UV-straling op de lange termijn. Opvallend is echter dat in een UV-overleving experiment – dat het biologische effect van UV-straling op de lange termijn meet – TTD-A cellen slechts een milde UV-gevoeligheid laten zien. Bij het uitvoeren van verschillende experimenten in TTD-A mutant cellen (hoofdstuk 1) merkten we dat UV schades minder snel worden gerepareerd. Op basis van deze verkregen resultaten veronderstelden we dat de reparatie-activiteit in TTD-A mutant cellen niet geheel afwezig is, maar waarschijnlijk minder efficiënt DNA beschadigingen verwijdert. De milde gevoeligheid tegen UV-licht is ook waargenomen bij relatief lage UV doses, wat suggereert dat niet alleen de beperkte TFIIH de waargenomen herstelcapaciteit veroorzaakt, maar pleit tegen meer directe rol van TTDA in NER.

Hoewel TTDA oorspronkelijk is geïdentificeerd als een TFIIH-geassocieerde factor, is de dynamische binding met TFIIH nog onbekend. Om te begrijpen hoe TTDA aan TFIIH bindt en hoe deze wordt beïnvloed wanneer het complex actief DNA schade repareert, hebben we met behulp van FRAP (fluorescence recovery after photobleaching) de mobiliteit van TTDA in levende cellen gemeten. Om dit doel te bereiken hebben we in

TTD-A patiënten cellen een groen fluorescerend gelabelde versie van het TTDA eiwit (TTDA-GFP; TTDA gefuseerd met een Green Fluorescent Protein of GFP) stabiel tot expressie gebracht (hoofdstuk 2). Uit de experimenten die zijn uitgevoerd, bleek dat TTDA slechts kortstondig gebonden is aan TFIIH en constant schakelt tussen een TFIIH-gebonden en een TFIIH-vrije vorm van TTDA. Echter, wanneer de cellen worden blootgesteld aan DNA schade, wordt dit evenwicht snel verschoven naar een TFIIH-gebonden vorm van TTDA die actief betrokken is in NER.

De analyse van geïsoleerde TTD-A patiënten fibroblasten (hoofdstuk 1) en de gemeten dynamische eigenschappen van TTDA in levende cellen (hoofdstuk 2) hebben waardevolle informatie verstrekt over de functie van TTDA in NER. Het merendeel van de ziekte-specifieke symptomen van TTD-A patiënten komen echter niet tot uiting in fibroblasten maar in de neuronale cellen of huidcellen (oorzakelijk voor de geestelijke achterstand, of broos haar en schilferige huid). Om belangrijke aanwijzingen te vinden over de etiologie en de moleculaire oorzaak van TFIIH-gerelateerde ziekten hebben we twee muismodellen gegenereerd: een *XpbYFP* knock-in muismodel en een TTDA knock-out muismodel (*Ttda*^{-/-}). De *XpbYFP* muizen werden gegenereerd door een geel fluorescerende eiwit (Yellow Fluorescent Protein of YFP, spectrale variant van GFP) in-frame toe te voegen aan het endogene *Xpb* allel. Hierdoor wordt er een fusie gecreëerd tussen het *Xpb* gen (coderend voor het TFIIH component XPB) en *YFP* (XPBYFP). Kruisingen tussen heterozygote *XpbYFP/Xpb* muizen resulteerden in muizen waarbij beide allelen het fluorescerende gelabelde *Xpb* tot expressie brengen. Hierdoor was het mogelijk om de dynamiek van *XpbYFP*, en dus ook het gehele TFIIH complex – omdat XPB een essentieel en integraal onderdeel is van TFIIH –, in verschillende celtypen en levende weefsels te bestuderen (hoofdstuk 3). Levende weefsels die werden geïsoleerd van deze muizen konden worden gebruikt voor het maken van video's en het uitvoeren van photobleaching experimenten. Deze proeven hebben ons voorzien van waardevolle nieuwe inzichten in de dynamische organisatie van transcriptie in verschillende celtypen. We zagen een opvallend verschil in transcriptie-afhankelijke dynamiek tussen gedifferentieerde post-mitotische cellen (bv. neuronale, spier-of levercellen) en delende cellen (bijvoorbeeld keratinocyten). TFIIH is op een transcriptie-afhankelijke manier vrijwel volledig geïmmobiliseerd op het chromatine in gedifferentieerde post-mitotische celtypen, terwijl in delende cellen de meeste TFIIH vrij verspreid en slechts een kortstondig interactie aangaat met het transcriptie complex. Deze verschillen in tijdsverloop van TFIIH in transcriptie kan ook de reparatie functie beïnvloeden en eventueel een rol spelen bij de weefselspecifieke fenotypische symptomen van de verschillende TFIIH mutanten. Bovendien werd het fluorescerende TFIIH ook te gebruiken om het lot van TFIIH bestuderen in de afwezigheid van TTDA in TTDA knock-out cellen (*Ttda*^{-/-}) (hoofdstuk 4). In dit hoofdstuk wordt het genereren en analyseren van het *Ttda*^{-/-} muismodel beschreven. Onverwacht en in schril contrast met TTD-A patiënten gaan *Ttda*^{-/-} embryo's dood tussen embryonale dag 10,5 en net voor de geboorte. We laten zien dat het verschil tussen de letale *Ttda*^{-/-} muis en de nogal milde TTD fenotype waargenomen in TTD-patiënten het gevolg is van de aanwezigheid van gedeeltelijke functionele mutant TTDA eiwitten in cellen van een patiënt. Omdat de cellen die zijn geïsoleerd uit de embryo's geen TTDA hebben, konden we voor het eerst zowel transcriptie als DNA reparatie bestuderen in de afwezigheid van TTDA. TTDA lijkt slechts een kleine rol te spelen in transcriptie, hoewel deze best van belang kan zijn tijdens specifieke transcriptionele programma's. De hoeveelheid TFIIH is sterk verminderd in afwezigheid van TTDA en is daarom dan ook mogelijk onvoldoende aanwezig om de hoge levels van transcriptie te ondersteunen die nodig zijn voor de verschillende stappen in embryogenese.

Cellen die zijn geïsoleerd uit *Ttda*^{-/-} muizen hebben een compleet inactief NER. Deze observatie staat in schril contrast met het milde NER defect in TTD-A patiënten cellen (beschreven in hoofdstuk 1). Dit verschil is te verklaren door de aanwezigheid van gedeeltelijk functionele mutant eiwitten in TTD-A patiënten cellen. Deze resultaten laten zien dat TTDA niet geheel onbelangrijke is, zoals eerder gesuggereerd werd, maar essentieel voor NER is gebleken. We merkten ook op dat TTDA-deficiënte cellen hypergevoelig zijn voor oxidatieve DNA beschadigende middelen, die normaal niet door het NER mechanisme worden gerepareerd. Oxidatieve DNA beschadigingen zijn de meest voorkomende endogene schades die door cellulaire processen worden geproduceerd. De gevoeligheid voor deze (endogene) oxidatieve DNA schades suggereert dat TTDA (en waarschijnlijk het gehele TFIIH complex) een extra functie heeft naast NER. De onnatuurlijke gevolgen van een gebrekkige transcriptie, een ernstige NER-deficiëntie en een verminderd vermogen om endogeen geproduceerde DNA beschadigingen te verwijderen, kan het waargenomen dodelijke fenotype in *Ttda*^{-/-} muizen verklaren.

List of Abbreviations

3'-OH	3'-hydroxyl group
5'-dRP	5'-deoxyribose phosphate
5'-P	5'-phosphate residue
6-4PP	Pyrimidine-(6-4)-pyrimidone product
8-oxoG	7,8-dihydro-8-oxoguanine
APE1	AP-endonuclease 1
AP-site	Abasic-site
ATM	Ataxia telangiectasia-mutated
ATR	Ataxia telangiectasia and Rad3-related kinase
BER	Base excision repair
CPD	Cyclobutane pyrimidine dimer
CS	Cockayne syndrome
CSA	Cockayne syndrome group A
CSB	Cockayne syndrome group B
DDR	DNA-damage response
Dmp52	p52 <i>D. melanogaster</i> mutants
DSB	Double strand break
ERCC1	Excision repair cross-complementing protein 1
FEN1	5'-flap endonuclease 1
GFP	Green fluorescent protein
GG-NER	Global genome nucleotide excision repair
HMGN1	High mobility group nucleosome-binding protein 1
HR	Homologous recombination
ICL	Interstrand crosslink
IPA	Ingenuity pathway analysis (IPA)
IR	Ionizing radiation
JNK	c-Jun NH ₂ -terminal kinases
LigI	Ligase I
LigIII	DNA ligase III
LP-BER	Long-patch BER
MAPK	Mitogen-activated protein kinases
MMR	Mismatch repair
NEIL1-3	Nei endonuclease VIII-Like 1-3
NER	Nucleotide excision repair
NGS	Next generation sequencing
NHEJ	Non-homologous end-joining
OGG1	8-oxoguanine DNA glycosylase
PARP1	Poly (ADP-ribose) polymerase 1
PCNA	Proliferating cell nuclear antigen
PIC	Pre-incision complex (PIC)
PMT	Post-translational modifications
Polβ	Polymerase beta
RFC	Replication factor C
RFC	Replication factor C
RNAP1	RNA polymerase I
RNAP2	RNA polymerase II
ROS	Reactive oxygen species

RPA	Replication protein A
RRS	Recovery of RNA synthesis
SP-BER	Short-patch BER
SSB	Single strand break
TC-NER	Transcription-coupled nucleotide excision repair
TDG	Thymine DNA glycosylase
TFIIH	Transcription factor II H
TFIIS	Transcription factor II S
TLS	Translesion synthesis
TTD	Trichothiodystrophy
TTDA	Trichothiodystrophy group A
UDS	Unscheduled DNA synthesis
USP7	Ubiquitin-specific protease 7
UV	Ultra violet
UV-DDB	UV-damaged DNA-binding
UVSSA	UV-stimulated scaffold protein A
XAB2	XPA-binding protein 2
XP	Xeroderma pigmentosum
XPA	Xeroderma Pigmentosum group A
XPB	Xeroderma pigmentosum group B
XPC	Xeroderma pigmentosum group C
XPD	Xeroderma pigmentosum group D
XPF	Xeroderma pigmentosum group F
XPG	Xeroderma pigmentosum group G
XRCC1	X-ray cross complementing protein-1
YFP	Yellow fluorescent protein

Curriculum Vitae

Name : Arjan F. Theil
 Date of Birth : 22 October 1977
 Place of Birth : 's-Gravenhage

Education	Year
Doctor of Philosophy (PhD), Erasmus MC, Department of Genetics, Rotterdam, The Netherlands	2009-2014
Bachelor in Biochemistry (BSc), Technician School, Rotterdam, The Netherlands	1995-2000

Research Experience	Year
PhD Student, Erasmus MC, Department of Genetics, Rotterdam, The Netherlands	2009-2014
Short-term Visit, Prof. P.C. Hanawalt, Department of Biology, Stanford, USA	2014
Assistant Researcher, Erasmus MC, Department of Genetics, Rotterdam, The Netherlands	2000-2009
Scientific Research Internship, Erasmus MC, Department of Cell Biology, Rotterdam, The Netherlands	1999-2000

List of Publications

Dinant C., Ampatziadis-Michailidis G., Lans H., Tresini M., Lagarou A., Grosbart M., **Theil A.F.**, van Cappellen W.A., Kimura H., Bartek J., Fousteri M., Houtsmuller A.B., Vermeulen W., Marteijn J.A.

Enhanced chromatin dynamics by FACT promotes transcriptional restart after UV-induced DNA damage

Molecular Cell 2013

Bergink S.*, **Theil A.F.***, Toussaint W.*, De Cuyper I.M., Kulu D.I., Clapes T., van der Linden R., Demmers J.A., Mul E.P., van Alphen F.P., Marteijn J.A., van Gent T., Maas A., Robin C., Philipsen S., Vermeulen W., Mitchell J.R., Gutiérrez L.

Erythropoietic defect associated with reduced cell proliferation in mice lacking the 26S proteasome shuttling factor Rad23b

Molecular and Cellular Biology 2013

Theil A.F., Nonnekens J., Steurer B., Mari P.O., de Wit J., Lemaitre C., Marteijn J.A., Raams A., Maas A., Vermeij M., Essers J., Hoeijmakers J.H.J., Giglia-Mari G., Vermeulen W.

Disruption of TTDA results in complete nucleotide excision repair deficiency and embryonic lethality

PLoS Genetics 2013

Nonnekens J., Perez-Fernandez J., **Theil A.F.**, Gadal O., Bonnart C., Giglia-Mari G.

Mutations in TFIIF causing trichothiodystrophy are responsible for defects in ribosomal RNA production and processing.

Human Molecular Genetics 2013

Kleppa L., Mari P.O., Larsen E., Lien G.F., Godon C., **Theil A.F.**, Nesse G.J., Wiksen H., Vermeulen W., Giglia-Mari G., Klungland A.

Kinetics of endogenous mouse FEN1 in base excision repair

Nucleic Acids Research 2012

Theil A.F., Nonnekens J., Wijgers N., Vermeulen W., Giglia-Mari G.

Slowly progressing Nucleotide Excision Repair in Trichothiodystrophy group A patients fibroblasts

Molecular and Cellular Biology 2011

Ahmad A., Enzlin J.H., Bhagwat N.R., Wijgers N., Raams A., Appeldoorn E., **Theil A.F.**, Hoeijmakers J.H.J., Vermeulen W., Jaspers N.G., Scharer O.D., Niedernhofer L.J.

Mislocalization of XPF-ERCC1 nuclease contributes to reduced DNA repair in XP-F patients

PLoS Genetics 2010

Giglia-Mari G., **Theil A.F.***, Mari P.O.*, Mourgues S., Nonnekens J., Andrieux L.O., de Wit J., Miquel C., Wijgers N., Maas A., Fousteri M., Hoeijmakers J.H.J., Vermeulen W.

Differentiation driven changes in the dynamic organization of Basal transcription initiation

PLoS Biology 2009

Giglia-Mari G.*, Miquel C.*, **Theil A.F.**, Mari P.O., Hoogstraten D., Ng J.M., Dinant C., Hoeijmakers J.H.J., Vermeulen W.

Dynamic interaction of TTDA with TFIIH is stabilized by nucleotide excision repair in living cells

PLoS Biology 2006

Niedernhofer L.J., Garinis G.A., Raams A., Lalai A.S., Robinson A.R., Appeldoorn E., Odijk H., Oostendorp R., Ahmad A., van Leeuwen W., **Theil A.F.**, Vermeulen W., van der Horst G.T., Meinecke P., Kleijer W.J., Vijg J., Jaspers N.G., Hoeijmakers J.H.

A new progeroid syndrome reveals that genotoxic stress suppresses the somatotroph axis

Nature 2006

Essers J., **Theil A.F.**, Baldeyron C., van Cappellen W.A., Houtsmuller A.B., Kanaar R., Vermeulen W.

Nuclear dynamics of PCNA in DNA replication and repair

Molecular and Cellular Biology 2005

Essers J., van Cappellen W.A., **Theil A.F.**, van Drunen E., Jaspers N.G., Hoeijmakers J.H., Wyman C., Vermeulen W., Kanaar R.

Dynamics of relative chromosome position during the cell cycle

Molecular Biology of the Cell 2005

van Veelen L.R., Cervelli T., van de Rakt M.W., **Theil A.F.**, Essers J., Kanaar R.

Analysis of ionizing radiation-induced foci of DNA damage repair proteins

Mutat Research 2005

Giglia-Mari G., Coin F., Ranish J.A., Hoogstraten D., **Theil, A.**, Wijgers N., Jaspers N.G., Raams A., Argentini M., van der Spek P.J., Botta E., Stefanini M., Egly J.M., Aebersold R., Hoeijmakers J.H., Vermeulen W.

A new, tenth subunit of TFIIH is responsible for the DNA repair syndrome trichothiodystrophy group A

Nature Genetics 2004

Niedernhofer L.J., Odijk H., Budzowska M., van Drunen E., Maas A., **Theil A.F.**, de Wit J., Jaspers N.G., Beverloo H.B., Hoeijmakers J.H.J., Kanaar R.

The structure-specific endonuclease Ercc1-Xpf is required to resolve DNA interstrand cross-link-induced double-strand breaks

Molecular and Cellular Biology 2004

PhD Portfolio

Name PhD Student : Arjan F. Theil
 PhD period : 2009-2014
 Erasmus MC Department : Genetics
 Research School : Medical Genetics Center (MGC)
 Promotor : Prof. Dr. J.H.J. Hoeijmakers
 Co-promotor : Dr. W. Vermeulen

General Courses	Year
Workshop on InDesign CS5, Erasmus MC, Rotterdam, The Netherlands	2012
Genome Maintenance & Cancer, MGC, Leiden, The Netherlands	2012
English Biomedical Writing and Communication, Erasmus MC, Rotterdam, The Netherlands	2012
The Microscopic Image Analysis: From Theory to Practice, Erasmus MC, Rotterdam, The Netherlands	2011
Literature Course, Erasmus MC, Rotterdam, The Netherlands	2010
PhD Teaching program, Erasmus MC, Rotterdam, The Netherlands - Cell and Developmental Biology course - Genetics course - Biochemistry and Biophysics course	2010
Training Handling Laboratory Animals in IVC cages, Erasmus MC, Rotterdam, The Netherlands	2006
Optical Imaging Course, Erasmus MC, Rotterdam, The Netherlands 2006	
Laboratory animal course (Art. 12), HR&O, Rotterdam, The Netherlands	2004
Laboratory animal course (Art. 9), Erasmus MC, Rotterdam, The Netherlands	2004
Working with radioactive substances (niveau 5B), Erasmus MC, Rotterdam, The Netherlands.	2002
FACS Vantage SE Operator Training, BD Biosciences, Erembodegem, Belgium	2001
Safe Microbiological Technology (ML-I and ML-II), Erasmus MC, Rotterdam, The Netherlands.	2000

International Conferences, Meetings & Workshops	Year
Meeting, Department of Cancer & DNA Damage Responses, Lawrence Berkeley National Laboratory, Berkeley, USA (oral presentation)	2014
FEBS DNA Repair Workshop, Smolenice, Slovakia (poster presentation)	2013
MGC PhD Workshop, Düsseldorf, Germany (oral presentation)	2012
DNA Damage, Mutations & Cancer, Ventura, CA, USA (poster presentation)	2012
MGC PhD Workshop, Maastricht, The Netherlands (poster presentation)	2011
Responses to DNA damage: from molecular mechanism to human disease, Egmond aan Zee, The Netherlands (poster presentation)	2011
MGC DNA Repair Meeting, Leiden, The Netherlands (oral presentation)	2010
Nucleic acids, Protein Research and Lipids & Biomembranes, Velthoven, The Netherlands (poster presentation)	2010
Seeberg Symposium, Alesund, Norway, (poster presentation)	2009
The Dynamic Organization of Nuclear Function, Cold Spring Harbor Laboratory, USA (poster presentation)	2008
DNA repair meeting, Strasbourg, France (oral presentation)	2007
Teaching & Coaching	Year
M. van der Zwalm, BSc Forensic Laboratory Research, Breda, The Netherlands	2013-2014
B. Steurer, MSc Molecular Medicine, Erasmus MC, Rotterdam, The Netherlands	2011-2012
S. Hoogendoorn, BSc Engineering and Applied Science, Rotterdam, The Netherlands	2010
C. Boumendil, MSc Biology, ENS Paris, France	2009
J. Nonnekens, MSc Molecular Medicine, Wageningen University, The Netherlands	2008-2009

Others	Year
Thursday Morning Work discussions	2009-2014
Literature discussions	2009-2014
Seminars (invited speakers)	2009-2014

Acknowledgements

Eindelijk is het dan zover, het laatste stukje van mijn proefschrift. Ik ben er lang mee bezig geweest en het traject ernaar toe is een samenwerking van zeer velen. Voor mij een gelegenheid om ieder die op de één of andere manier bij de totstandkoming ervan betrokken is geweest te bedanken.

Beste Wim, ik ben je enorm dankbaar voor je vertrouwen, ondersteuning en wetenschappelijke training. Het proefschrift was nooit in zijn huidige vorm verschenen zonder jouw inzet. Ik heb altijd met veel plezier voor je gewerkt en ik hoop dat onze samenwerking nog lang zal voortduren.

Dear Ambra, thank you for your support and guidance from day one that you entered the lab. You really inspired and stimulated me in my scientific development. You were the first person that “pushed” me in doing a PhD. I hope that I will be able to visit you and PO many times, as I consider you both as very dear friends.

Beste Jan, bedankt voor de mogelijkheden die je mij hebt geboden. Jouw enthousiasme is een inspiratiebron voor mij en vele anderen.

Beste commissieleden, bedankt voor het lezen van mijn proefschrift en alle nuttige tips.

Karen en Nils, bedankt dat jullie mijn paranimfen willen zijn.

Kishan, bedankt voor je hulp met de opmaak van mijn proefschrift.

I would like to thank everybody for their support.

Als laatste wil ik mijn vrienden, schoonfamilie en familie bedanken voor alle steun. Pa en ma, bedankt voor alle goede zorg toen, nu en in de toekomst.

Judith, bedankt voor alles.

Arjan.

Stellingen behorende bij het proefschrift

“Functional Analysis of TTDA: From Human to Mouse – Big impact of a small protein”

1. Contrary to initial observations, TTDA is an essential NER factor. (*this thesis*)
2. The equilibrium between a TFIIH-bound and dissociated form of TTDA shifts towards the bound state when the complex is actively engaged in NER. (*this thesis*)
3. The finding that *Ttda*^{-/-} embryos die in utero between 10.5 days of gestation and birth, and that *Ttda*^{-/-} cells are viable, makes this mutant unique compared to deletions of the other TFIIH subunits. (*this thesis*)
4. The sensitivity of *Ttda*^{-/-} cells to oxidative DNA damage suggests that TTDA (and likely the whole TFIIH complex) has additional functions in DNA repair extending beyond NER. (*this thesis*)
5. A complete absence of TTD-A expression in humans will most likely be embryonic lethal. (*this thesis*)
6. Architecture is an underestimated aspect in science that can promote people to work together effectively. (*K. Lee et al., PLoS One 2010*)
7. Although biology makes significant progress in many areas, it is a sobering fact that the vast majority of species still awaits description. (*C. Mora et al., PLoS Biology 2011*)
8. The problem of endogenously produced DNA lesions is one of the major black holes in our knowledge on DNA repair.
9. It is important to understand the evolution and function of non-coding RNAs (ncRNAs), as the number of non-coding RNA transcripts surprisingly exceeds the number of protein-coding genes. (*A. Fatica et al., Nature 2014*)
10. Like in sports, high performance in science requires a team of highly qualified and experienced professionals who are not only selected on the basis of scientific skills, but also on their personal characteristics.
11. One of the striking differences between an iPhone and this thesis is the fact that this thesis cannot be financed by the “Personal budget for development”. (*CAO UMC 2013-2015*)